SIMULATING THE EFFECTS OF LAND USE LAND COVER CHANGE ON HYDROMETEOROLOGICAL PARAMETERS OVER WEST AFRICA

BY

ACHUGBU, IFEANYI CHUKWUDI

B. Tech., M. Tech. (MET/04/3597)

A Thesis in the Department of Meteorology and Climate Science, School of Earth and Mineral Sciences, Submitted to the School of Postgraduate Studies in the partial Fulfillment of the Requirements for the Award of Doctor of Philosophy (Ph.D) in Meteorology and Climate Science of the Federal University of Technology, Akure, Nigeria.

FEBRUARY, 2020

DECLARATION

I hereby declare that the Thesis was written by me and is a correct record of my own research work. It has not been presented in any previous application for any degree of this or any other University. All citations and sources of information are clearly acknowledged by means of references.

Candidate's name: Achugbu Ifeanyi Chukwudi

Signature:…… Date:……..

CERTIFICATION

We certify that this Thesis/Desertation/Project entitled “Simulating The Effect of Land Use Land Cover Change on Hydrometeorological Parameters of West Africa” is the outcome of the research carried out by Achugbu, Ifeanyi Chukwudi in the Department of Meteorology and Climate Science, The Federal University of Technology, Akure, Nigeria.

Major Supervisor’s Name: Prof. A. A. Olufayo

Signature:……. Date:…….

Co - Supervisor’s Name: Dr. I. A. Balogun

Signature:……. Date:…….

Co - Supervisor’s Name: Dr. E. A. Adefisan

Signature:……. Date:…….

DEDICATION

This research work is dedicated to the Almighty God.

ACKNOWLEDGEMENT

First and above all, I thank the Almighty God for His grace upon me through the PhD program. I express my utmost gratitude to the German Federal Ministry of Education and Research (BMBF) for providing the fund for this research through the West African Climate System (WACS) Graduate Research Program (GRP) in Federal University of Technology Akure (FUTA). I really appreciate my wife, Mrs. Juliet Ujunwa Achugbu for her encouragement and immeasurable support all through the program. I appreciate my first daughter, Chiazam Glory Ifeanyi and my second daughter (Ph.D daughter), Uchechukwu Favour Ifeanyi for being able to bear with me all through my programme.

I sincerely appreciate my main supervisor, Prof. A. A. Olufayo for his support, guidance, patience and cooperation in this work. The almighty God will continue to bless you and grant you your heart desire. Also, my appreciation goes to my co-supervisors, Dr. I. A. Balogun and Dr. E. A. Adefisan for their support through the program. I acknowledge Prof. K. O. Ogunjobi for his encouragement during the course of this program. God will continue to lift you higher. My special appreciation goes to my Advisor, Dr. Jimy Dudhia for his support, insightful comments, and advice throughout my visit to the National Center for Atmospheric Research (NCAR) in the United States. My Appreciation also goes to Mike Dixon for his support and for also making my stay in the US a memorable one. I would like to acknowledge the Mesoscale and Microscale Meteorology (MMM) Laboratory, NCAR and the Research Applications Laboratory for their supports, and also acknowledge the NCAR's Conputational and Information System Laboratory for providing the computing facilities for the research. Also, many thanks to Ming Chen,

Micheal Duda, Micheal Barlage, Molly McAllister, Katelyn FitzGerald and other NCAR staffs who provided technical support.

I appreciate the entire staff of WASCAL Center FUTA, especially the Director, Prof. E. C. Okogbue for their cooperation and prompt response to render assistance.

Thank you all.

ABSTRACT

Land Use Land Cover (LULC) in Sub-Sahara Africa has undergone rapid transformation in the last century. So comprehending the impact of land use land cover change and its interaction with the atmosphere by means of modeling, and its impact on some hydrometeorological variables is an interesting area both for present and future research. The land use land cover change (LULCC) over West Africa was analysed using the Moderate Resolution Imaging Spectroradiomater (MODIS) MCD12Q1 land use land cover data. The Weather Research and Forecasting (WRF) model was used to examine the effect of Land Surface Model (LSM) options of WRF model on temperature, precipitation and dew point temperature (DPT) in West Africa (WA). Eight simulations were performed using the Noah, Noah-multi-physics (Noah-MP), Community Land Model version 4 (CLM4) and Noah-MP LSM with a ground water option, all with same and other physics combinations. In order to assess the impacts of LULCC on some hydrometeorological parameters over WA, series of WRF simulations were carried out with 2001 and 2016 land use data, and 6 LULC scenarios which includes Built-up (Bu), Partial Deforest I (PDI), Partial Deforest II (PDII), Partial Afforest (PA), Total Afforest (TA) and Total Deforest (TD) were generated. The WRF-hydrological (WRF-Hydro) model was used to simulate the LULC change impact on streamflow over Sokoto Rima River Basin (SRRB) and 3 Forecast Points (FP) (Sokoto, Goronyo and Bakolori) were analysed. Analysis of the LULCC over West Africa (WA) between 2001 and 2016 revealed that there was a general decrease in all forest parameters and a steady increase in built up lands over the period of study. Results show that the LSMs performed differently for different variables in different land-surface conditions. However, Noah-MP was the

overall best performing LSM for all the variables in all season, while Noah performed least. The differences in the simulations could be attributed to the differences in vegetation representation, soil column depth, number of soil layers and other processes in the LSMs. Experiment with 2001 and 2016 land use data revealed that WRF model is sensitive to changes in the land cover parameters. The integration of updated MODIS land use data into WRF model showed improvement in its outputs. Result also shows that for the entire area (10W, 10E, 5N, 15N), Bu scenario decreased DPT, evapotranspiration (ET) and precipitation, but increased 2m temperatures (T2m) and Sensible heat (SH). PDII and PDI scenario increased DPT, T2m, and decreases SH, ET, and Pr, while PA scenario slightly increases DPT, ET, Pr, SH and caused a decrease in T2m. TA scenario increased DPT, ET, Pr, but decreased T2m, and SH while TD decreased DPT, ET, but increases T2m, SH, and Pr. For all the FPs in the SRRB, Bu scenario caused the highest increase in streamflow, while TA scenario shows the highest decrease. The deforestation scenario generally led to an increase in streamflow, while the afforestation scenario led to a decrease. Higher streamflow occurs as a result of increased agricultural lands and decreased forest areas within the basin. The study has shown that land cover has changed over the years, and that the adverse effects of LULCC to the extreme will be increased temperature and discomfort as well as flooding as streamflow increases. The combination of Remote Sensing, GIS, WRF and WRF-hydro model provides a useful technique in assessing the impact of LULC on catchment hydrology. This is essential in selecting and developing feasible catchment management options that will promote sustainable utilization of land and water resources.

TABLE OF CONTENT

LIST OF TABLES

LIST OF TABLES (Continued)

LIST OF FIGURES

LIST OF FIGURES (Continued)

LIST OF FIGURES (Continued)

LIST OF FIGURES (Continued)

LIST OF FIGURES (Continued)

LIST OF FIGURES (Continued)

LIST OF ABBREVIATIONS

ACRU	Agricultural Catchments Research Unit
AEJ	African Easterly Jet
ALMIP	AMMA Land Surface Model Intercomparison Project
AMMA	African Monsoon Multidisciplinary Analysis
ANN	Artificial Neural Networks
ANN	Artificial Neural Networks
ARW	Advanced Research WRF
BATS	Biosphere Atmosphere Transfer Scheme
BGC	BIOME-Biogeochemical Cycles
BL	Boundary Layer
Br	Barren
BU	Built Up
CCM	Community Climate Model
CISL	Computational and Information System Laboratory
CLCV	Chinese Land Cover derived from Vegetation map
CLM	Community Land Model
Co	Control
Cr	Croplands
CS	Closed Shrublands
CVM	Cropland/Natural Vegetation Mosaics
DBF	Deciduous Broadleaf Forests
DJF	December January February

LIST OF ABBREVIATIONS (Continued)

DNF	Deciduous Needleleaf Forests
EASM	East Asian Summer Monsoon Simulation
EBF	Evergreen Broadleaf Forests
ECMWF	European Centre for Medium-Range Weather Forecasts
ENF	Evergreen Needleleaf Forests
FAO	United Nations Food and Agriculture Organisation
FNL	Final Analysis
G	Ground Heat flux
GCM	General Circulation Model
GIS	Geographic Information System
GLACE	Global Land-Atmosphere Coupling Experiment
GPCP	Global Precipitation Climatology Project
Gr	Grasslands
GVF	Vegetation Greenness Fraction
HCA	Hydrologic Characteristics Analysis
IBIS	Integrated Biosphere Simulator
ICTP	International Center for Theoretical Physics
IGBP	International Geosphere-Biosphere Programme
ISA	Impervious Surface Area
ISBA	Soil Biosphere and Atmosphere
ITD	Inter-Tropical Discontinuity
JAS	July August September

LIST OF ABBREVIATIONS (Continued)

LAI	Leaf Area Index
LBC	Lower Boundary Condition
LC	Land Cover
LCC	Land Cover Change
LCCS	Land Cover Classification System
LCP	Land Cover Parameters
LH	Latent Heat flux
LSM	Land Surface Model
LU	Land Use
LUCID	Land Use and Climate, IDentification of robust impacts project
LULC	Land Use And Land Cover
LULCC	Land Use And Land Cover Change
MF	Mixed Forests
MODIS	Moderate Resolution Imaging Spectroradiometer
MYNN2.5	Mellor-Yamada Nakanishi and Niino Level 2.5
NCAR	National Center for Atmospheric Research
NCEP	National Centers for Environmental Protection
NCL	NCAR Command Language
NETW	North East Trade Wind
Noah-MP	Noah-Multi-Parameterisation
NSE	Nash-Sutcliffe Efficiency
NWM	Numerical Weather Models

LIST OF ABBREVIATIONS (Continued)

OS	Open Shrublands
PA	Partial Afforest
PAR	Photosynthetically Active Radiation
PBL	Planetary Boundary Layer
PD	Partial Deforest
PFT	Plant Functional Type
PSI	Permanent Snow and Ice
PW	Permanent Wetlands
RAMS	Regional Atmospheric Modeling System
RCM	Regional Climate Model
RDA	Research Data Archive
RegCM3	Regional Climate Model Version 3
RMSE	Root Mean Square Error
RRTMG	Rapid Radiative Transfer Model
RS	Remote Sensing
RUC	Rapid Update Cycle
Sa	Savannas
SH	Sensible Heat flux
SRRB	Sokoto Rima River Basin
SSiB	Simplified Simple Biosphere
STD	Soil Thermal Diffusion
SWAT	Soil and Water Assessment Tool

LIST OF ABBREVIATIONS (Continued)

SWTW	South West Trade Wind
TA	Total Afforest
TD	Total Deforest
THMB	Terrestrial Hydrology Model with Biogeochemistry
TRIP	Total Runoff Integrating Pathway
TRMM	Tropical Rainfall Measurement Mission
UBL	Urban and Built-up Lands
UHI	Urban Heat Island
UMD	University of Maryland
USGS	United States Geological Survey
VAPOUR	Visualization and Analysis Platform for Ocean, Atmosphere, and Solar Researchers
WA	West Africa
WAM	West African monsoon
WB	Water Bodies
WHC	Water Holding Capacity
WPS	WRF Preprocessing System
WRF	Weather Research and Forecasting
WRF-DA	WRF Data Assimilation
WS	Woody Savannas

CHAPTER ONE

INTRODUCTION

1.1 Background

The terms Land Use (LU) and Land Cover (LC) tend to be used in exchange for each other, although they have little differences. Land cover (LC) is the material (like vegetation, bare ground, asphalt e.t.c) physically covering the surface. Land use (LU) refers to how land is used by humans. Land use and land cover change (LULCC) is a main driving force of regional and global climate change (Vitousek *et al*., 1997; Feddema *et al.,* 2005; Foley *et al.,* 2005). It plays a crucial role in water and energy balance between the land and the atmosphere. For instance, land cover change (LCC) alters the albedo, surface roughness, soil water and thermal characteristics, which in turn have effects on climate parameters. For centuries, humans have changed the global environment. Ramankutty and Foley (1999) noted that approximately 12 million km^2 of forests and woodlands have been removed globally since 1700AD. The impacts of this have escalated over the modern decades as a result of increase in population and industrial activity (Trail *et al*., 2013). Owing to the combined effects of natural climate variability, overgrazing, land reclamation for cultivation, deforestation, and other human activities, there has been a notable change in the land cover and this has further influenced the natural environment, climate variability and extreme weather events (Li and Ding, 2004).

The sub-Saharan West African environment has been subjected to a sequence of disruptions as a result of land degradation over the last three decades (Brink and Eva, 2009) which are manifested in changes of the natural vegetation cover, where agricultural

expansion and other human activities are degrading natural vegetation cover. Studies by Chase *et al*. (1996), Zhou *et al*. (2003), Georgescu *et al*. (2009), Ge *et al*. (2014), Kumar *et al*. (2014) and Zhou *et al*. (2015) have all demonstrated that regional climate can be very sensitive to even small changes in land surface properties. According to Mkaya, (2013), the conversion of forestland to agricultural land and urban settlement always increases soil erosion, and volume of storm runoff in a catchment. For example, deforestation, subdivision of land to small units and urbanization have all significantly changed the seasonality and magnitude of discharge, and annual distribution of stream flows (Karanja *et al*., 1986; Donner, 2004; Mustafa *et al*., 2005).

Some researchers in this field use more complex land models that account for LULCC induced changes in albedo, Bowen ratio, and surface roughness (Xue and Shukla, 1993; Taylor *et al*., 2002; Hagos *et al*., 2014) together with feedback due to vegetation dynamics (Zeng *et al*., 1999; Wang and Eltahir, 2000a, b). Taylor et al. (2002) used a land use model to generate land use change scenarios for the Sahel between 1960 and 2015 that were implemented in a General Circulation Model (GCM) to quantify the impact of land use change and found a small magnitude of precipitation decrease. However, as a result of lack of large scale observation before the satellite era, knowledge of how and by how much the land cover in West Africa might have changed before and after the onset of the late twentieth century drought remain largely unknown, and are subjective to a high degree of uncertainty (Gornitz 1985; Fuller and Ottke 2002; Xue *et al*. 2004a).

Charney, (1975), Zeng *et al*. (1999) and Wang and Eltahir (2000a) have all maintained that the Sahelian drought, which has been constant since the 1960's, could to

some extent be regarded as being caused by vegetation changes. Impacts of land use and climate changes could have instantaneous and gradual effects on terrestrial hydrology and thereby make alterations to the balance between rainfall and evapotranspiration and the resultant run-off. Land use change could disrupt the hydrological cycle either through increasing the water yield or by reducing or at times completely removing the low flow (Bruijnzeel, 1990; Pereira, 1992; Croke *et al*., 2004), and the reductions in evapotranspiration and water recycling as a result of changes in LULC could trigger a feedback mechanism in which the consequence is reduced rainfall (Savenije, 1995).

Looking into the effect of the interaction between the land surface and the atmosphere in a region like West Africa (a climatically consequential region in the world) is bound to improve the future climate change projections as there will be more understanding on the behavior of the models and the associated uncertainties. Comprehending the impact of LULCC and its interaction with the atmosphere by means of modeling and its impact on some meteorological, biogeophisical and hydrometeorological variables is an interesting area both for present and future research in regards to climate change projections. Hydrometeorological variables includes, precipitation, evapotranspiration, air temperature, dew-point temperature, atmospheric pressure, humidity, solar radiation, albedo, streamflow, water levels, wind speed and direction, horizontal visibility, soil moisture content, lightning, soil types, vegetation cover, water infiltration, soil moisture e. t. c. The United Nations Food and Agriculture Organisation (FAO) suggested that 9% of forest have been lost within 1990-2005. However, ability to find out the effect of the past and future land use change is significant in the world of modeling, and this can be well achieved by understanding if models can

precisely delineate changes that occurred in climate as a result of land use land cover change.

1.2 Statement of Problem

Rapid population growth and high level of poverty in Sub-Sahara Africa have led to increased agricultural expansion into forests and high reliance on natural resources for subsistence and income; completely leading to more and more deforested areas (WFSE Working Group, 2009). Substantial percentage of poor families in Sub-Sahara Africa, for instance, get their energy requirements from charcoal and wood fuel which are sourced directly from the forest, and these still goes on in most parts of the region. Poor governance in most of the countries of the Sub-Sahara Africa is also not helping matters in this regards as corruption, poor policies and lack of will to enforce the laws that has to do with forest regulation and protection still persist in the region till date and have made the LULC to keep changing without check.

Semazzi and Song (2001) estimated that as much as 80% of African countries either suffer from deforestation or desertification. Remarkable population increase, migration, and accelerated socio-economic activities have intensified these environmental changes over the last several centuries as the impacts of these changes on the climate are prevalent in local, regional, and global trends in modern atmospheric temperature records and other relevant climatic indicators **(**Mahmood *et al.,* 2009**)**. Herein lies a consequence; greater land use change to support agricultural land (i.e. through removal of tropical forest and Savannah) leads to undesirable change to the climate variables, which it is relying on presently. LULCC exposes the soil and lead to soil erosion, and could also close up the soil and reduce infiltration thereby encouraging more run off and flooding.

However, studies have revealed that there are still some uncertainties in the research on the effect of LULCC on hydrometeorological variables. Previous studies on this topic over West Africa have all used idealized land use data from the default data in respective models, but in this research, an updated satellite data was incorporated into the model for a better representation of the land surface parameters and a more realistic scenarios. This research improves on the model configuration by carrying out a sensitivity study to check the suitability of the four most recent Weather Research and Forecasting (WRF) land surface schemes in representing the prevailing physical phenomenon and land surface properties over the region, and also the suitability of the available in-build WRF land cover data and an external remote sensing data in simulating the prevailing situation over West Africa.

LULCC could lead to series of interconnected issues from discomfort through increase in temperature to severe health challenges. It is an important characteristic in the runoff process that affects infiltration, interception, erosion, and evapotranspiration. Also, changes and agricultural demands of irrigation water, cattle feeding, all constitute pressure on water availability and quality. This also can result in alteration of stream patterns, altered pattern of global atmospheric circulation in the long run, and long term extinction of species. The Sokoto Rima River Basin (SRRB) is highly prone to those changes imposing impact on hydrological processes and resulting in degradation of raw water in the reservoir. Because of the semi-arid nature of most parts of the catchment, it suffered heavily during the 1970's and the 80's Sahelian drought. The catchment is also facing high erosion by the effects of intense rainfall between July and September each year, which also aggravates the land cover change of the catchment. Continuous change

in land cover has the potential to affect the water balance of the catchment by changing the size and pattern of the components of stream flow, which includes surface runoff, and ground water flow. Hence, there is a need to undertake a research with a tool that takes both the land surface and the atmospheric component of the area into consideration in assessing the effects of land cover changes on the response of hydrometeorological parameter in the catchment.

1.3 Research Aim and Objectives

The aim of this research is to simulate the impact of land use land cover change on hydrometeorological parameters of West Africa.

The specific objectives are to:

i. analyse the land use land cover change over West Africa;
ii. evaluate the performance of four WRF land surface schemes to simulate some hydrometeorological parameters in West Africa;
iii. assess the impact of land use land cover change on the WRF outputs over West Africa;
iv. examine the response of the hydro-meteorological parameters to different land cover scenarios in West Africa.

1.4 Justification of the Study

Land use land cover changes attributable to urbanization and agricultural practices have affected the physical and biological properties of the earth's surface. Such effects change the radiative forcing and have a potential impact on regional and global climate (IPCC, 2001). However, the study of LULCC impacts on hydrometeorological variables has been one area that is sparsely carried out in West Africa. This could be because, high-

quality hydrometeorological data are very scarce over the region (Jones *et al*., 2015). Snce the practice of agriculture also entails deforestation, the question is how has land cover changed over the years, and how has it affected some hydrometeorological variables over the region? Another important question is that what will be the future situation if deforestation is not checked, and if afforestation is greatly practiced. Do integration of remotely sensed land cover data into the models produce improved simulations of the hydrometeorological variables?

For now, land surface model sensitivities to different land cover data will be explored and an appropriate parameterization scheme that is suitable for the West African domain for land surface modeling studies will be sought for. Gong and Eltahir, (1996) have pointed out that local convective vapor accounts for about 27% of the annual precipitation in West Africa, and can be described as a major source of moisture in West Africa. This shows that the terrestrial hydrology and land cover changes play a very important role on the local climates. Therefore, it is clear that comprehending the impact of LULCC effect on the hydrometeorological parameters of West Africa and also, streamflow in the Sokoto Rima River Basin (SRRB) are important step to prudent water resources management within the region. Also, the existence of a basin especially in a Sudano-Sahelian environment is sure to increase livelihood, assure food security, reduce hunger, improve production and provide job for the people around and beyond. However, assessments of the existing and future land use (LU) changes on hydrometeorology are absolutely necessary in land use planning, which is a sine qua non for a beneficial water resources management. Hence, it is justified to carryout this research in other to find out how LULCC affects the hydrometeorological parameters of West Africa.

1.5 Scope of the Study

This study is designed to study the LULCC over West Africa (WA), and select the best performing Land Surface Model (LSM) in WRF model for WA. The research use the ensemble of the best LSM, WRF and WRF-hydrological model to study the impact of LULCC on some hydrometeorological parameters over the entire West African region and finally over the SRRB in WA.

CHAPTER TWO

LITERATURE REVIEW

2.1 Hydrometeoroloical Variables in West Africa

Hydrometeorology is an interdisciplinary field of research that marries knowledge from two well-expanded disciplines, which includes meteorology and hydrology in other to study the transfer and exchange of water and energy between land and the lower atmosphere. The scope of hydrometeorology research is clearly interdisciplinary and includes analysis of the space-time properties of proxy parameters such as precipitation, maximum precipitation amount, minimum and maximum temperatures and their influence on river systems and dams (Botai *et al*., 2015). In this regard, this field of research is concerned with a broad understanding of the complex interactions between weather and the water resources of the earth (Mora *et al*., 2004).

Figure 2.1 represents a simplified process of water transfer between the land, oceans and the atmosphere. The real hydrological process is, nevertheless, very complex and needs an exhaustive understanding of how each process interacts with the other, energy transformation between the different water phases (e.g., solid, liquid and gas), movement and distribution of water on Earth and consequently their effects on water resources (Kinter and Shuka, 1999).

There are various hydro-meteorological products like Precipitation (which include rainfall in liquid form or snow, sleet, and hail in solid form), evapotranspiration, temperature, atmospheric pressure, humidity, solar radiation, stream flow, water levels (surface and groundwater), wind speed and direction, horizontal visibility, soil moisture content, lightning, vegetation cover, etc. These form the basis for knowledge, decision

making and actions in fields such as water management, agriculture, energy, aviation, transport, risk management, etc. Precipitation data are the most important data used in hydro-meteorological analysis as it forms the bedrock for runoff generated in basins and sub-basins. Evaporation is one of the primary inputs to catchment rainfall runoff models and is consequently used to deduce water losses from wetlands, reservoirs, and aquifers and the water requirements of crops under irrigation (Botai *et al*., 2015). However, water resources, particularly in arid and semi-arid regions of the world, (which the Sokoto Rima River Basin is an example of such) are of great concern, as they are closely linked to the wellbeing of humankind (Botai *et al*., 2015).

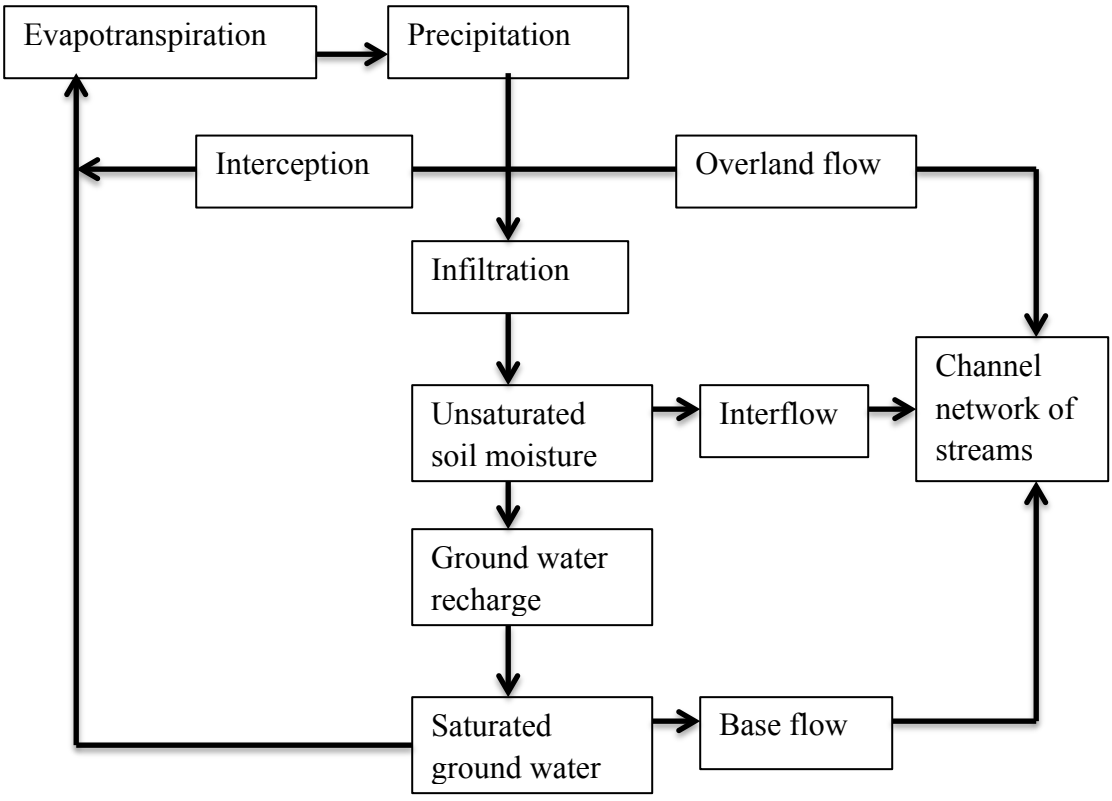

Figure 2.1: Schematic Representation of Hydrologic Cycle. Adapted from Domenico and Schwartz, (1990).

West Africa is a region for which high-quality hydrometeorological measurements are very scarce (Jones *et al*., 2015), and according to Ndehedehe (2019), lack of sufficient in-situ data for the parameterizations and adequate initialization of outputs from hydrological models and reanalysis data for hydrological applications results in poor representation of the West African land surface and hydrological state variables. Observational hydro-meteorological data are however needed for a better scientific understanding of hydrological processes and their interactions with the atmosphere and the biosphere, and it also form the basis for the development of reliable modeling approaches for climate change analyses, as well as for determining the impact of land cover changes in hydrology and other disciplines.

According to Ouedraogo *et al*., (2009) and Knauer *et al*., (2017), a lot of regions in West Africa are marked by significant LC changes due to an extensive conversion of savanna and other ecosystems into agricultural land. This is expected to continue in the future, and LC change analysis is the basis for the development of sustainable land management practices that strengthen the resilience of socio-ecological systems against climate extremes, and improve food security (Bliefernicht *et al*., 2018). Moreover, substantial biosphere–precipitation feedbacks have been detected for the West African savanna (Klein *et al*., 2016). This was found to be linked to their transitional character between energy and water limitation (Green *et al*., 2017), rendering them particularly sensitive to land use changes.

2.2 Deforestation and Forest Degradation

Africa, particularly the Sub-Sahara Africa, has been identified as cheif player in the global carbon dynamics (Houghton and Hackler, 2006) with forest cover in the humid

and sub-humid part of the region spanning about 366 million hectares (Vågen et al., 2005). The various forests and woodlands in Africa apart from sustaining a huge amount of biodiversity and protecting water sources, also store huge quantity of carbon (WFSE Working Group, 2009). Congo DR; Madagascar; South Africa and Tanzania are listed among seventeen (17) most ecologically diverse countries on earth (WFSE Working Group, 2009; mongabay.com). Furthermore, the Congo Basin is only second to the Brazilian Amazon tropical rainforest in its large and continuous stretch containing more than two-thirds of Africa's biodiversity (WFSE Working Group, 2009). Central African forests alone have the capacity to mitigate against the current international human emissions of CO_2 for a period of four (4) years due to its large storage of carbon (25-30 billion tonnes) (WFSE Working Group, 2009). The forests, apart from sequestering carbon, also deliver vital ecosystem goods and services, which include food, maintenance of clean and healthy watersheds water, housing, cycling of nutrients and biodiversity preservation (Morales-Hidalgo *et al*., 2015). Notwithstanding these critical roles that forests play, deforestation is accelerating in Sub-Sahara Africa and even the entire Africa continent resulting in diminished ecosystem's resilience. Soil degradation, permanent loss of species, global warming and climate change are the environmental degradation resulting from loss of forest cover (Malick and Inoussa, 2009).

2.2.1 Causes and Drivers of Deforestation

Different sectors have various contributing factors driving deforestation (Mahapatra and Kant, 2003), and in consequence, impacts of deforestation differ across the global, national and local boundaries. These factors generally are either due to natural or anthropogenic activities. Human needs and activities have been the greatest drivers

and causes of deforestation going by the increased recognition of their footprints on the earth system (Olorunfemi *et al*., 2018). It is important to note the human drivers of environmental change (deforestation) differ in nature and scope but generally be grouped together as economic, conflict and governance, demographic, social and science and technology (UNEP, 2006). An important demographic factor leading to LUC is migration (Angelsen and Kaimowitz, 1999; Matthews, 2001) as some policies leading to LUC could either instigate (Indian *et al*., 2001) or are intricately connected with migration increase (Fearnside, 1997).

In other to develop appropriate policies and measures for the changing of the current trends of deforestation, forest degradation and the consequent global warming and climate change, thereby promoting a favourable outcome for ecological diversity and human welfare, we must fully understand the core drivers/causes of these changes (theredesk.org). Globally, four-fifths of deforestation is approximately linked to agriculture while 70% of the entire forest degredation comes from commercial timber extraction and logging activities most especially in Latin America and Sub-tropical part of Asia (Kissinger *et al*., 2012). Industrial activities are the major drivers of deforestation and degradation of forest globally, while subsistence farming and wood extraction for fuel causes considerable deforestation most especially in Africa (www.mongabay.com). Greater and faster decline of tropical forest in emerging economies as a result of industrialization is expected within decades (Laurence and Bierregaard, 1997; Laurence, 2007).

In Sub-Saharan Africa, more than two thirds of the population depends on forests and woodlands for survival and an estimated 20% of the daily income of poor families come from forest (World Bank, 2017). Forest area survey in Ghana between 2004 and 2008, showed that the pay revenue or incomes by persons engaged in the chainsaw timber production process ranged from less than 5,000 to 50,000 Ghanian Cedi (Obiri and Damnyag, 2011). Rapid population growth and high level of poverty in Sub-Sahara Africa has led to increased agricultural expansion into forests and high reliance on natural resources for subsistence and income completely leading to more and more deforested areas (WFSE Working Group, 2009). Most forest degradation in Sub-Sahara Africa are a result of collection of wood for fuel, activities of charcoal merchants, and livestock grazing to a lesser extent (Kissinger *et al*., 2012) and population pressure. Ninety (90) percent of poor families in Sub-Sahara Africa, for instance, get their energy requirements from charcoal and wood fuel (UNEP, 2006). In addition, corruption, inadequate governance, poor policies and political uncertainty (Geist and Lambin, 2001), low capacity of public forestry agencies, uncertainties in land tenure system, and lack of planning and monitoring of natural resources (Rademaekers *et al*., 2010) are fundamental factors influencing deforestation and forest degradation.

Fallow system of farming, activities of legal and illegal loggers, oil exploration and mining companies are also one of the feasible causes of deforestation. Environmental changes caused by deforestation and forest degradation are big threats to biodiversity. Loss of biodiversity, species annihilations and fast-tracked emissions of carbon into the atmosphere due to continuous loss of native forest in tropical countries have been reported (Laurance, 2007). In view of the above, making a living outside the forest by

reducing the demands of forest-based commodities, sustainable use of current agricultural lands and expansion of croplands into grassland rather than forests will bring favourable outcome (Boucher *et al*., 2011).

2.2.2 Rates of Deforestation

In 1990s, global forest cover stood at 4123 billion ha, 4033 billion ha in 2005 (FAO, 2010), while in 2015, forest cover had reduced to 3999 billion ha recording a 3% loss in the global forest cover between 1990 and 2015 (Keenan *et al*., 2015; Han *et al*., 2017). A record of 29.7 million ha of tree cover loss was recorded in 2016 according to the Global Forest Watch. Currently, forest occupies 31% of the earth surface (Han et al., 2017). In Tropical Africa, fast decline of tropical forests concentrated in the west and central part of the continent has been reported. During the 80s, the highest rate of deforestation was recorded in Africa than any other region, a trend that persisted from 1990-1995 (www.mongabay.com). Between 1990 and 2010, Africa and South America continue to have the highest net loss of forest cover (FAO, 2010) (Figure 2.2). The mean annual deforestation rate of 0.8% in Sub-Sahara Africa was far more than the global average rate of 0.15% between 1990 and 2010 (FAO, 2010). In Africa, Nigeria and Sudan has the highest deforestation rates during the 2001-2005 period mainly as a result of small scale activities. Currently, Nigeria is losing her forest at an alarming rate of 3.5% amounting to 350, 000 to 400, 000 ha annually (FAO, 2015) as shown in Figure 2.2. With a loss of 47% (about 8, 193,000 ha) of its forest cover between 1990 and 2010, Nigerian forest cover now stands at 9.9% (about 9, 041, 000 ha) of its land area (FAO, 2010; mongabay.com). This is far below the recommendation of 25% national minimum forest

cover by Food and Agriculture Organisation of the United Nations (FAO) (Ojekunle, 2014).

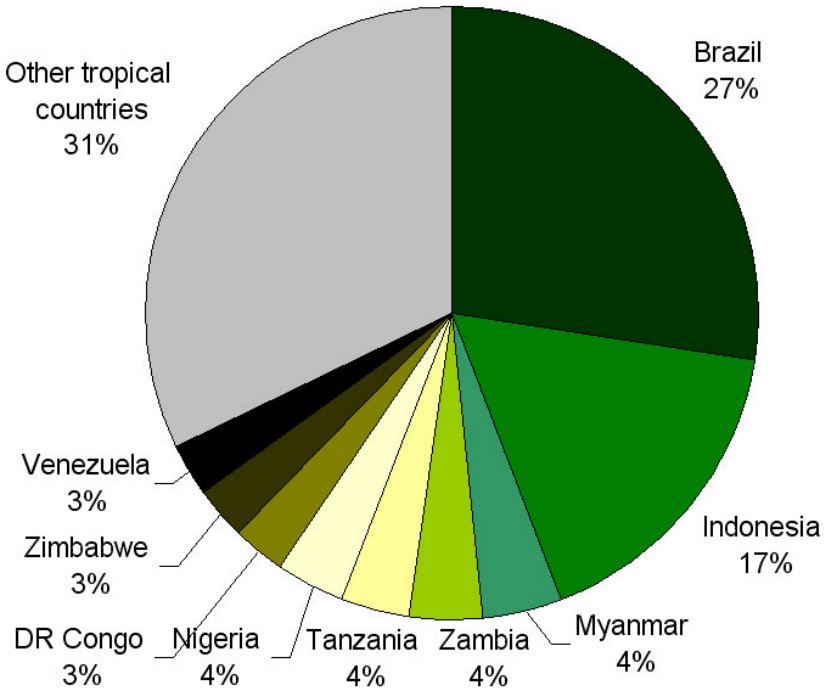

Figure 2.2: Share of Tropical Deforestation, 2000-2005.
(Source: mongabay.com, using FAO data).

2.3 Land Use Land Cover Changes in Sub-Sahara Africa: the Drivers

According to Mengistu, (2008), most human activities take place on land and many materials for such human activities come from it. These anthropogenic activities are the main cause of Land Use Land Cover Change (LULCC) (Weng, 2001). Land use Land Cover (LULC) consist of two separate concepts, which are often, used interchangeably (Rawat and Kumar, 2015). Land Use (LU) is any human purpose or intents applied to a specific portion of land initiated to cause an alteration or maintain it (FAO/UNEP, 1999) while Land Cover (LC) is the biological and physical state of the Earth's surface and the sub-surface immediately below it (He *et al*., 2002). Land use and

land cover changes may be categorized into conversion and modification. Conversion involve changing one land use or cover to another, while modification refers to the conversion of the wide-ranging land use or cover type regardless of changes in its features. LULCC has become one of the key elements in global environmental change and sustainable development (Zheng *et al*., 2015) due to its pervasiveness on the local scale and its globally recognized environmental trend. Researchers, planners, and policy makers utilize LULC information in evaluating urban growth patterns and determining changes in natural resources (Adeel, 2010) as the design of an effective land management programs requires proper knowledge of LULCC.

Land covers in Sub-Sahara Africa have undergone rapid transformation in the last century, which is mostly due to the increasing population being experienced in Africa. Currently, about 60% of Africans are rural dwellers, exerting considerable pressure on the environment thereby leading to loss of forests and forest resources (Pellikka *et al*., 2009). Also, Sub-Sahara Africa is the only major region globally where the population of rural dwellers is projected to increase until the 2040s (WFSE Working Group, 2009).

Furthermore, 16% of Africa's forest and 5% of its woodlands and grasslands were converted to other land uses at a rate of 5 million ha per year between 1975 and 2000 with West Africa witnessing the greatest change (Eva *et al*., 2006). Thus, Agricultural land witnessed 57% growth between 1975 and 2000 having increased from 215 million ha to 338 million ha at an annual rate of 2.3% (Eva *et al*., 2006). Additionally, 10% of the total forestland (approximately 75 million ha) in Africa was lost majorly due to subsistence and commercial agriculture between 1990 and 2010 (FAO, 2016). Rapidly increasing agricultural activities and urbanization brought about by soaring population

have led to significant changes in LULC and greater demands on natural resources lodged in the land (Hegazy and Kaloop, 2015). Precisely, rapid population growth, demographic pressure, agricultural expansion, and collection of fuelwood and charcoal are the drivers of land use change in Sub-Sahara Africa.

2.4 General Land-Atmosphere Interaction and Review over West Africa

The land surface and the overlying atmosphere are tightly coupled systems. The planetary boundary layer (layer where intense turbulence takes place) is the interface that regulates the feedbacks. Despite the significant influence of land-atmosphere exchange on the daytime Planetary Boundary Layer (PBL), uncertainty remains in the parameterization of surface heat and moisture fluxes in numerical weather models (Trier *et al*., 2010a, b). The LSM in WRF provides heat and moisture fluxes over land to provide a lower boundary condition for vertical transport in the PBL scheme. These fluxes of sensible heat and latent energy are dependent on the surface meteorology, radiative forcing, soil properties and land use type. Thus, an accurate description of the land surface and vegetation characteristics is needed in any numerical weather prediction model (Wharton *et al*., 2013). The Surface energy exchange is determined by the terrestrial radiation budget, as shown in equation 2.1,

$$R_{net} = SH + LH + G \quad (2.1)$$

where R_{net} is the net radiation flux (W m^{-2}),

SH is the sensible heat flux (W m^{-2}),

LH is the latent heat flux (W m^{-2}) and

G is the ground heat flux (W m^{-2}).

The surface available fluxes (i.e. SH and LH) is net radiation minus ground heat flux. The net radiation is balanced by outgoing fluxes of LH, SH, and G, whose partitioning strongly depends on the prevailing surface conditions. Some energy is absorbed by the ground G, this is in fact much lower than average value of LH and SH for most plant canopies, as most part of available energy will be transferred back into the atmosphere as sensible and latent heat (Betts *et al*., 1996). LH is the quantity of heat absorbed or released by water undergoing a change of state. LH is most often the heat released by water as it changes from a liquid to gaseous state over a plant canopy through evapotranspiration.

However, the exact magnitudes of SH, LH, G are dependent on many variables, including the amount of incoming radiation, soil moisture availability (the most crucial), groundwater availability and plant access, soil properties, canopy properties (e.g. albedo, biomass density, leaf area index, rooting depth, species), temperature, and entrainment of dry air into the boundary layer from the free atmosphere. The ratio of sensible heat to latent energy transfer is called the Bowen ratio and is usually expressed as a midday average. A higher Bowen ratio shows that a larger portion of available energy is partitioned into sensible heat than latent heat. Therefore, one would expect a high Bowen ratio over a desert and less Bowen ratio over tropical forest as the later has high evapotranspiration (Wharton *et al*., 2013). The partitioning of the energy available at the surface into latent and sensible heat depends crucially on the soil moisture as earlier mentioned. Vegetated surfaces have the ability to draw water from a depth of order 1 m (the root layer), while for bare ground only the water in the top few cm of soil contributes to evaporation.

In explaining the role of SH and LH in the atmosphere, sensible heat at the bottom means energy immediately available to the atmosphere, and contributes to the heating and/or deepening of the planetary boundary layer (BL), which is the shallow portion of the atmosphere directly affected by the surface. The surface evaporation flux does not directly heat the atmosphere, but provides moisture to the BL or, in the case of deep convection, to the whole troposphere. This contributes to precipitation generation mechanisms in favourable conditions, with the associated release of latent heat into the whole troposphere. However, LH is the key surface flux, which couples the surface to the atmosphere via the hydrological cycle (Boone *et al*. 2009a). For an entire atmospheric column, the net radiative cooling is balanced by energy involved in phase changes inside the column (condensation of water vapour and evaporation of rain) and sensible heat flux at the surface. Land surface processes affect directly or indirectly this balance.

One of the ways in which the land surface affects the climate system is the fact that due to the direct contact of the land surface with the atmosphere, the land surface reacts as a source and sink of heat and moisture through the sensible heat flux and evaporation. The surface conditions regulate the important feedback cycles in the climate system (Viterbo, 2002). Also, the partitioning of the surface net radiation into sensible and latent heat fluxes determines the soil wetness development. The surface energy fluxes to a large extent, control the surface weather parameters like the temperature, humidity and wind speed and to a lesser extent, low-level cloudiness and precipitation (Viterbo, 2002). According to Tiwari *et al. (2015),* as the surface and the atmosphere affect prognostic variables such as surface temperature, precipitation, etc., it is significant to have a better representation of surface boundary conditions in a model.

According to Zheng and Eltahir (1998), vegetation cover and soil moisture content play a comparable role in the concept of land–atmosphere interactions. The main difference is that soil moisture anomaly patterns could last for many days to weeks, while vegetation is capable of mobilizing the root zone soil moisture that would otherwise not be in contact with the atmosphere. It therefore imposes a lower boundary condition on the atmosphere that is effective over much longer time scales and moreover reacts much slower on single precipitation events than surface soil moisture. Taylor (2008) propose that such slow intra-seasonal modulations could be more important in the densely vegetated southern regions of West Africa as opposed to the barren Sahel, where the main response in latent heat fluxes is within a few days.

The atmosphere–land surface interactions are modulated by the magnitude of the associated north–south gradient of heat and moisture in the lower atmosphere (Eltahir and Gong, 1996). A number of regions in the world, such as the Sahel (Koster et al., 2004; Xue *et al*., 2004a), Amazon (Nobre *et al*., 2004), and Asian monsoon regions (Fu *et al*., 2004; Xue *et al*., 2004b), have been identified as hot spots of land–atmosphere interactions, where interactions through feedback loops play a critical role in the surface water and energy balances as well as regional climate. Numerous modeling studies have examined the influence of the land surface on the WAM in terms of surface albedo (e.g., Sud and Fennessy 1982; Laval and Picon 1986), the vegetation spatial distribution (e.g., Xue and Shukla, 1996; Li *et al*., 2007), and the soil moisture (e.g., Walker and Rowntree, 1977; Cunnington and Rowntree, 1986; Douville *et al*., 2001). However, explanation of the results, from any one of such studies, ought to be tempered by the fact that there are considerable discrepancies in African land–atmosphere coupling strength among current

state-of-the-art GCMs (Koster et al., 2002). Studies have demonstrated that land surface processes play a crucial role in the climate system (Li *et a*l., 2015). In regions where the land–atmosphere coupling is strong, land surface processes, such as soil-precipitation feedback (Schär *et al*., 1999; Koster *et al*., 2004; Sörensson *et al*., 2010), soil moisture initial conditions (Sörensson et al., 2010; Sato and Xue, 2013) and vegetation feedbacks (Xue et al., 2010a; Lu and Kueppers, 2012), have significant impacts on the dynamic downscaling of Regional Climate Models (RCMs).

The land surface has been shown to be an important factor in modulating the West African monsoon (WAM) (Boone *et al*., 2016). For example, based on observations, the land surface characteristics and processes have been shown to have a significant impact on the inter-annual variability of rainfall in the Sahel region (Nicholson, 2013). The importance of surface-atmosphere interactions was one of the main tenets of the recent international African Monsoon Multidisciplinary Analysis (AMMA) project (Redelsperger *et al*., 2006) which was later investigated in several studies. According to Dirmeyer (2011), the WA region typically appears as one where the soil moisture feedbacks with the atmosphere are among the strongest over the globe. The Sahel region has been identified as one of strong soil moisture-atmosphere coupling (Koster *et al*. 2004). Furthermore, it has been resolved to be the region of the world with the highest impact of biophysical processes on the climate (Xue *et al*., 2004a). As reviewed by Xue *et al*. (2012), studies like Steiner *et al*. (2009) and Lavender *et al*. (2010) have shown the importance of the land surface on modulating the WAM. For example, previous studies have examined the role of changes in the surface albedo (e.g. Charney, 1975; Sud and Fennessy, 1982; Laval and Picon, 1986) and the vegetation (e.g. Xue *et al*., 1990; Xue,

1997; Zheng and Eltahir, 1997; Li *et al*., 2007) on modulating the WAM. All of these studies lead to the general conclusion that reduced vegetation leads to reduced rainfall.

2.5 Modeling and the Impacts of Land Use Land Cover Change

Land Use modeling have attracted the interest of many researchers, namely, those who try to model spatio-temporal patterns of Land Use Change (LUC), those who want to understand the drivers and impact/consequence of LULCC (Veldkamp and Verburg, 2004). Models have become a great tool to study the past, present and forecast the future effects of LULCC on the environment including weather, climate and water resources. However, changes in vegetation (the major LULC variable) can have a noticeable effect on the local, regional and indeed global mean climate along with climatic extremes and variability (Charney *et al*., 1977; McGuffie *et al*., 1995; Zhang *et al*., 1996; Zeng and Neelin, 1999; Clark *et al*., 2001; Semazzi and Song, 2001; Pielke, 2001; Legesse *et al.,* 2003; Xue *et al*., 2010b; MacKeller *et al*., 2010; Swann *et al*., 2012). In the tropics where West Africa situates, interaction of the atmosphere with the land surface are supposed to have a high effect on the climate as a result of the high net radiation and moisture which in turn, generates high evaporation rates. Researchers like Clark and Arrit (1995) and Xue *et al*. (1996) have stressed that proper understanding and parameterization of the land surface atmosphere interactions is most important for the forecast of accurate rainfall amounts.

Alterations in the land surface characteristics affect the surface water balance; change in the nature of vegetation affects interception and transpiration; change in the distribution of vegetation alters the balance between fluxes from the soil and those from canopy processes; and changes in evapotranspiration, soil evaporation, re-evaporation of

intercepted water, etc. affect runoff and soil moisture content (Pitman, 2003). Thereafter, other processes are affected by means of the connection with surface energy balance. Vegetation store and transmits water, also absorbs radiation and plays a great part in the regional water and energy balance in which depending on the vegetation type in the canopy, interception and storage of rainfall happens in differing amounts. For example, shorter vegetation reduces the surface roughness layer, also reducing surface eddy transport of water vapour, heat and momentum and also leads to less evaporation and higher surface temperature.

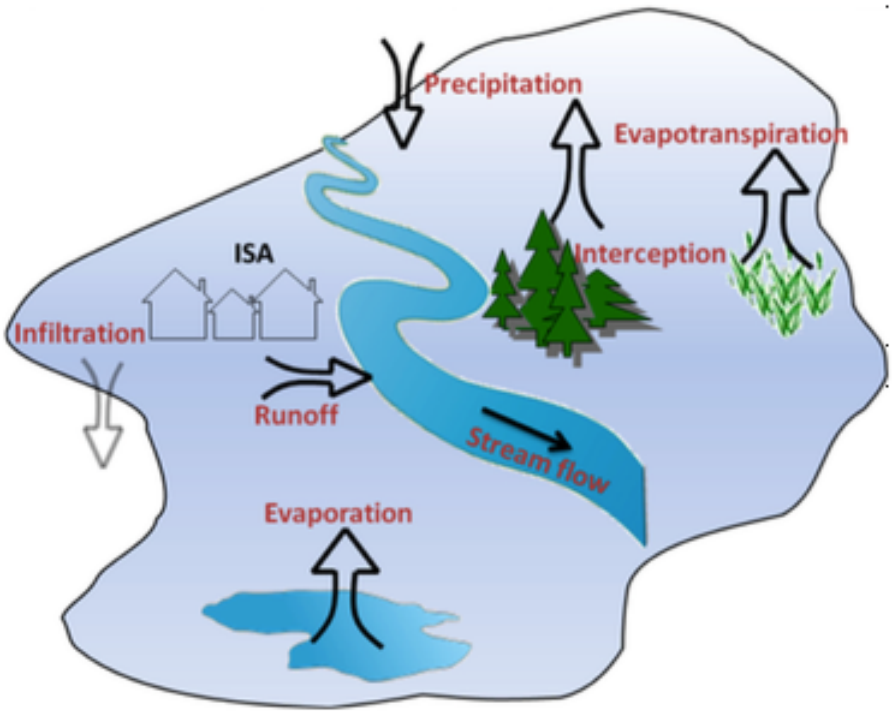

Figure 2.3: Typical Hydrologic Processes in the Urbanizing Environment. ISA means Impervious Surface Area (Source: Zhou, 2014)

Regarding the hydrologic implication of LULCC, according to Shuster et al. (2005) and Zhou and Wang (2008), Impervious Surface Area (ISA) of an urban

settlement is often used to study the environmental impact of urbanization. As shown in Figure 2.3, expansion of the ISA affects a series of hydrologic processes as it reduces infiltration, increases runoff, increases peak flow and duration, reduces baseflow, and raises sediment loading (Zhou, 2014), The impact of the expansion of ISA on the above listed hydrologic processes lead to environmental problems such as flooding, erosion, sedimentation, increased temperatures, habitat changes, and loss of fish populations. In spite of the fact that the magnitude of hydrologic change due to urbanization remarkably differ in many studies, increasing peak flow has been generally taken as the major hydrologic implication of urbanization (Zhou, 2014).

The best way to comprehend the impact of land cover change on variables and the complex nature of land surface-atmosphere interactions is by means of land use sensitivity studies. According to Koster, et al. (2006), the strength of the coupling is varied with individual models because of dissimilarity in the representation of biophysical processes. Koster *et al.* (2006) sought to understand the various land-atmosphere coupling strengths of about 12 weather and climate models in the Global Land-Atmosphere Coupling Experiment (GLACE) project and found out a wide variation in the strength of land–atmosphere coupling. They investigated the capacity of soil moisture to have an effect on precipitation in two stages, that is, its capacity to affect evaporation, and the capacity of evaporation to have an effect on precipitation. Koster *et al*. (2006) stressed that an evaporation rate that varies strongly and consistently with soil moisture tends to lead to a higher coupling strength. The first-stage differences reflect identifiable differences in model parameterization and model climate. Also, that the Inter-model differences in the connection between evaporation and precipitation, also play an

important role. From Koster *et al*., (2006), notable agreement between the 12 models in the coupling strength is presented as a hot spot which also exist over tropics in the precipitation and surface temperature fields, and this shows a good agreement between the models.

Researchers like Eltahir and Bras (1993), McGuffie et al. (1995) and Swann *et al*. (2012), have suggested that afforestation will result into an increase in precipitation. This might not be the same in every region with different tools and models as Xue *et al*. (1996) and some others have put forward that there is an increase in rainfall as a result of deforestation. Some studies also suggested that large scale afforestation would result into reduced surface temperatures, reduced evaporation and precipitation. The discrepancies in the studies on impact of LULC change could be attributed to the fact that simulations could be carried out with different spatial resolutions, different LULC data (which could be unrealistic), and different parameterization schemes. So, improvement in these could better the model outputs.

With a series of 10 deforestation experiments, Polcher (1995) found out that the increase in sensible heat flux leads to more deep convective activities thereby increasing rainfall. Reduction of evaporation generally accompanying deforestation decreases precipitation, and this is only of slight significance for the regional rainfall. Polcher (1995) also stressed that both increase and a decrease in rainfall due to deforestation can be possible depending on the change in type and spatial distribution of vegetation, and that this is region specific and could be attributed to the complexity of land surface-atmosphere interaction.

Zhang et al. (1996) examined the potential impacts of deforestation in the humid

tropics using the NCAR's CCM1 coupled with the Biosphere-Atmosphere Transfer Scheme package. They conclude that replacement of rainforest with tall grassland in tropical Africa results into a decrease in evapotranspiration by 7%, which amounts to a 62.6 mm/year loss of rainfall. Zhang et al. (1996) however found a seasonal variation with precipitation during the main rainy season, decreasing by 15-30 mm/month and increasing in March and April. Also, evapotranspiration shows the highest reduction in October-November and moisture convergence increased through February-April and weakened during August-October.

For Clark et al. (2001), a general circulation model was used to assess the impact of degradation (replacement of vegetation with shrubs and bare soil) of five regions within tropical Africa (i.e. areas between 0N-25N and 20W-50E). Using idealized degradation scenarios, they found that the impact of degradation varies between the regions. There was considerable reduction in precipitation over the degraded area of the Sahel (12°N-18°N) in West Africa. A reduction of rainfall 0.5-1 mm/day was prominent as a result of the general weakening of the circulation accompanied by a southward displacement of convection. Also, both surface evaporation and atmospheric moisture convergence are reduced. Clark *et al*. (2001) also stressed that degradation of a southern area close to the Gulf of Guinea has insignificant consequence on precipitation owing to the compensatory growth of moisture convergence.

All the past studies on LULC sensitivity studies over West Africa have used idealized land use data from the default data in respective models, but in this research, a satellite data (with is more or less an observation data) was incorporated into the model for a better representation of the land surface parameters and a little more realistic

scenarios. Some researchers like Miller *et al*. (2006), Liu *et al*. (2009), Sertel *et al*. (2011), Case *et al.* (2012), Zhao *et al*. (2012), Zhao *et al*. (2014), have replaced the land-use data in each respective models, by incorporating remote sensing data into the model for more updated and realistic LULC data which in a way improved the model outputs over their region of study.

2.6 Review on Land Surface Models over West Africa

Different climate variables are found to be sensitive to different physical parameterizations (Evans *et al*., 2012) making the need for an all-inclusive sensitivity analyses more pressing and the procedure of physics parameterization selection more demanding (Zittis *et al*., 2014). The land surface is the principal constituent located in the space separating the atmosphere and the lithosphere and it obviously impacts the exchanges of energy and moisture with the boundary layer. Through the controlling of the surface energy balance and water balance, land-surface processes strongly affect the weather and climate from local to regional and global scale (Zhao and Li, 2015). Land surface models (LSMs) differ in the number of soil and canopy layers and also in the treatment of vegetation-related processes, and hence are able to perform differently. Several sensitivity and evaluation studies have been carried out in different regions such as Miao *et al.*, 2007; Singh *et al.*, 2007; Jin *et al.,* 2010; Wharton *et al.,* 2013, etc. This is necessary in order to help firstly, the model developers for further improvements, secondly, the users in the selection of LSM options especially in the WRF model, and thirdly, improving the simulations for the area under study. Therefore, considering the number of LSMs currently in the WRF model, it remains a difficult task for researchers

to choose a suitable land surface scheme that fits their needs (Chen *et al*., 2012) especially over a data sparse region like West Africa.

Variations in surface conditions are shown to influence the position and intensity of the African Easterly Jet (AEJ) (Cook, 1999). The AMMA Land Surface Model Intercomparison Project (ALMIP) was conceived as a step towards a better understanding and description of surface processes over West Africa (Boone *et al*., 2009b). The first ALMIP phase included simulations with the land surface running in off-line or uncoupled (without atmospheric feedbacks) mode. The idea was to develop a forcing database with the best quality and highest spatial and temporal resolution data available and use this database to force state-of-the-art LSMs in order to better understand key processes at different scales (Ruti *et a*l., 2011). Regarding the LSMs, the AMMA results showed that they tend to underestimate surface sensible heat flux and possibly baseflow runoff and overestimate evaporation from the vegetation canopy. During the monsoon season, evapotranspiration is generally the most significant component of the water budget, acting to recycle much of the rainfall, in particular, over the Sahel. However, qualitative estimates of recycling by the LSMs must be interpreted in view of the fact that the LSMs have a large inter-model scatter over the Sahel.

Steiner et al. (2009) studied the Land surface coupling in regional climate simulations of the West African monsoon. They coupled the Community Land Model (CLM3) and the Biosphere Atmosphere Transfer Scheme (BATS) with to the International Center for Theoretical Physics ICTP Regional Climate Model Version 3 (RegCM3) and found out that CLM3 improves the timing of the monsoon advance and retreat across the Guinean Coast, and reduces a positive precipitation bias in the Sahel

and Northern Africa. This led to a higher simulated temperature, thereby reducing the negative temperature bias found in the Guinean Coast and Sahel in the BATS. Also, in BATS simulation, warmer temperatures in northern latitudes and wetter soils near the coast create excessively strong temperature and moist static energy gradients, which shifts the African Easterly Jet further north than observed. In the CLM3 simulation, the migration and position of the African Easterly Jet more closely match reanalysis winds. They also emphasized that the improvement in CLM3 is triggered by drier soil conditions in the simulation and an increase in evapotranspiration per unit precipitation.

In spite of the notable impact of the land-atmosphere exchange on the daytime planetary boundary layer, there are still some uncertainties in the parameterization of surface heat and moisture fluxes in numerical weather models (NWM) (Trier *et al*., 2010b). WRF has many LSM options that range from simple treatment of sub-surface processes like absence of vegetation or snow cover prediction to advanced physical models with sophisticated vegetation and soil models and snow cover prediction. Moreover, WRF LSMs use seasonally adjusted or annually fixed land-use properties read from look-up tables in order to allocate surface variables (albedo, emissivity, roughness length, vegetation fraction), yet some land cover parameters like vegetation can change often within a short time.

Researchers such as Evans *et al*. (2012) examined the performance of various physics scheme combinations on the simulation of a series of rainfall events near the southeast coast of Australia. They created a thirty-six member multi-physics ensemble such that each member had a unique set of physics parameterisations. They found out that no single ensemble member was found to perform best for all events, variables and

metrics, and this also reflects the fact that different climate variables are found to be sensitive to different physical parameterisations.

Hagos *et al*. (2014) compared the response of WRF LSMs to monsoon precipitation over West Africa. They compared Noah, SSIB and Pleim-Xui (PX) LSMs for the JJAS against three reference datasets, and found out that the models consistently differ from the references over the Gulf of Guinea, with the model apparently overestimating precipitation. They also revealed that the simulations differ in their northward incursion of precipitation over land as the 2–4 mm/day precipitation band reaches Lake Chad in the case of Noah LSM, a little to the south for SSIB and further north for Pleim-Xiu. That is to say, on average, the SSIB simulations are relatively dry and the Pleim-Xiu experiments are relatively wet in comparison to Noah LSM. Their analysis also showed that the African Easterly Jet (AEJ) position for the simulations with the NOAH land surface scheme is in best agreement with that of ERA-Interim, while it is too far south for SSIB and too far north for Pleim-Xiu. They proposed that simulations that are climatologically too dry or too wet compared to observations and reanalyses have weak response to land use change because they are in moisture or energy limited regimes respectively. Also that the evaporation from soils that are close to saturation or close to the wilting point does not vary significantly, even under land use change conditions.

Wharton *et al*. (2013) used WRF model to investigate the impact of land surface model (LSM) physics on the simulated surface energy balance and the near surface wind profile, including heights reached by a modern wind turbine in Oklahoma. They tested 10 common LSM configurations in WRF including Noah scheme, Noah-multi-parameterisation (Noah-MP) scheme, Simplified Simple Biosphere (SSiB), Pleim-Xiu

(PX), Rapid Update Cycle (RUC), and others. WRF model was simulated for four, 2-week periods covering different canopy, surface meteorology and soil moisture conditions. They found that LSM performances varied by simulation period and errors were greatest during periods with high soil moisture and live crop cover, indicating highest LSM sensitivity when PBL behaviour is most coupled to land-atmosphere exchange. Higher wind speed errors also occurred at night during the spring, possibly from some difficulty with simulating nocturnal low-level jets. They also found that the choice of land-surface model led to about 10% improvement in simulating hub-height wind speed and that the overall best performing models were Noah and Noah-MP. They emphasized that the variability of LSM performance across different soil moisture and vegetation canopy conditions suggests LSM representation of surface energy exchange processes in WRF remains a large source of model uncertainty.

Lee *et al*. (2016) studied the performance evaluation of four different LSMs in WRF over the Haean Basin in South Korea. They carried out a four-day period high-resolution simulation over a complex terrain during autumn. They evaluated the 5-layer Soil Thermal Diffusion (STD) LSM, the Noah LSM, RUC LSM and the PX LSM, and found Noah to be the overall best performing LSM over the area. Also, WRF with RUC has a very good agreement with temperature profiles, whereas, WRF with PX and with TD performed insufficiently for the simulation of heat fluxes. They both overestimated the sensible heat and underestimated the latent heat fluxes during the daytime.

Jin *et al*. (2010) studied the sensitivity of Four Land Surface Schemes in the WRF namely the simple Soil Thermal Diffusion (STD) scheme, Noah scheme, RUC scheme and Community Land Model version 3 (CLM3). They carried out WRF simulations with

all four land surface schemes over the western United States for 1 October 1995 through 30 September 1996. Their results show that land-surface processes strongly affect temperature simulations over the area. They also found out that WRF CLM3 with the highest complexity level significantly improves temperature simulations, except for the wintertime maximum temperature as compared to the observations. Also, precipitation was dramatically overestimated by WRF with all four land-surface schemes over the area and does not show a close relationship with land-surface processes.

To further explore the physical and dynamic mechanisms behind the Regional Climate Model (RCM) sensitivity to LSP schemes, Li et al. (2015) investigated the differences in the surface energy budget between simulations of ensemble mean averaging of Noah and CLM, and ensemble mean averaging PX and SSiB and their subsequent impacts on the atmospheric circulation were analyzed. They found that the intensity of simulated sensible heat flux over Asian continent in ensemble mean averaging of Noah and CLM is stronger than that in PX and SSiB, which induces a higher tropospheric temperature in Noah-CLM than in PX-SSiB over land. They further stressed that RCM simulation does add more information to the East Asian Summer Monsoon Simulation (EASM) compared to reanalysis that imposes the Lower Boundary Condition (LBC) because the RCM provides 2-m temperature and precipitation that are with higher resolution and more realistic compared to the LBC. Also, the simulated 2-m temperature and precipitation are more consistent with observations in PX and SSiB than in Noah and CLM.

2.7 Review on LULC Change Impact on some Hydrometeorological Parameters.

The interaction between land and the atmosphere is important in every weather prediction model. Changes in LU have the capacity to affect the output of weather models owing to the fact that the incoming and outgoing radiations are altered by the modification of biophysical features on the earth's surface. West Africa was selected for this study because it has become a focal point in debates over biophysical impacts of desertification, deforestation and climate change. (Fuller and Ottke, 2002).

The role of land surface processes in the regional climate was investigated by several modeling studies: Charney (1975), Charney *et al*. (1977), Yeh *et al*. (1984), Sud and Fennessy (1984), Sud and Molod (1988), Cunnington and Rowntree (1986), Kitoh *et al.* (1988), Rowell and Blondin (1990), Rodriguez- Iturbe *et al*. (1991), and Xue and Shukla (1993). Charney (1975) was the trailblazer on land–atmosphere interaction studies in West Africa. He introduced a hypothesis, which proposed a significant role for vegetation in the dynamics of rainfall over the Sahel. By implication, the rainfall-producing circulation over West Africa is sensitive to changes in the state of vegetation at the desert border with the Sahara, i.e. the Sahel-Sahara interface.

Baidya Roy and Avissar (2002) studied the Impact of deforestation on regional hydrometeorology in Amazonia using the Regional Atmospheric Modeling System (RAMS). They found out that the Coherent mesoscale circulations were triggered by the surface heterogeneity, and that synoptic flow did not eliminate the circulations but advected them off from the location that they were generated. They also stressed that the circulations affected the transport of moisture and heat at the synoptic scale and have the ability to affect the climate. Recent studies on the Amazon deforestation problem predict

that removal of the forest will result in a higher surface temperature, a significant reduction in evaporation and precipitation, and possibly significant changes in the tropical circulation.

Eltahir and Bras (1993) discussed the basic mechanisms instrumental to the response of the tropical atmosphere to deforestation using a simple linear model and revealed that deforestation causes an increase in surface temperature and a decrease in heating to the upper-troposphere due to reduction in rainfall. As a result of the nature of the deforestation complications, (an increase in surface temperature with a decrease in precipitation) it is possible to have notable anomalies in surface temperature and precipitation with only a negligible effect on the circulation (Eltahir and Bras, 1993).

Qu *et al*. (2013) studied the Impacts of Land Cover Change on the Near-Surface Temperature in the North China Plain for 1992 and 2005. Their results indicated that the land cover change in the North China Plain, which was characterized by the regional urbanization, had led to significant changes in the near-surface temperature, increasing the regional near-surface temperature by 0.03°C/year on average. The spatial pattern of the climate change basically corresponded to that of the land cover change; for example, the temperature increased most significantly in the regions mainly consisting of cities and built-up area. Besides, there were some variations in the degree and range of influence of the land cover change on the temperature among seasons.

Yu and Xie (2013) investigated the regional climate effects of land cover change over China using RegCM4. They carried out two 24-year simulations (1978–2001), one with the land cover derived from the Moderate Resolution Imaging Spectroradiometer (MODIS) data and the other with the CLCV (Chinese land cover derived from vegetation

map) data. Their results indicated that the land cover change has important impacts on local climate through mechanisms related to changes in surface energy, water budgets and macro-scale circulation. During the summer period, the land cover change leads to a decrease in surface air temperature over southern China, a reduction in precipitation and an increase in surface air temperature in the transitional climate zone and the northern Tibetan Plateau, and an increase in inter-annual variability of surface air temperature in the marginal monsoon zone and northwestern China in the summer period.

Cao *et al*. (2015) examined how different land use and land cover patterns affect regional climate in the agro-pastoral transitional zone of North China, whose environmental and socio-economic conditions are sensitive to climate change. They parameterized WRF using LULC maps corresponding to 2001 and 2010 conditions, which differ in the representation of four land surface biophysical parameters: vegetation fraction, Leaf Area Index (LAI), albedo, and emissivity. Cao *et al*. (2015) found out that vegetation fraction and LAI increased in summer, emissivity increased and albedo decreased in winter, and that there was widespread reduction in summer temperature with local cooling on the order of 1°C, and extensive increase in winter temperature with local warming exceeding 0.8 °C. Their findings demonstrate that LUCC in Northern China has altered the regional climate over the past decade.

Li *et al*. (2018) studied two scenarios including an urbanization scenario in which all the wetlands and croplands would be converted to built-up areas, and an irrigation expansion scenario in which all wetlands and dry croplands would be substituted by irrigated croplands in India. Results showed that conversions of wetland and cropland to built-up areas would substantially increase temperature in the region and stimulate

sensible heat fluxes but reduce latent heat fluxes and albedo. Expansion of irrigated croplands could contradictorily decrease temperature and sensible heat fluxes but however increase latent heat fluxes and albedo. They stressed that the impacts of LULC change on precipitation were complex and that a shifting of maximum rainfall rates was seen in the urbanization scenario as a result of the downwind effect. In line with expansion of built-up areas, increased temperature has been reported due to the Urban Heat Island (UHI) effect, which is mostly caused by increased heat emissions from human-related sources (Weng *et al*., 2004; Chen *et al*., 2006; Tan *et al*., 2010). Increase of precipitation in the downwind areas of urbanized land has been observed and attributed to urbanization (Shepherd *et al*., 2002).

Laux *et al*. (2017) studied the impacts of land-use/land-cover change and climate change on the regional climate in the Central Vietnam. Using WRF model with an updated LULC map, they found that the impacts of the outdated LU map in WRF exceed those of climate change, at least for the period 2001 to 2030. In addition, the deforestation scenario does not provide statistically significant signals of the most crucial surface climate variables, whereas the urbanization scenario provides evidence for a temperature signal (temperature increase) over the converted area, but no clear signal for precipitation is found.

Pitman *et al*. (2012) studied the effects of land cover change on temperature and rainfall extremes in multi-model ensemble simulations over some parts of North America, Europe and Sourh East Asia using four climate models within the Land Use and Climate, IDentification of robust impacts project (LUCID). Pitman *et al*., (2012) found out that consistent changes in both high and low temperature extremes are similar to the

simulated change in mean temperature caused by LULCC and are restricted to regions of intense modification. While they find some evidence that individual models respond consistently to LULCC in the simulation of changes in rainfall and rainfall extremes, LULCC's role in affecting rainfall is much less clear and less commonly statistically significant, with the exception of a consistent impact over South East Asia.

Fuller and Ottke (2002) examined albedo time series and their relationships with rainfall, land cover, and population in West Africa. They found out that albedo and rainfall were related only modestly at short time scales (monthly and annual) and that mean annual albedo values remained relatively stable from 1982–1989 over a wide range of climatic and vegetation zones in West Africa. The relationship between long-term mean rainfall and mean albedo was strong and curvilinear ($r^2 = 0.802$). Also, same was true for the relationship between percentage trees cover and mean albedo ($r^2 = 0.659$). They also suggested that long-term climate patterns that control vegetation type and canopy structure have considerable effect on albedo than short-term fluctuations in rainfall.

Kutzbach *et al*. (1996) used a climate model to study the role of vegetation and soil moisture in African paleo-climate studies and revealed that changes in vegetation and soil may have increased the climate response to orbital forcing. They found out that replacing today's orbital forcing with that of the mid-Holocene increases summer precipitation by 12% between 15 and 22°N. They also found out that replacing desert with grassland, and desert soil with more loamy soil, enhances the summer precipitation more by 6 and 10% respectively, giving a total precipitation increase of 28%. When the simulated climate changes are applied to a biome model, vegetation becomes established

north of the current Sahel-Sahara boundary, thereby shrinking the area of the Sahara by 11% owing to orbital forcing alone, and by 20% owing to the combined influence of orbital forcing and the prescribed vegetation and soil changes. They therefore found out from the study, that the incorporation of the vegetation and soil feedbacks consequently brings the model simulations and palaeo-vegetation observations into closer agreement. The results of these studies suggest that the conditions of the land surface as characterized by vegetation cover and soil moisture play a significant role in rainfall variability over West Africa.

Abiodun *et al*. (2007) investigated the feedback mechanisms between land cover and the monsoon in West African using the RegCM3 model. They performed series of multi-year simulations under three idealised vegetation states, i.e. potential, desertified and deforested. Their findings revealed that both desertification and deforestation tend to increase the monsoon flow over the Guinean region, although the mechanisms for change were different in each case. They emphasized that desertification increases the flow mainly by increasing the meridional temperature gradient. As this reduces rainfall over the desertification region, rainfall is increased to the south. Deforestation however, increases the monsoon flow largely because of the reduced surface friction experienced by the flow over the Guinean region and also reduces rainfall over the entire West African region. They concluded that state of the biosphere could play an important role in determining the characteristics of the monsoon and rainfall pattern in West Africa.

Hagos *et al*. (2014) examined the uncertainties of model response in the African monsoon system and Sahel precipitation due to LULC change using WRF model simulations with different combinations of land surface and cumulus parameterization

schemes. They discovered that most of the simulations show a decline in Sahel precipitation due to the expansion of pasture and croplands at the expense of trees and shrubs and an increase in surface air temperature. Simulations that are not too dry or too wet were seen to have stronger response to the LULC changes. Also, that much of the change in precipitation is related to changes in circulation, particularly to the response of the intensity and latitudinal position of the African Easterly Jet, which varies with the changes in meridional surface temperature gradients.

Diba *et al*. (2018) used RegCM4.5 to investigate the potential impacts of land cover change of the Sahel–Sahara interface on the West African climate. They carried out simulations with three vegetation change experiments namely; forest, tall grass, and short grass savanna at 50 km grid resolution. Their results show that the presence of forest, tall grass, and short grass savanna at the Sahel–Sahara interface tends to decrease the mean summer surface temperature in the whole region, but more conspicuous over the Central Sahel for the forest experiment. They suggested that the temperature decrease is associated with a weakening of the sensible heat and strengthening of the latent heat flux in the whole region. They also show that the afforestation options tend to alter the precipitation in the considered sub-domains substantially by increasing it in the whole Sahel region, with strong interannual variability, and also tend to increase the frequency of the number of rainy days in regions located south of 18°N, and that the vegetation change experiments also affect the Tropical Easterly Jet (TEJ), mostly during wet years, by increasing its intensity over the southern Sahel.

Among those studies on the impact of vegetation cover (e.g., Charney, 1975; Xue and Shukla, 1993), it is generally concluded that the desertification near the sub-Saharan

desert border reduces rainfall within the region of vegetation perturbation and increases rainfall south of the perturbation region. The soil moisture–rainfall interactions are often found to be able to sustain rainfall anomaly and thus provide a positive feedback (e.g., Yeh *et al*., 1984; Zheng and Eltahir, 1997).

2.8 Review on LULC Change and its Impact on Streamflow

Land use changes and their related effects are known to impact the hydrology of the catchment area (Bronstert *et al*., 2002; Ott and Uhlenbrook, 2004; Foley, 2005; Tang *et al*., 2005; e.t.c). Researchers like Lal, 1997; Pereira, 1989 and Ngana, 2002 have stated that the impact of vegetation cover in improving the capacity of basins, moisture conservation and water yield increase cannot be disregarded. This is because, it can alter the hydrological flow regime of the river catchments. According to Newson (1995), alterations in the vegetation cover tend to affect the degree of infiltration, run-off, and evaporation rate and precipitation pattern. Although vegetation holds a lot of precipitation by means of interception and infiltration, Hough (1986) states that trees evaporate much more. Heat change between land and the atmosphere could be affected by loss of wetlands, which can considerably adjust evapotranspiration and runoff (Kalnay and Cai, 2003; Bartzen *et al*., 2010). Also, the changing of wetlands to croplands can likewise lead to alterations in structure and function of vegetation layer that further affects energy fluxes in the climate system (Kutzbach *et al*., 1996; Stohlgren *et al*., 1998; Carrington *et al*., 2001). Furthermore, the conversion of wetlands to built-up areas increases impervious surfaces like roofs, parking lots, and roads allow no infiltration, hence will force all water that falls onto them to run-off, and thus influence regional water cycling. According to Zheng *et al*. (2008), changes in LU types in a catchment could have a

considerable effect on the stream flow/discharge and its response to storms.

Aduah *et al*. (2017) assessed the impacts of LU changes on the hydrology of a rainforest catchment in Ghana using the Agricultural Catchments Research Unit (ACRU) hydrological model. They developed three LU scenarios for baseline, current and potential future LU maps. Aduah *et al*. (2017) found out that for the current LU, peak and dry season streamflows between 1991 and 2011 have increased by 21% and 37% respectively in comparison to the baseline due to a decrease in evergreen and secondary forests by 18% and 39%, respectively, and an increase in settlements, mining areas and shrubs/farms by 81%, 310% and 343%, respectively. They also revealed that variability of streamflow changes was higher at the subcatchment scale than at the catchment scale.

Legesse *et al*. (2003) evaluated the hydrological response of a catchment to climate and land use changes in Tropical Africa and found that a 10% decrease in rainfall produced a 30% reduction on the simulated hydrologic response of the catchment, while a 1.5 °C increase in air temperature would result in a decrease in the simulated discharge of about 15%. Moreover, they indicated that a conversion of the present day dominantly cultivated/grazing land by woodland would decrease the discharge at the outlet by about 8%.

Ward *et al*. (2009) evaluated the impact of land use and climate change on future sediment yields and found out that conversion of forest to agricultural land increases yield in all simulations. Ward *et al*. (2009) also revealed that the sensitivity of sediment yield to changes in climate increases as the percentage of deforested land increases.

Mahe *et al*. (2005) modeled the impact of land use change on soil water holding capacity and river flow in West Africa and found that the total reduction in water holding

capacity is estimated to range from 33% to 62% between 1965 and 1995. This was explained by the decline in the extent of natural vegetation from 43% to 13% of the total basin area, whilst the cultivated areas increased from 53% to 76% and the area of bare soil nearly tripled from 4% to 11%.

Li *et al*. (2007) modeled the hydrological impact of land use change (West Africa) using terrestrial ecosystem model IBIS (Integrated Biosphere Simulator) and an aquatic transport model THMB (Terrestrial Hydrology Model with Biogeochemistry). From the research, they pointed out that total deforestation increases the simulated runoff ratio from 0.15 to 0.44, and the annual streamflow by 35%–65%, depending on location in the basin, although forests occupy less than 5% of the total catchment area. They mentioned that there is no significant impact on the water yield and river discharge when the deforestation percentage is below 50% or the overgrazing percentage below 70% for savanna and 80% for grassland areas. They also affirmed that when LCC exceeds these thresholds the water yield was increased substantially.

Ghaffari *et al*. (2012) simulated the hydrological impact of land-use changes in 1967, 1994 and 2007 in Iran using the Soil and Water Assessment Tool (SWAT) model. The study reveals that during 1967 a 34.5% decrease of grassland with concurrent increases of shrubland (13.9%), rain-fed agriculture (12.1%), bare ground (5.5%) irrigated agriculture (2.2%), and urban area (0.7%) led to a 33% increase in surface runoff and a 22% decrease in groundwater recharge. Also, the area of sub-basins that was influenced by high runoff (14–28 mm) increased, as there was a substantial increase in runoff when more than 60% of the rangeland was removed.

Akpoti *et al*. (2016) assessed the potential implications of rainfall variability along with Land Use and Land Cover Change (LULC) on stream flow in the Black Volta basin using the SWAT model. Using year 2000 and 2013 land use data with LU classes like bare land, urban areas, water bodies, agricultural lands, deciduous forests and evergreen forests increasing respectively by 67.06%, 33.22%, 7.62%, 29.66%, 60.18%, and 38.38%, while only the grasslands decreased by 44.54% within the period, the dry season discharge increased by 6% while the discharge of wet season increased by 1%. The overall effect was that the water yields to stream flow increased by 4%.

Githui *et al.* (2009) used the SWAT model to investigate the impact of land-cover changes on the runoff of the River Nzoia catchment, in Kenya. They generated land cover change scenarios and compared the results over 2 periods of six years, each which are 1970–1975 and 1980–1985. It showed that land-cover changes accounted for a difference in surface runoff ranging from 55 to 68% between the two periods. The land-cover scenarios used showed the magnitude of changes in runoff due to changes in the land covers considered. The land-cover scenarios generated changes in runoff of about –16% and 30% for the best and worst case scenarios respectively as compared to the 1980–1985 runoff.

Petchprayoon *et al*. (2010) integrated remote sensing, Geographic Information System, statistical methods, and hydrological modelling to determine the hydrological impacts of land use/land cover (LULC) change in the Yom watershed in central–northern Thailand over a 15-year period. They found out that Yom River's daily discharge long-term trend significantly increased at most of the measurement stations, and the rate of increase in discharge at areas downstream of the rapid urbanisation was significantly

greater than that at areas upstream. There were no significant long-term trends in precipitation characteristics in the basin, except for one station. The rate of change in discharge after changes in LULC showed a systematic increase.

In the study of how to manage high runoff discharge in the urbanized basins of Asa river catchment area of Ilorin, Jimoh and Iroye (2010) examined the relationship between runoff discharge and basin characteristics in Ilorin using rainfall data and satellite land use map. They found out that basin size and land use have overwhelming influence on the explanation of discharge in the basins.

Okpara *et al.* (2013) explored and assessed the potential impacts of projected climate change on water resources of the Nigerian sector of Niger River basin using both parametric and non-parametric approaches and simulation models i.e. Thornthwaite water balance accounting scheme and Artificial Neural Networks (ANNs). They observed that the humid portion in the lower Niger sub-basin are also vulnerable to the changing climate and its impacts, and that the observed changes are likely to be connected to the long time variability in the climatic variables of the region, and land use changes due to increasing anthropogenic activities and gas flaring and population pressure.

Mahe (2006) stressed that the joint effect of climate change and human activities on land cover is responsible for an increase in the runoff coefficients of the West African Sahelian rivers since the 1970s, as revealed by the analysis of runoff time series of rivers from Mauritania, Burkina-Faso and Niger. They studied the relationship between hydrology and LULCC using hydrological modeling and concluded that the hydrological changes correlated with LULCC, which leads to the impermeabilization of the soil top

layer, and thus to the reduction of the Water Holding Capacity (WHC) by using conceptual hydrological models which uses WHC as the soil water reservoir.

Ifatimehin *et al*., (2012) evaluates the impact of urbanization on Meme river catchment area (sub basin of the Lower Niger basin) in Lokoja. They applied multiple regression analysis to analyse the impact of urbanization on the Meme river catchment. Their results showed that urbanization has greatly impacted on the river via loss of flood plains, river flow, as well as reduction in capacity of the water channel to keep water. They suggested controlled siltation of the river and that developers should be educated about the environmental and economic implications.

Amoo and Dzwairo (2017) extend the versatility and usefulness of Arc Hydro tool in GIS and statistical analysis as a methodology for any river basin Hydrologic Characteristics Analysis (HCA) with case study at the Gurara river basin within the lower Niger basin. The result of the downstream unit hydrology indicates that streamflows from high altitude, lithological variation and moderately steep slopes, elevation, drainage pattern of the area, slope, LULC, soil type, vegetation and drainage network are factors affecting the distribution of runoff in the basin.

Research by Casse *et al*. (2016) provides a better understanding of the roles of rainfall and surface conditions (LULC and drainage area) in observed changes, using hydrological simulation based on the Interaction between Soil Biosphere and Atmosphere (ISBA)–Total Runoff Integrating Pathway (TRIP) model in Niger red floods. The simulations based on current surface conditions are able to reproduce the observed trend in red flood occurrence and intensity since the 1980s. They found out that increasing the vegetation cover and reducing the drainage area decreases the runoff production in the

model and simulates discharges closer to the observations in the 1950s and 1960s. This result implies that changes in the environmental conditions are responsible for the change in hydrological behaviour between the 1950s–1960s decades and the 1970s to present period.

Zhou, (2014) emphasized that although much progress has been made in the study of hydrologic impact of LULCC, there are still numerous uncertainties and even controversies. There are uncertainties from data sources, LULCC quantification, and hydrologic modeling in the evaluation. The hydrologic impact of LULCC may vary with study area, climate condition, geography, and spatial scale, and it is also dependent on the temporal scale analyzed. All of these factors make the evaluation of the hydrologic impact of LULCC more challenging.

However, many researchers have worked on the impact of LULC change on different river catchment areas in the Niger basin and in West Africa within and outside Nigeria using different tools and approaches like remote sensing, statistical and modeling tools, but none have either used the WRF-Hydro model, or incorporated a satellite data into the model. The integration of land use change models and climate change models with hydrologic models can improve the efficiency of predicting the hydrologic response, since these models are capable of providing more realistic forecasts. Models are differing in terms of complexity, processes considered, and the data required for model calibration and model use. In general there is no 'best' model for all applications (Merritt et al., 2003). The selection of a particular model is a key issue to get satisfactory answers to a given problem. Currently, there are numerous numerical weather prediction (NWP) and hydrological models simulating the hydrological process at different spatial and temporal

scales. This research uses the WRF and WRF-Hydro model to simulate the impact of land cover change on the hydrometeorological parameters over West Africa and tailored down to the Sokoto Rima River Basin (SRRB) in West Africa.

2.9 Climate Modelling

One of the techniques to study climate dynamics is the use of General Circulation Models (GCM). The major difference between General Circulation Models (GCMs) and Regional Climate Models (RCMs) has to do with their spatial and temporal resolutions. Global models can distinguish the large-scale weather systems affecting a region; but not to a resolution capable of capturing the activities that are associated with the local landscape and land cover. In other to capture smaller scale features, a simulation at sufficiently high spatial resolution of the local complex terrain and the heterogeneous land surfaces is required (Alpert *et al.* 2008).

2.10 Weather Research and Forecasting Model (WRF)

WRF model is a fully compressible and non-hydrostatic model (Skamarock, *et al*. 2008). It is suitable for use in a wide range of scales, from thousands of kilometers to a few meters. It is intended to be a flexible, state-of-the-art atmospheric simulation system, which is portable and efficient on available parallel computing platforms (WRF user's guide). WRF model has several options that relates to the model core and most physical parameterizations. The WRF modeling system consists of the following program:

- WRF Preprocessing System (WPS)
- WRF Data Assimilation (WRF-DA) system
- Advanced Research WRF (ARW) Solver
- Post-processing and Visualisation tools.

2.10.1 WRF Preprocessing System (WPS)

The WRF Preprocessing System (WPS) is a component of WRF model with a set of three programs including geogrid, ungrib and metgrid, having a common role, which is to formulate input to the real program for real-data simulations in WRF. The geogrid program defines the model domains and interpolates static geographical data to the model grids; the ungrib extracts the meteorological fields from GRIB-formatted files like ERA-Interim, e.t.c.; and the metgrid program horizontally interpolates the extracted meteorological fields from ungrib program to the model grids as defined by the geogrid program.

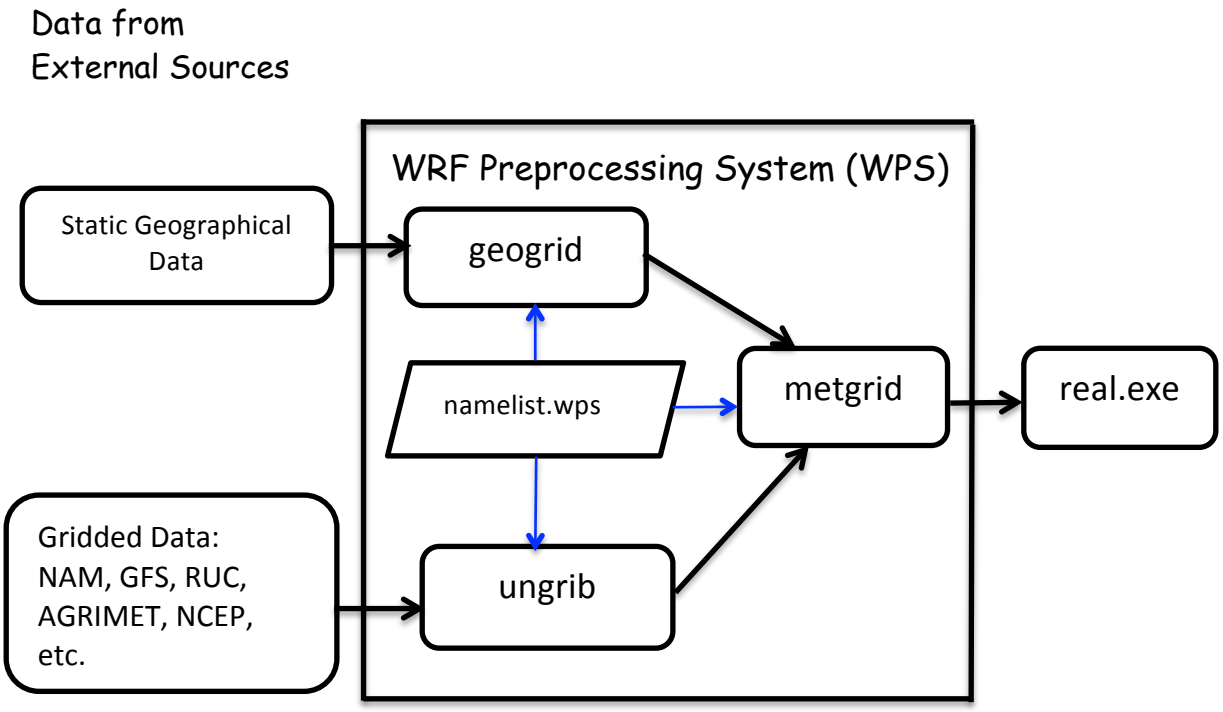

Figure 2.4: The Data Flow Between the Programs of the WPS (Adapted from Wang *et al*., 2008a)

All the WPS programs read in variables from the same namelist file with both the separated and shared namelist records. Each WPS program uses the separated namelist

records, while the shared namelist records determine the variables, which are utilized by two or all the WPS programs. Vertical interpolation of the meteorological fields from metgrid to WRF eta levels is carried out within the *real* program in WRF model.

The features of WPS component of WRF model include;

- GRIB 1-2 meteorological data from various meteorological centers worldwide
- USGS 24 category and MODIS 20 category land datasets; USGS GTOPO30 elevation data sets, Global 5 minutes United Nations FAO, and North America STATSGO 30 sec Soil category dataset; MODIS leaf area index, monthly surface albedo; and other few supplementary specialized datasets.
- Map projections for; 1) polar stereographic, 2) Lambert conformal, 3) Mercator and 4) Latitude-longitude
- Nesting
- User-interfaces to input other static data as well as met data

2.10.2 WRF-DA

The WRF-DA component of the model is an optional program; nevertheless can be utilzed to ingest observational data into the interpolated analysis from WPS. It can be used to update WRF model's initial boundary conditions when the WRF model is run in cycling mode (warm-start). Details of the WRF-DA description and features are well outlined in the WRF-user guide.

2.10.3 ARW Solver

It is the major component of the modeling system. It consists of several initialization programs for idealized and real-data simulations, and the numerical integration program. The features of the WRF model include but not limited;

- Fully compressible non-hydrostatic equations with hydrostatic equations
- Regional and global applications
- Complete Coriolis and curvature terms
- Two-way nesting with multiple nests and nest levels
- Concurrent one-way nesting with multiple nests and nest levels
- Offline one-way nesting with vertical nesting
- Moving nests (prescribed moves and vortex tracking)
- Map-scale factors for Polar stereographic, Lambert, Mercator, Latitude and longitude projections
- Arakawa C-grid staggering
- Runge-Kutta 2nd and 3rd order time integration options
- 2nd to 6th order advection options (horizontal and vertical)
- Upper boundary absorption and Rayleigh damping
- Lateral boundary conditions
- Full physics options for land-surface, planetary boundary layer, atmospheric and surface radiation, microphysics and cumulus convection
- Ocean models e.t.c

Descriptions of more of these features are mentioned in the WRF-user guide (WRF-ARW V3: User's Guide).

The Weather Research and Forecasting (WRF) Model, is a mesoscale numerical weather prediction (NWP) system which provides both the operational forecasts and atmospheric research requirements (Skamarock *et al*., 2008). In spite of the fact that it is invented to improve forecast accuracy across scales ranging from cloud to synoptic, the

special importance on horizontal resolutions of 1-10km makes it satisfactorily suited for the newly emerging Numerical Weather Prediction (NWP) applications in the non-hydrostatic system. Although individual models have their specific strengths and weaknesses, selection is based on the model performance, cost, popularity of the model among researchers, ease access to the ground and satellite meteorological data that will be used as boundary and initial conditions. The performance of WRF model have been analyzed by many studies like in Santos-Munoz *et al*. (2009), Matsangouras *et al*. (2011) and have shown a better performance.

It would be too simplistic and far from truth to describe meteorological processes for a spherical planet as having no water and vegetation, but rather, more equations are required to account for features including oceans, mountains, ice, biotic factors, e.t.c which emphasizes the need for many equations. Parameterization options use mathematical formula (derived from theoretical understanding of atmospheric processes) to compute values of parameters of interest (www.yarkerconsulting.com). Parameterization is a method of replacing processes that are of a very small-scale or very complex to be physically represented in the model through a simplified process. These parameterizations are usually a major source of model uncertainty. As regards to parameterized physics and dynamics, and also as a regional climate model, WRF has some common features with global climate models. WRF model possess a wide range of physical parameterizations schemes that include options for Microphysics, Longwave Radiation, Shortwave Radiation, Surface Layer, Land Surface, Urban Surface, Lake Physics, Planetary Boundary Layer, Cumulus Parameterization e.t.c which allow setting

the model to better describe the physical processes based on model domain, resolution, location, and application (Ruiz –Arias *et al.,* 2008).

The capability of any physics scheme depends largely on the principal feature of atmospheric processes in the domain of interest, the model resolution and the suitable choice of parameterization scheme for the particular issue (Klein *et al*., 2015). Researchers like Jankov *et al*. (2005), Gallus and Bresch (2006), Kain *et al*. (2006), Borge *et al*. (2008), Deb *et al*. (2008), Hong *et al*. (2009), Kwun *et al*. (2009), Li and Pu (2009), Nolan *et al*. (2009), Crétat *et al.* (2012), Evans *et al.* (2012) and García-Díez *et al.* (2013) have focused on the appropriate selection of Weather Research and Forecasting (WRF) parameterizations schemes for varying conditions and applications. Some of these studies concluded that the performance of the physics schemes varies according to the region of study including the time of the year. Hence, care should be taken in applying each for a specific study area.

However, an indispensable feature of a regional climate model is the need to simulate the interaction between the land surface and atmospheric fluxes of energy, moisture, and momentum, which is usually handled through a Land Surface Model (LSM) component (Okalebo *et al.* 2016). In the IPCC report (2013), the effect of LULCC was ranked as one of the largest uncertainties in global climate models. LSMs are used to compute the hydrological, biogeophysical and biogeochemical processes involved in latent, sensible and soil heat land surface atmospheric fluxes (Wei *et al*., 2009). They use atmospheric information from the surface layer scheme, radiative forcing from the radiation scheme, and precipitation forcing from the microphysics and convective schemes, in conjuction with internal information on the condition of the land variables

and land-surface properties, in other to provide heat and moisture fluxes over land points and sea-ice points (Skamarock *et al*., 2008). A wide range of LSMs is currently in use today, each varying in their temporal and spatial scales and especially in their degree and type of physical parameterization.

2.10.4 WRF land surface models (LSMs)

WRF version 3.9.1.1 has about seven different land surface physics options from the simple 5-layer soil model simply with thermal diffusion in soil layers and no vegetation or snow cover prediction to Noah LSM, Noah-MP, RUC LSM, PX LSM, CLM4, SSiB LSMs with sophisticated vegetation models and snow cover prediction. The WRF LSMs are driven by surface energy and water fluxes and predict soil temperature and moisture in different layers depending on the LSM option in which Noah and Noah-MP has 4 layers, RUC has 9 layers, PX has 2, SSiB has 3 and 10 for CLM4. Noah-MP, RUC, SSiB and CLM4 may predict snow water equivalent on ground. All the WRF land surface models utilize the wind and stability information from the atmospheric surface layer scheme. In this research, the four most recent and most sophisticated LSM options in WRF model is tested in combination with other parameterization schemes for the West African region.

The Noah LSM (Chen and Dudhia 2001) was developed jointly by National Center for Atmospheric Research NCAR and National Centers for Environmental Prediction NCEP. It has been validated by many inter-comparison studies both in coupled (Betts *et al*., 1997) and uncoupled (Wood *et al*., 1998; Schlosser *et al*., 2000) mode. Its moderate complexity and computational efficiency has made it effective in both operational weather and climate models. It has the advantage of being compatible with

the time-dependent soil fields made available by NCEP in the global analysis datasets. It has a 4-layer (0.10, 0.30, 0.60 and 1 m thick) soil temperature and moisture model in addition to canopy moisture and snow cover prediction. It has a rooting depth fixed at 1m including three layers at the top and also has one snow layer and one canopy layer. The mass conversation law and the diffusive form of the Richard's law controls the vertical water mass movement between soil layers, while a conceptual parameterization for the sub-grid treatment of soil moisture and precipitation controls the infiltration (Schaake *et al*., 2004). Total evapotranspiration in Noah is the sum of the canopy intercepted water evaporation, transpiration from vegetation canopies, and evaporation from bare soil as weighted by the respective land surface coverage fractions (McNally *et al*., 2017). The drainage is due to the gravitational percolation below the soil layers. The surface skin temperature is calculated from a surface energy balance equation. The surface energy fluxes of Noah are calculated over a combined surface layer of vegetation and bare soil surface. A model of such structure impedes its further development as a process-based dynamic leaf model, because it cannot explicitly compute photosynthetically active radiation (PAR), canopy temperature, and related energy, water, and carbon fluxes (Niu *et al*., 2011). Prediction includes a root zone, evapotranspiration, soil drainage, and runoff, taking into account vegetation categories, monthly vegetation fraction, and soil texture. It also predicts soil ice, and fractional snow cover effects, has urban treatment options, and takes surface emissivity and albedo properties into consideration.

The Noah MP (multi-physics) Land Surface Model (Niu *et al*., 2011) is an augmented version of the Noah LSM. The vital augmentation is the introduction of (a) a vegetation canopy layer for individually computing the canopy and the ground surface

temperatures, achieved by introducing a semitile subgrid scheme to represent land surface heterogeneity (Niu *et al*., 2011), (b) a modified two-stream scheme (Yang and Friedl, 2003; Niu and Yang, 2004) for transfer of radiation through vegetation canopy and considering the canopy gaps, (c) a Ball-Berry scheme for the canopy stomatal resistance (Ball *et al*., 1987; Collatz *et al*., 1991, 1992; Sellers *et al*., 1996; Bonan, 1996) which connects stomatal resistance to the photosynthesis of sunlit and shaded leaves, (d) a short-term dynamic vegetation model (Dickinson *et al*., 1998) with two options (off and on) in which Leaf Area Index (LAI) and Vegetation Greenness Fraction (GVF) can be predicted from the model when turned on. Also, a simple TOPMODEL runoff model for the computation of surface runoff and groundwater discharge, a 3-layer snow model (Yang and Niu, 2003), and a frozen soil scheme with exceptional soil permeability from Niu and Yang, (2006). The Noah-MP uses multiple options for key land-atmosphere interaction processes. It contains a separate vegetation canopy defined by a canopy top and bottom with leaf physical and radiometric properties used in a two-stream canopy radiation transfer scheme that includes shading effects. Noah-MP contains a multi-layer snow pack with liquid water storage and melt/refreeze capability and a snow-interception model describing loading/unloading, melt/refreeze, and sublimation of the canopy-intercepted snow. Multiple options are available for surface water infiltration and runoff, and groundwater transfer and storage including water table depth to an unconfined aquifer. Horizontal and vertical vegetation density can be prescribed or predicted using prognostic photosynthesis and dynamic vegetation models that allocate carbon to vegetation (leaf, stem, wood and root) and soil carbon pools (fast and slow).

CLM4 (Community Land Model Version 4, Oleson *et al*. 2010) is a state of the science land surface model more often used in climate applications, developed at the National Center for Atmospheric Research alongside many external collaborators and includes sophisticated handling of biogeophysics, hydrology, biogeochemistry, and dynamic vegetation. The vertical structure comprises of a single-layer vegetation canopy, a five-layer snowpack, and a ten-layer soil column. It has 3.8m soil depth divided into 10 layers approximately at 1.8 cm, 4.5 cm, 9.1 cm, 16.6 cm, 28.9 cm, 49.3 cm, 82.9 cm, 138.3 cm, 229.6 cm, and 342.3 cm below the surface. The Soil water is predicted from the modified Richards equation by Zeng and Decker (2009). CLM4 centers on biogeophysics of land surface including vegetation dynamics modules. The overland flow is calculated with a simple conceptual TOPMODEL approach to parameterize the surface runoff. An exchange of water between an unconfined aquifer and the overlying soil column is incorporated in the soil hydrology scheme (Niu *et al*., 2011). The parameterization schemes of Niu and Yang (2006) and Wang and Zeng (2009) is used to calculate the snow cover and snow burial fraction. Some of the major differences between the LSMs are highlighted in Table 2.1.

Table 2.1: Highlights of Some Major Differences Between the LSMs.

Description	Noah	Noah-MP	CLM4
Reference	Chen and Dudhia (2001)	Niu *et al*. (2011)	Lawrence *et al*. (2011)
No. of model soil layers	4	4	10
Depth of total soil column (m)	2	2	3.8
Model soil layer thickness	0.1, 0.3, 0.6, 1.0	0.1, 0.3, 0.6, 1.0	0.018, 0.028, 0.045, 0.075, 0.124, 0.204, 0.336, 0.553, 0.913, 1.506
Tiling vegetation	Not present	Present	Present
Soil water vertical diffusion	Not present	Present	Present

Description	Noah	Noah-MP	CLM4
No. of snow model layers	1	3	5
TOPMODEL for surface runoff	Not present	Present	Present
Dynamic vegetation	Not present	Present	Present
Explicit vegetation	Not present	Present	Present

Moreover, Recent WRF modification has two land surface options (i.e. MODIS IGBP 21-category data and the 24 category USGS land-cover classification). By default, the geogrid program in WRF will interpolate land use categories from the MODIS IGBP 21-category data. However, the user may select an alternative set of land use categories based on the 24 category USGS land-cover classification, or incorporate an alternative data source for a field (e.g. Land Use) which must be used with an existing source. The later involves writing the data in the proper Geogrid binary format, creating an index metadata file for the data set, and adding or editing the entry for the data in the GEOGRID.TBL file in the WPS program. http://www2.mmm.ucar.edu/wrf/users/docs/user_guide_V3/users_guide_chap3.htm

Sertel et al. 2010 stressed that accurate representation of the land surface is an important factor for climate modeling studies because land surfaces control the partitioning of available energy and water and is important to precisely model the effects of past, current and future land cover. Therefore, in other to better represent the land surface, this research will also use remote sensing technique to analyze the effects of land cover data quality on modeling the climate of West Africa. Latest and accurate land cover data for the study area derived from MODIS land cover data will be fed into the WRF model and the results will be assessed so as to have a preferable numerical simulation output.

2.10.5 Post-processing and Visualisation tools.

The supported post-processing and visualisation tools includes the Visualization and Analysis Platform for Ocean, Atmosphere, and Solar Researchers (VAPOUR), NCAR Command Language (NCL), Model Evaluation Tool (MET) e.t.c.

2.11 WRF-Hydro (Hydrological Model)

WRF-Hydro has been developed to expedite improved representation of terrestrial hydrologic processes related to the spatial redistribution of surface, subsurface and channel waters across the land surface and to make coupling of hydrologic models with atmospheric models possible (Gochis et al., 2018). Gochis and Chan (2003) employed a simple subgrid disaggregation procedure as a means of mapping land surface hydrological situations from a coarsely resolved LSM grid to a much more finely resolved terrain routing grid able to adequately resolve the dominant local landscape gradient features responsible for gravitational redistribution of terrestrial moisture. WRF-Hydro could work as a coupling architecture or layer between weather and climate prediction models and terrestrial hydrologic models and land data assimilation systems, and also in a standalone mode as a conventional land surface hydrologic modeling structure (Gochis et al., 2018).

The model is invented to allow better simulation of land surface hydrology and energy states and fluxes at a high spatial resolution of about 1 km or less. It could be used as either a land surface model in both standalone (uncoupled) mode and fully-coupled (to an atmospheric model) mode. This presents the opportunity for a physics-based, fully coupled land surface hydrological and regional atmospheric modeling capability useful in hydrometeorological and hydroclimatological research and applications (Gochis et al.

2018). Moreover, both time evolving "forcing" and static input datasets are needed for model operation. The accurate specification of both forcing and static data is dependent on the selection of model physics and component options that will be utilized. The principle model physics options in WRF-Hydro include:

- 1-dimensional (vertical) land surface parameterization
- surface overland flow
- saturated subsurface flow
- channel routing
- reservoir routing
- conceptual/empirical baseflow

Noah land surface and Noah-MP land surface model options are available now for use in the WRF-hydro version used in this research (version 5.0) and the newer versions, but the future versions will include other land surface model options (Gochis et al. 2018). The required meteorological forcing parameters are listed in the table 2.2 below.

Table 2.2: Required Input Meteorological Forcing Variables for the Noah and Noah-MP LSMs

Variable	Units
Incoming shortwave radiation	(W/m^2)
Incoming longwave radiation	(W/m^2)
Specific humidity	(kg/kg)
Air temperature	(K)
Surface pressure	(Pa)
Near surface wind in the u - component	(m/s)
Near surface wind in the v-component	(m/s)
Liquid water precipitation rate	(mm/s)

When WRF-hydro is coupled to the WRF regional atmospheric model, the model provides the forcing data with a frequency determined by the LSM time-step specified in WRF. When run in a standalone mode, meteorological forcing data must be provided as gridded input time series. Geographic Information System (GIS) tools in ArcGIS softwrae are used to outline a stream channel network, open water (i.e., lake, reservoir, and ocean) grid cells and groundwater basins. Water features are mapped onto the high-resolution terrain-routing grid and post-hoc consistency checks are performed to ensure uniformity between the coarse resolution Noah/Noah-MP land model grid and the fine resolution terrain and channel routing grid (Gochis *et al*., 2018). The WRF-Hydro model calculate fluxes of energy and moisture either back to the atmosphere or also, in the case of moisture fluxes, to stream and river channels and through reservoirs (Gochis *et al*., 2018).

CHAPTER THREE

RESEARCH METHODOLOGY

3.1. Study area

3.1.1 West Africa

The study area lies between longitude 20^{o}W and 22^{o}E and latitude 0^{o} and 25^{o}N, bounded to the west and south by the Atlantic Ocean and by the neighboring countries to the north and east. The climate of West Africa is mostly controlled by two main air masses namely the dry, dusty North East Trade Wind (NETW) originating from the desert region, and the moist, warm South West Trade Wind (SWTW) originating from the Atlantic Ocean. Mostly the movement of the Inter-Tropical Discontinuity (ITD) decides the effect of the two air masses on the region. The ITD represents the surface meeting point/separation of the two air masses. However, the interaction between the NETW and SWTW bring about the two clear seasons (i.e. the wet and dry) in the region. West Africa lies within a range of climatic zones with variation of rainfall in each region. In regards to rainfall distribution, West Africa can be categorized into five climatic zones according to Amani *et al*. (2007) namely Saharan zone (mostly less than 150mm of rainfall per year), Sahelian zone (average of 150-400mm of rainfall per year), Sudano-Sahelian zone (average annual rainfall in the range of 400-900mm), Sub-humid Sudanese zone (has an average annual rainfall of 600-900mm) and humid Sudanese-Guinean and Guinean zone (annual average rainfall varies between 900-1500mm, but could be more in some places). Rainfall over this region is dependent on the inland movement of the rain band associated to the ITD.

3.1.2 Sokoto Rima River Basin

In other to analyse the impact of land use land cover on streamflow, hydrological simulations were carried out for the Sokoto Rima River Basin (SRRB). The SRRB is a semi arid basin, which lies in the Sudano-Sahelian zone of West Africa with mostly Savanna vegetation and marked with a separate wet and dry seasons. The full SRRB lies between latitudes 10°**N** and 16°N with northern extension to Niger having the Tarka and N'Kaba rivers (from the dryer part of the basin) and longitudes 3°E and 9°E and covering an area over 100,000 square kilometres and bodering with Niger Republic on the north and Benin Republic on the southwest. The main river that drains the basin is the Sokoto river having the Rima, Gaminda, Zamfara and Ka rivers as its major tributaries. The Rima river (which also has a clear basin) is at the upper part of the SRRB also has the Tarka, N'Kaba, Goulbin Maradi, Bunsuru and Gagere rivers as its main tributaries. It covers Sokoto, Zamfara, Kebbi, and large part of Katsina States to the East; it also borders Niger State to the South-east, shares borders with Niger Republic to the north, and Benin Republic to the west. Two major Dams, which include the Goronyo and Bakolori dams were situated in the basin mainly for irrigation and agricultural purposes.

According to Ekpoh and Ekpeyong (2011), average annual temperature for Sokoto is 34.5°C, even though dry season temperatures in the region many a times exceed 40°C around February/April. The daily minimum temperature may be lower than 18°C during the harmattan season. According to Abdulahi *et al*. (2014), the basin is characterized by high evaporation ranging from 80mm in July to about 210mm in April to May, and that a monthly average evaporation range of about 140mm symbolises 30% of monthly average precipitation into the basin. The hottest months of April to May are

periods of highest evaporation. Relative humidity is low most of the year and only increases during the wet seasons of June to September. Rainfall is highly seasonal and controlled by the movement of the ITD. The rainy season usually commences from May/June and could last till September/early October based on the yearly rainfall pattern, so nearly all the rain falls between the month of May to September. Also, the northern part is dominantly shrubby and thorny vegetation known for the Sahel region of West Africa. The area under study is a sub basin in the SRRB which lies between latitudes 11°30'N and 15 N and longitudes 5 and 9 E (Figure 3.1) and covering an area of about 65,000 square kilometres. It covers Sokoto, Zamfara, Katsina, small part of Jigawa and Kano. The Sub-basin was selected due to the high computational cost of running WRF-hydro simulations over such a very large domain.

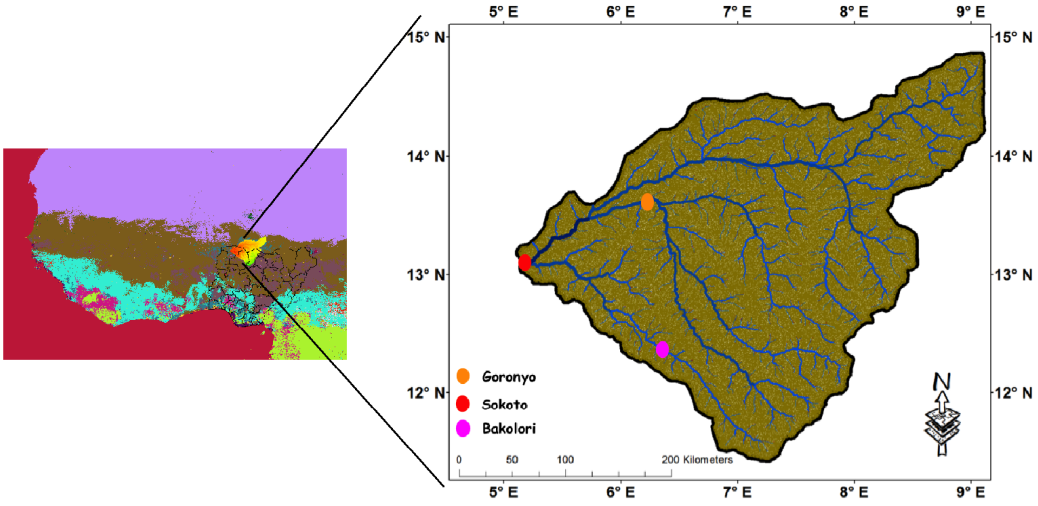

Figure 3.1**:** Location of Sokoto Rima River Basin Basin in West Africa also showing the Streamflow Order and the location of the three Forecast Points.

The dominant LULC parameters in the basin (based on the 2012 LULC obtained from MCD12Q1 data) includes Open shrublands occupying 0.011% of the area, Grasslands occupying about 22.18% of the area, Permanent Wetlands occupying 0.001%, Croplands occupying about 50.126% of the area, Urban and built-up lands occupying

about 0.63% of the area, Cropland/Natural vegetation Mosaics occupying about 26.54% of the area and Barren lands covers 0.51% of the area.

3.2 Land Use Land Cover Data

The WRF model has two available land use options for the users to choose, the United States Geological Survey (USGS) and Moderate Resolution Imaging Spectroradiometer (MODIS). The MODIS option in the model is based on the 2001 data collection, which has not been updated for West Africa. This research study therefore integrated the raw and updated collection 6 (C6) MODIS Land Cover Type Product (MCD12Q1) into the model. The MODIS Land Cover Type Product (MCD12Q1) provides global land cover maps at annual time steps and 500 m spatial resolution for 2001 till present. According to Sulla-Menashe and Friedl (2018), six different classification schemes which include the International Geosphere-Biosphere Programme (IGBP) land cover classification (Loveland and Belward, 1997; Belward et al., 1999), the University of Maryland (UMD) classification scheme (Hansen et al., 2000), the BIOME-Biogeochemical Cycles (BGC) classification scheme described by Running et al. (2004), the Leaf Area Index (LAI) Biome scheme described by Myneni et al. (2002), the Plant Functional Type (PFT) scheme described by Bonan (2002) and the Land Cover Classification System (LCCS) scheme were provided in other to maximize the utility of the C6 MCD12Q1 data to science community. The land cover data is created applying supervised classification of MODIS reflectance data (Friedl *et al*., 2002, 2010).

According to Sulla-Menashe *et al*. (2018), accuracy assessment of the MCD12Q1 data shows that the Collection 6 product has an all-inclusive accuracy of 73.6% for the primary LCCS layer and that the amount of bogus land cover change has been

substantially reduced in Collection 6 relative to Collection 5 (1.6% in C6 and 11.4% in C5). The data are provided as tiles approximately 10° x 10° with a sinusoidal grid in HDF4 file format. However, the IGBP land cover classification was selected for this research as it is in close match with the default land use data in WRF. Table 3.1 shows the IGBP land use parameter's name, designated name value and the description of the features that made up the parameter name. Some of the parameters in some instance could not fill up the size of the pixel due to its lower resolution, and hence were mixed with other parameters as shown in Table 3.1.

Table 3.1: MCD12Q1 International Geosphere-Biosphere Programme (IGBP) legend and class descriptions.

Name	Value	Description
Evergreen Needleleaf Forests (ENF)	1	Dominated by evergreen conifer trees (canopy >2m). Tree cover >60%.
Evergreen Broadleaf Forests (EBF)	2	Dominated by evergreen broadleaf and palmate trees (canopy >2m). Tree cover >60%.
Deciduous Needleleaf Forests (DNF)	3	Dominated by deciduous needleleaf (larch) trees (canopy >2m). Tree cover >60%.
Deciduous Broadleaf Forests (DBF)	4	Dominated by deciduous broadleaf trees (canopy >2m). Tree cover >60%.
Mixed Forests (MF)	5	Dominated by neither deciduous nor evergreen (40-60% of each) tree type (canopy >2m). Tree cover >60%.
Closed Shrublands (CS)	6	Dominated by woody perennials (1-2m height) >60% cover.
Open Shrublands (OS)	7	Dominated by woody perennials (1-2m height) 10-60% cover.
Woody Savannas (WS)	8	Tree cover 30-60% (canopy >2m).
Savannas (Sa)	9	Tree cover 10-30% (canopy >2m).
Grasslands (Gr)	10	Dominated by herbaceous annuals (<2m).
Permanent Wetlands (PW)	11	Permanently inundated lands with 30-60% water cover and >10% vegetated cover.
Croplands (Cr)	12	At least 60% of area is cultivated cropland.
Urban and Built-up Lands (UBL)	13	At least 30% impervious surface area including building materials, asphalt, and vehicles.

Name	Value	Description
Cropland/Natural Vegetation Mosaics (CVM)	14	Mosaics of small-scale cultivation 40-60% with natural tree, shrub, or herbaceous vegetation.
Permanent Snow and Ice (PSI)	15	At least 60% of area is covered by snow and ice for at least 10 months of the year.
Barren (Br)	16	At least 60% of area is non-vegetated barren (sand, rock, soil) areas with less than 10% vegetation.
Water Bodies (WB)	17	At least 60% of area is covered by permanent water bodies.
Unclassified	255	Has not received a map label because of missing inputs.

Table 3.2: List of some Reclassified Land Cover Parameters

	Value	Name
All Forests	1 + 2 + 3 + 4 + 5	ENF + EBF + DNF + DBF + MF
All Shrublands	6 + 7	CS + OS
All Savannas	8 + 9	WS + Sa
All Croplands	12 + 14	Cr + CVM

*Value and Name is same as in Table 3.1

In other to get a more generalized classification, some close land cover parameters (LCPs) were reclassified into one unique class as ENF, EBF, DNF, DBF and MF were reclassified into All Forests, CS and OS were reclassified into All Shrublands, WS and Sa were re-classed into All Savannas, Cr and CVM into All Croplands (Table 3.2).

3.3 Climate Data

3.3.1 Gridded Station data

Simulated precipitation is assessed using the Tropical Rainfall Measurement Mission (TRMM; Huffman *et al*. 2007) and the Global Precipitation Climatology Project (GPCP; Huffman *et al*. 2009, 2016). The 0.25^{o} resolution TRMM 3B42 product was used as the standard for evaluating the model outputs because of its reliability and also that it is a merged dataset (i.e. combination of in-situ and satellite products) with high quality

precipitation estimates (Huffman *et al*. 2007). The GPCP is another genuine source for merged estimates computed from microwave, infrared, and sounder data observed by the international constellation of precipitation-related satellites and precipitation gauge analysis (Huffman *et al*. 2009). These datasets were used for the validation because the region (West Africa) is a data sparse region with a poorly spread synoptic weather station network, which is inadequate for validating the spatiotemporal distribution of the model results. In other to have a good comparison, all the data involve were interpolated to same horizontal resolution. However, TRMM and the simulated precipitation were interpolated to GPCP's horizontal resolution using the first order conservative remapping.

3.3.2 Boundary Condition Data

Initial and lateral boundary conditions are from European Centre for Medium-Range Weather Forecasts (ECMWF) Interim Re-Analysis (ERA-Interim) 6 hourly data, which has a horizontal resolution of 0.75° (Dee *et al*. 2011) and 6 hourly National Centers for Environmental Protection (NCEP) Final Analysis (FNL) initial soil data (sea surface temperature, soil moisture and temperature) from the NCAR's Computational and Information System Laboratory Research Data Archive (CISL RDA) with resolution of 1°. Simulated surface air temperature and dew-point temperature were assessed using the ERA-Interim dataset from the ECMWF. In other to enable good comparison with the simulations, FNL and the simulated temperature and dew point temperature were interpolated to the horizontal resolution of ERA-Interim using the bilinear interpolation.

3.4 Streamflow Data

The all-important in-situ streamflow data available is located at Goronyo in Sokoto state. The data is available since the inception of the dam, but due to

inconsistency, loss of records and in order to have a climatologically normal year, 2012 was chosen among the number of years made available. Promises were made to make more years available in the future.

3.5 Set-up of WRF model to Evaluate the Performance of Four LSMs

In this study, version 3.9.1.1 of WRF model (ARW) was used. For the first objective, eight different 3-month simulations of the December-February (DJF) 2011/2012 dry season and July-September (JAS) 2012 rainy season was carried out over West Africa. The periods were chosen to study the impact of choice of land surface model over different land surface conditions (i.e. wet and dry) that would affect the surface energy budget. West Africa has two distinct seasons; the dry season (November-April) and wet season (May-September), but JAS and DJF months were chosen because these are the periods that have the deep monsoon and high influence of Saharan dust respectively over the region.

The simulations were performed with a 12km horizontal resolution for a domain that encompasses latitude 10°S-30°N and longitude 28°W-28°E as shown in Figure 3.2. The first 15 days were used as spin-up, hence 16th of July to 29th September 2012 (JAS) for the rainy season and 16th of December 2011 to 28th February 2012 (DJF) for the dry season. Due to the absolute different behaviour of rainfall across the latitudes in the region, rainfall was analysed separately for each agroclimatological region according to Omotosho and Abiodun (2007), while air temperature and dew point temperature were analysed over 10°W – 10°E and 5° – 15°N so that the domain of interest is moved away from the errors introduced by boundary values. Regionalization is a normal practice in studying large regions that have spatial heterogeneity, as it enables in-depth comparative

examination of the sub-regions to characterize the distinctions in their behaviors with regard to phenomena of interest (Dezfuli and Nicholson, 2013).

The Noah LSM (as the most commonly used LSM) was used to test for four other different physics combinations (results not shown) in which the best combination was used with other three LSMs, which includes the Noah-MP, CLM4 and the Noah-MP GW. The Noah-MP GW is a new option including a free drainage soil lower boundary condition, a variable water table, 1-dimensional interaction with horizontal aquifer transport, but no river routing or overland flow scheme as in hydrological models. All parameterisation schemes apart from the LSMs were the same for all simulations. The new version of Rapid Radiative Transfer Model (RRTMG) based on Iacono *et al*. (2008) is selected for describing long wave and short wave radiative transfer within the atmosphere and to the surface, Mellor-Yamada Nakanishi and Niino Level 2.5 (MYNN2.5) scheme by Nakanishi and Niino (2006) was used for boundary-layer processes with a consistent MYNN surface layer scheme, new Tiedtke scheme (Zhang *et al*., 2011) is applied to parameterise the unresolved deep cumulus clouds and WRF Single-Moment 6-class (WSM6) scheme (Hong and Lim, 2006) for the microphysics scheme (as shown in Table 3.3). These were selected based on some preliminary tests that also agreed with the findings of Gbode *et al*. (2018) who carried out a verification study of many atmospheric physics combinations over West Africa.

Table 3.3: WRF Physics Options Used

Physics Categories	Selected scheme options	Reference
Cumulus Parameterisation	New Tiedtke scheme	Zhang et al. (2011)
Longwave Radiation	New version of Rappid Radiative Transfer Model (RRTMG)	Iacono et al. (2008)
Microphysics	WRF Single-Moment 6-class (WSM6)	Hong and Lim (2006)

Physics Categories	Selected scheme options	Reference
Planetary Boundary layer	Mellow-Yamada Nakanishi and Niino Level 2.5 (MYNN2.5)	Nakanishi and Niino (2006)
Shortwave Radiation	New version of Rappid Radiative Transfer Model (RRTMG)	Iacono et al. (2008)

3.6 Method of Model Evaluation

In other to examine how each model performs when compared with the observation, Taylors diagram was used for the evaluation. The Taylor diagram can concisely summarize the degree of agreement between simulated and observed variables (Taylor, 2001). The correspondence amongst different patterns is quantified by their correlation, their centred root mean square difference and their standard deviations. Houghton *et al*. (2001) stressed that the diagram is useful specifically in evaluating multiple aspects of complex models or in gauging the relative skills of many dissimilar models. The Taylor diagram generally characterizes the statistical relationship between two fields, a forecast field (representing a field simulated by a model) and an observation field, which serves as the reference for the comparison. (Taylor, 2001). The location of each model on the diagram describes how closely the model's output pattern corresponds with the observations. However, each model point in the diagram represents the correlation, the standard deviation and the centered RMS and are related by the following equations:

$$E'^2 = \sigma_f^2 + \sigma_o^2 - 2\sigma_f\sigma_o R \qquad (3.1)$$

where: R is the correlation coefficient between the forecast and observation fields;

E' is the centered root mean square (RMS) difference between the fields; and

σ_f^2 and σ_o^2 are the variances of the forecast and the observation fields respectively. The second order statistics can be calculated with the equations 3.2 to 3.5:

$$R = \frac{\frac{1}{N}\sum_{n=1}^{N}(f_n - \bar{f})(r_n - \bar{r})}{\sigma_f \sigma_o} \tag{3.2}$$

$$E' = \frac{1}{N}\sum_{n-1}^{N}\left[(f_n - \bar{f}) - (r_n - \bar{r})\right]^2 \tag{3.3}$$

$${\sigma_f}^2 = \frac{1}{N}\sum_{n-1}^{N}(f_n - \bar{f})^2 \tag{3.4}$$

$${\sigma_r}^2 = \frac{1}{N}\sum_{n-1}^{N}(r_n - \bar{r})^2 \tag{3.5}$$

where the overall mean of a field is indicated by an overbar. In the case of a time-independent field, the sum is computed over all grid cells.

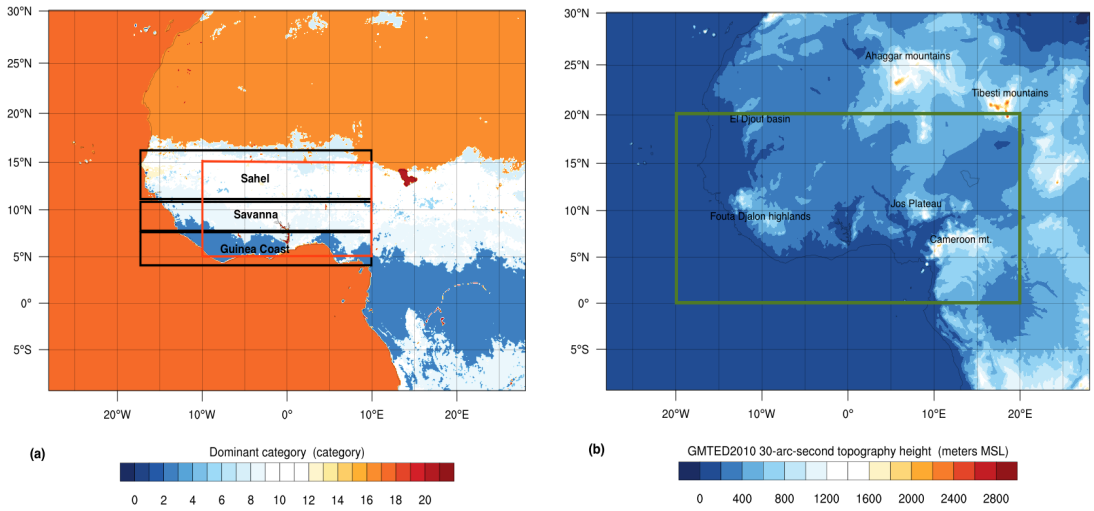

Figure 3.2: (a) Map showing the Model domain with different land use categories. The different regionalization of West Africa according to Omotosho and Abiodun (2007) i.e. Guinea (coast – 8°N), Savana (8°N – 11°N), and the Sahel (11°N –16°N) for precipitation analysis. The red box (5°N – 15°N, 10°E – 10°W) is the domain for area average of the parameters, (b) Elevation map of West Africa. The green box is the evaluation area for the spatial plots.

3.7 Setup of WRF to Assess the Impacts of LULC Change on WRF Outputs Over West Africa

The study utilizes version 3.9.1.1 WRF model for six different runs of 3-month simulations for December-February (DJF) 2011/2012 dry season and July-September (JAS) 2012 rainy season over West Africa. Apart from the simulation with the default land use data in the model for both the dry and rainy season, which serves as the control simulation, two other experiments were carried out; experiment 1 was carried out using the 2016 MCD12Q1 MODIS LULC data incorporated into the model, and experiment 2 using 2001 MCD12Q1 MODIS LULC data incorporated into the model also for both dry and rainy season. The simulations were carried out with a 12km horizontal resolution for a domain that encompasses latitude 10°S-30°N and longitude 28°W-28°E, same as shown in Figure 3.2. The Initial and lateral boundary conditions are ERA-Interim data, which has horizontal resolution of 0.75° (Dee et al., 2011) and NCEP FNL initial soil data (sea surface temperature, soil moisture and temperature) from the NCAR's CISL RDA (NCEP FNL 2000) with resolution of 1°. The first 15 days were used as spin-up. Same physics combination as in Table 3.3 was used except for the LSM in which Noah LSM was used here.

Thirteen (13) granules of MCD12Q1 satellite data covering West Africa was downloaded from MODIS website https://search.earthdata.nasa.gov/. The data was mosaiced, reprojected and resampled using the MODIS reprojection tool (MRT) in other to make it compatible with WRF projection. Each LULC data files were converted to a single binary file that supports the format required by WRF model using some specialized tools. The preprocessed LULC data were interpolated in each domain by the

nearest neighbor method using the Geogrid program in the WRF Processing System (WPS). Also, the Ungrib program was used to extract the meteorological fields from GRIB-formatted files. The Metgrid program was used to horizontally interpolate the extracted fields from Ungrib with the land surface data that was processed through Geogrid program. Hoewver, the incorporated satellite data would impact the LSM that have the potential to adjust the variables of the vapourisation, vegetation fraction, albedo e.t.c of each grid in each grid for every domain and would affect the WRF model in simulating the parameters. Hence, the default land use data in WRF were changed with each new MCD12Q1 LULC data and were incorporated into the WRF model and hence, any difference in the output from experiment 1 and 2 is as a result of the change in LULC data between 2001-2016. Table 3.4 shows the set up of the time and land cover data used for each experiment.

Table 3.4: Arrangement of the Simulation Tests

Test	Test period	Land cover data used
Control Simulation	July-September JAS 2012 and December-February DJF 2011/2012	WRF default land cover data
Experiment 1	July-September JAS 2012 and December-February DJF 2011/2012	MODIS MCD12Q1 land cover data of 2016
Experiment 2	July-September JAS 2012 and December-February DJF 2011/2012	MODIS MCD12Q1 land cover data of 2001

3.8 Response of The Hydro-Meteorological Parameters to Different Land Cover Scenarios in West Africa

3.8.1 Comparison Between WRF Simulations with Default LULC Data and the Incorporated Satellite Data

In other to justify the incorporation of satellite data in the model over West Africa, two 5 months (May-September) simulations were carried out with the WRF default LULC data and the MCD12Q1 satellite data, using with same domain as in Figure 3.2, and same physics option as in Table 3.3. Noah-MP LSM was used and the first 20 days was used as spin-up. Analysis was carried out for 2 m air temperature and precipitation and the two outputs compared against the observation. Precipitation is compared against TRMM while 2 m temperature was compared against ERA-Interim.

3.8.2 Response of Air Temperature, Dew Point Temperature, Sensible Heat, Rainfall, Evapotranspiration to Different Land Cover Scenarios in WA

In other to study the response of air temperature, dew point temperature, rainfall and evapotranspiration to different land cover scenarios in West Africa, six different land cover scenarios were generated for Built Up (BU), Partial Deforest I (PDI), Partial Deforest II (PDII), Partial Afforest (PA), Total Afforest (TA) and Total Deforest (TD) as shown in Figure 3.3. The LULC scenarios were generated by changing some LU variables into another type as follows: for BU scenario, all parameter value 11 and 12 (description of parameter value is shown in Table 3.5) were changed into 13; for PDI, parameter value 8, 9, 12 and 14 were changed into 10 (i.e. Grasslands), then, all parameter Value 1-7 were changed into parameter value 9 (i.e. Savanna); for PDII, all parameter Value 1-8 were changed into parameter Value 9 (i.e. Savanna); for PA, parameter value 8 was changed into parameter value 2, parameter value 9 was changed

into parameter value 8, then parameter value 10 was changed into 9; for TA, all parameter value 5-10, 12 and 14 were changed into parameter value 2 (i.e. Evergreen Broadleaf Forests); for TD, all parameter value 1-10, 12 and 14 were changed into parameter value 16 (i.e. Barren lands).

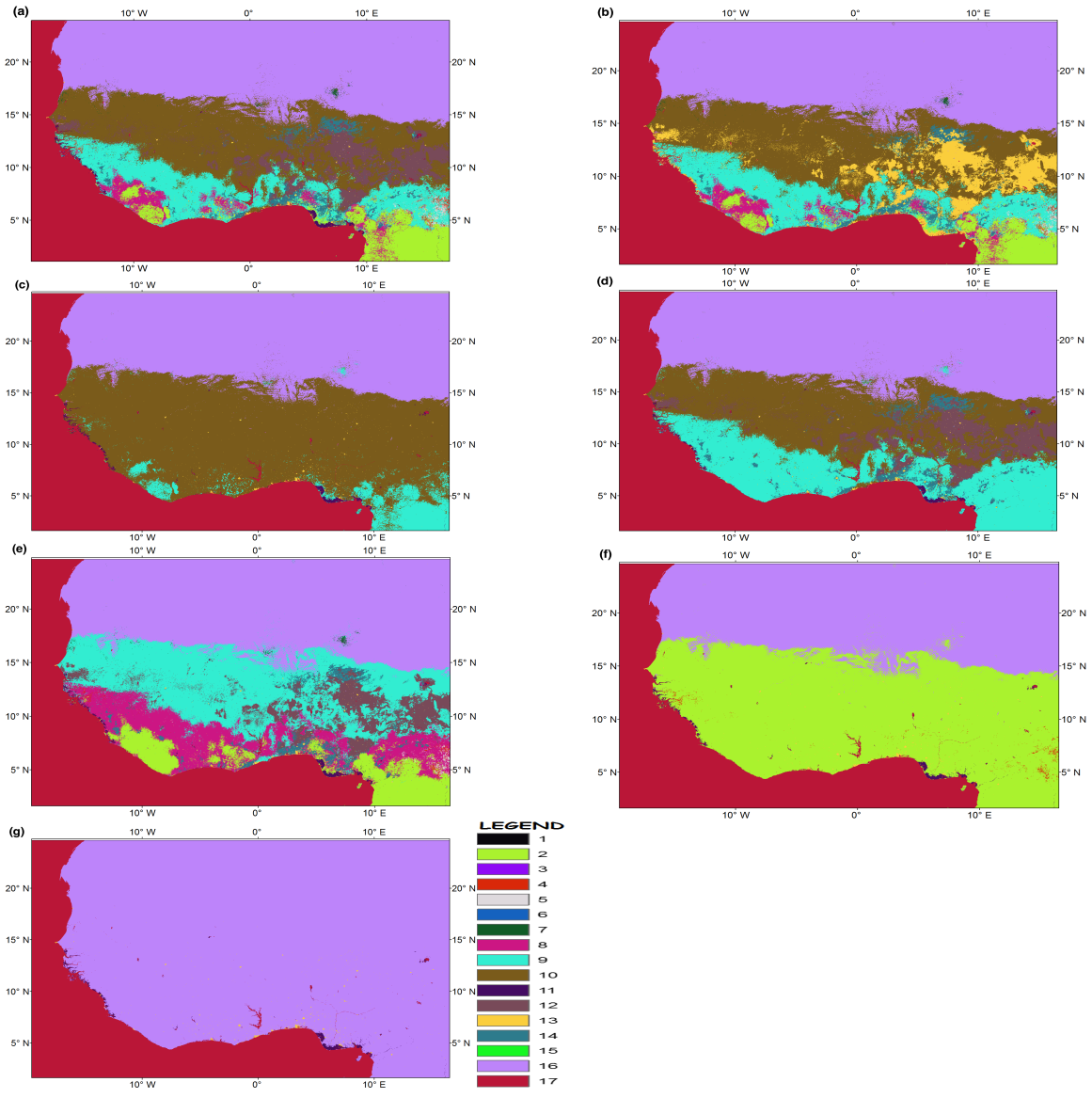

Figure 3.3: Different LULC scenarios Used for the Simulations over West Africa (a) 2012 control, (b) Built Up, (c) Partial Deforest I, (d) Partial Deforest II (forest to savanna), (e) Partial Afforest, (f) Total Afforest, (g) Total Deforest. Legend value is same as in Table 3.5

Table 3.5: Percentage Cover of Each LULC Parameters in Terms of Pixel Counts for Each Scenario Over West Africa

LULC variables	Value	Co	BU	PDI	PDII	PA	TA	TD
Evergreen Needleleaf Forests	1	0.0	0.0	0.0	0.0	0.0	0.0	0.0
Evergreen Broadleaf Forests	2	5.0	5.0	0.0	0.0	7.0	41.1	0.0
Deciduous Needleleaf Forests	3	0.0	0.0	0.0	0.0	0.0	0.0	0.0
Deciduous Broadleaf Forests	4	0.4	0.4	0.0	0.0	0.4	0.4	0.0
Mixed Forests	5	0.3	0.3	0.0	0.0	0.3	0.0	0.0
Closed Shrublands	6	0.0	0.0	0.0	0.0	0.0	0.0	0.0
Open Shrublands	7	0.1	0.1	0.0	0.0	0.1	0.0	0.0
Woody Savannas	8	1.9	1.9	0.0	0.0	8.6	0.0	0.0
Savannas	9	8.6	8.6	5.8	16.4	18.6	0.0	0.0
Grasslands	10	18.6	18.6	35.7	18.6	0.0	0.0	0.0
Permanent Wetlands	11	0.3	0.0	0.3	0.3	0.3	0.3	0.3
Croplands	12	5.2	0.0	0.0	5.2	5.2	0.0	0.0
Urban and Built-up Lands	13	0.2	5.7	0.2	0.2	0.2	0.2	0.2
Cropland/Natural Vegetation Mosaics	14	1.4	1.4	0.0	1.4	1.4	0.0	0.0
Permanent Snow and Ice	15	0.0	0.0	0.0	0.0	0.0	0.0	0.0
Barren	16	33.1	33.1	33.1	33.1	33.1	33.1	74.6
Water bodies	17	24.9	24.9	24.9	24.9	24.9	24.9	24.9

Co, BU, PDI, PDII, PA, TA and TD are the LULC scenarios for West Africa, i.e. Control, Built Up, Partial Deforest I, Partial Deforest II, Partial Afforest, Total Afforest and Total Deforest respectively.

Table 3.5 shows the percentage cover of each LULC parameters in terms of pixel counts for the Control (Co) and each Scenario over West Africa. Each created LULC scenario data files were converted to a single binary file that supports the format required by WRF model, and Seven 5 months (May-September) simulations were carried out using Noah-MP LSM, and the first 20 days as spin-up. Noah-MP LSM was used here as it proved to be the best LSM for West Africa from the previous analysis in this research. Other physics combination used was the same as in Table 3.3.

3.8.3 Response of Stramflow to different Land Cover Scenarios in Sokoto Rima River Basin (SRRB), West Africa

In other to study the response of streamflow to different land cover scenarios in the Sokoto Rima River Basin (SRRB), five different land cover scenarios were generated for Built Up (BU), Partial Deforest (PD), Partial Afforest (PA), Total Afforest (TA) and Total Deforest (TD) as shown in Figure 3.4. The LULC scenarios were generated by changing some LU variables into another type as follows: for BU scenario, all parameter value 12 (description of parameter value is shown in Table 3.6) was changed into 13; for PD, parameter value 12 and 14 were changed into 10 (i.e. Grasslands), then, all parameter Value 7 was changed into parameter value 9 (i.e. Savanna); for PA, parameter value 10 was changed into 9; for TA, all parameter value 7, 10, 12 and 14 were changed into parameter value 2 (i.e. Evergreen Broadleaf Forests); for TD, all parameter value 7, 10, 12 and 14 were changed into parameter value 16 (i.e. Barren lands). However, Table 3.6 shows the percentage cover of each LULC parameters in terms of pixel counts for the Control (Co) and each Scenario over West Africa.

WRF-Hydro modelling system version 5.0 (Gochis *et al*., 2018) forced with WRFV3.9.1 was used to simulate the response of streamflow to different land cover scenarios over the Sokoto Rima River Basin (SRRB) in the Niger River catchment. The setup of the atmospheric model (WRF) to generate the parameters to force the hydrological model (WRF-hydro) as shown in Figure 3.5, comprises of a parent domain (Figure 3.5a) at 12 km horizontal resolution and the nested domain (Figure 3.5b) at 4 km. The Simulation was carried out for 2 years (2011-2012). Noah-MP LSM was used with other physics combination as in Table 3.3.

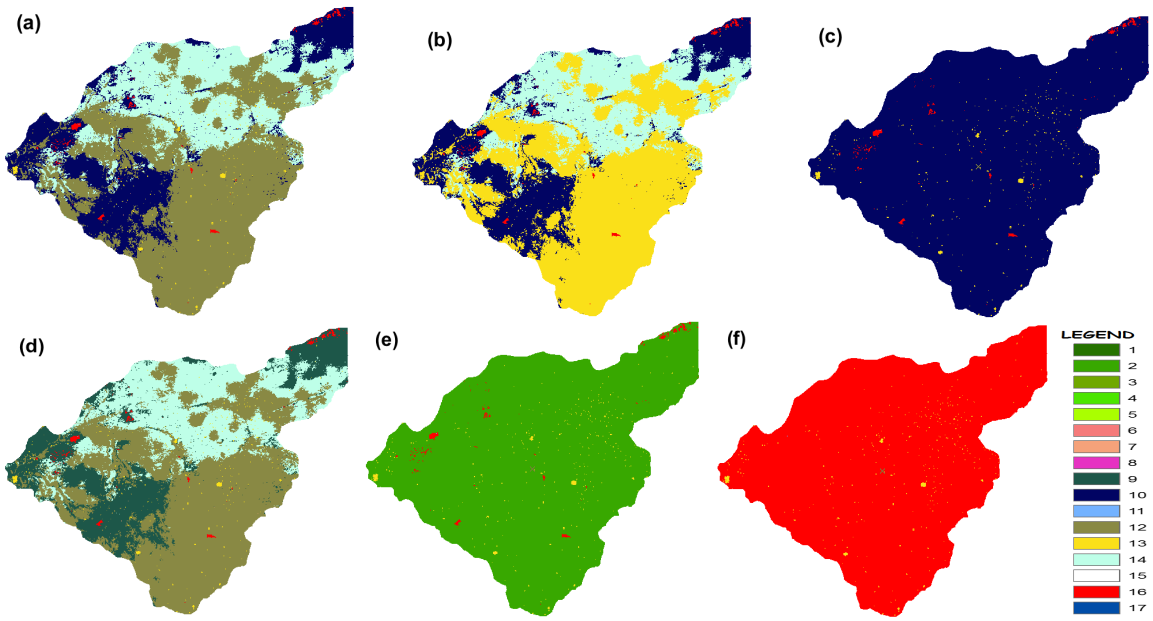

Figure 3.4: Different LULC scenarios Used for the Simulations Over the SRRB (a) 2012 control, (b) Built Up, (c) Partial Deforest, (d) Partial Afforest, (e) Total Afforest, (f) Total Deforest. Legend Value is same as in Table 3.5

Table 3.6: Percentage Cover of Each LULC Parameters in Terms of Pixel Counts for Each Scenario Over SRRB

LULC Parameters	Value	Co	BU	PD	PA	TA	TD
Evergreen Broadleaf Forests	2	0.000	0.000	0.000	0.000	98.859	0.000
Open Shrublands	7	0.011	0.011	0.000	0.011	0.000	0.000
Savannas	9	0.000	0.000	0.011	22.180	0.000	0.000
Grasslands	10	22.180	22.180	98.849	0.000	0.000	0.000
Permanent Wetlands	11	0.001	0.000	0.001	0.001	0.001	0.001
Croplands	12	50.126	0.000	0.000	50.126	0.000	0.000
Urban and Built-up Lands	13	0.630	50.757	0.630	0.630	0.630	0.630
Cropland/Natural Vegetation Mosaics	14	26.543	26.543	0.000	26.543	0.000	0.000
Barren	16	0.510	0.510	0.510	0.510	0.510	99.369

Co, BU, PD, PA, TA and TD are the LULC scenarios for SRRB, i.e. Control, Built Up, Partial Deforest, Partial Afforest, Total Afforest and Total Deforest respectively.

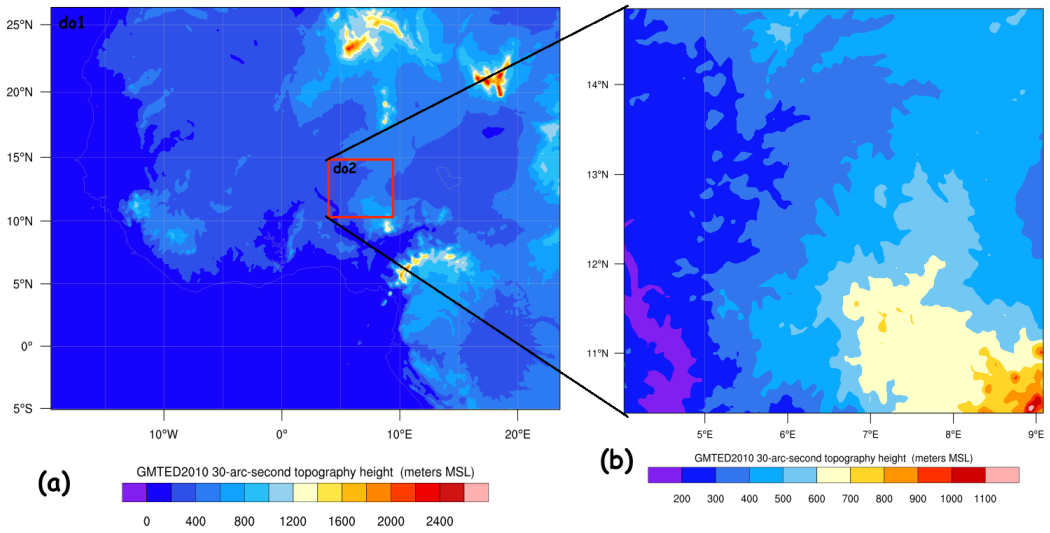

Figure 3.5: Map showing the terrain of the WRF domain for the WRF-Hydro Simulations, do1 is the main domain and do2 is the nested domain for WRF-hydro Simulations (a) is at 12 km and (b) the nested domain at high resolution of 4 km.

Nevertheless, considering the fact that the spatial resolution of the nested domain is within the convective permitting scale (i.e. between 3 and 5 km) in which the cumulus activities would be resolved, the cumulus scheme for the nested domain was switched off. The routing grid is determined by the nested domain from WRF at 400 m horizontal resolution in other to compute the overland routing. Furthermore, Geographic Information System (GIS) tool is used to delineate of the basin. The processing workflow used in creating the WRF-Hydro routing grids is available as an ArcGIS Python Toolbox, which is implemented in the ArcGIS Desktop. The motive of the WRF Hydro GIS Pre-Processing Tool is for the creation of the data layers for terrestrial overland flow, subsurface flow and channel routing processes vital for the WRF Hydro simulations.

The geogrid files generated from the WRF Processing System (WPS) version 3.9.1 component of WRF model were processed as the input static data for WRF-Hydro model. Another input for creating the WRF-Hydro routing grids is a Comma-Separated Values

(CSV; .csv) formatted file format of Goronyo guage location and other locations (i.e. forecast points FP) for Sokoto and Bakolori in latitude/longitude coordinates (WGS84).

The high quality and high-resolution terrain dataset (digital elevation model-DEM) is a very important input parameter required in this process, which drives the output layers. Hydrologically conditioned DEM datasets are often integrated with hydrographic data such as shapefiles of rivers or lakes. However, the terrain processing is only successful when the input DEM has been hydrologically processed to ensure continuous flow paths. For this research, multiple tiles of the 3 arc-second GRID USGS HydroSHEDS DEM datasets from http://hydrosheds.cr.usgs.gov. These tiles were mosaicked and the area that matches the size of the geogrid file was masked out. A required Regridding Factor (RF) parameter of 10 was chosen. The RF allows the user to set the output cell size for the derived datasets based on a relationship to the cell size in the GEOGRID file inputted. Consequently, the output high-resolution datasets from the WRF-Hydro preprocessing must have the capacity to nest perfectly with the coarse geogrid resolution, and the resolute on of the geogrid is divided by the regridding factor to obtain the horizontal resolution of the WRF-Hydro. So, the sub-grid for this study is obtained by dividing the inner domain by a regridding factor of 10. The least possible number of pixels to define a stream segment for this simulation was chosen as 4. Smaller value of this number will yield higher drainage density of the resulting channel network (i.e. CHANNELGRID) file. Henceforth, the geogrid file could be processed from the ArcGIS tool and a series of netCDF format output files that becomes the WRF-Hydro simulations static data are generated.

3.8.4 WRF-Hydro Model Calibration

The calibration of the hydrological models is important in other that the model will simulate the right flow over a particular area of study before applying it for any hydrological study. The calibration was carried out based on the discharge at Goronyo forecast point. The stations coordinates were placed in the preprocessing of the basin data for the hydrological model. The calibrated model was used to simulate streamflow for each LULC scenario as described. For gauged rivers, calibration information (studies) of another watershed of similar geographical characteristics could be used as a basis in the calibration process (Naabil *et al*. 2018). This however justifies the use of the model for other FPs in the study. The calibration of the model was focused on the infiltration factor (REFKDT). The REFKDT is a turnable parameter in the WRF-hydro model that significantly influences the surface infilteration, and hence the partitioning of total runoff into surface and sub-surface runoff. Increaseing the value of REFKDT decreases the surface run off and vice versa. This approach ensures that the model is capable of simulating the streamflow at the gauges, and then the amount of water is correctly distributed in time (Yucel *et al*., 2015). In tuning the model parameters the optimum streamflow estimates during calibration were assessed using statistical measures (e.g Root Mean Square Error RMSE, Percentage Bias PBias, Pearson's correlation coefficient and Nash-Sutcliffe efficiency NSE index). The bias statistic shows sensitivity toward hydrograph volumes, R^2 shows sensitivity toward temporal variation of discharge, whereas Nash-Sutcliffe and RMSE statistics describes both characteristics (Gupta *et al*., 2009; Yucel *et al*., 2015). The choice of different REFKDT values influences the amount

of water that infiltrates or makes it to the channel network as streamflow. Tested values of REFKDT during calibration were 3, 1.5, 1.0, 0.7, 0.6, and 0.5.

3.8.5 Assessment of WRF-Hydro Model Calibration

In other to ensure that the WRF-hydro simulation is comparable to the reality, three error statistics, which includes, PBias, NSE, and Pearson correlation coefficient (r) were performed. The equations for computing the listed statistical approaches are described below;

$$PBias = \sum_{t=1}^{N}\left(q_t{}^{obs} - q_t{}^{sim}\right) / \sum_{t=1}^{N} q_t{}^{obs} \; X \; 100 \tag{3.6}$$

$$NSE = 1 - \sum_{t=1}^{N}\left(q_t{}^{sim} - q_t{}^{obs}\right)^2 / \sum_{t=1}^{N}(q_t{}^{obs} - q^{mean})^2 \tag{3.7}$$

$$r = \frac{n(\sum xy) - (\sum x)(\sum y)}{\sqrt{\left[n\sum x^2 - (\sum x)^2\right]\left[n\sum y^2 - (\sum y)^2\right]}} \tag{3.8}$$

where x is the observed and y is the simulated value

These statistical equations provide some perspectives regarding the performance of the model. The PBias measures the average tendency of the simulated value to be larger or smaller than the observed. Positive values indicate a model bias toward overestimation, whereas negative values are an indication of underestimation (Gupta *et al*., 1999). The Nash-Sutcliffe efficiency (NSE) gives normalized indicators of model performance. It measures the relative magnitude of the residual variance (called "noise") to the variance of the flows ("information") (Nash and Sutcliffe, 1970). The optimal value for NSE is 1.0, and therefore for a "minimally acceptable" performance of the model, values should be larger than 0.0. Where the value is less than 0.0, it indicates that the mean observed

flow is a better predictor than the model. The closer the NSE is to 1, the more accurate the model is. The Pearson's Correlation (r) measures the similarity in the spatial or temporal patterns between two datasets. A perfect linear relationship having a positive slope will have correlation coefficient r = 1, and perfect linear relationship having a negative slope will have correlation coefficient r = -1. So, in this case, it is the relationship between simulated streamflow and observed streamflow. However, a correlation coefficient of zero shows there is no relationship.

CHAPTER FOUR

RESULTS AND DISCUSSION

4.1 Land Use Land Cover Change analysis over West Africa

Figure 4.1 show the spatial LULC map of the study area derived from MODIS data, although the changes could not be easily seen from the map due to the size of the area. Most of the areas were covered by Water body (WB) (although this composed mostly the Atlantics), Barren (Ba), Grasslands (Gr) and Savannas (Sa). The Evergreen Broadleaf Forests (EBF) is mostly dominant around the Cameroon forests in the area. Table 4.1 shows the number of pixels covered by each Land Cover Parameter (LCP). The average number of pixels count of each LCP in decreasing order is as follows; Baren (Br) (16865008), Water Bodies (WB) (12679762), Grasslands (Gr) (9323662), Savannas (Sa) (4439618), Croplands (Cr) (2709204), Evergreen Broadleaf Forests (EBF) (2563741), Woody Savannas (WS) (926769), Cropland/Natural Vegetation Mosaics (CVM) (718074), Deciduous Broadleaf Forest (DBF) (216468), Permanent Wetlands (PW) (151755), Mixed Forest (MF) (131794), Urban and Built-up Lands (UBL) (74504), Open Shrublands (OS) (42536), Closed Shrublands (CS) (416) and Evergreen Needleleaf Forests (ENF) (28). The percentage coverage of each parameter as presented in Table 4.2, shows that Br, WB, Gr, Sa and Cr have the highest average coverage of 33.17% (of the entire area), 24.94% (mostly the Atlantic ocean), 18.34%, 8.73% and 5.33% respectively over the study period (Fuller and Ottke, 2002). Others like ENF, EBF, DBF, MF, CS, OS, WS, PW, UBL, CVM each covered 0.0%, 5.04%, 0.43%, 0.26%, 0.0%, 0.08%, 1.82%, 0.30, 0.15% and 1.41 of the entire area respectively. In general, all forest covers 5.73%, all shrublands covers 0.08%, all savannas covers 10.55% and all croplands covers

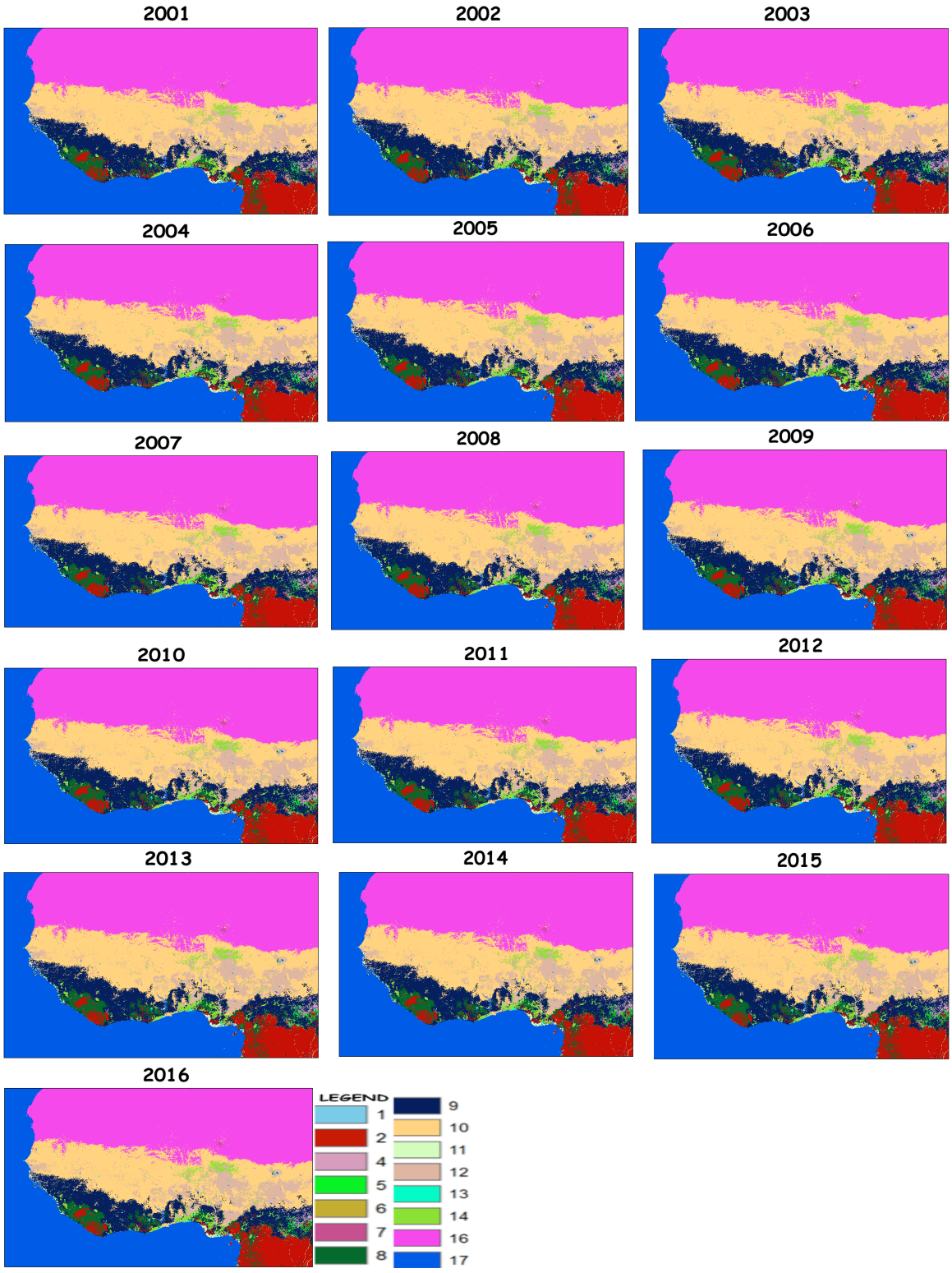

Figure 4.1: LULC Analysis for West Africa From 2001 to 2016.
Legend Value (1 – 17) is the same as in Table 3.5

Table 4.1: Number of Pixels covered by each LCP between 2001 and 2016 over West Africa

LCP*	2001	2002	2003	2004	2005	2006	2007	2008
ENF	35	22	25	24	27	22	23	22
EBF	2515270	2572737	2600934	2622621	2629566	2611793	2587701	2575327
DBF	237664	237821	241138	240073	233528	229630	230960	226832
MF	102448	107676	112308	116382	113844	110218	117456	124462
CS	870	642	758	977	469	282	177	173
OS	47725	46341	42430	39976	38892	38796	39369	40431
WS	913922	888414	858850	851439	850684	859185	867907	892703
Sa	4486105	4508769	4518110	4507484	4507723	4513300	4504687	4484971
Gr	9057297	9060404	9131587	9211426	9286418	9329716	9349075	9337578
PW	144056	145379	149389	151874	149587	153125	149331	148371
Cr	2866859	2839998	2781865	2701650	2685268	2678910	2688578	2700000
UBL	66436	68001	68797	70036	70846	72232	73221	74085
CVM	711389	676457	686107	706735	704806	707781	721186	717353
Br	17013104	17010642	16971123	16942827	16891889	16858543	16833945	16841300
WB	12680108	12679989	12679872	12679770	12679748	12679762	12679679	12679687

2009	2010	2011	2012	2013	2014	2015	2016	Average
21	24	33	34	34	35	32	33	28
2573143	2564777	2569763	2552879	2540647	2516315	2501395	2484985	2563741
211978	210520	208815	201700	191802	188168	188754	184103	216468
139883	147075	150208	153290	150918	151241	154459	156114	131749
247	747	402	252	163	174	161	165	416
42531	43934	44660	44319	43725	42871	42471	42102	42536
915884	945877	963613	982616	994892	1006908	1010510	1024898	926769
4448913	4413140	4384569	4379504	4370965	4354348	4330683	4320624	4439618
9348237	9385435	9424226	9454243	9465310	9462613	9452902	9422127	9323662
152290	153681	153274	152437	154070	156513	158318	156383	151755
2688576	2677476	2654573	2647556	2646995	2660017	2697971	2730976	2709204
75104	75998	77175	78171	79040	79921	81117	81888	74504
719206	713025	707984	708952	729664	752128	756436	769980	718074
16847643	16831944	16824362	16807843	16795135	16792211	16788274	16789339	16865008
12679638	12679642	12679637	12679498	12679935	12679831	12679812	12679578	12679762

*See Table 4.4 for definition of Land Cover Parameters (LCPs)

Table 4.2: Percentage Coverage of each Land Cover Parameter (LCP) Between 2001 and 2016 Over West Africa

LCP*	2001	2002	2003	2004	2005	2006	2007	2008	2009	2010	2011	2012	2013	2014	2015	2016	Mean Perc.
ENF	0.00	0.00	0.00	0.00	0.00	0.00	0.00	0.00	0.00	0.00	0.00	0.00	0.00	0.00	0.00	0.00	0.00
EBF	4.95	5.06	5.12	5.16	5.17	5.14	5.09	5.07	5.06	5.04	5.05	5.02	5.00	4.95	4.92	4.89	5.04
DBF	0.47	0.47	0.47	0.47	0.46	0.45	0.45	0.45	0.42	0.41	0.41	0.40	0.38	0.37	0.37	0.36	0.43
MF	0.20	0.21	0.22	0.23	0.22	0.22	0.23	0.24	0.28	0.29	0.30	0.30	0.30	0.30	0.30	0.31	0.26
CS	0.00	0.00	0.00	0.00	0.00	0.00	0.00	0.00	0.00	0.00	0.00	0.00	0.00	0.00	0.00	0.00	0.00
OS	0.09	0.09	0.08	0.08	0.08	0.08	0.08	0.08	0.08	0.09	0.09	0.09	0.09	0.08	0.08	0.08	0.08
WS	1.80	1.75	1.69	1.67	1.67	1.69	1.71	1.76	1.80	1.86	1.90	1.93	1.96	1.98	1.99	2.02	1.82
Sa	8.82	8.87	8.89	8.87	8.87	8.88	8.86	8.82	8.75	8.68	8.62	8.61	8.60	8.56	8.52	8.50	8.73
Gr	17.81	17.82	17.96	18.12	18.26	18.35	18.39	18.37	18.39	18.46	18.54	18.59	18.62	18.61	18.59	18.53	18.34
PW	0.28	0.29	0.29	0.30	0.29	0.30	0.29	0.29	0.30	0.30	0.30	0.30	0.30	0.31	0.31	0.31	0.30
Cr	5.64	5.59	5.47	5.31	5.28	5.27	5.29	5.31	5.29	5.27	5.22	5.21	5.21	5.23	5.31	5.37	5.33
UBL	0.13	0.13	0.14	0.14	0.14	0.14	0.14	0.15	0.15	0.15	0.15	0.15	0.16	0.16	0.16	0.16	0.15
CVM	1.40	1.33	1.35	1.39	1.39	1.39	1.42	1.41	1.41	1.40	1.39	1.39	1.44	1.48	1.49	1.51	1.41
Br	33.46	33.46	33.38	33.32	33.22	33.16	33.11	33.12	33.14	33.11	33.09	33.06	33.03	33.03	33.02	33.02	33.17
WB	24.94	24.94	24.94	24.94	24.94	24.94	24.94	24.94	24.94	24.94	24.94	24.94	24.94	24.94	24.94	24.94	24.94

*See Table 4.4 for definition of Land Cover Parameters (LCPs)

Table 4.3: Percentage Change in the Analysis of Land Cover Parameters (LCP) Between 2001-2016 Over West Africa

LCP*	Percentage change
Evergreen Needleleaf Forests (ENF)	-5.71
Evergreen Broadleaf Forests (EBF)	-1.2
Deciduous Broadleaf ForestsDBF)	-22.54
Mixed Forests (MF)	52.38
Closed Shrublands (CS)	-81.03
Open Shrublands (OS)	-11.78
Woody Savannas (WS)	12.14
Savannas (Sa)	-3.69
Grasslands (Gr)	4.03
Permanent Wetlands (PW)	8.56
Croplands (Cr)	-4.74
Urban and Built-up Lands (UBL)	23.26
Cropland/Natural Vegetation Mosaics (CVM)	8.24
Barren (Br)	-1.32
Water bodies (WB)	0.00

*See Table 4.4 for definition of Land Cover Parameters (LCPs)

6.74% (Fuller and Ottke, 2002), Fairhead and Leach, (1998) however indicated that that additional large-scale tropical moist forest covered the humid belt in Guinea, Sierra Leone, Liberia, Ghana, Cote d'Ivoire, and Nigeria before the 20th century.

Between 2001 and 2016, Br decreased from 17013104 to 16789339 pixel count (33.46% in 2001 to 33.02 % in 2016) (Table 4.1 and 4.2), WB decreased from 12680108 to 12679578 pixel count, Gr increased from 9057297 to 9422127 pixel count (17.81% in 2001 to 18.53% in 2016), Sa decreased from 4486105 to 4320624 pixel count (8.82% in 2001 to 8.50% in 2016), Cr decreased from 2866859 to 2730976 pixel count (5.64% in 2001 to 5.37% in 2016). Also, EBF decreased from 2515270 to 2484985 pixel count (4.95% in 2001 to 4.89% in 2016), WS increased from 913922 to 1024898 pixel count (1.80% in 2001 to 2.02% in 2016), CVM increased from 711389 to 769980 pixel count (1.40% in 2001 to 1.51% in 2016), DBF decreased from 237664 to 184103 pixel count

(0.47% in 2001 to 0.36% in 2016). In addition, PW increased from 144056 to 156383 pixel count (0.28% in 2001 to 0.31% in 2016), MF increased from 102448 to 156114 pixel count (0.20% in 2001 to 0.31% in 2016), UBL increased from 66436 to 81888 pixel count (0.13% in 2001 to 0.16% in 2016), OS decreased from 47725 to 42102 pixel count (0.09% in 2001 to 0.08% in 2016), CS decreased from 870 to 165 pixel count (0.09% in 2001 to 0.08% in 2016), and ENF decreased from 35 to 33 pixel count.

From Table 4.3, CS has the highest percentage change between 2001 and 2016 (-81.03%), while EBF has the least percentage change. Also, in terms of change in pixel count coverage, Gr has the highest increase (364830), Br has the highest decrease (223765 pixel count) (Figure 4.3).

Figure 4.2 shows the behavior of each LCP over the years from 2001 to 2016. EBF increased between 2001 and 2005 and start decreasing till 2016. The DBF decreased all through the years, while the MF increased all through the study period. ENF decreased sharply between 2001 and 2002, and became a little steady till 2010, and then start increasing till 2016. The CS increased in 2004 and 2010 and decreased in all other years while OS decreased till 2006 and starts increasing from 2007, but begin to decrease again in 2012. The Gr increased all through the period while PW also averagely increases throughout the period (although there were instances of decrease in 2005 and 2008). Cr decreased 2006, from then increased till 2008, and again decreases till 2013 and thereafter increased till 2016. CVM decreased in 2002 and then increased all through with a little decline in 2010, 2011 and 2012. The UBL increased throughout the entire period, while Br decreased throughout the period except for 2008 and 2009. The WB decreased from 2001 till 2012, increased in 2013, thereafter decreased from then till

2016. The re-classified classes were also analysed and presented in Figure 4.4. The croplands were seen to decrease from 2001 to 2006 and then increase up till 2008 and then decreases till 2012 and kept going higher till 2016. The Savannas decreased till 2005, increases from then till 2008 and went down until 2011. It then goes up again in 2013 and finally gets to the lowest decrease in 2015. The forests increased to the highest size in 2004 and then decreased till 2016 (the year with the lowest size).

From Table 4.4, EBF, DBF, CS, OS, Sa, Cr, Br, WB, All Forests, All Shrublands, All Savannas and All Croplands showed decreasing trend over the years while ENF, MF, WS, Gr, PW, UBL, CVM showed increasing trend over the period.

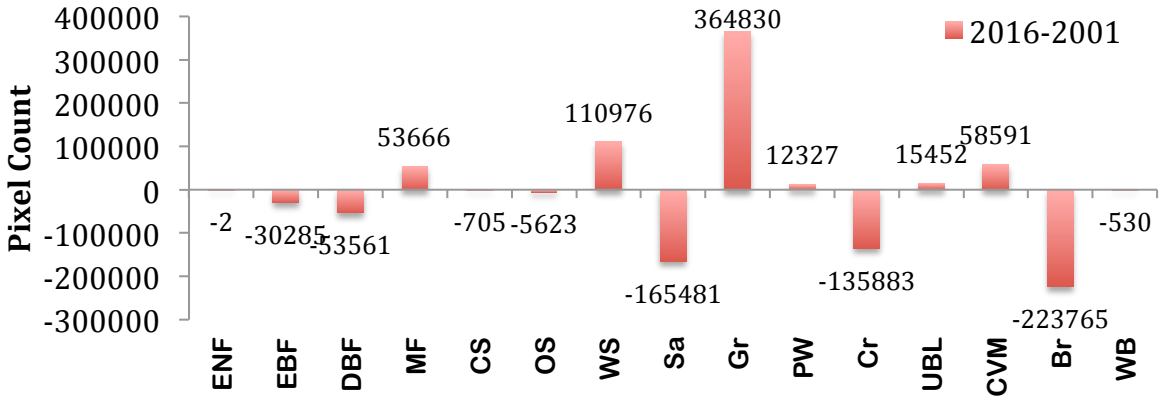

Figure 4.2: Land Use Land Cover Change Difference Between 2001 and 2016. Horizontal axis label is same as Table 4.4

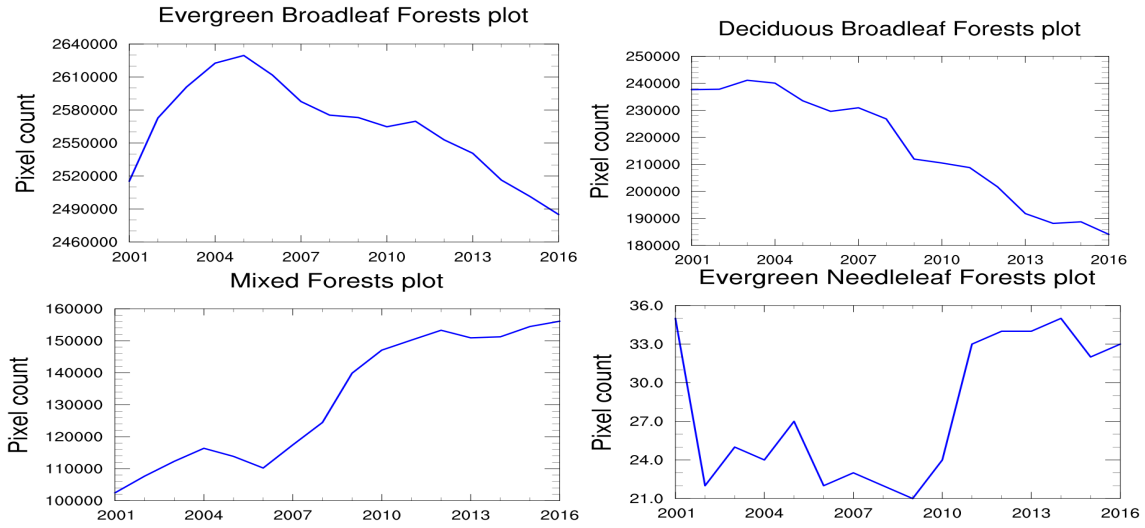

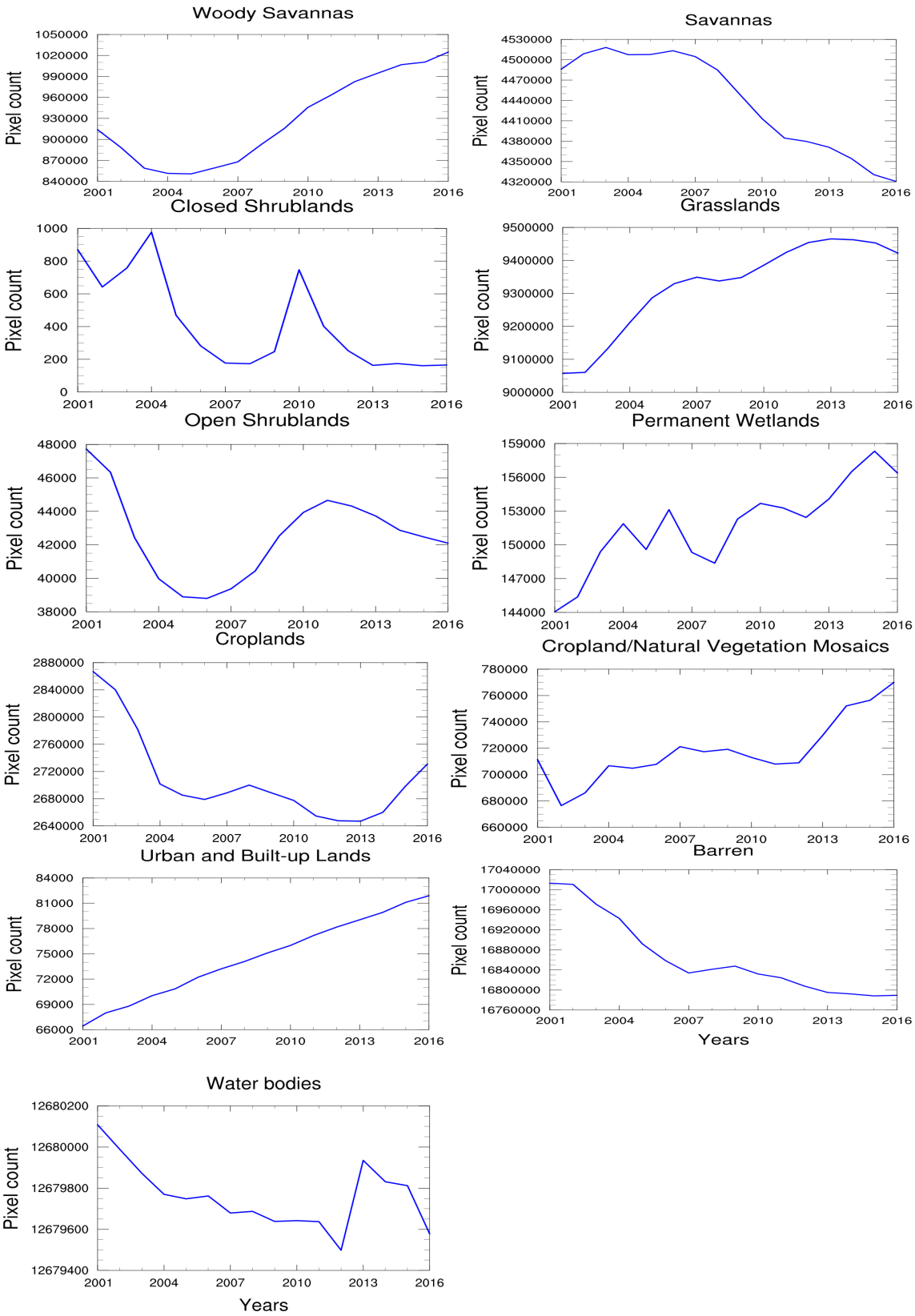

Figure 4.3: Time Series of the Land Use Parameters From 2001 to 2016

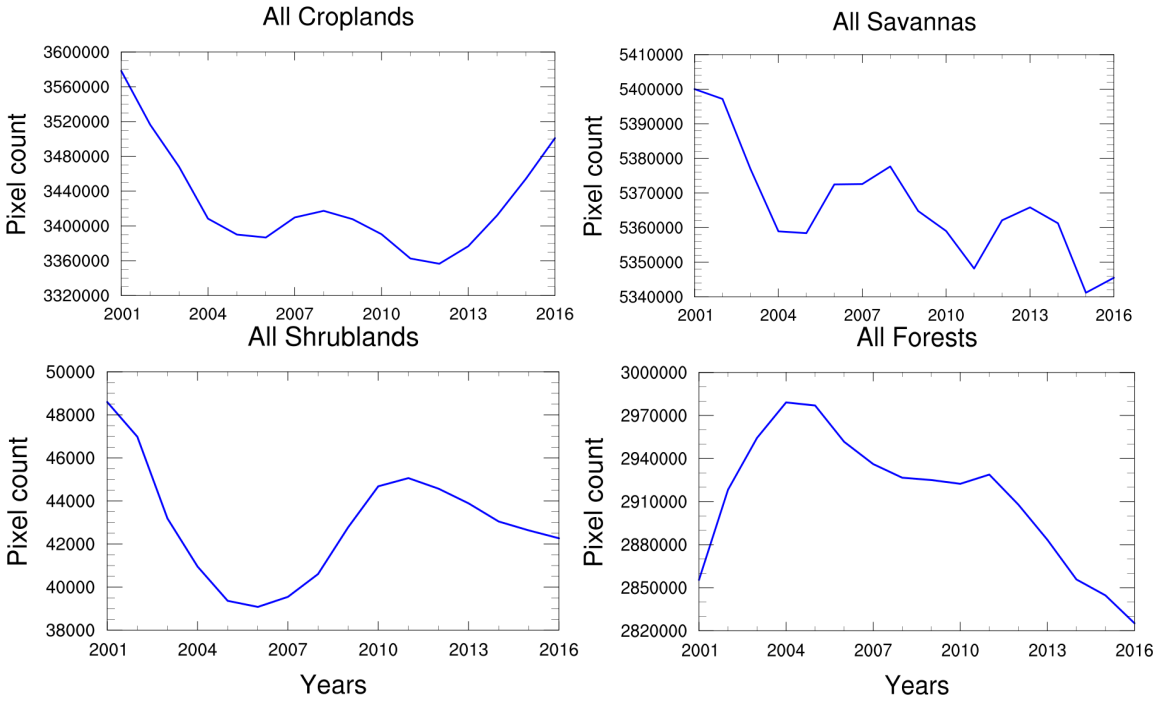

Figure 4.4: Time Series of some Reclassified Land Use Parameters From 2001 to 2016

Table 4.4: Trend analysis of LULCC parameters with Time

Land Cover Parameters (LCPs)	Trend
Evergreen Needleleaf Forests (ENF)	0.51
Evergreen Broadleaf Forests (EBF)	-0.63
Deciduous Broadleaf ForestsDBF)	-0.97
Mixed Forests (MF)	0.95
Closed Shrublands (CS)	-0.72
Open Shrublands (OS)	-0.03
Woody Savannas (WS)	0.87
Savannas (Sa)	-0.93
Grasslands (Gr)	0.92
Permanent Wetlands (PW)	0.88
Croplands (Cr)	-0.66
Urban and Built-up Lands (UBL)	0.99
Cropland/Natural Vegetation Mosaics (CVM)	0.82
Barren (Br)	-0.93
Water bodies (WB)	-0.52
All Forests	-0.60
All Shrublands	-0.11
All Savannas	-0.77
All Croplands	-0.38

However, analysis has shown that there is a mutual exchange between different types of LCP depending on the year understudy; for instance, savanna may be converted to cropland in a particular year, while the opposite happens in a different year in a particular location (Ichoku *et al.,* 2016). This is in line with the result of this study as in the case of all the LCPs except for the UBL that has steady increase throughout the study period. Yang *et al*., (1992) have emphasized that evergreen forests perform outstanding water conservation functions, therefore there is a need to put up a proactive measures to curb or reduce the rate at which the EBF, DBF and all forest in general, decreases as deduced in this research. This is necessary because, the time it takes for a destroyed forest to grow back to its earlier state is much longer than for savanna or grassland (Ichoku *et al.* 2016). Moreover, several other reasons could be accountable for the decline in EBF, DBF and all forests in general like rapid increase in human population. High number of people in an area would lead to increased deforestation because of buildings and construction purposes for settlements, food and basic infrastructural development (Boori *et al*., 2015, Antwi *et al*., 2014; Semwal *et al*., 2004). Other cause could be as a result of increase in the demand for timber and wood by the local people (Butt *et al*., 2015a).

Analysis of the WB revealed a decreasing trend over the study period. It cannot be denied that this is connected to the increase in UBL, which steadily increased over the period. This is in line with studies of Nwaogu *et al*. (2017) which states that a small decline in water bodies could be connected to anthropogenic activities of land uses for housing, and road constructions. Studies like Cai (2008) have also found that the increase in urban areas leads to an increase in non-agricultural water demand, as there is a transfer

from agricultural use to municipal and industrial needs, which further increase the regional water stress and aggravate the issues of effective water management. Increased exploitation of water resources by the increasing population can lead to the drying up of some streams and river tributaries (Butt *et al*., 2015a). Increased rate of surface run-off due to the absence of the plants roots to withhold water could also be an additional explanation for the decrease in water areas in the study area (Butt et al., 2015b). However, the steady increase of UBL LCP is clear evidence that urban sprawl is imminent in most cities across West Africa as there is generally a high increasing trend within the study period. This also corroborate the reports of earlier researches like Taylor (1993), Braimoh and Onishi (2007), Qi and Chopping (2007), Antwi *et al.* (2014), Alfred *et al*. (2016), Kilianova *et al*. (2017) on the role of population growth in LULCC.

From this study, the increase in croplands in some years and the CVM is in line with the findings of Wang *et al*. (2008b) stressed that increase in croplands cover is a possible consequence of a growing population and economy. It could also be the consequence of the convertion of water bodies into croplands. Also, decrease in croplands could be a result of internal population displacement, which is now common in the zone because of the increasing rate of terrorism and communal clashes.

4.2 Assessment of WRF LSM performance over West Africa

Figure 4.5 shows the spatial distribution of mean daily JAS average dew-point temperature. It can be seen that all the models can reasonably simulate the spatial pattern of dew-point temperature over West Africa. They all show a similar increase in dew-point temperature from north to south. All the LSMs (just as the reference) show reduced dew-point temperature around the Jos plateau and the Cameroon-Adamawa Mountains. Also, all the models show the incursion of dew-point value of 20-22°C from the Atlantic Ocean into the continental bulges at the boundary between Liberia and Cote d'lvoire and in Ghana. From the spatial bias of JAS dew point temperature in Figure 4.6, the dew point temperature in the models differ from ERA within the range of about −2 to 8 °C. The white color map in all the spatial bias plots indicates areas with bias value <1 and >-1 (i.e. -1< bias <1 close to zero). Noah-MP, Noah-MP GW and CLM4 show a high positive bias in the area Northwest of 15-20°N. Noah LSM however behaved differently by showing negative bias all through the areas 15-20°N and bias close to zero in most areas below 15°N. CLM4 shows a higher positive bias than others in the north-western part. From the spatial plot of daily DJF dew-point temperature in figure 4.7, all the LSMs show the drier dewpoints extending more south to about 7°N. Also, all the models show a little higher dew point temperature around Lake Chad in which the analysis did not depict. However, CLM4 shows scattered higher dew point temperature in areas within 15°N and 20°N than the others.

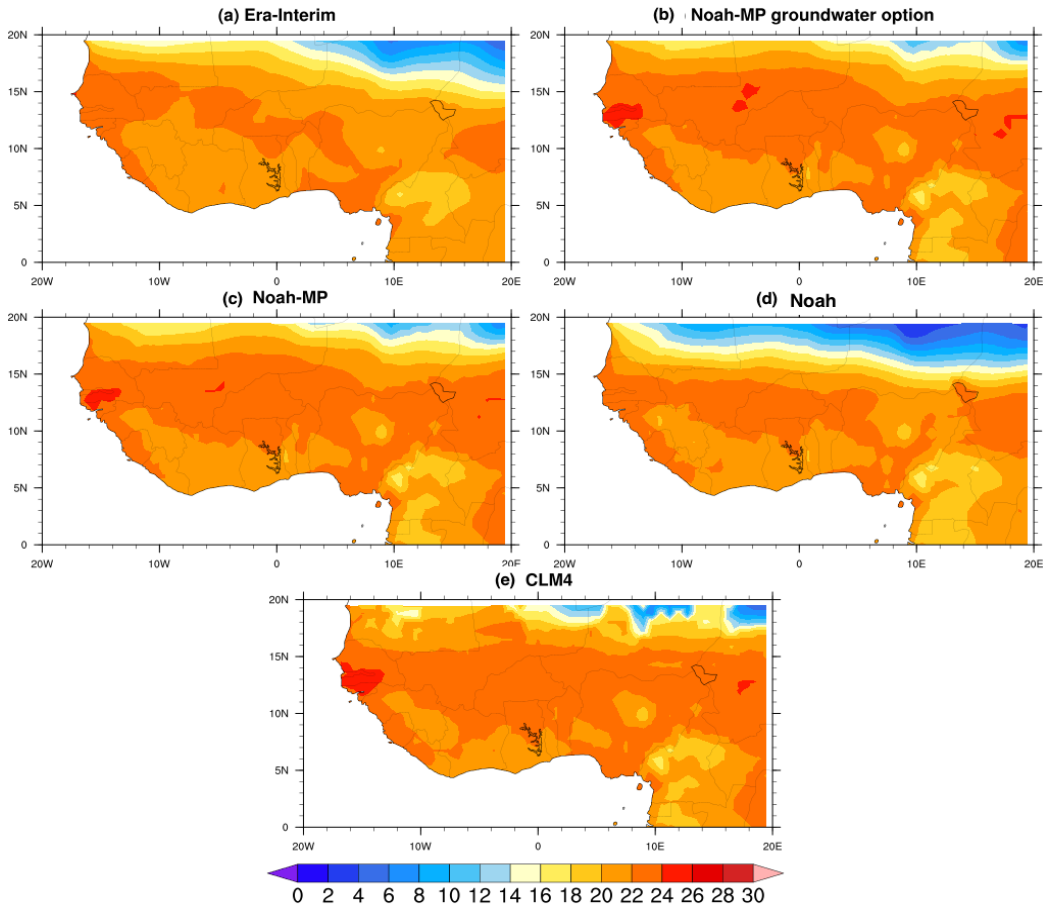

Figure 4.5: Spatial distribution of Average dew point temperature (^{o}C) for July 16th – Sept. 29th, 2012

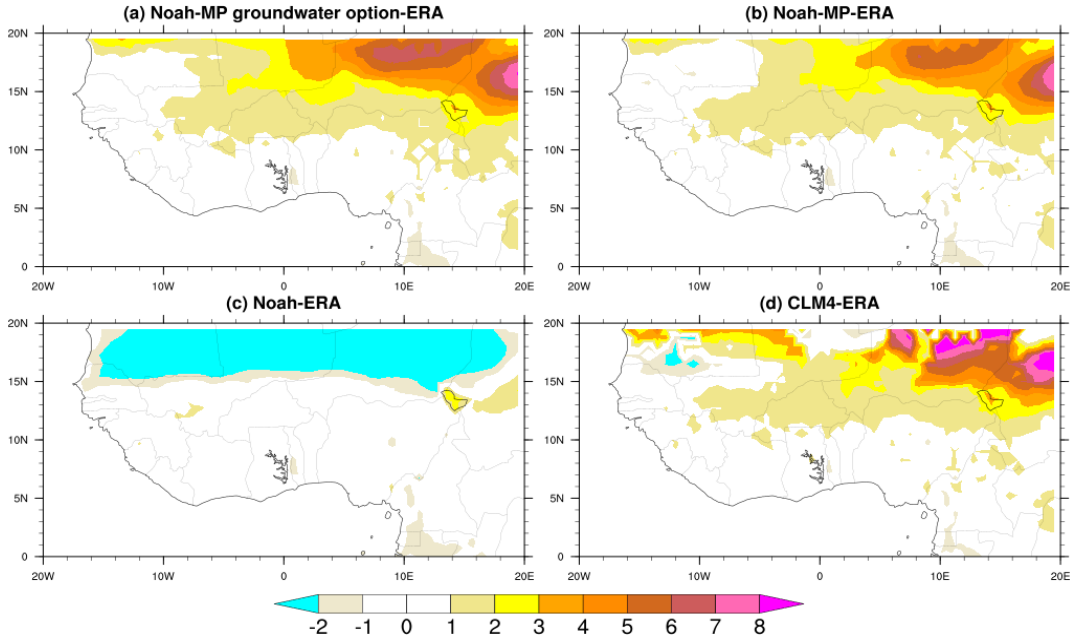

Figure 4.6: Spatial bias of Dew point temperature (°C) for July 16th –Sept. 29th 2012

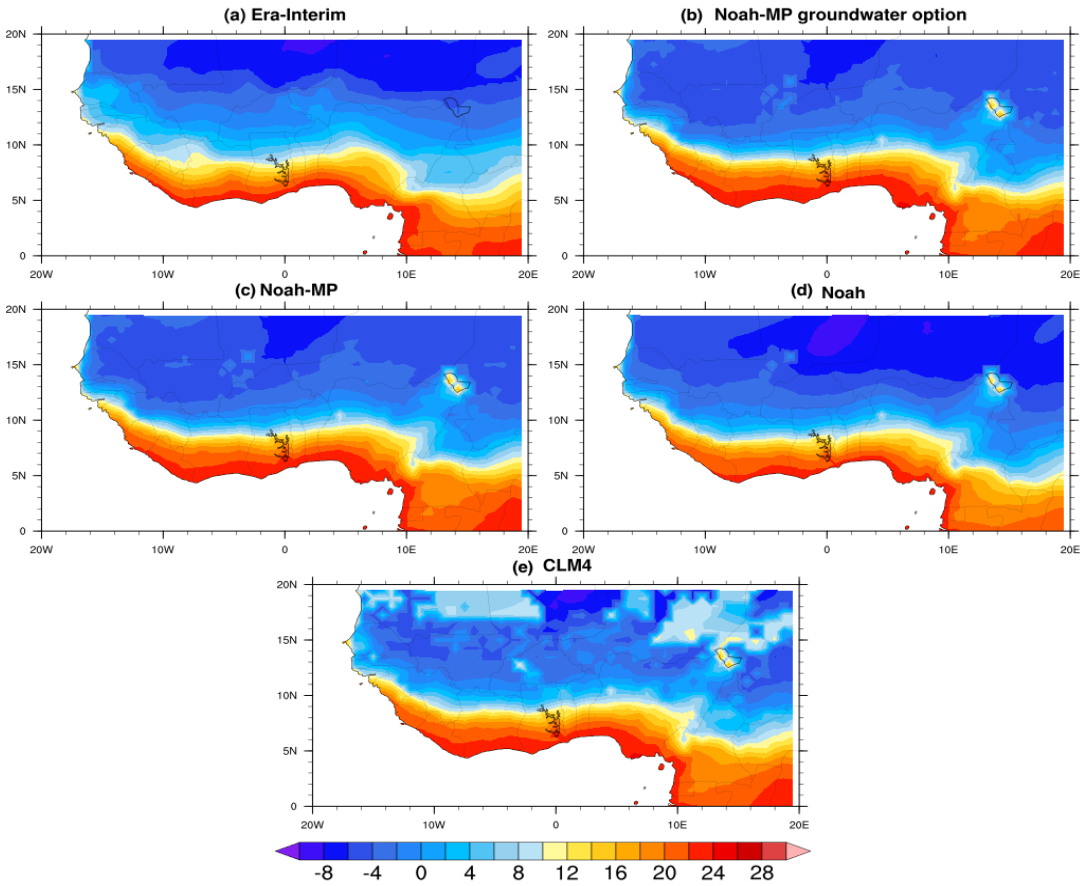

Figure 4.7: Spatial distribution of Average Dew Point Temperature (°C) for Dec. 16th 2011 to Feb. 28th 2012.

Obvious systematic errors were prevalent in all the dew point temperature simulated outputs both for DJF and JAS. For DJF outputs, as depicted in Figure 4.8, all the simulations show high positive bias around Lake Chad, possibly due to a bias in the lake temperature, but CLM4 also showed high positive bias in areas between 15°N and 20°N. The region between 10 and 15°N mostly showed negative bias (underestimation) for all the simulations. Also, areas around Fouta Djalon Highlands showed between -4 and -8°C bias for all the LSM outputs except for Noah, which showed less. Noah LSM has the lowest range of bais ranging from -8 to about +3 apart from over the Lake Chad where all the LSMs over-estimated the dew point temperature. It is therefore clearly seen that Noah simulates the Dew point temperature better than others. Figure 4.9 (a) shows

the time series of the average dew point temperature for JAS over the 3 months period. It shows that ERA has a lower dew point temperature than all the models. Although, the models have similar pattern with the reference, they were out of phase at some points like

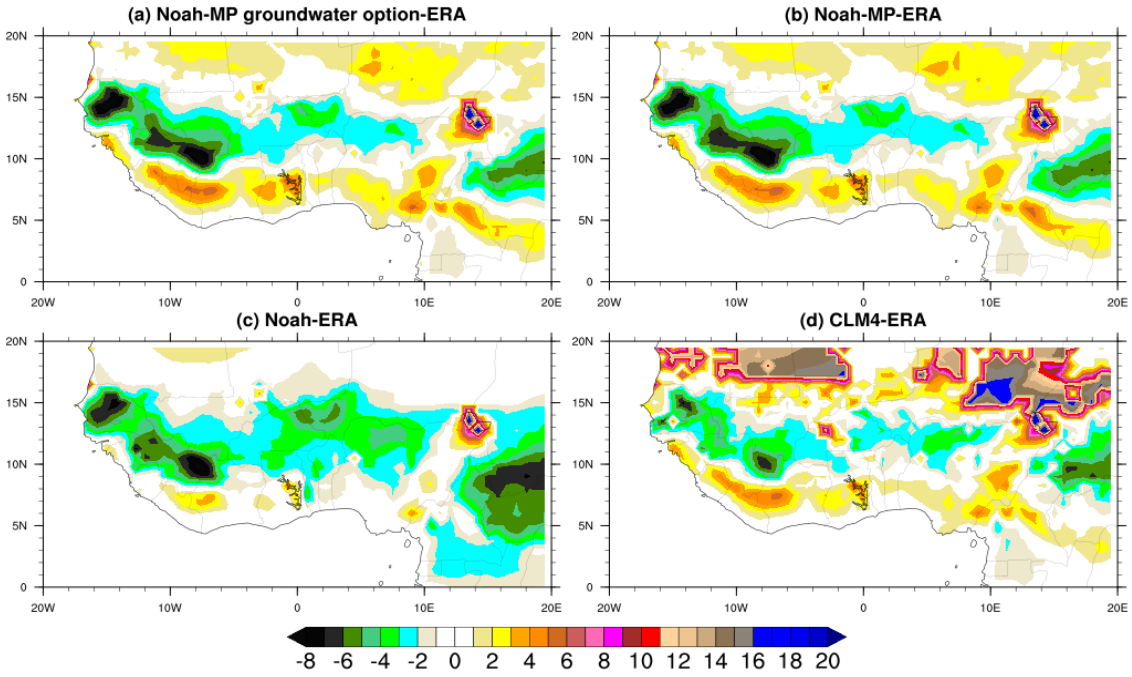

Figure 4.8: Spatial bias of Dew point temperature (°C) for Dec. 16, 2011-Feb. 28, 2012

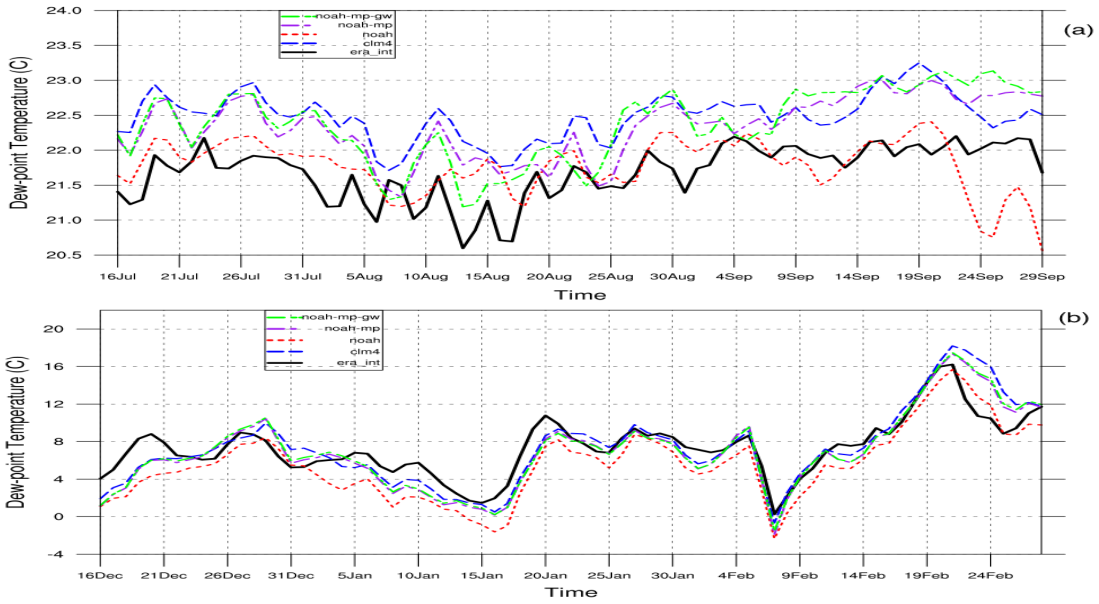

Figure 4.9: Time Series of 2m Daily Dew Point Temperature Averaged Over 10°W-10°E and 5°-15°N for (a) JAS, and (b) DJF

August 7th and 8th. On average, the series seem to vary between 21.7°C and 22.9°C in July, 21.0°C and 22.3°C in August and subsequently 21.5°C and 23.1°C in September. From the average daily time series of dew point temperature for DJF as illustrated in Figure 4.9 (b), all the LSMs have a similar pattern with the reference except for period around early January. For most of the periods, Noah LSM underestimates the DJF dew point temperature while CLM4 was the closest to the reference. All the simulations obviously have a clear lower dew point temperature than ERA-interim between December 16-21 and January 5-20. The range of fluctuation of the values in the dry season is larger than the rainy season. From December 16 to January 17, the series fluctuate between 0 and 9°C, there is a sharp increase between January 17 and 20 from 1 to 10°C (on average). There is also a sharp decrease on February 5 till 7th from 8 to -1°C after which a steady increase took place thereafter till February 21st to about 17°C. Except at the end, most of these changes do not correspond to rainfall, so they are likely advective moisture changes from the large-scale flow.

From the plot of the average air temperature for JAS (Figure 4.10), all the simulations were in close resemblance to ERA-interim as well as FNL used as reference. The areas of high and low values in the two reference sets were captured by all the four LSMs. Using ERA-Interim only for bias, the average temperature bias plot for JAS in Figure 4.11 shows that the outputs of all the model simulations agrees with ERA-interim within the range of -4 to 3.5°C. The maximum positive bias was shown around the EL Djouf basin in Mauritania and Northern Mali, while the maximum negative bias was found around Lake Chad, again possibly due to a bias in the lake temperature in the model, for all simulations. But Noah shows a cold bias relative to ERA-interim in areas above 16°N at

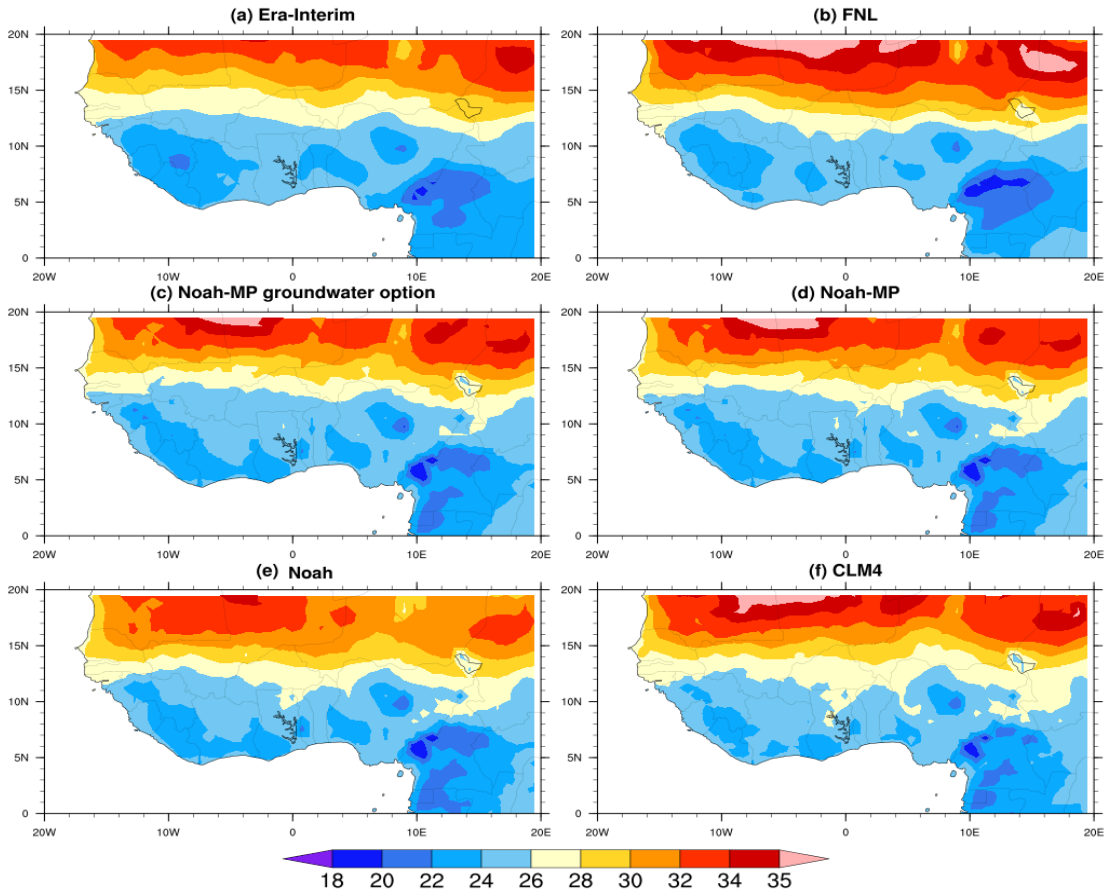

Figure 4.10: Spatial Distribution of Average 2 Meter Temperature (°C) for July 16-Sept 29th, 2012

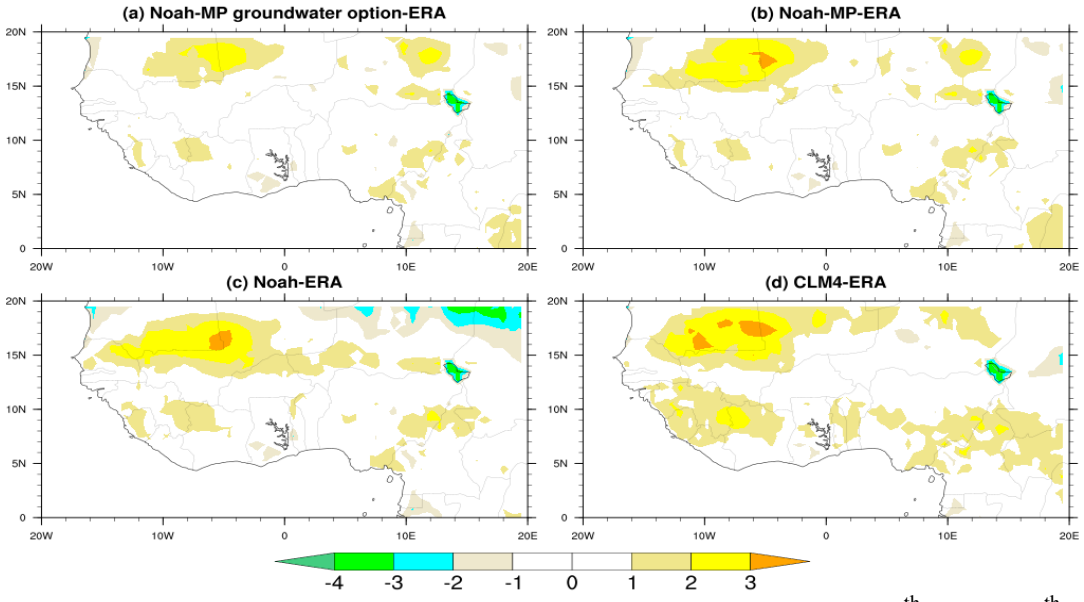

Figure 4.11: Spatial Bias of Average 2m Temparature (°C) for July 16th -Sept. 29th , 2012

the North-eastern part which other models did not reveal. Areas below 15°N mostly showed bias value close to zero except for CLM4. However, it shows that all the models could fairly predict rainy season air temperature.

Figure 4.12 shows that the spatial distribution of average 2m surface temperature for DJF decreases with increasing latitude just like the reference from areas above 10°N. All the models and ERA-interim were able to capture reasonably well the cooling around the highlands of Jos Plateau, Guinea and Cameroon, however, FNL has more rainfall around the coastal areas than ERA-Interim. From Figure 4.13, the average temperature bias between ERA-interim and the models for DJF ranges between -4° and 5°C. There is a maximum warm bias around Fouta Djallon highlands in all the simulations. Noah LSM output tends to have the coldest bias while CLM4 LSM tends to have the warmest. From the time series of JAS daily 2m surface temperature averaged over 10°W-10°E and 5°-15°N (as shown in Figure 4.14a), the general biases between ERA-interim and the models can be clearly seen as ERA is predominantly cooler than the models. On average, August is the coolest period while September is the warmest, but the model tended to be too warm in September for all LSMs. Also, the models behave differently at some times and were in line with the reference pattern at some other times. From the time series of average daily temperature for DJF (Figure 4.14b), the model patterns were very similar to the reference. Noah-MP and the ground water option were the closest while Noah was the furthest being 1-2°C colder than ERA-interim.

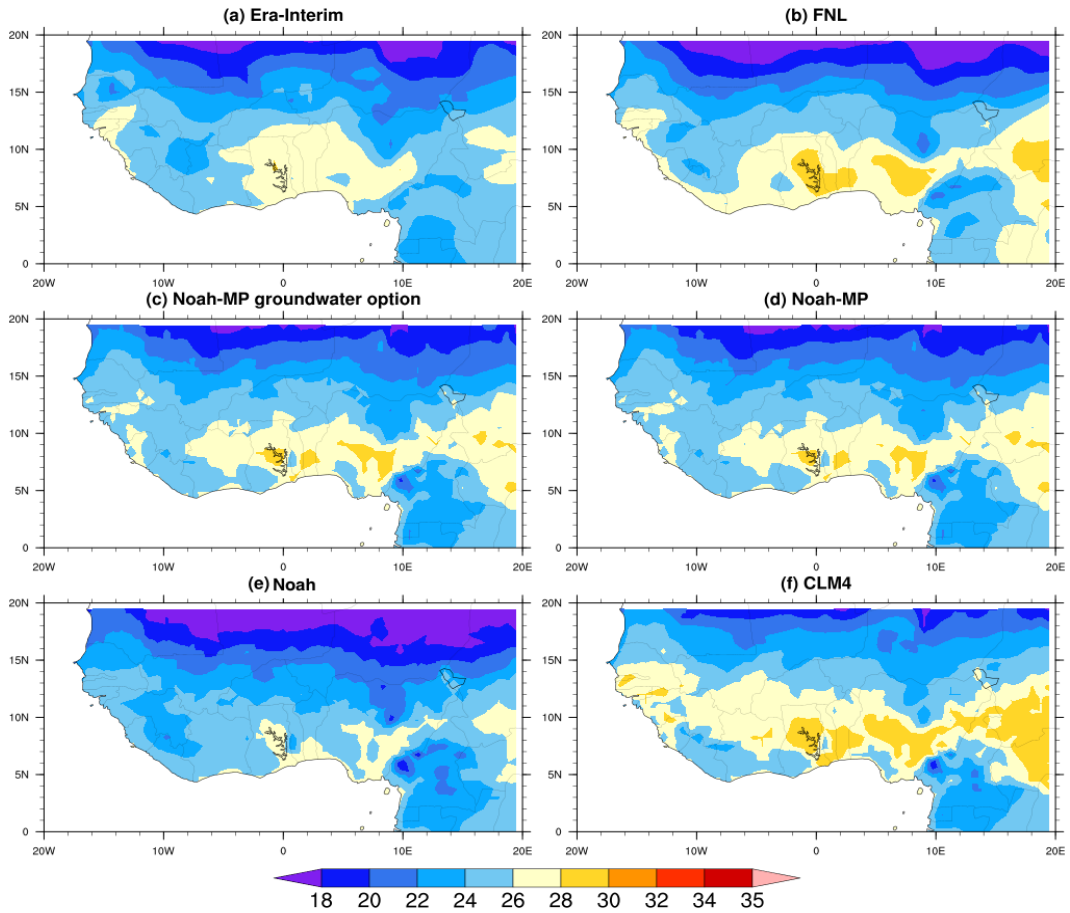

Figure 4.12: Spatial Distribution of Average 2m Surface Temperature (°C) for Dec. 16th 2011-Feb. 28th, 2012

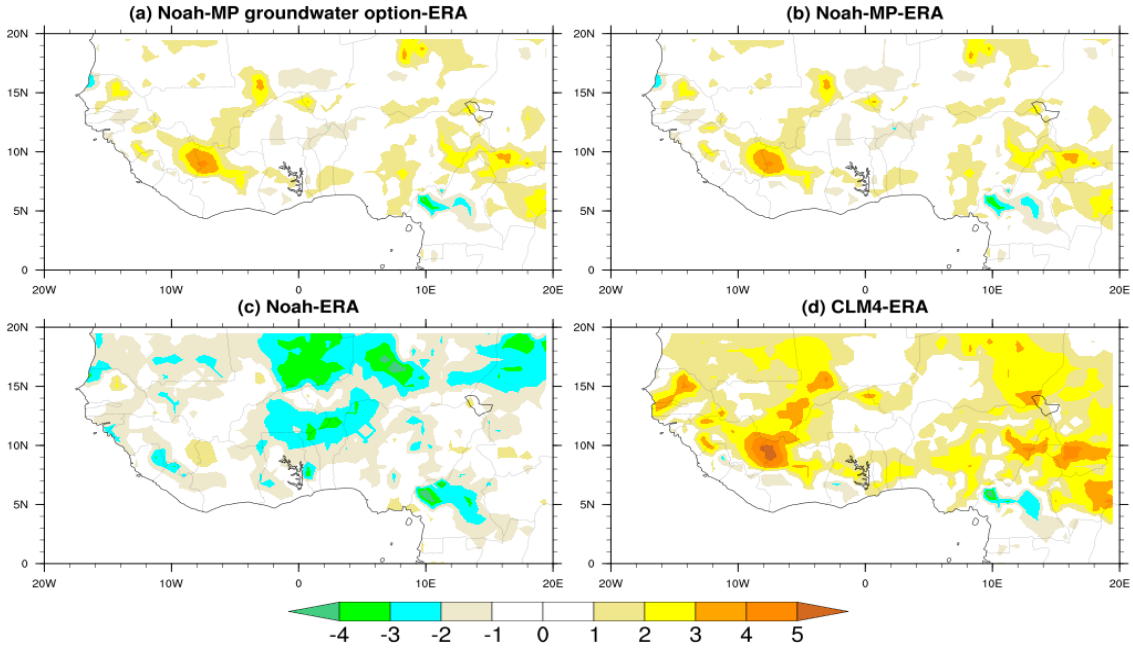

Figure 4.13: Spatial Bias of Average Temparature (°C) for Dec., 2011-Feb. 28, 2012

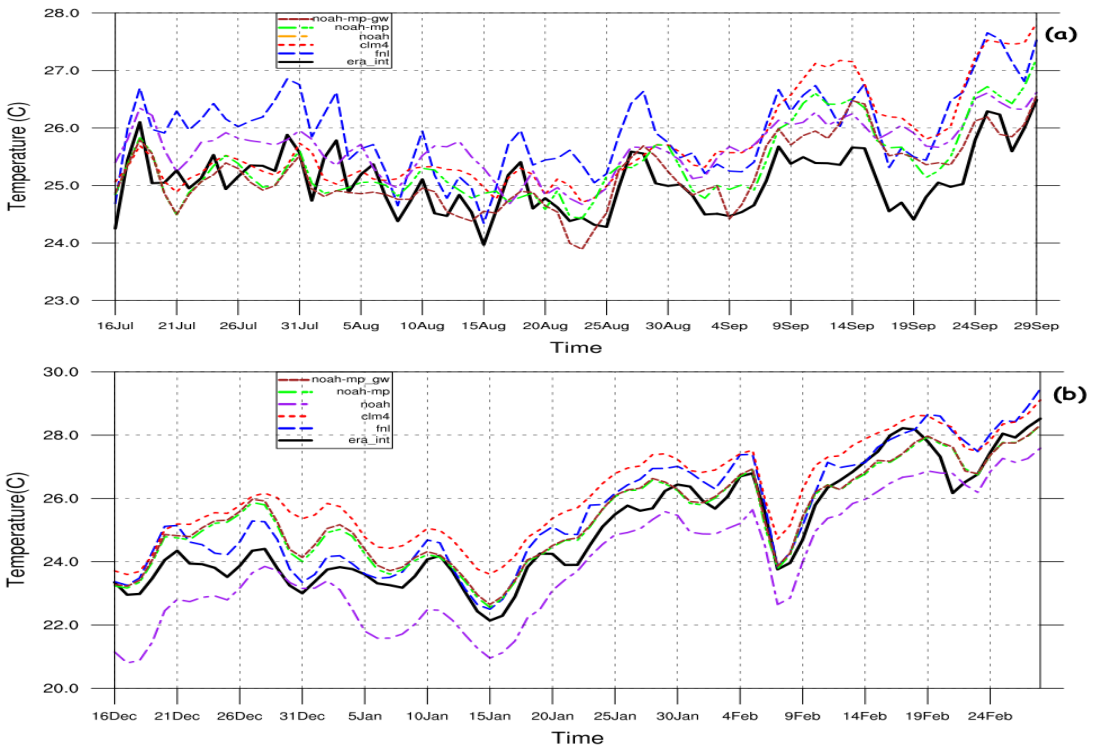

Figure 4.14: Time Series of Daily 2m Temperature Averaged Over 10°W-10°E and 5°-15°N for (a) JAS (b) DJF

Figure 4.15 spatially displays the average JAS daily precipitation. All the models with TRMM and GPCP showed maximum precipitation concentrated around Fouta Djallon highlands, Jos Plateau and Cameroon Mountains. There seems to be a more intense precipitation core formed around the Fouta Djallons in Guinea both in TRMM, GPCP and all the models. Also, the models seem to produce more intense precipitation around the highlands than TRMM and GPCP. The orographic effect of the highlands is the reason the models deliver a high precipitation amount but it appears to be more than reference in those areas. Outputs from Noah and CLM4 models showed almost no rainfall from latitude 17°N northwards whereas; TRMM, GPCP, Noah-MP and Noah-MP with groundwater option displayed some amount of precipitation. Also, the models differ in their northward advance of precipitation as compared with the reference. The 1-3mm/day precipitation belt stopped around 16°N for Noah, 17°N in CLM4 and 19-20°N

for Noah-MP and the ground water option and by implication, it shows that Noah is driest in comparison to other LSM understudy.

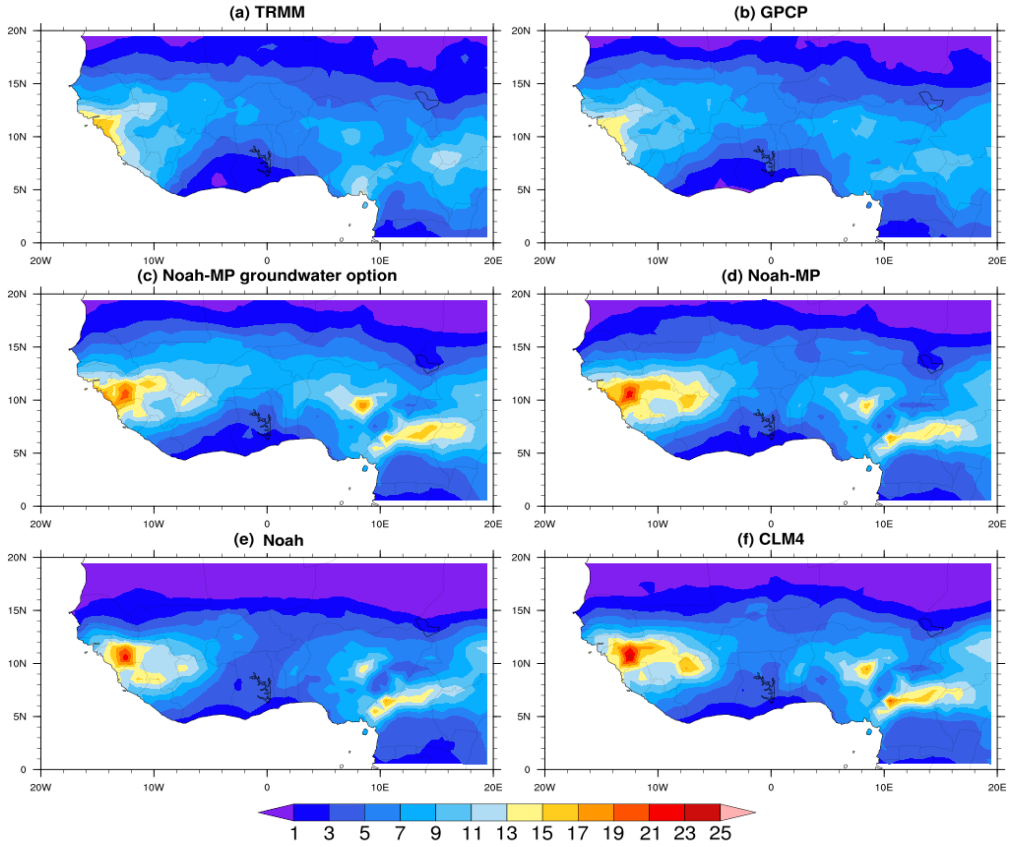

Figure 4.15: Spatial Distribution of Average Precipitation for July 16, -Sept. 29, 2012

From the spatial bias of JAS precipitation as presented in Figure 4.16, the difference between the models and TRMM ranges between -5 and 10mm/day. There was prevalence of positive precipitation bias of amount >9mm/day around Fouta Djallon highlands and precipitation bias amount >5mm/day. Noah-MP with groundwater showed the largest area of high precipitation bias among all the LSMs tested. From Figure 4.17, all the models showed good pattern of the West African precipitation, which follows the movement of the inter tropical discontinuity (ITD). Areas above 7°N were dry as a result of the influx of the dry north easterlies during this period. The dry coasts of Ghana, Togo,

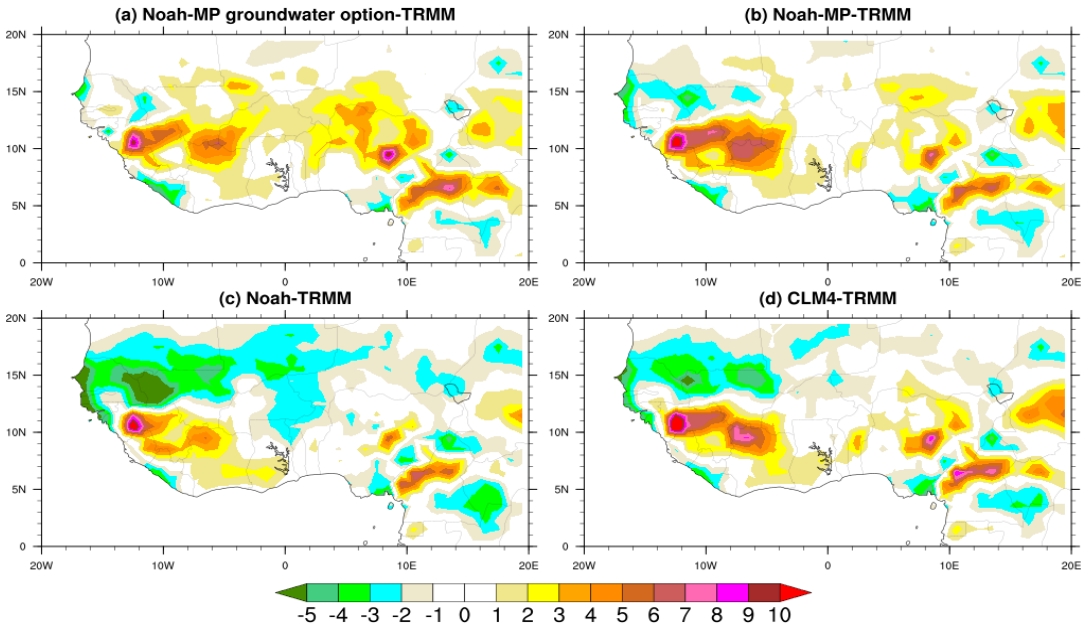

Figure 4.16: Spatial Bias Of Precipitation for July 16-Sept. 29, 2012

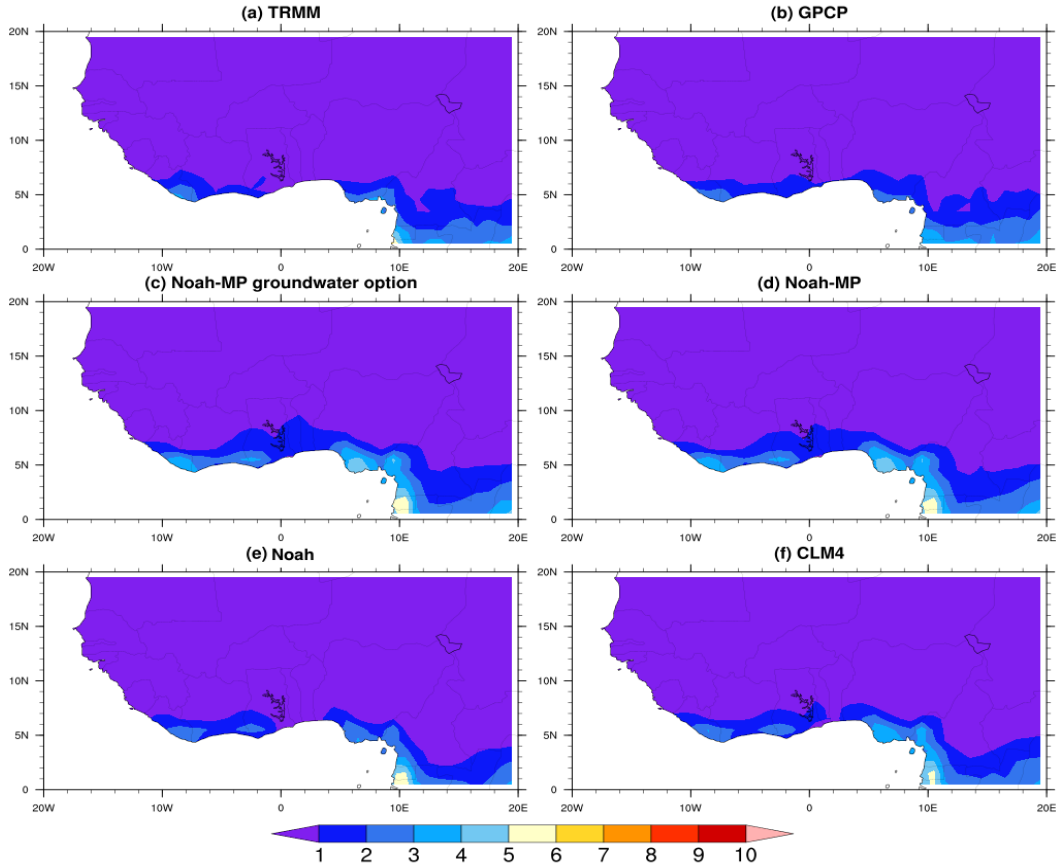

Figure 4.17: Spatial Distribution Of Average Precipitation for Dec. 16th 2011-Feb. 28th, 2012

Benin and some parts of Nigeria as seen in TRMM and GPCP were also demonstrated in Noah and a little in CLM4. From the spatial bias of precipitation for DJF in Figure 4.18, there was evidence of bias as the difference between TRMM and the models ranges from -6 to 2mm/day.

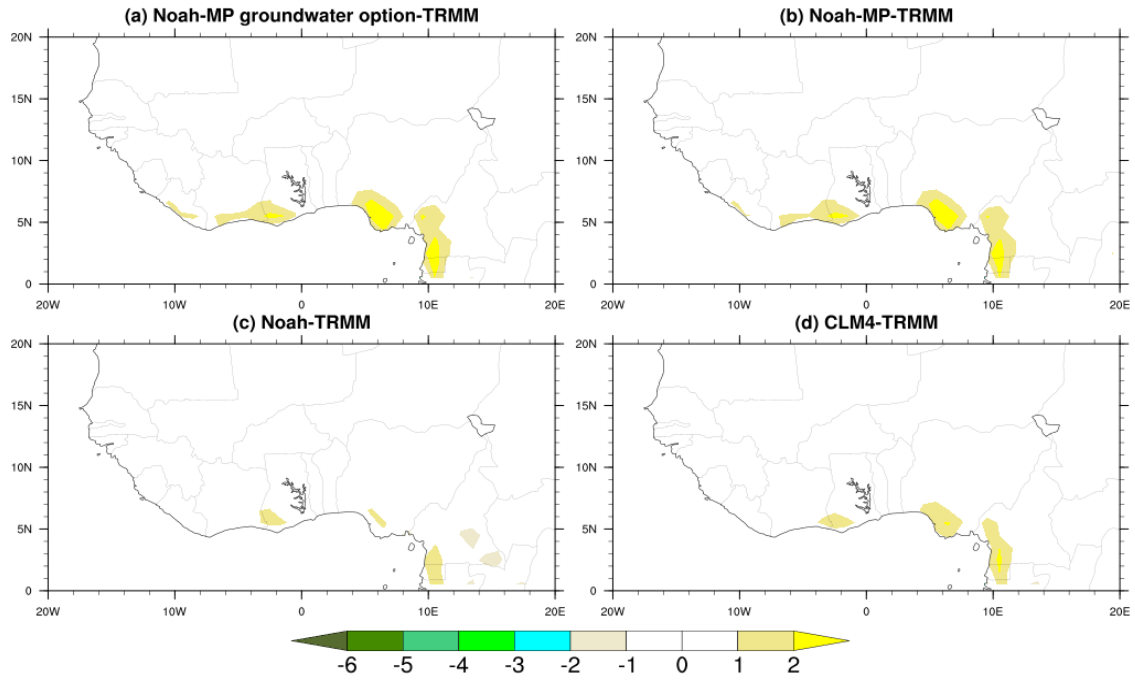

Figure 4.18: Spatial Bias Of Precipitation for Dec. 16, 2011-Feb. 28, 2012

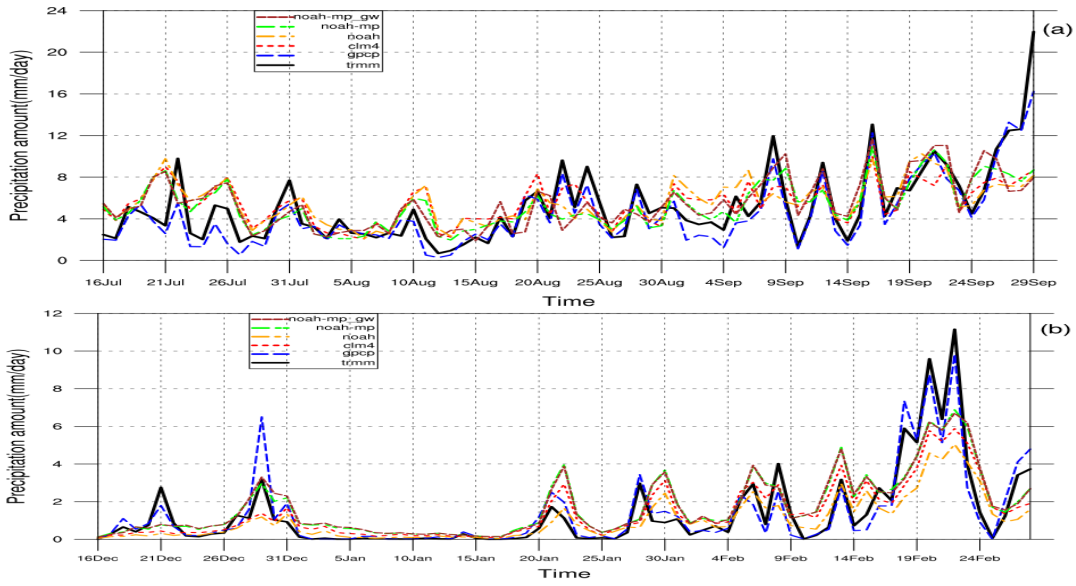

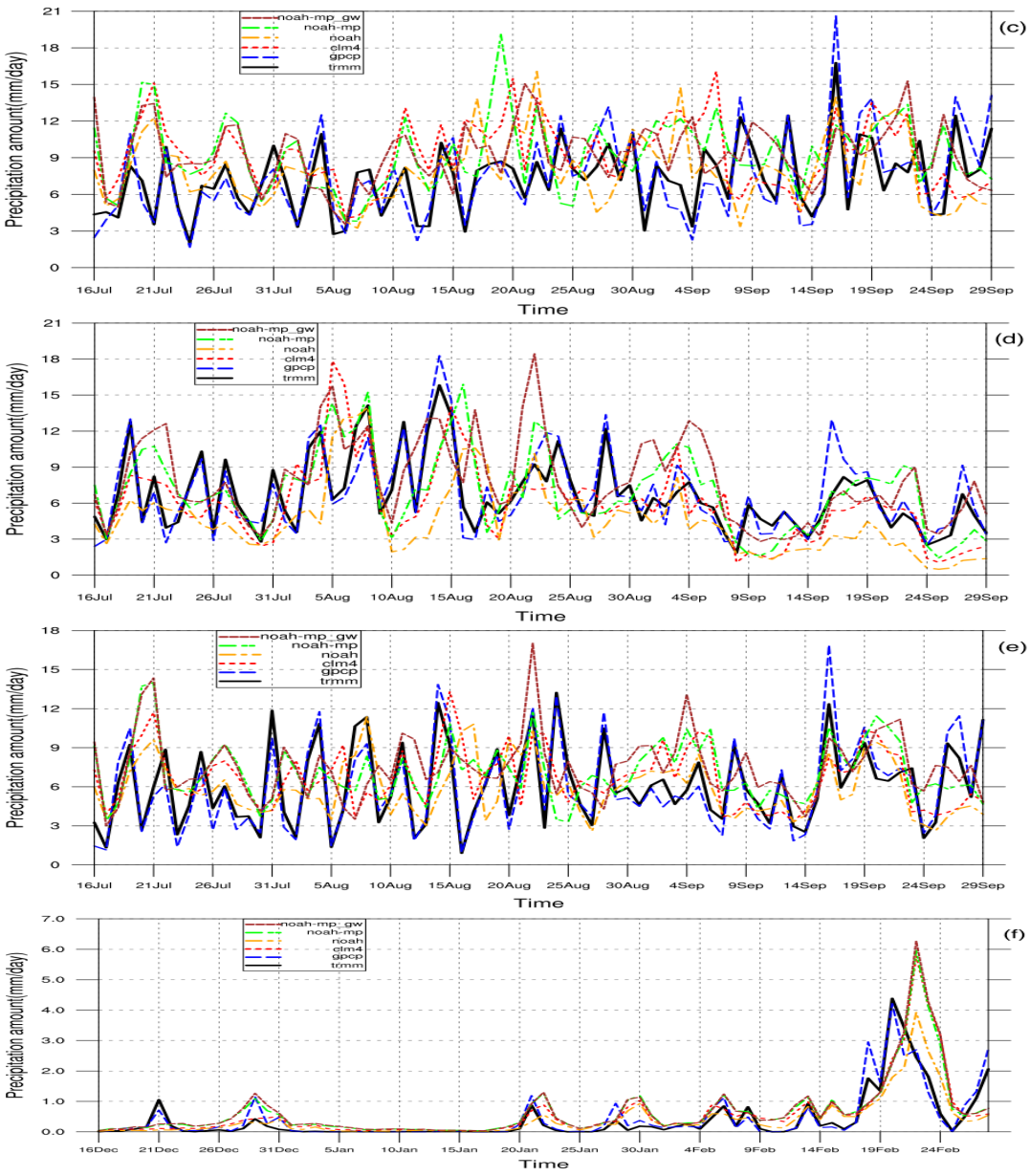

Figure 4.19: Time Series of Daily Precipitation Averaged Over (a) Coastal JAS 4°-8°N, (b) Coastal DJF 4°-8°N, (c) Savannah JAS 8°-11°N, (d) Sahel JAS 11°-16°N, (e) 5°N – 15°N, 10°E – 10°W JAS, (f) 5°N – 15°N, 10°E – 10°W DJF.

Figure 4.19 shows the time series of precipitation averaged over the entire area (i.e. evaluation area) and the sub-regions. From Figure 4.19a for the Coastal JAS period, the models have the same pattern with the reference except for September 27, 28, 29 and July 21st. The average amount of September precipitation was more than that of July and August, which could be attributed to the prevalence of the little dry season or monsoon

jump as described by Sultan and Janicot (2000) and (2003), and Gbobaniyi *et al*. (2013) (popularly known as August break) that usually occurs in the rain band between June and July resulting to the northward shift of the monsoon rainfall up to about 10°N in West Africa. However, the consequence of this is high precipitation amounts in the Sahel region (shown later), in coexistence with an instantaneous cessation in precipitation intensities along the coasts. Figure 4.19b shows the time series of daily DJF precipitation over the coastal area. The models were able to capture the December and late January and February precipitation peculiar to some of the coastal areas in West Africa. Also, there were some overestimations and underestimations of precipitation at some times. From the time series of the daily JAS rainfall amount over the Savanna (8°-11°N) (Figure 4.19c), the simulation patterns agree with the reference in some instances and disagree in others. There was clear over-estimation from the simulations mostly in July and August. All the simulations were in disagreement with the reference on September 21 and 22, and July 21st as well as other cases that were overestimated.

The time series of daily JAS precipitation averaged over the Sahel (Figure 4.19d) shows that the simulated pattern agrees with the reference but there were over-estimation and under-estimation at some times. There was a clear disagreement between the simulations and the reference on August 5. Also, August marks the month with the highest amount of average precipitation while September has the lowest within the months under consideration. This could be as a result of the southward shift in the rain band (i.e. the ITD) towards the Guinea coast, and it goes with a decrease in the amount of rainfall over the Sahel. From Figure 4.19(e), all the JAS simulations were completely in disagreement with TRMM on July 20th and 21st, August 2nd, 24th and September 1st. All the series have

similar pattern with the reference aside from the listed points. There was a clear overestimation from Noah-MP with groundwater option on 21st of August. From Figure 4.19(f), the simulated DJF precipitation pattern disagree with the reference on 29th of January and 22nd of February but have a similar pattern in other periods. The very little or no precipitation notable for this period of the year in the region was well captured in all the models.

Table 4.5: Daily Mean Bias Value for All the Simulations and Variables

	Noah	Noah-MP	Noah-MP GW	CLM4	FNL	GPCP
Dew point Temp. (°C) DJF	1.79	0.46	0.38	0.04		
Dew point Temp. (°C) JAS	-0.09	-0.65	-0.69	-0.80		
Air Temp. (°C) DJF	1.02	-0.39	-0.45	-1.15	-0.55	
Air temp. (°C) JAS	-0.57	-0.30	-0.11	-0.63	-0.84	
All region precip. DJF (mm/day)	-0.01	-0.25	-0.27	-0.18		-0.05
All region precip. JAS (mm/day)	0.22	0.11	0.09	-0.57		0.12
Coastal precip. (mm/day) JAS	-0.42	-0.12	-0.35	-0.38		0.74
Coastal Precip. (mm/day) DJF	0.32	-0.36	-0.37	-0.04		-0.02
Savannah precip (mm/day) JAS	-0.67	-2.02	-2.00	-1.97		-0.13
Sahel precip. (mm/day) JAS	2.00	-0.28	-1.13	0.72		-0.15

Using the same frequency and data as used in Figure 4.9, 4.14 and 4.19 (i.e. daily averaged data series), Taylor diagrams (Taylor 2001) evaluate the models performance with the ERA-interim (for surface temperature and dew-point temperature) and TRMM (for precipitation) for all the regions combined and also separately for the study period and season. Surface air temperature, dew point temperature and precipitation outputs from the eight different WRF runs at 12km resolution for rainy (JAS) and dry (DJF) seasons with four different land surface schemes and options are compared in the diagrams as shown in Figure 4.20 a-e. The outputs were averaged over 5°-15°N and 10°W-10°E for the entire West African region and 10°W-15°E and 4°-8°N for the coastal

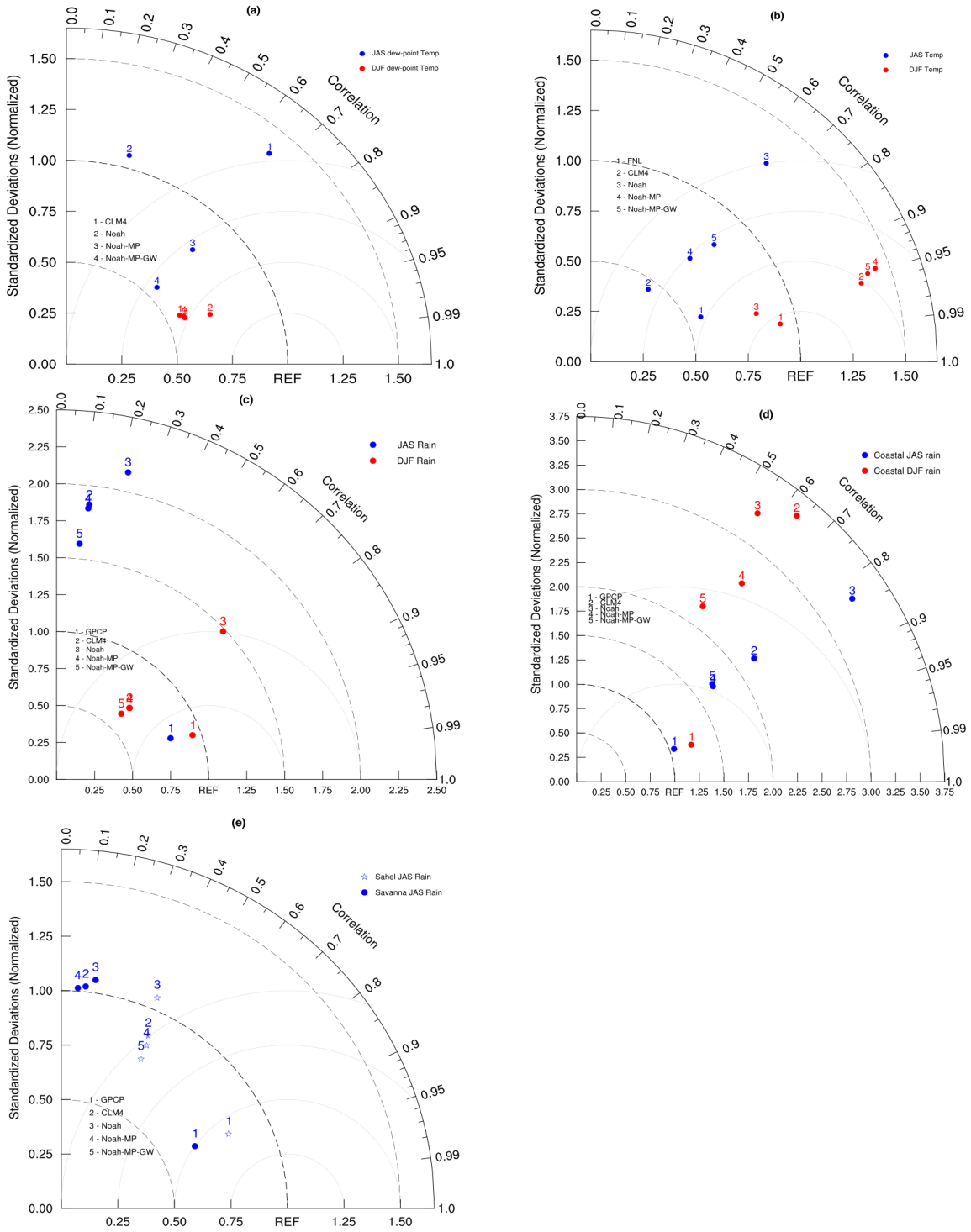

Figure 4.20: Taylor Diagrams (a) Dew Point Temperature, (b) Surface Air Temperature, (c) Precipitation for all Region, (d) Coastal Precipitation (e) Savannah and Sahel Precipitation. (Blue colours are for the rainy season and red colours are for dry season), a and b were compared against ERA-interim (REF), while c, d and e were compared against TRMM (REF). The RMS error and the standard deviation have been normalized according to Taylor (2001) before plotting the Taylor diagram.

region, 13°W-15°E and 8°-11°N for the Savannah, and 13°W-15°E and 11°-16°N for the Sahelian region. For dew point temperature (Figure 4.20a), all the simulations have high correlation coefficient with ERA-interim and are between 0.91 and 0.94 during the dry season and between 0.27 and 0.74 for the rainy season. Noah has the highest correlation coefficient with mean bias of 1.79°C (as shown in Table 4.5) during the dry season and the lowest during the rainy season with mean bias of -0.09°C as shown in Table 4.5. The standard deviation (normalised) ranges from 0.55 to 0.7 in the dry season, which is a low range but has a wider range in the rainy season (0.55 – 1.38). This shows that Noah could be best to simulate dew point temperature during the dry season and Noah-MP is best for dew point in the rainy season. From Figure 4.20b, FNL shows a high correlation coefficient of 0.98, while the simulations correlation coefficient ranges between 0.96 and 0.95 during the dry season. The standard deviation ranges from 0.87 to 1.48 for the simulations during the dry season and 0.45 to 1.30 for the rainy season. Noah LSM however performs best in simulating the dry season surface air temperature while the Noah-MP with the groundwater option performs best in simulating the rainy season surface air temperature.

For precipitation over the whole region (Figure 4.20c), the correlation coefficient for dry season rainfall ranges from 0.69 to 0.74 for the simulations, while the GPCP has a correlation coefficient of 0.95. Standard deviations range from 0.62 to 1.48 for the simulations. For the rainy season precipitation over the whole region, the correlation coefficient ranges from 0.09 to 0.22 for the models, and 0.94 for the GPCP. Standard deviations range from 1.6 to 2.13 for the models and 0.8 for GPCP. Therefore, there were higher standard deviations for precipitation during the rainy season whereas; there were

higher values for dew point temperature and surface air temperature during the dry season. Rainy season precipitation is best simulated with the Noah-MP groundwater option, while CLM4 and Noah-MP equally performed equally for dry season rainfall simulations over the study region. For the coastal rainfall as shown in Figure 4.20d, the JAS correlation coefficient ranges from 0.56 to 0.64 for the models, while GPCP has a correlation coefficient of 0.95. Standard deviation ranges from 1.7 to 3.4 for the simulation, with GPCP having 1.02. For the coastal DJF, correlation coefficient ranges from 0.81 to 0.83 for the simulations, while GPCP has a correlation coefficient of 0.95. Standard deviation ranges from 2.2 to 3.52 for the dry season, and GPCP has 2.07 standard deviation. However, Noah-MP performed best for the coastal JAS precipitation, while Noah performed worst, and Noah-MP with groundwater option performed best for the DJF precipitation.

For the Savannah and Sahel rainfall analysis, the DJF season was not analysed because the area is completely dry during this period. For the Savannah JAS rainfall as in Figure 4.20e, the correlation coefficient is less than 0.14 for the models, while GPCP has a correlation coefficient of 0.90. Standard deviation is less than 1.2 for the simulations, while GPCP has a value of 0.65. For the Sahel JAS rainfall, correlation coefficient ranges from 0.40 to 0.46 for the models, while GPCP has a correlation coefficient of 0.91. Standard deviation ranges from 0.77 to 1.06 for the simulations, and GPCP has a value of 0.82. Noah-MP performed best for the Savanna rainfall while Noah-MP GW performed worst. Noah-MP GW performed best for Sahel rainfall and Noah performed worst. On average, from the four compared schemes with the variables used, Noah-MP GW best simulates the rainy season events while Noah is good for dry season events over the

region. All the simulated parameters from all the models have high correlateon with the reference for the dry season simulations.

Table 4.6: Average Value of the Reference and Simulations for Temperature, Dew Point Temperature and Precipitation.

	Variable	REF	Noah	Noah-MP	Noah-MP GW	CLM4
DJF	Air Temperature (°C)	25.00	23.98	25.39	25.45	26.15
	Dew point Temperature (°C)	7.36	5.57	6.90	6.98	7.32
	Coastal Precipitation (mm/day)	1.35	1.02	1.71	1.71	1.39
JAS	Air temperature (°C)	25.08	25.66	25.38	25.19	25.71
	Dew point Temperature (°C)	21.69	21.78	22.34	22.37	22.49
	Coastal precipitation (mm/day)	5.16	5.57	5.27	5.51	5.53
	Savannah precipitation (mm/day)	7.24	7.91	9.26	9.25	9.21
	Sahel precipitation (mm/day)	6.65	4.64	6.93	7.77	5.93
	All region precip. (mm/day)	6.11	5.89	7.10	7.50	6.68

From the table showing the average values of the Reference and all the model outputs (Table 4.6), it can be seen that most of the simulations have average values close to the reference value both for rainy and dry season except for precipitation with a little wide range in some instances. Also, Noah LSM gives a little different average value from other LSM, which could be related to the fact that it is the least sophisticated LSM among the ones under study. However, the change in WRF LSM does not significantly change the average output of temperature and dew point temperature over the area, and this could mean that the differences in some values could be as a result of atmospheric changes and also the data used for the initial and boundary conditions. From Table 4.7 and 4.8, minimum and maximum values of the coastal rainfall has the widest range of values, hence could be the most difficult to predict in all the regions, but maxima in other regions were well captured. Other parameters (i.e. surface air temperature and dew point temperature) have close minimum and maximum values with the reference.

Table 4.7: Daily Minimum and Maximum Values in Comparison with the Reference

		REF		CLM4		Noah		Noah-MP		Noah-MP GW	
		Min	Max	Min	Max	Min	Max	Min	Max	Min	Max
DJF	Air Temp. (°C)	22.14	28.52	23.60	29.11	20.80	27.59	22.56	28.31	22.65	28.31
	Dew point Temp. (°C)	0.25	16.22	-0.67	18.20	-2.33	15.67	-1.88	17.37	-1.54	17.48
	Coastal Precip. (mm/day)	0.00	11.16	0.10	5.88	0.04	5.04	0.13	6.88	0.12	6.70
JAS	Air Temp. (°C)	23.97	26.49	24.70	27.82	24.66	26.62	24.43	27.20	23.89	26.56
	Dew point Temp. (°C)	20.60	22.20	21.71	23.25	20.56	22.41	21.33	23.00	21.19	23.13
	Coastal Precip. (mm/day)	0.68	21.97	2.06	10.00	2.10	10.24	1.96	10.91	1.90	11.66
	Savannah Precip. (mm/day)	2.01	16.77	4.06	16.08	3.23	16.08	3.81	19.10	3.55	15.28
	Sahel Precip. (mm/day)	1.85	15.83	1.05	17.85	0.49	13.99	1.43	15.89	2.80	18.44
	All region precip. (mm/day)	0.90	13.23	3.31	13.30	2.59	11.36	3.28	14.00	2.99	17.02

Table 4.8: Difference Between the Daily Minimum and Maximum Values for the Reference and the Simulations

		REF	Noah	Noah-MP	Noah-MP GW	CLM4
		max-min	max-min	max-min	max-min	max-min
DJF	Air Temperature. (°C)	6.38	6.79	5.75	5.66	5.51
	Dew point Temp. (°C)	15.97	18	19.25	19.02	18.87
	Coastal Precip. (mm/day)	11.16	5	6.75	6.58	5.78
JAS	Air Temperature. (°C)	2.52	1.96	2.77	2.67	3.12
	Dew point Temp. (°C)	1.6	1.85	1.67	1.94	1.54
	Coastal Precip. (mm/day)	21.29	8.14	8.95	9.76	7.94
	Savannah Precip. (mm/day)	14.76	12.85	15.29	11.73	12.02
	Sahel Precip. (mm/day)	13.98	13.5	14.46	15.64	16.8
	All region precip(mm/day)	12.33	8.77	10.73	14.03	9.99

Table 4.9: Positions of Each Model in Regards to Their Performance

	Variable	Noah	Noah-MP	Noah-MP-GW	CLM4
1	DJF air temp	1ST	4th	3rd	2nd
2	JAS air temp	4th	2nd	1st	3rd
3	DJF dew point temp.	1st	2nd	3rd	4th
4	JAS dew point temp	4th	1st	2nd	3rd
5	JAS all region precip.	4th	2nd	1st	3rd
6	DJF All region precip	4th	2nd	3rd	1st
7	JAS Savannah precipitation	3rd	1st	4th	2nd
8	JAS Sahel precipitation	4th	2nd	1st	3rd
9	JAS Coastal precipitation	4th	1st	2nd	3rd
10	DJF Coastal Precipitation	4th	2nd	1st	3rd

Although, each LSM performed well for some variable and worse for others as shown in Table 4.9, but with a view to get the overall best preforming LSM for all parameters, a score table was formulated for each set of variables as named A, B, C, D, E (Table 4.10). Four points was assigned to each model that performed best for each variable, three was assigned for model that came second, two for third and one for the worst performing model, i.e. fourth position. For variable combination A, **Noah-MP GW** got the highest score, **Noah-MP** got the highest for B, **Noah-MP** and **Noah-MP GW** option both got the same score for variable combination C, **Noah-MP** got highest score for precipitation for

all seasons, and **Noah-MP** was the overall best for all the variables and seasons in combination.

Table 4.10: Scores

	(A)	(B)	(C)	(D)	(E)	Total	Score
Noah	11	6	10	17	7	51	4th
Noah-MP	14	17	11	31	20	93	1st
Noah-MP GW	15	13	11	28	18	85	2nd
CLM4	10	13	8	23	15	69	3rd

(A) JAS Air Temperature, DJF Temperature, JAS Dew Point Temperature, DJF Dew Point Temperature And JAS Precipitation for all the Area, (B) DJF Precipitation for all Area, Sahel Precipitation, Savanna Precipitation, DJF And JAS Coastal Precipitation, (C) JAS Air Temperature, DJF Temperature, JAS Dew Point Temperature, DJF Dew Point Temperature and (D) All The Variables for all Seasons, (E) Precipitation for all Seasons.

Land surface models have become more important in numerical weather prediction models like WRF as more complex and sensitive planetary boundary layer schemes are used (Chen, 2007). However, from the overall performance based on the point system on Table 4.9, the Noah-MP (the overall best performing model) had an overall improvement of about 14.1% when compared against Noah (the overall worst performing model) which is a significant inprovement. CLM4 had an overall improvement of about 6% against Noah while Noah-MP-GW had about 11.4%. All the models showed maximum positive temperature bias around the EL Djouf basin in Mauritania and Northern Mali which could be as a result of the effect of the West African heat low prevalent in this area. This a low surface pressure region, which develops during the summer, linked with high insolation and seasonal surface temperatures. However, the lower bias prevalent for Noah-MP and the groundwater option than Noah in areas between latitude 11° and 14°N (which falls to the Savanna region) shows that the inclusion of a dynamic vegetation and groundwater process (as in the Noah-MP with groundwater option) can improve the simulation of temperature over this semi-arid

region of West Africa to some extent especially during the monsoon season. But the region within 15°N and 20°N (the Sahel-Sahara interface) showed high positive bias more than any other region. Noah has a strong negative bias for the desert areas in the north. According to Chen *et al*. (2014), Noah has less absorbed solar radiation resulting in colder surface and lower (or negative) sensible heat flux, which could be the reason behind the cold bias especially seen at the north-eastern part for Noah LSM. This is unique to Noah among the LSMs under study, and could also be because of the fact that among the LSMs, it is the only model that has no upward groundwater flow into the lowest soil layer that is prescribed with a lower boundary.

CLM4 has the strongest positive bias in some major highlands and the El Djouf basin, and also has the most sophisticated snow, soil, and vegetation physics among the LSMs. The El Djouf area is an arid basin, which consists of a typical African broad and shallow sedimentary basin, separated by divides formed by fault blocks, plateaus and mountain ranges, where rock waste eroded from higher surfaces has been deposited at the base. CLM4 has a very deep soil column and water table that might need a considerably long time period for temperature and soil moisture to reach equilibrium, mostly in the cold and dry regions (Liang *et al*., 2003). This could make it require more spin up time than other LSMs especially the Noah-MP, and might be its reason for high bias around the semi-arid/arid areas of the region for both temperature and dew point temperature, which in turn lowers its overall performance.

Hagos *et al*. (2014), demonstrated that different land surface schemes simulate different ET response to land use change and this leads to differences in the precipitation response through differences in local precipitation recycling, and that land surface

schemes determine the meridional structure of the evaporative fraction (or equivalently Bowen ratio), which shows a steep meridional gradient across the Sahel. As a result of this, the meridional location of the model peak temperature response is modulated, and thereby leading to differences in the response of the model mean zonal wind and thereafter precipitation.

Noah-MP introduces a TOPMODEL concept (Niu *et al*., 2004) in order to improve the separation of surface runoff and subsurface runoff, and links both flows to the water table depth through exponential functions. This might have been the reason for the high bias recorded for temperature and dew point temperature over the region during the dry season (when the water table depth is very deep and infiltration-excess runoff is dominant) for all the models with the TOPMODEL concept for surface runoff (i.e. CLM4 and Noah-MP). However, Noah LSM with no such model simulates dry season temperature and dew point temperature better than the others. Noah-MP has the closest minimum air temperature value to ERA-interim (as the reference) while CLM4 has the highest, and Noah-MP with Noah-MP GW has the closest maximum value while Noah has the highest for DJF air temperature. But for JAS air temperature, Noah-MP GW has the closest minimum air temperature value to the reference while CLM4 has the highest, and Noah-MP GW has the closest maximum value while CLM4 has the highest for JAS air temperature. This is an indication that CLM4 could overestimate both the minimum and maximum air temperature for the area. For the Coastal precipitation, there were obvious high differences in maximum precipitation for all the simulations which shows that all the simulations underestimate daily high intensity rainfall over the coastal region of West Africa and also overestimate the minimum precipitation.

4.3 Impact of Land Use Land Cover Change on WRF Outputs Over West Africa

From the average spatial plot of temperature for JAS (Figure 4.21 a-d), it can be seen that there is increasing temperature gradient with increasing latitude just like the

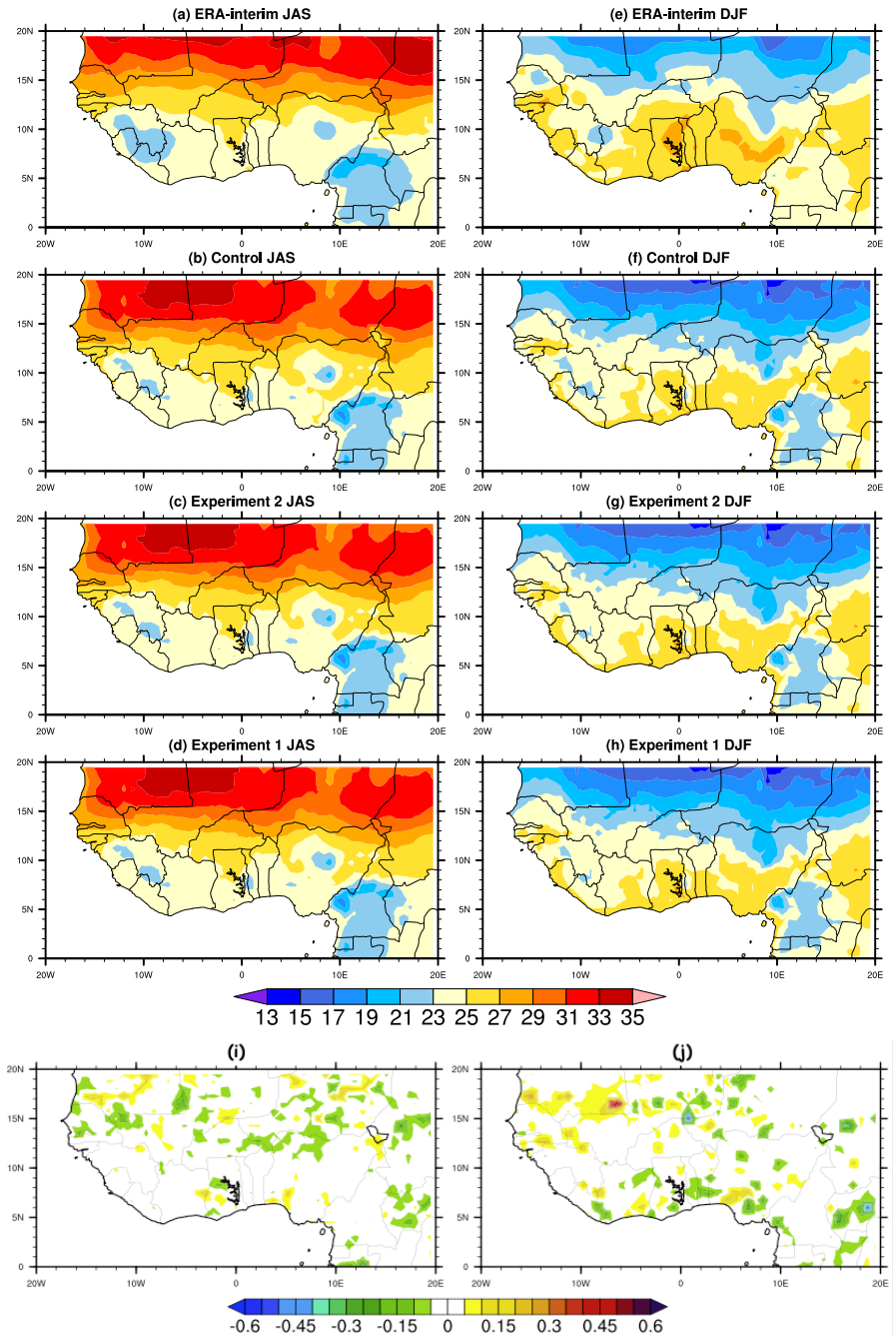

Figure 4.21: Spatial Distribution of 2m Air Temperature (°C) (a-d are for JAS season while e-h are DJF season) (i) is the difference between the 2m air temperature output from JAS experiment 1 and 2 (j) is the difference between the 2m air temperature output from DJF experiment 1 and 2.

reference from areas above 10°N for both the control simulation and ERA-interim. This is necessary to show that the control simulation is in line with the reference. There were clear cooling areas around the highlands of Jos Plateau, Guinea and Cameroon for the reference, the control and the experiments. The output for DJF (Figure 4.21 e-h) shows decreasing temperature with increasing latitude just like the reference from areas above 10°N. The control simulation with the experiments and ERA-interim were able to capture the cooling's around the highlands of Jos Plateau, Guinea and Cameroon satisfactorily. Figure 4.21 i and j reveal the spatial difference between the two experiments for both JAS and DJF season. Also, there were higher difference around 15-18°N for the DJF season. Also, there was more difference in temperature as a result of LULC change over the southern and northern part of the area especially in the DJF season.

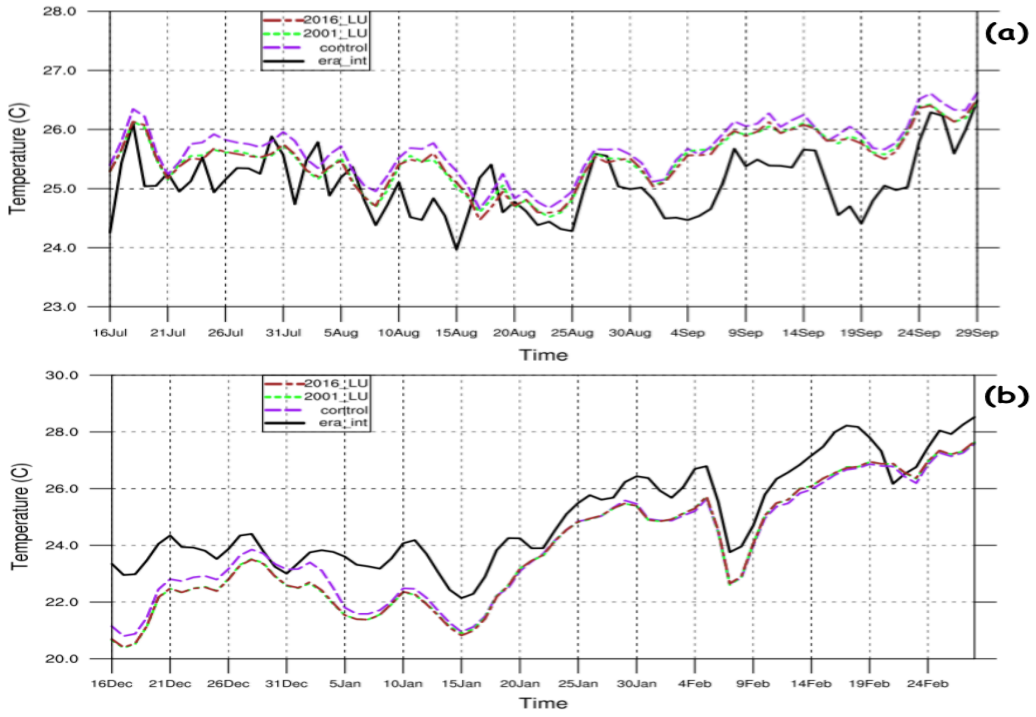

Figure 4.22: Time series of daily 2m air temperature averaged over 10°W-10°E and 5°-15°N (a) JAS (b) DJF (2016_LU is experiment 1, 2001_LU is experiment 2)

From the time series of JAS daily 2m surface temperature averaged over 10°W-10°E and 5°-15°N (as shown in Figure 4.22. a), the control simulation seems to have higher temperature than the experiments throughout the period. Also, the outputs from the two experiments differ with either higher or lower values at different point. This shows that the output was really affected with the change in the land cover data. The difference between the control and the experiment was obvious in December to mid-January (as seen in Figure 4.22 b). The values were closer from late January to early February.

Figure 4.23 a-e spatially displays the average JAS daily precipitation, a-e showed maximum precipitation concentrated around Fouta Djallon highlands, Jos Plateau and Cameroon Mountains. There seems to be a more intense precipitation core formed around the Fouta Djallons in Guinea both in TRMM, GPCP, control and the experiments. The control seems to produce more intense precipitation around the highlands than TRMM and GPCP. From Figure 4.23 f-j, areas above 7°N were dry as a result of the influx of the dry north easterlies during this period. Obvious difference was seen between experiment 2 and 1 especially around longitude 0°, and there was a more intense precipitation around Fouta Djalon highlands in the control simulation than the experiments. Also, the effect of the LULCC was prevalent on the precipitation rate over the region as seen in Figure 4.23 k and l, but clearly in Figure 4.23 k (JAS) as there were precipitation increase in some area and decrease in some parts. It however shows that land cover change affects the output of WRF simulations, and that the model is sensitive to LULC change.

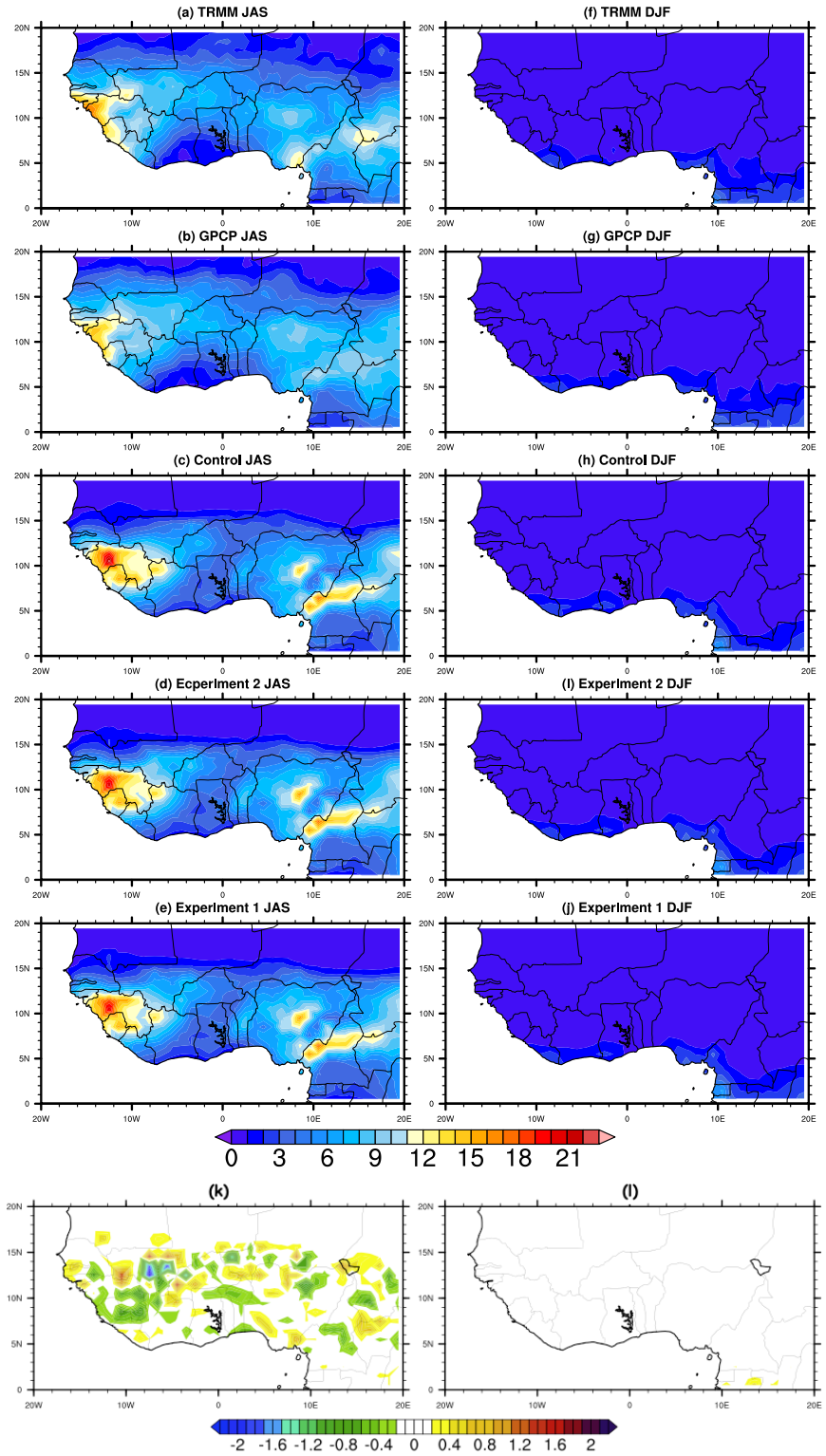

Figure 4.23: Spatial distribution of average precipitation (a-e are for JAS season while f-j are DJF season) (k) is the difference between the precipitation output from JAS experiment 1 and 2 (l) is the difference between the precipitation output from DJF experiment 1 and 2

Figure 4.24 a shows the time series of daily precipitation amount averaged over longitude 10°W-10°E and latitude 5°-15°N for 16th of July to 29th of September 2012. The pattern of the control simulation and the experiments agree with the reference in some instances and disagree in others. From Figure 4.24 b, it can be shown that that the control simulation and the experiments disagree with the reference pattern on 21st and 29th of December and 22nd of February but have similar pattern in other periods. The little or no precipitation notable for this period of the year in the region was well captured in both the control simulations and the experiments.

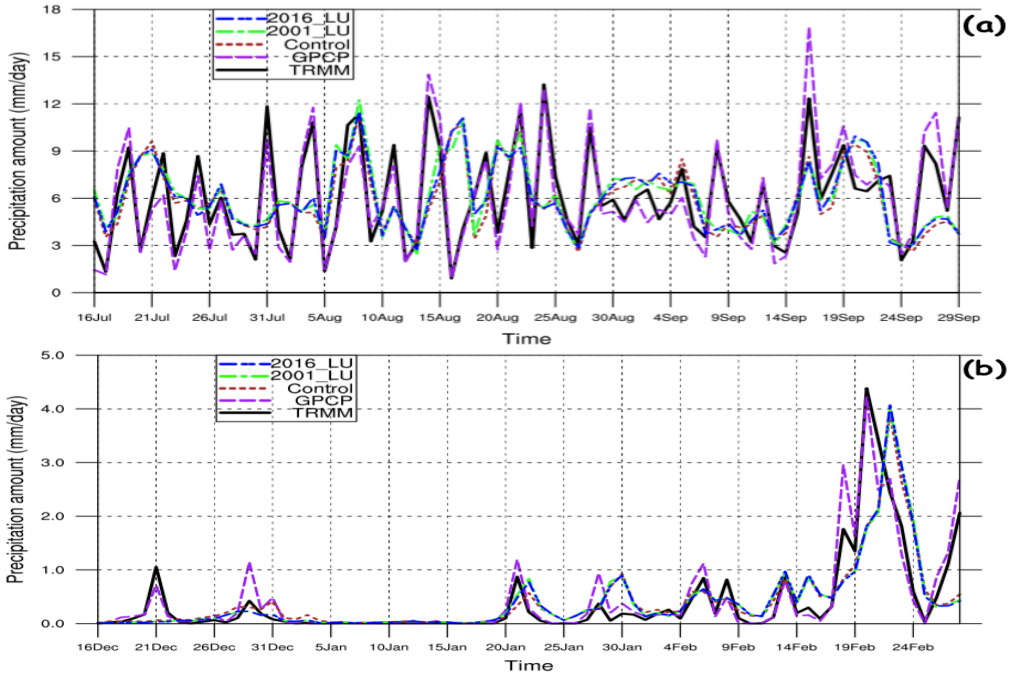

Figure 4.24: Time series of daily value for precipitation averaged over 10°W-10°E and 5°-15°N (a) JAS (b) DJF. (2016_LU is experiment 1, 2001_LU is experiment 2).

Figure 4.25 a-h shows the spatial distribution of daily JAS average dew-point temperature. It can be seen that the control simulation and the experiments can reasonably simulate the dew-point temperature over West Africa.

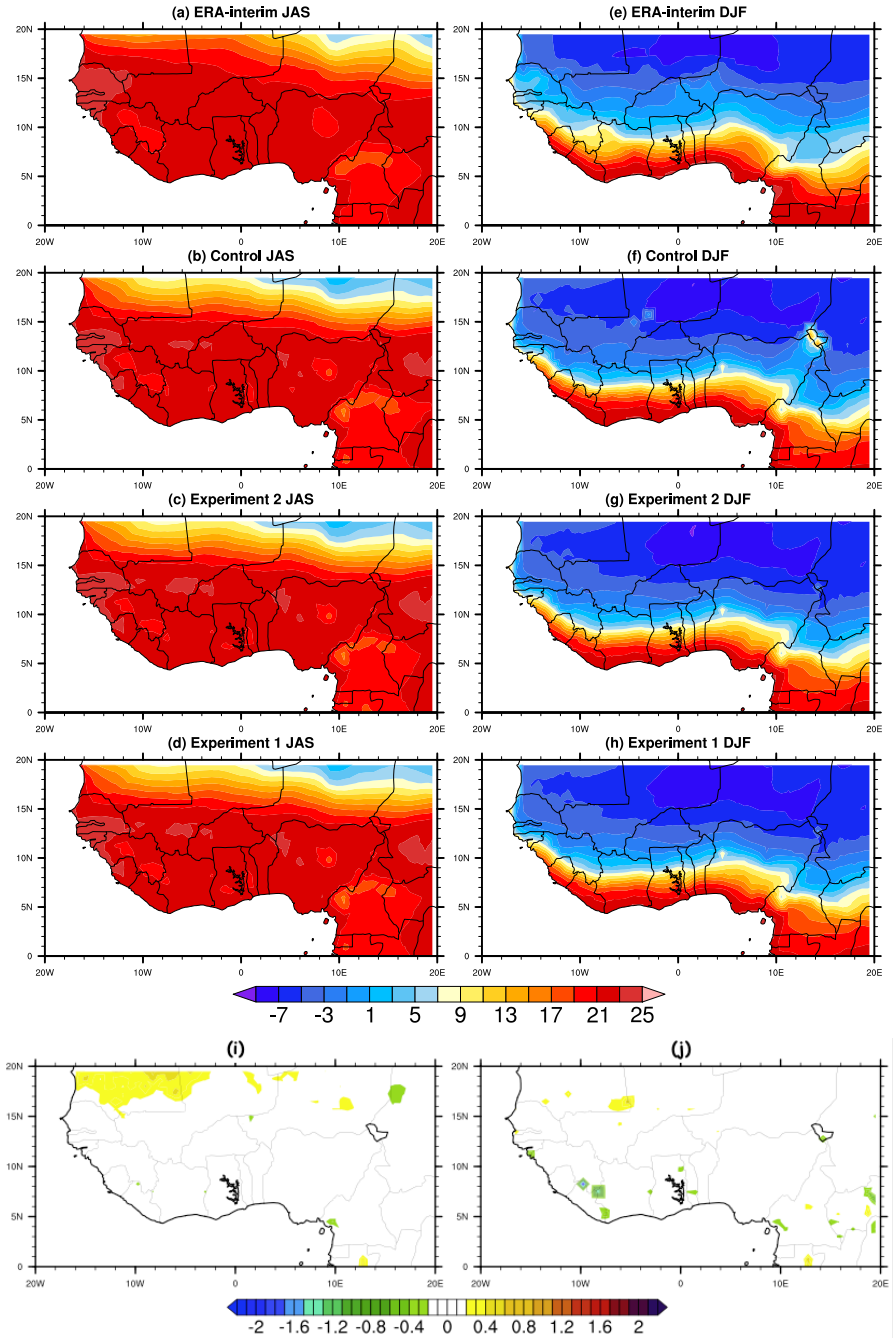

Figure 4.25: Spatial distribution of 2m dew point temperature (°C) (a-d are for JAS season while e-h are DJF season) (i) is the difference between the 2m dew point temperature output from JAS experiment 1 and JAS experiment 2 (j) is the difference between the 2m dew point temperature output from DJF experiment 1 and DJF experiment.

It also shows increase in dew-point temperature from the Northern to the southern part. A reduced dew-point temperature was obvious around the Jos plateau and the Cameroon-Adamawa Mountains.

From the spatial plot of daily DJF dew-point temperature as shown in e-h, all the experiments show the drier dew points extending more south to about 7°N. Also, all the models show a little higher dew point temperature around Lake Chad in which the reference did not depict. However, the effect of the land use change was notable in areas between 15-20°N (The Saharan-Sahelian interface) especially during the JAS season. This also shows that LULCC affects dew-point temperature in this region.

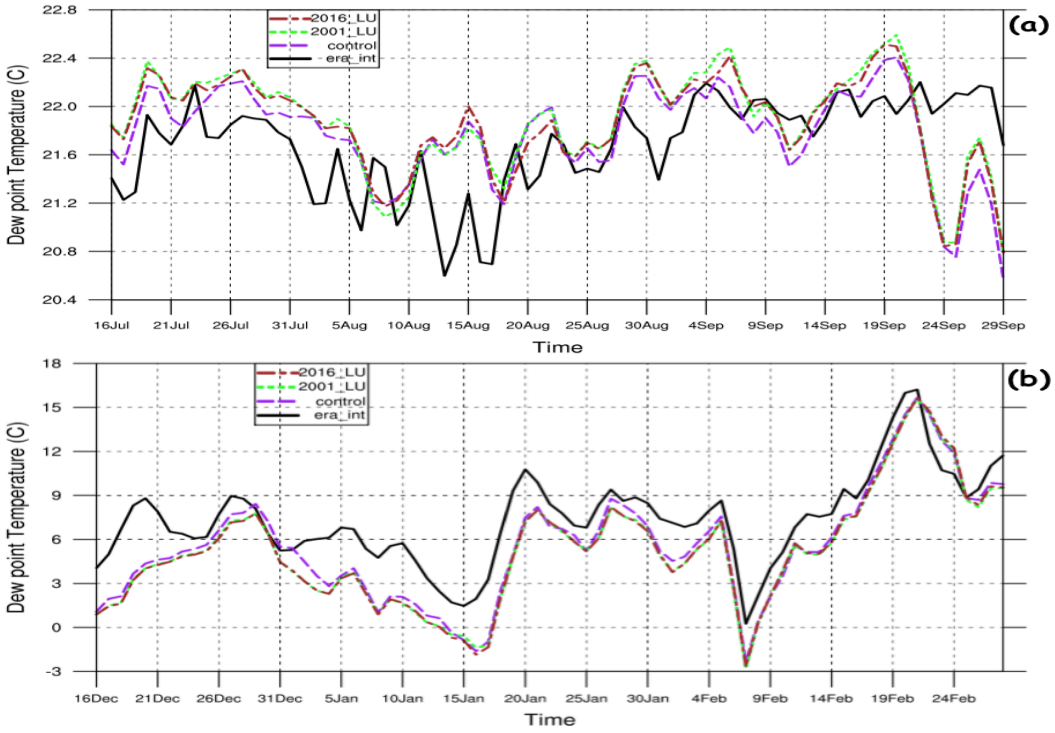

Figure 4.26: Time Series of Daily Dew Point Temperature Averaged over 10°W-10°E and 5°-15°N (a) JAS (b) DJF. (2016_LU is Experiment 1, 2001_LU is Experiment 2).

Figure 4.26 (a) shows the time series of the average dew point temperature for JAS over the 3 months period. The control simulation was lower than the experiments throughout the period of study. Also, experiment 2 has higher values than 1, except for August 6-10. For the DJF season Figure 4.26 b, the control simulation is higher than the experiments, while the two experiments have close values throughout the period.

Albedo is the fraction of incident radiation that is reflected. The surface albedo plays a vital role in the land and ocean surface atmosphere interaction, as it substantially influences the absorption of shortwave radiation. A decrease in albedo would result into a reduction in the quantity of the shortwave radiation that is reflected to the atmosphere, and consequently increases the amount of shortwave radiation that is absorbed. From Figure 4.27 a, b, c and d, it can be seen that the albedo value was maximum (>0.36) in areas above 15°N which is mostly covered with dessert sand or barren land, for both experiments in both season. For the rainy season in both experiments (Figure 4.27 a and c), areas between latitude 9°N and 15°N consist mostly of grasslands, croplands and Natural vegetation mosaics in the JAS season with albedo value ranging mostly between 0.14 and 0.22, whereas in the in the dry season, (Figure 4.27 b and d), the albedo value for the same area ranges mostly between 0.22 and 0.26. The minimum values of albedo were found in area around latitude 7°N and bellow, which are mostly covered with evergreen broadleaf forests with albedo value of about 0.08. From Figure 4.27 e and f, there was a sharp decrease at the boundary between the barren land and the grassland (i.e. the Sahel-Sahara interface). Also, there is a decrease in albedo in most part of the study area in both the dry and rainy season. This indicates that land use change affects albedo.

From Figure 4.28, albedo decreased during the rainy season and increased during the dry

season. The peak value of albedo was recorded in February and the least in September.

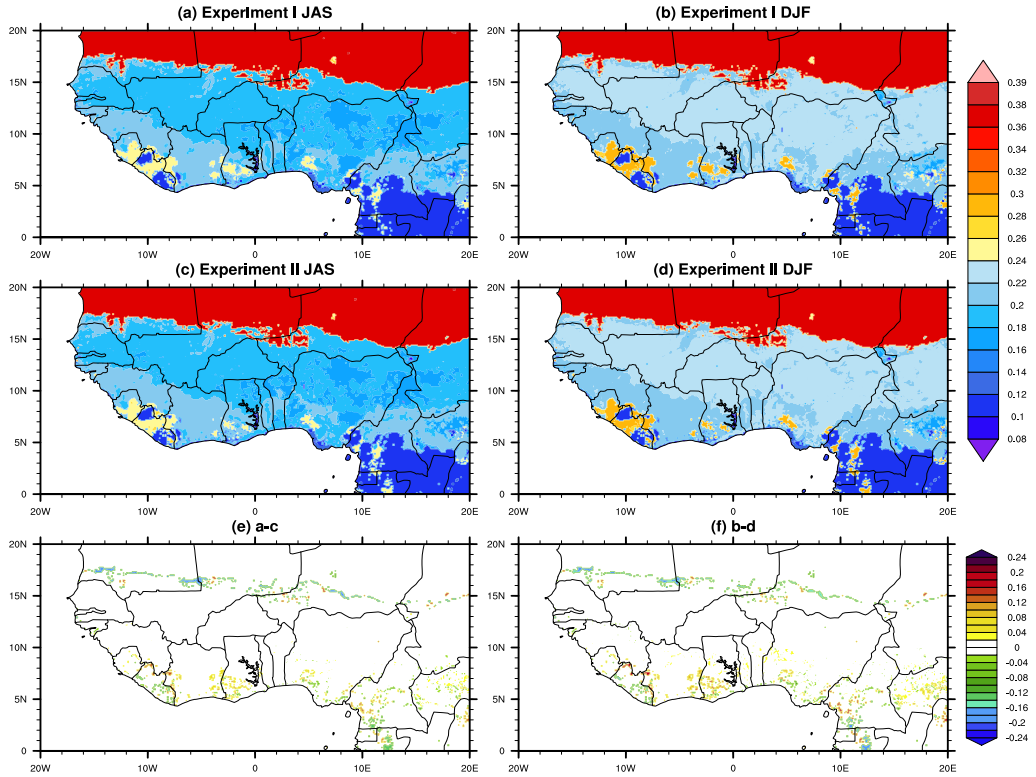

Figure 4.27: Spatial distribution of Albedo (a) experiment 1 JAS, (b) experiment 1 DJF, (c) experiment 2 JAS (d) experiment 2 DJF, (e) is a – c, (f) is b – d.

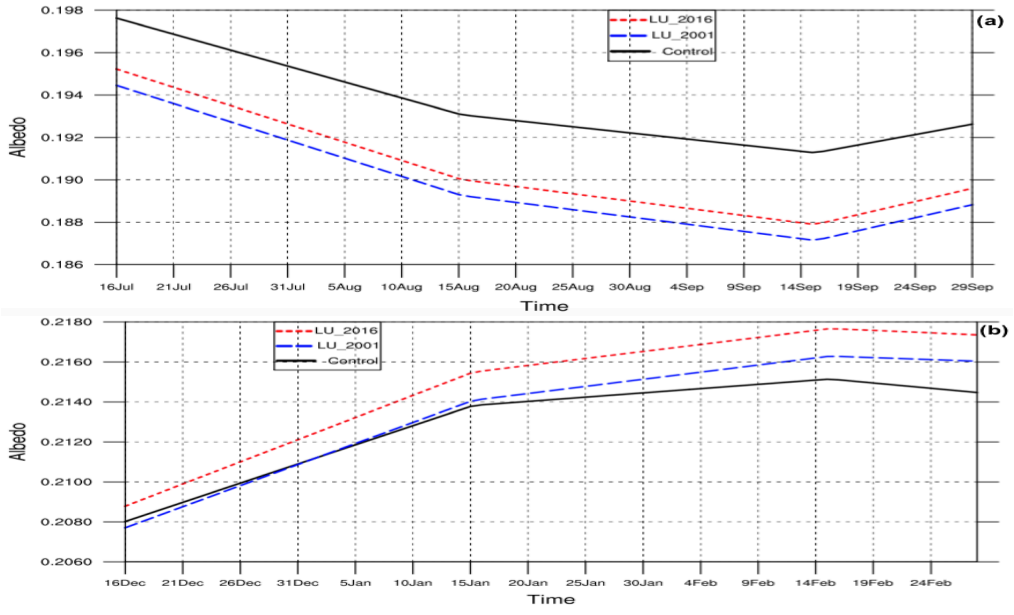

Figure 4.28: Time series of Albedo averaged over 10E-10W, 5°N-15°N for (a) JAS and (b) DJF.

From 4.29 a, b, c and d, the emissivity is minimum at the areas above the 15°N for both experiment in the two seasons. For the rainy season, in both experiment (Figure 4.29 a and c), areas covered with water and croplands has the maximum amount of emissivity, whereas, the dry season (Figure 4.29 b and d) has lower value in the same area which could be caused by the lack of rainfall during this period of the year. Figure 4.29 e and f also showed that land cover change in WRF model has effect on the output of the model as the difference between the value of emissivity between the two experiment show increase in some areas and decrease in some area. Also, there was more increase in the difference between experiment 1 and 2 for the rainy season than for the dry season. There was a pronounced increase in emissivity at the boundary between the

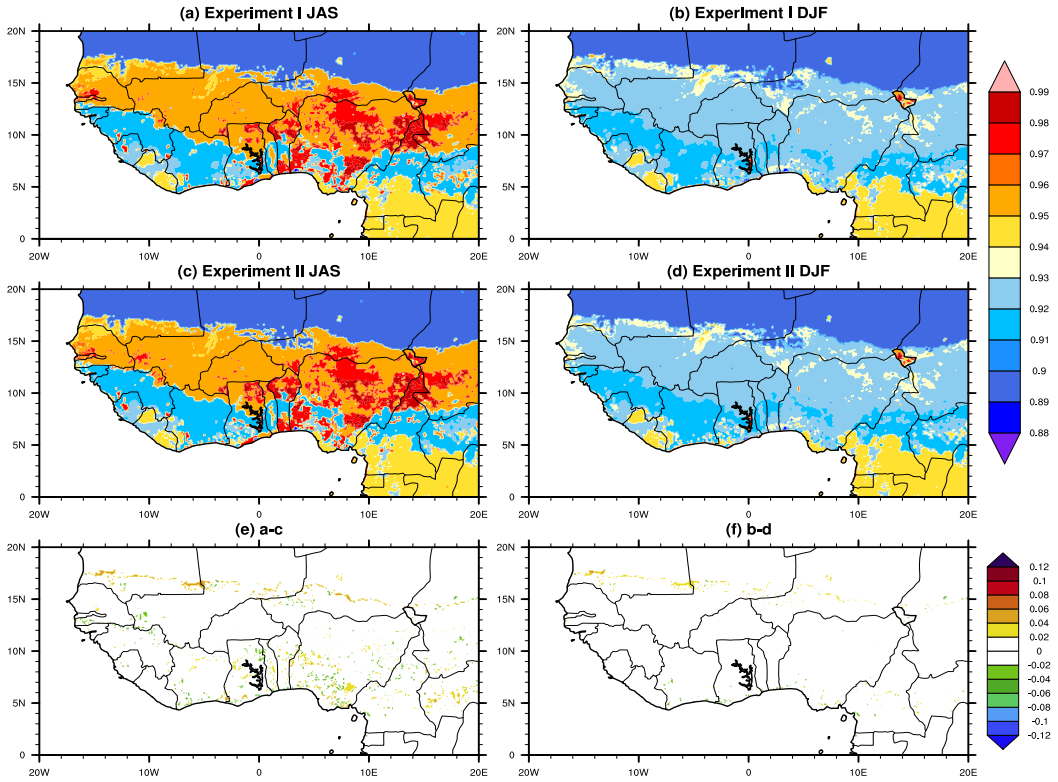

Figure 4.29: Spatial Distribution of Emissivity (a) Experiment 1 JAS, (b) Experiment 1 DJF, (c) Experiment 2 JAS (d) Experiment 2 DJF, (e) a – c, (f) b – d.

barren land and the grassland for both seasons. The time series of daily emissivity as presented in Figure 4.30 a, shows that emissivity increased during the wet season and peaked in September. The value started dropping after September. Also, from Figure 4.30 b, its value continued to drop all through the dry season.

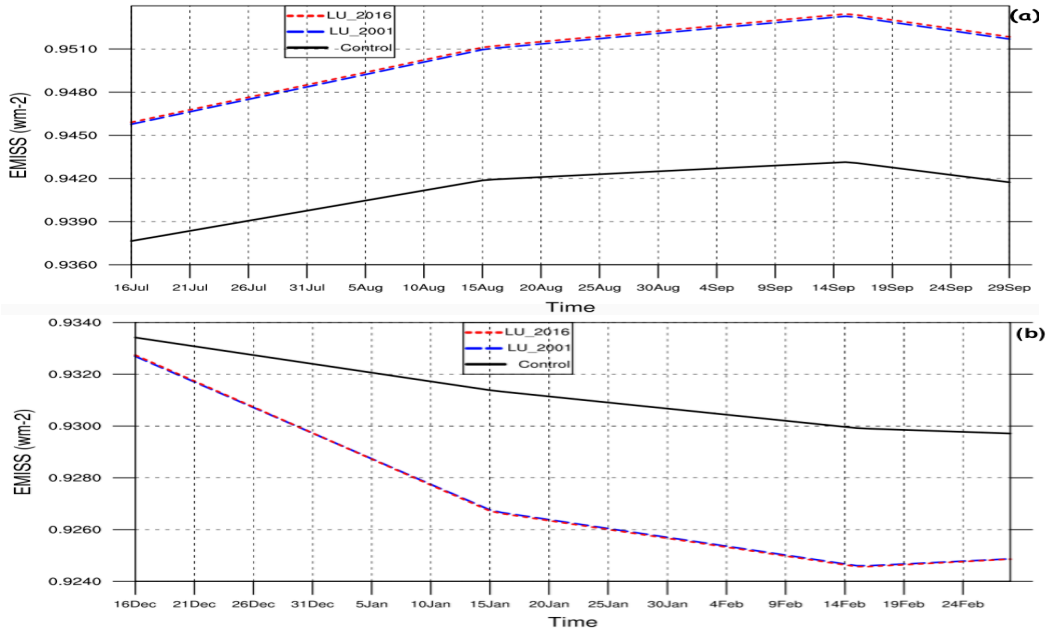

Figure 4.30: Time series of daily Emissivity averaged over 10W-10E and 5-15°N for (a) JAS and (b) DJF

Leaf Area Index (LAI) is a dimensionless quantity that describes plant canopy, and can be defined as the area of green leaves per unit area of the ground, and is taken as a critical crop parameter (Jonckheere *et al.,* 2004). High value of LAI is a sign of a denser or healthier crop canopy, while a low value symbolizes sparse or drier canopy. From Figure 4.31 a - d, the LAI is minimum at the areas above the 15°N for both experiment in the two seasons. For the rainy season, in both experiment (Figure 4.31 a and c), the forests and croplands has the maximum amount of LAI, whereas, the dry season (Figure 4.31 b and d) has lower value in most of the area due to the lack of rainfall during this period of

the year. Figure 4.31 e and f also showed that land cover change in WRF model has effect on the output of the model as the difference between the value of LAI between the two experiment show increase in some areas and decrease in some other area. Also, there was more increase in the difference between experiment 1 and 2 for the rainy season than for the dry season. Also, the time series as shown in Figure 4.32 a and b revealed that LAI increases during the JAS season and decreased during the DJF season. The highest LAI was reference in September, while the lowest was in February. This happens because most of the vegetation in the region is usually lost due to the long period of dryness experienced during the DJF period. The value picks up again at the advent of rainfall over the region.

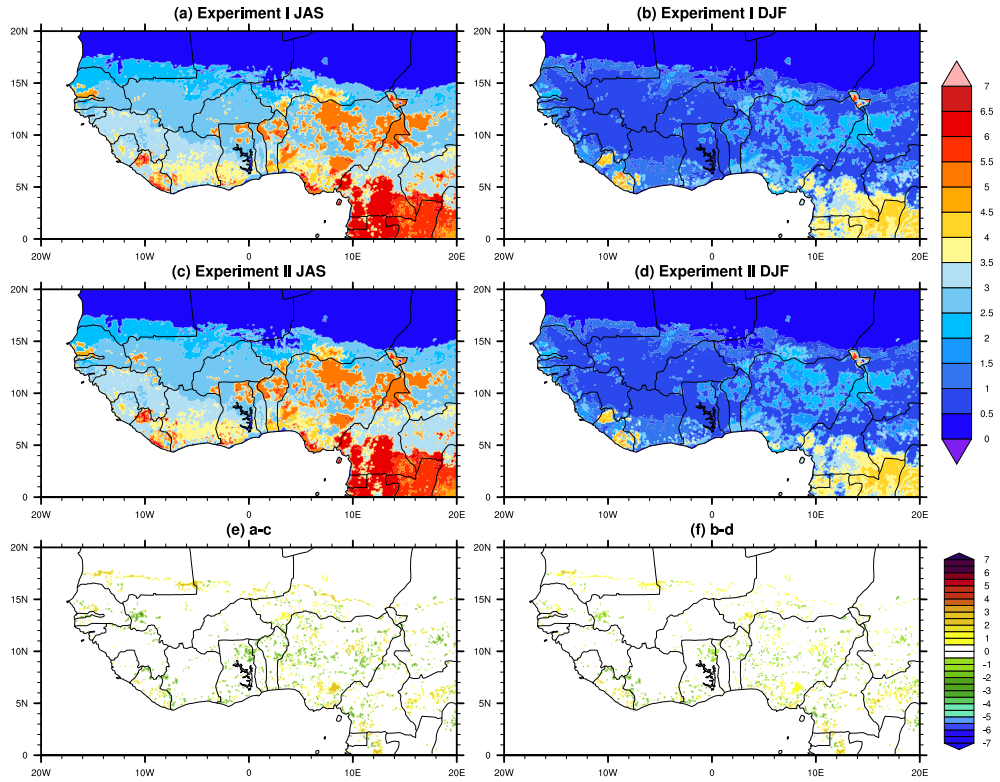

Figure 4.31: Spatial Distribution Of Leaf Area Index LAI (a) Experiment 1 JAS, (b) Experiment 1 DJF, (c) Experiment 2 JAS (d) Experiment 2 DJF, (e) a – c, (f) is b – d.

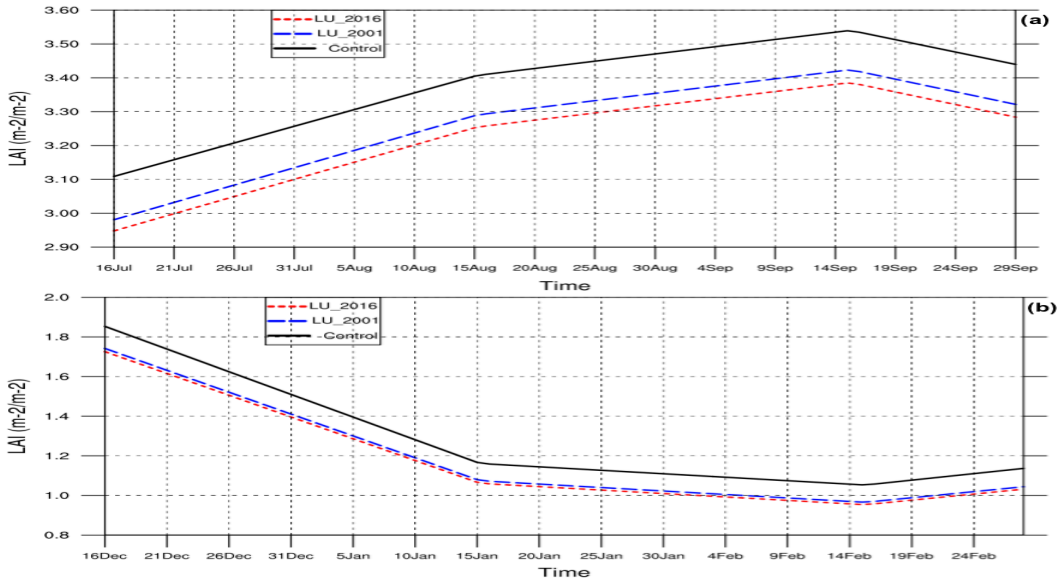

Figure 4.32: Time series of daily LAI averaged over 10W-10E and 5-15°N for JAS (a) JAS and (b) DJF

The Outgoing Longwave Radiation (OLR) at the top of the atmosphere provides significant information concerning the Earth's outgoing energy and overall energy budget at the Top Of the Atmosphere (TOA). It is among the radiation variables that dictate the Earth radiation budget at the TOA. From Figure 4.33 a and c, the OLR is maximum at the areas above the 15°N for both experiment and also decreases southwards during the rainy season, while it increases southward during the dry season. Also, there were generally a higher OLR during the dry season than the rainy season. However, Figure 4.33 e and f also showed that land cover change in WRF model has effect on the output of the model as the difference between the value of OLR between the two experiment show increase in some areas and decrease in some area. Also, The difference between experiment 1 and 2 for the rainy season is higher than for the dry season. Figure 4.34 a and b, shows that using the updated land use data (2016 LU), there was a little shift in the outputs of the model and also showed that the model is sensitive to the changes in land use and land cover.

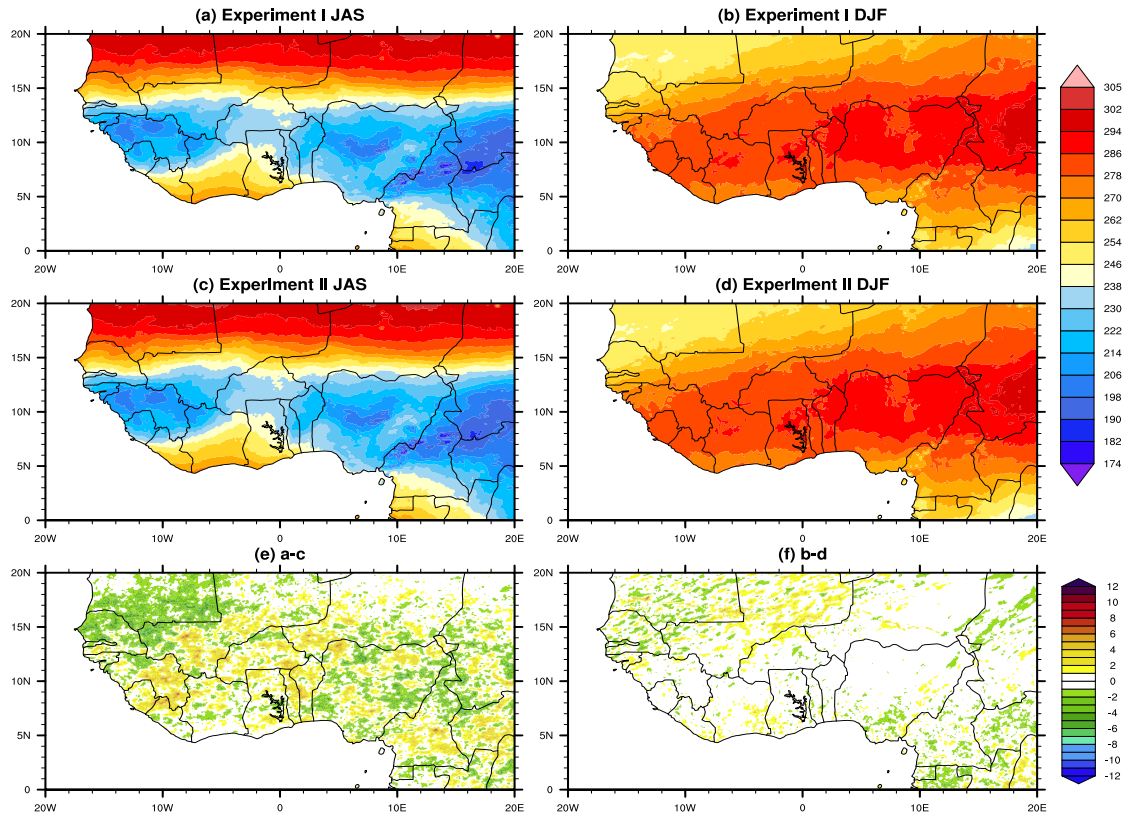

Figure 4.33: Spatial Distribution of Outgoing Long Wave Radiation OLR (a) experiment 1 JAS, (b) experiment 1 DJF, (c) experiment 2 JAS (d) experiment 2 DJF, (e) is a – c, (f) is b – d.

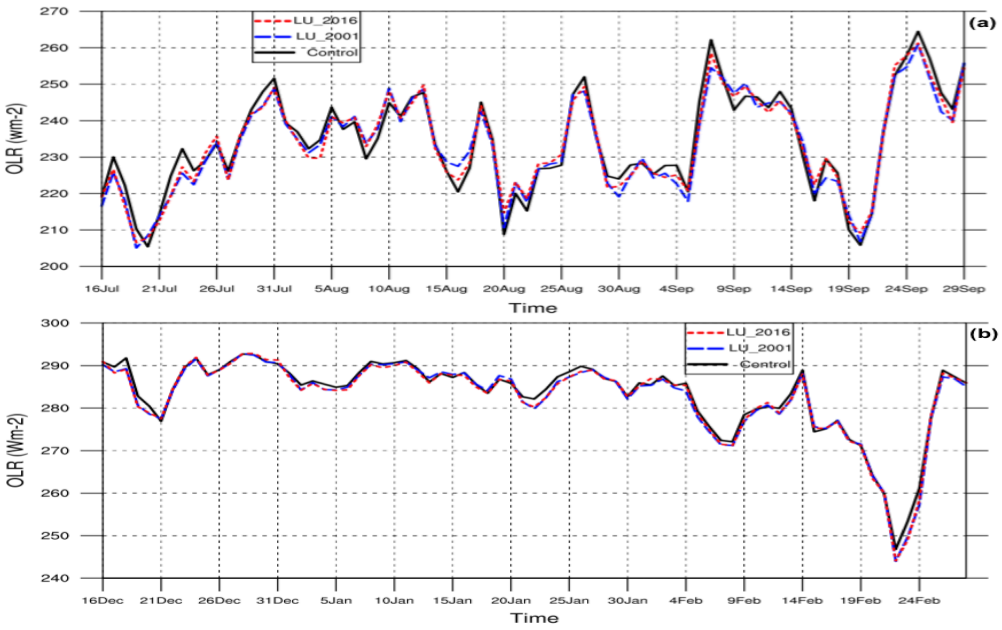

Figure 4.34: Time Series of Daily Outgoing Longwave Radiation (OLR) Averaged Over 10W-10E and 5-15N for (a) JAS and (b) DJF

From Figure 4.35 a-d, the spatial soil moisture averaged for the four Noah levels showed an increasing value towards the south. The JAS period has more moisture because of the presence of monsoon rainfall in the area. Also, Figure 4.35 e and f revealed the difference between the two experiments for JAS (e) and for DJF (f). The time series of the soil moisture for JAS and DJF for the four LSM layers were presented in Figure 4.36 a and b respectively. The surface layer (0.1m from the surface) and the root zone (1.0 m down from the middle layer) will exhibit the strongest influence on the surface evaporation fluxes. In general, the surface soil moisture affects ground evaporation, while the root zone soil moisture has a greater influence on the transpiration by vegetation (Steiner *et al*., 2009). Therefore, the greatest impact of the deep reservoir of soil moisture will be found in regions with high tree cover, such as the Guinean Coast

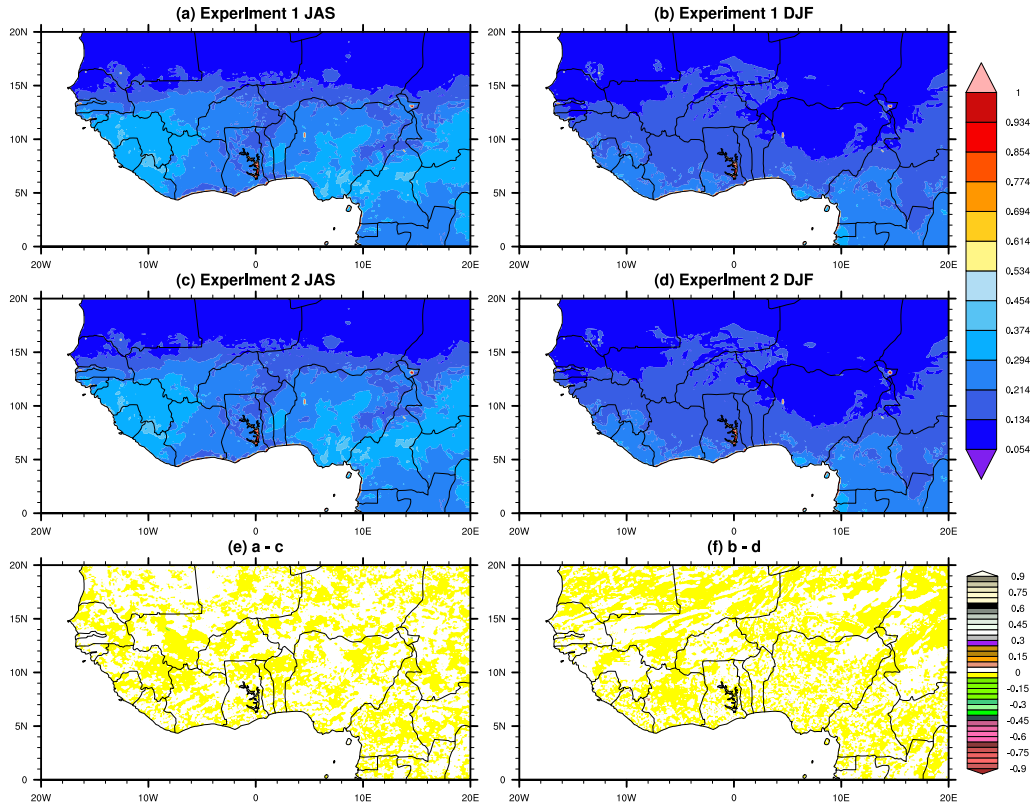

Figure 4.35: Spatial Distribution of Soil Moisture Averaged for the Four Levels (0.10, 0.30, 0.60 and 1 m)

(Steiner *et al*., 2009). This is in line with the outputs from the result as the soil moisture value decreases with increasing latitude as in Figure 4.35. The uppermost layer (surface layer) for both seasons has varying amount over the period while the lowest level has more steady increase for the JAS season and decrease for the DJF season. The effect of LULC change was more visible in August. However, it shows that the model is sensitive to changes in soil moisture due to land cover change.

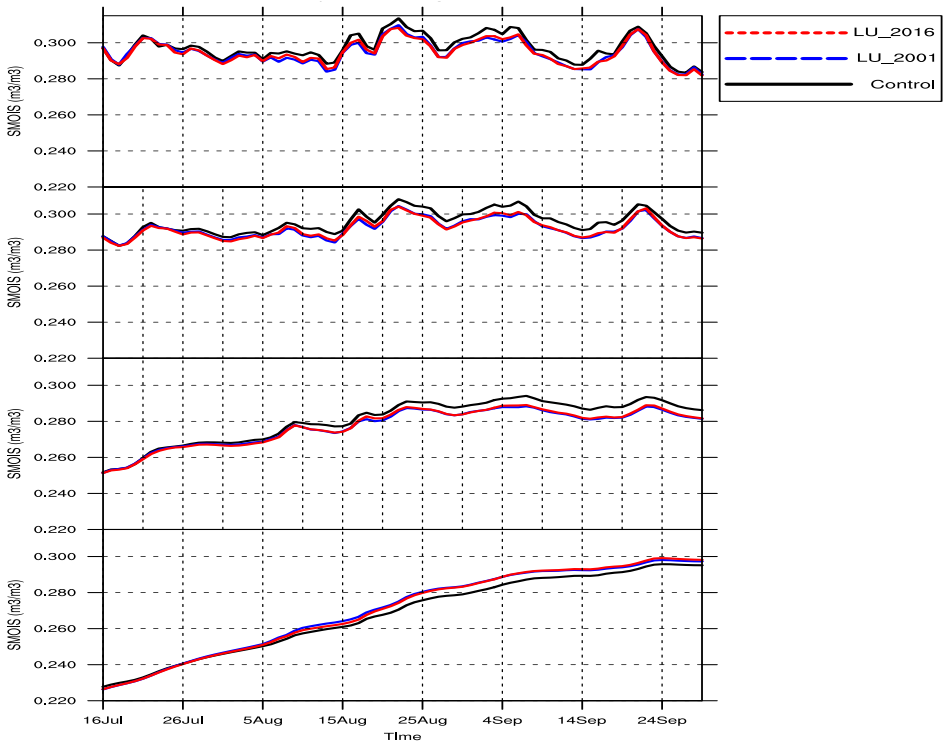

(a)

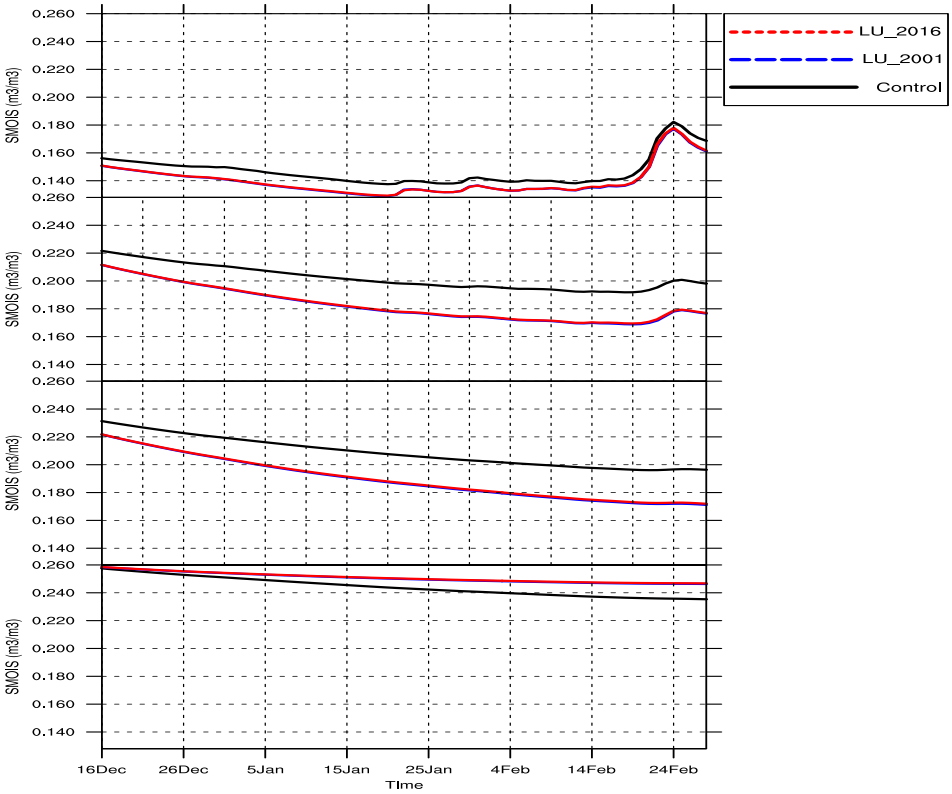

(b)

Figure 4.36: Time Series of Daily Soil Moisture Averaged for (a) JAS and (b) DJF for the 4-layer (0.10, 0.30, 0.60 and 1 m)

Figure 4.37 and 4.38 displays the differences between the outputs of experiment 1 and 2 for JAS and DJF seasons. All the parameters displays differences regards to LULCC. However, the results have shown that LULCC affects meteorological and biogeophysical parameters like rainfall, temperature, albedo, emissivity, dew point temperature, soil moisture and TOA OLR through some simulations using two different land use data and keeping all other parameters constant. The feedback of the land – atmosphere interaction can alter the albedo and soil moisture. It can also alter the evaporation process, and as a result affect the response of weather variables. Results from Fuller and Ottke, (2002) proposed that other factors apart from rainfall influence the temporal behavior of land-surface albedo in West Africa including land use and woody vegetation cover. According to Pitman (2003), albedo changes naturally with solar insolation angle. It can also change

seasonally with changes in vegetation and stochastically with precipitation. Albedo can also be altered through land cover change and other human factors that alter the physical characteristics of vegetation.

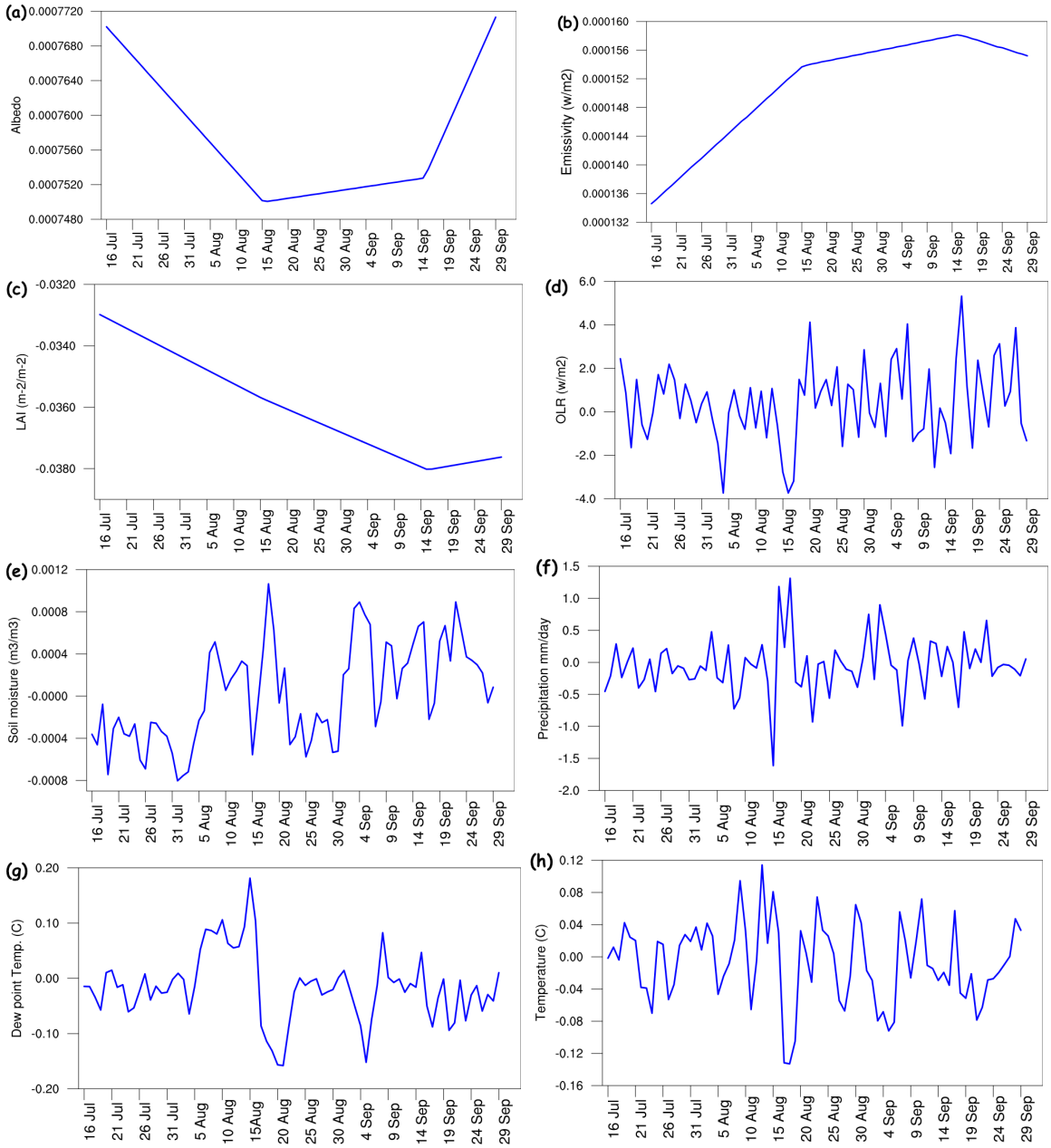

Figure 4.37: Daily JAS Time Series of the Difference between the outputs of the simulations from experiment 1 and 2 (i.e. 2016_LU-2001_LU) for: (a) Albedo, (b) Emissivity, (c) LAI, (d) OLR, (e) Soil Moisture, (f) Precipitation, (g) Dew Point Temperature, (h) Temperature.

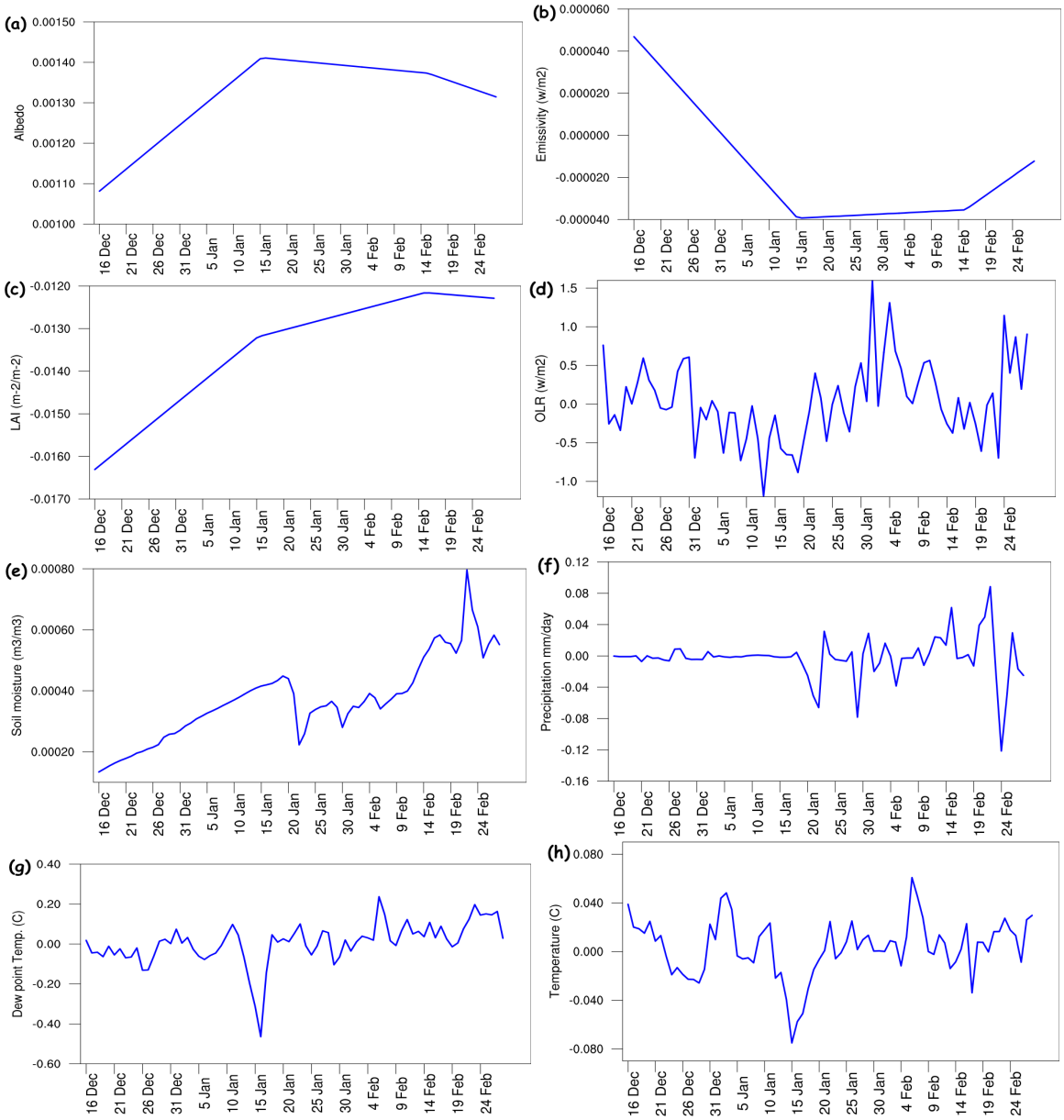

Figure 4.38: Daily DJF Time Series of the Difference between the outputs of the simulations from experiment 1 and 2 (i.e. 2016_LU-2001_LU) for: (a) Albedo, (b) Emissivity, (c) LAI, (d) OLR, (e) Soil Moisture, (f) Precipitation, (g) Dew Point Temperature, (h) Temperature.

Consequently, increase in albedo could reduce the absorption of shortwave radiation, decreases latent and sensible heat flux. This reduces water vapour and boundary layer heating, and both consequently decrease convective clouds which results into decrease in Precipitation (Pitman, 2003). Decrease in soil moisture could decrease latent heat flux

and increase surface temperature, and in a way reduces water vapour, decrease clouds and precipitation. Decreased moisture could also cause a change in evaporation rate of the model. However, in depth study is still needed to establish the said relationship. According to Eltahir (1998), decrease in initial soil moisture results into a: decreased latent heat fluxes, increased sensible heat, decreased in total fluxes, increased PBL height, decreased moist static energy in the PBL, increased stability (weaker gradient of equivalent potential temperature) and eventually decreased precipitation. Although in the work of Kunsman and Jung (2006) where they studied the impact of decreased and increased initial soil moisture on total rainfall and on precipitation recycling indicators. They found a scale dependent, positive (increased precipitation at increased initial soil moisture) as well as negative (decreased precipitation at increased initial soil moisture) feedback mechanisms. Negative feedback mechanisms were prevalent on a small scale while positive feedback was prevalent on the large scale. Therefore, according to Kuntsman and Jung (2006), sensitivity of precipitation with respect to soil moisture was very variable over space.

4.4 Impact of Land Use Land Cover Change (LULCC) on Some Hydrometeorological Parameters Over West Africa

In other to justify the incorporation of satellite data in the model, the simulation of precipitation and temperature from the updated satellite data were validated. Figure 4.39 shows the spatial plot of daily average precipitation for 21 May – 28 September 2012 using the default land use data in the model and the updated MODIS satellite data for 2012, as the first 20 days was taken as spin up. Comparing the precipitation outputs from the two simulations simulation, the TRMM and GPCP shows a zonal distribution with

precipitation decreasing from the south to the North (Figure 4.39 a and b). Also, precipitation peaks were found on the highlands of Fouta Jallon, Jos, and Cameroon. The simulations with the default LU and the updated satellite data also shows a zonal distribution with precipitation decreasing from the south to the North with maximum precipitation also in the highlands, but with higher values (Figure 4.39 c and d). The difference between the outputs from default LU and that from the updated satellite LU is presented in Figure 4.39 e and f. The high precipitation bias prominent around Lake Chad for simulations with the default LU was normalised to almost zero when satellite data was incorporated as shown in Figure 4.39 f. Figure 4.40 represents the simulation of the daily average May-September (MJJAS) 2m temperature with the default LU (b) and the incorporated satellite data (c). Both simulations show north south gradient, with coldest temperature of 19°C over the orographic areas and higher temperature of about 36°C over the area close to 20°N. The high temperature bias prominent around Lake Chad for simulations with the default LU was also normalised to almost zero when satellite data was incorporated as shown in Figure 4.40 f. This is in line with the findings of some researchers like Miller *et al*. (2006), Liu *et al*. (2009), Sertel *et al*. (2011), Case *et al.* (2012), Wen and Lu (2012), Zhao *et al*. (2012), Zhao *et al*. (2014), whom have also shown that incorporation of remotely sensed data into a model improves the outputs.

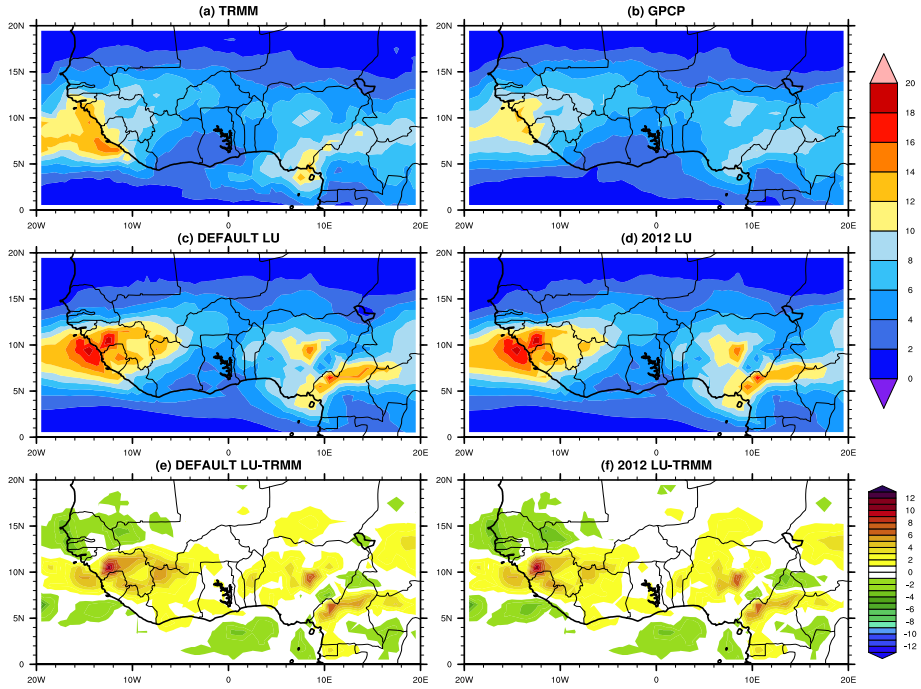

Figure. 4.39: Spatial Plot of Daily Average Precipitation for 21 May – 28 September 2012 (a) TRMM, (b) GPGP, (c) simulation with the WRF default land use data, (d) simulation with the MCD12Q1 MODIS 2012 data, (e) c-a, (f) d-a.

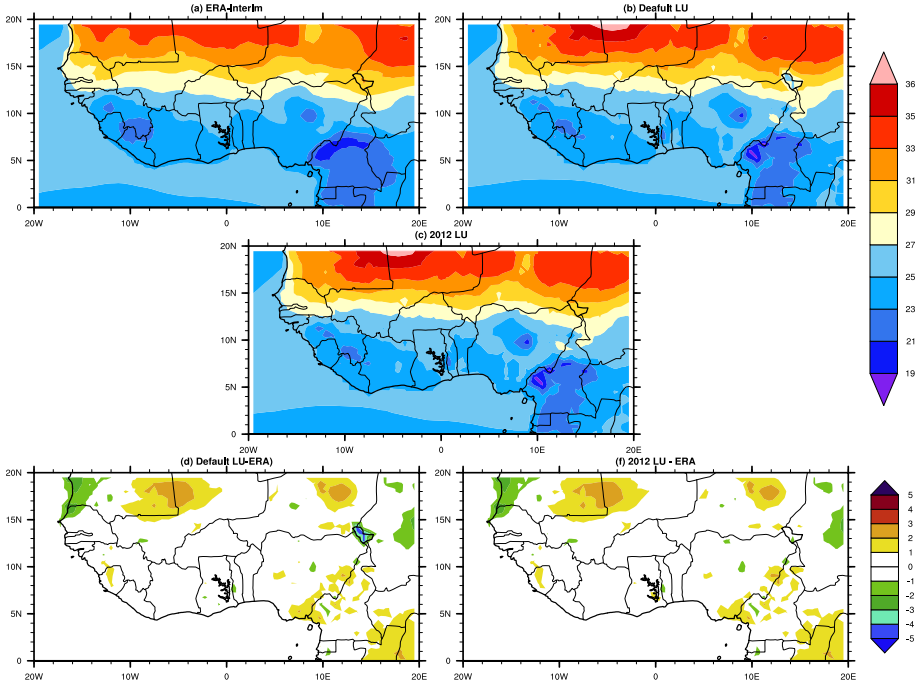

Figure 4.40: Spatial Plot of Daily Average 2m Temperature for 21 May – 28 September 2012 (a) TRMM, (b) GPGP, (c) simulation with the WRF default land use data, (d) simulation with the MCD12Q1 MODIS 2012 data, (e) c-a, (f) d-a.

From Figure 4.41a, increased built up lands (i.e., changing croplands and wetlands to built up lands) caused a decrease in dew point temperature in the area. The white colormap in the plots are areas with insubstantial increase or decrease. Researchers like Carrington *et al*. (2001) and Bai *et al*. (2013) have stressed that the conversions of wetlands to other land use types could alter local hydrological cycling and influence the microclimate of regions. For both Partial Deforest I (PDI) and Partial Deforest II (PDII) scenarios (Figure 4.41 b and c), the dew point temperature is not affected much over West Africa, although, there is a decrease in dew point temperature for both scenario.

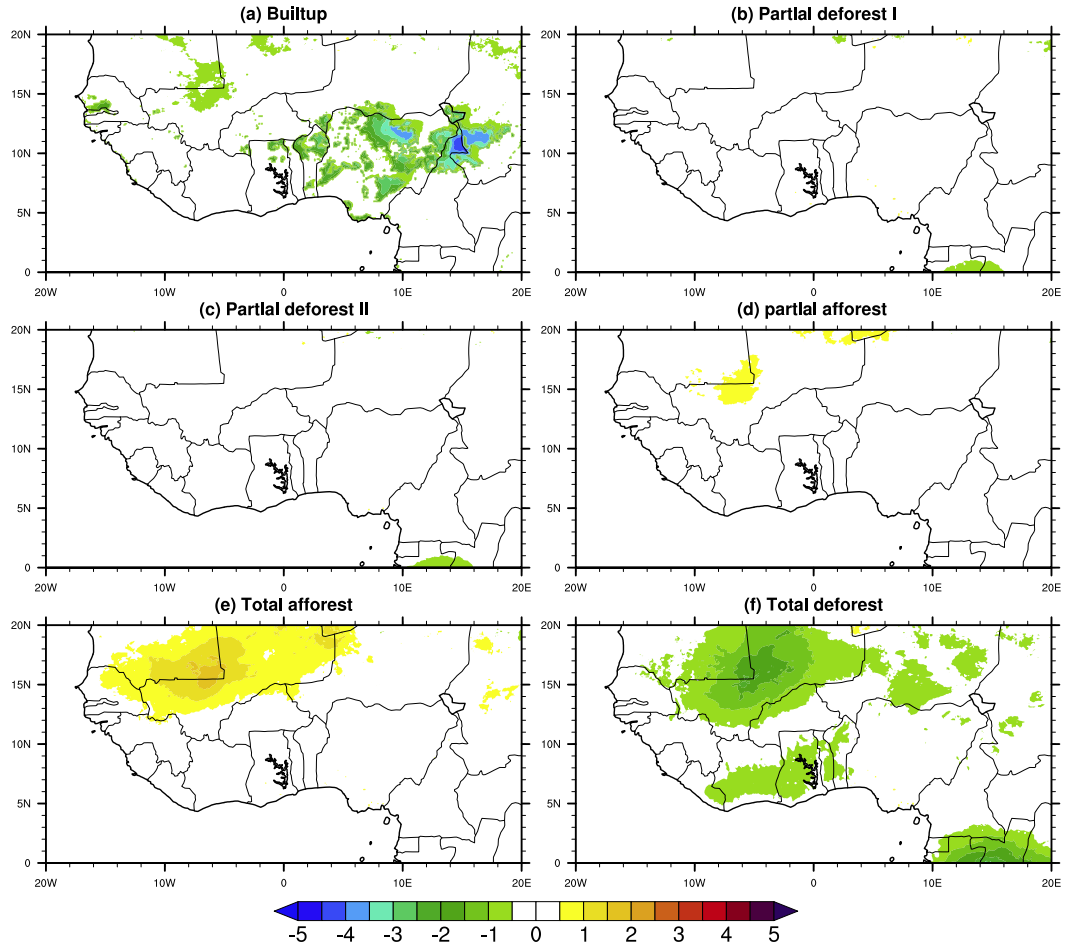

Figure 4.41: Average Dew Point Temperature Difference Between the Control Output and the Land Use Land Cover Experiments.

The partial afforest (PA) scenario increased dew point temperature around the 15°N and 20°N, which intensified in the Total Afforest (TA) scenario in area around 13°N and 20°N. In the Total Deforest (TD) scenario, dew point temperature reduced in most part of the area. Figure 4.42 shows the difference of the May-September dew point temperature between the simulations using the scenario LULC changes and the simulation with the un-altered LULC (i.e. the control run). The built up scenario (Figure 4.42a) tends to generally decrease dew point temperature. Maximum dew point changes are prominent over the Sahel-Sahara interface with high daily variations and Guinea with lower variability. Every other region apart from the Sahel-Sahara interface, follow the same pattern of distribution. These however have shown that urbanization could decrease the dew point temperature over the entire West African region, although the level of effect varies for each zone. This is in line with the results from Ray *et al*. (2006), which indicated that deforestation increases surface sensible heat fluxes and decreases latent heat fluxes, and thereby raising the air temperature and lower the dew point temperature of air masses. Also, Table 4.11 shows the percentage of change of dew point temperature due to each LULC scenario. It reveals that Sudan and the Sahel region will feel the highest impact of converting all croplands and Wetlands into built up lands over West Africa. However, the Guinea zone will have the least effect, which could be attributed to the high moisture influx into the zone from the Atlantic Ocean providing West Africa with most of its moisture (Abiodun *et al*. 2007). Researchers like Georgescu, (2008) have also confirmed that irrigated agriculture-to-urban land conversion, decreases dew point to the order of 1.5K in his study in Phoenix. Also, all the zones showed a reduced dew point

temperature due to conversion of permanent wetlands and Croplands into built up lands over West Africa.

The difference between the control simulation and the simulation with the Partial Deforest I (i.e. conversion of forests to savanna and croplands to grasslands) scenario and Partial Deforest II (conversion of forests to savanna) is presented in Figure 4.42 b and c. From Figure 4.42 b and c, the pattern of distribution of the Sahel-Sahara interface is quite different from others. The difference is higher in PDI that in PDII. This shows that conversion of forests to savanna and grasslands have little effect on the variation of dew point temperature over West Africa. Furthermore, the PDI scenario has more impact on the dew point temperature than the PDII scenario as the later showed less percentage change as shown in Table 4.11. However, other factors could be playing behind this, which includes moisture advection, convective activity and upward transport of moisture from the low-level monsoon in the zone (Abiodun et al. 2007). From Figure 4.42d, simulation with the Partial Afforest (PA) scenario (i.e. conversion of Woody Savanna into Evergreen Broadleaf Forests, and conversion of Savanna into Woody Savannas, and then converting Grasslands into Savanna) show that the effect was more prominent over the Sahel-Sahara interface. Also, from Table 4.11, there was a decrease in dew point temperature over the Guinea and Sudan zone, while an increase was detected over the Sahel and the Sahel-Sahara interface. The Total Afforest (TA) scenario (Figure 4.42e) is the extreme side of afforestation in which all the LULC parameters were converted into Evergreen Broadleaf Forests except the deserts (i.e. the barren lands), the permanent wetlands and built up lands. Simulation with the TA scenario have little effect on the on the dew point temperature of the Guinea zone with little decrease, but with a high and

higher diurnal variation over the Sahel and Sahel-Sahara interface respectively. Table 4.11 also showed that the TA scenario have high impact on the dew point temperature over the Sahel-Sahara interface and the Sahel far more than in the Gunea and Sudan zone. The Total Deforest (TD) scenario (Figure 4.42f) is the extreme side of deforestation in which all the LULC parameters were converted into barren lands except the permanent wetlands and built up lands. Simulation with the TD scenario impacted all the zones with a decrease in dew point temperature and higher daily variation over the period. The Sahel-Sahara interface has the highest percentage decrease of -3.83% while the Guinea zone has the least (-0.94).

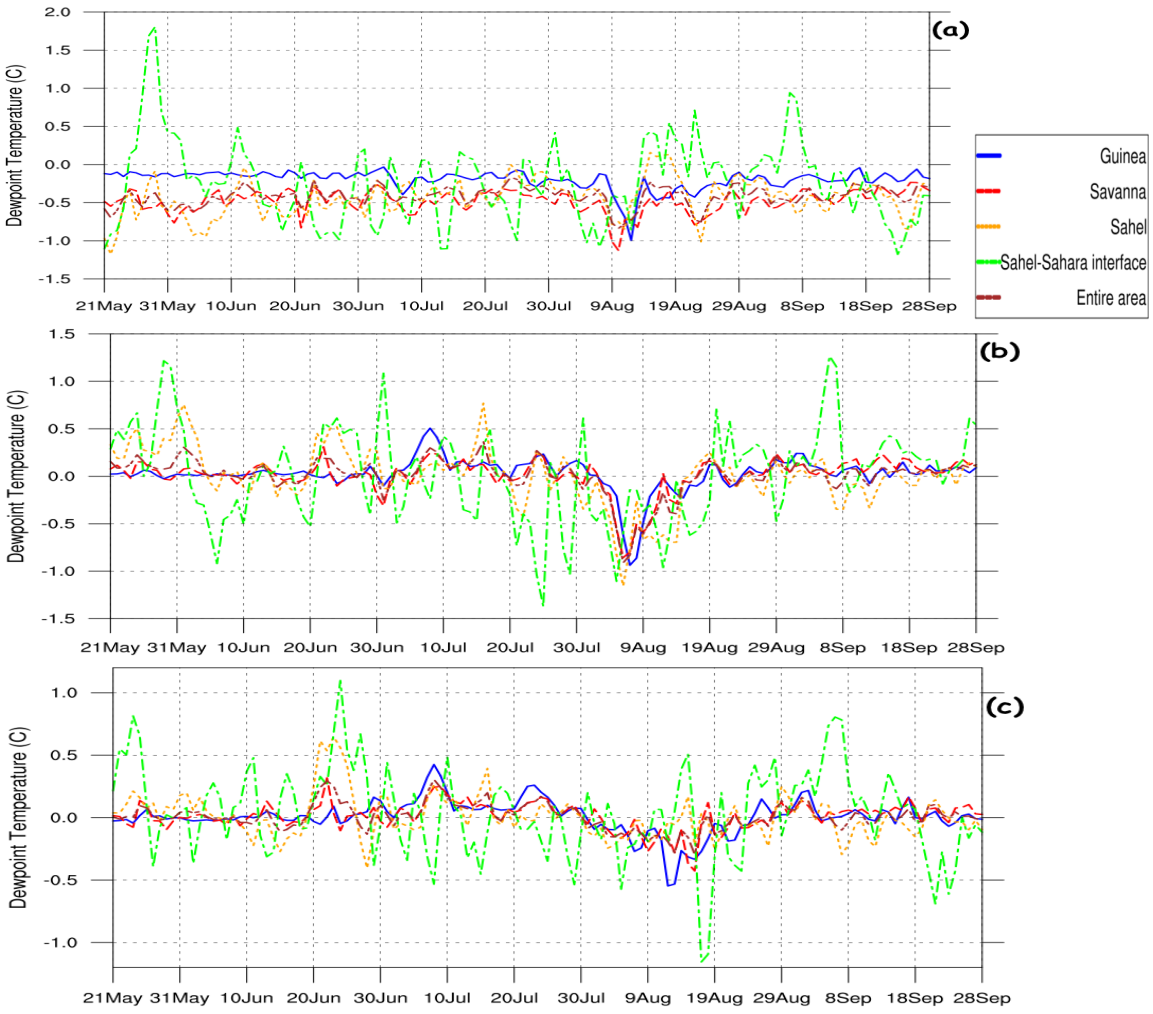

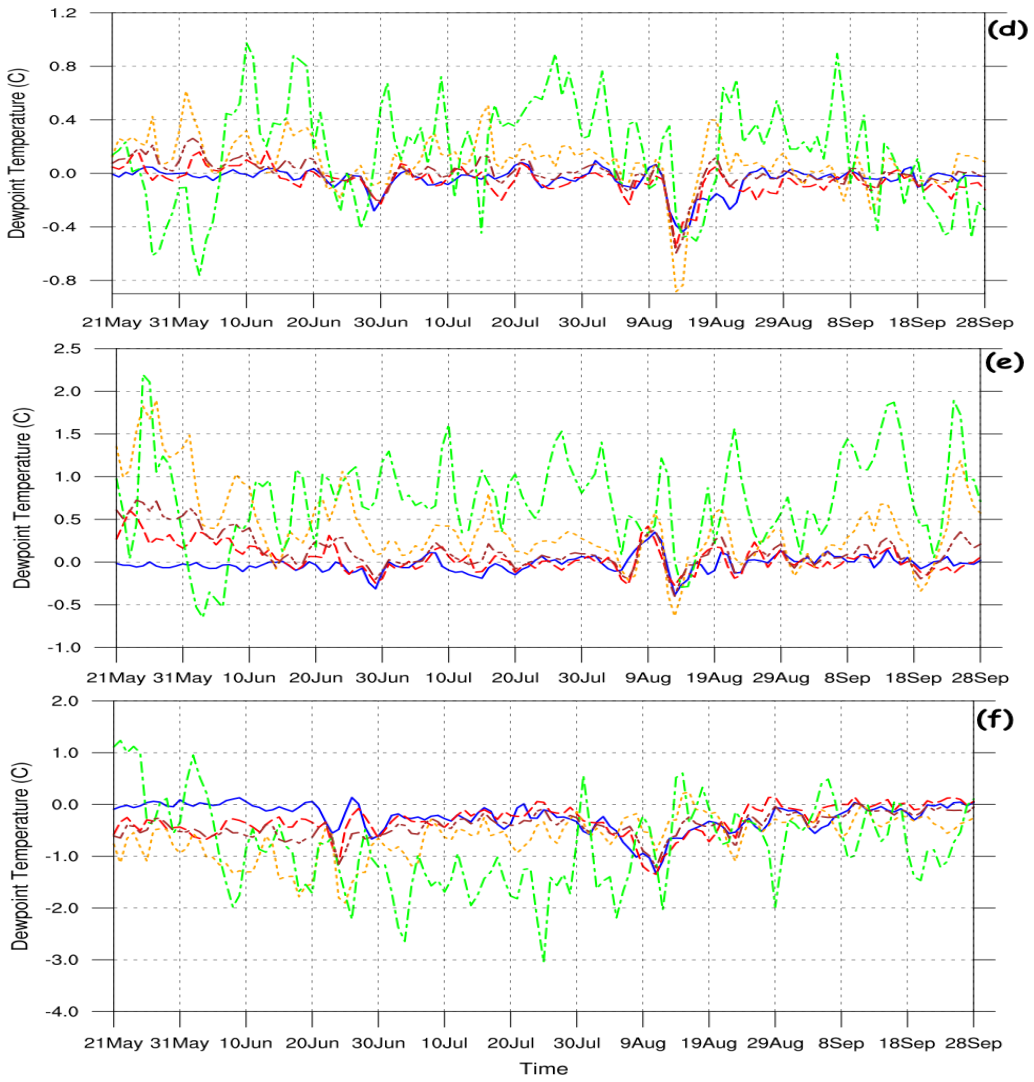

Figure 4.42: Time Series of Daily Dew Point Temperature Difference for (a) Built Up, (b) Partial Deforest I, (c) Partial deforest II (d) Partial Afforest, (e) Total Afforest, (f) Total Deforest.

Table 4.11: Percentage Change of Dew Point Temperature for Each LULC Scenario

Zone	Built Up	Partial Deforest II	Partial Deforest I	Partial Afforest	Total Afforest	Total Deforest
Guinea	-0.84	0.12	0.03	-0.16	-0.11	-0.94
Sudan	-2.13	0.09	0.05	-0.19	0.36	-1.41
Sahel	-2.07	0.21	0.09	0.43	2.40	-2.91
Sahel-Sahara interface	-1.04	0.56	0.39	0.67	4.52	-3.83
Entire area	-1.90	0.12	0.05	0.05	0.86	-1.83

From Figure 4.43a, conversion of croplands and wetlands to built up lands led to about 0.4°C decrease in temperature in the area between 6°N and 8°N and increase in areas around 9°N-11°N. The PDI scenario has some patches of increase and decrease temperature, while the PDII scenario (Figure 4.43c) has insubstantial change in temperature over most of the area. Simulations using the PA and TA scenarios are similar spatially with a more intense increase in the western pert of the Sahel zone. The TD has more intense increase in temperature around the Sudano-Sahelian zone than any other zone. Figure 4.44 presents the temporal changes of 2 m temperature as induced by LULCC. Simulation with the built up scenario (Figure 4.44a) brought about an increase

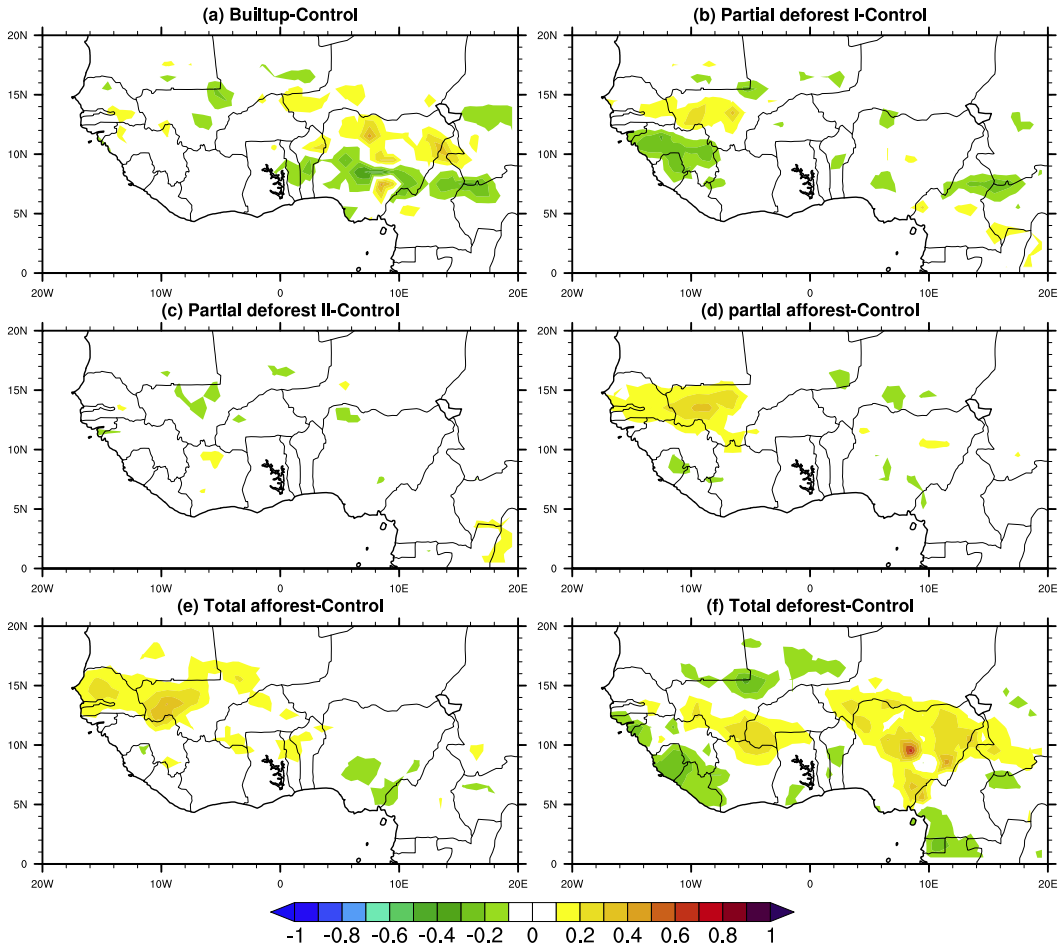

Figure 4.43: Average Temperature Difference Between the Control Output and the Land Use Land Cover Experiments.

in temperature over all the zones. Table 4.12 shows that SahelSahara interface has the least increase, while the Sudan-Sahel zone having the highest increase. This could also be because higher percentage of the converted wetlands and croplands are domiciled within the Sudan-Sahel zones. Land conversion has been considered as one of the most significant and comprehensive modifications to natural ecosystems (Van Asselen and Verburg, 2013). Built-up areas dramatically alter surface areas, thermal characteristics, and moisture pathways and tend to add extra energy supply to ecosystems (Grimmond, 2007). Zhang *et al*. (2010) also found that conversion of croplands to urban areas increased both temperature and precipitation but decreased surface humidity. Conversions of wetland and cropland to built-up areas would substantially increase regional temperature and stimulate sensible heat fluxes (Li *et al*., 2018). According to Li *et al*. (2018), urban sprawl could dramatically increase average temperature. Ren *et al*. (2008) stressed that urban area tends to have higher temperature than other land covers due to the changing albedo and hydrological cycles. This could truly be confirmed in this study provided the entire study area is converted into built up areas as in the total deforest scenario.

From Figure 4.44 b and c simulation with the PDI and PDII scenario follows almost the same pattern with slight difference in some days. However, from the table showing the percentage change of temperature for each LULC scenario (Table 4.12), the temperature decreases for the simulation with PDI for Guinea zone, while it increases in all other zones. For the simulation with PDII, temperature decreases across the Guinea, Sudan and the entire area (10°E-10°W, 5°N-15°N), but increases in the Sahel and Sahel-Sahara interface. The PA, PDI and PDII scenario do not have appreciable change in temperature

over the study area. The Total Afforest (TA) scenario caused a decrease in temperature in all the zones (Figure 4.44e) with the Sudan having the highest percentage change in temperature. However, the Total Deforest (TD) scenario led to an increase in temperature in all the zones (Figure 4.44f) with higher diurnal variation in Sahel and the Sahel-Sahara interface. Also, Sudan has the highest percentage increase while the Sahel-Sahara interface has the lowest.

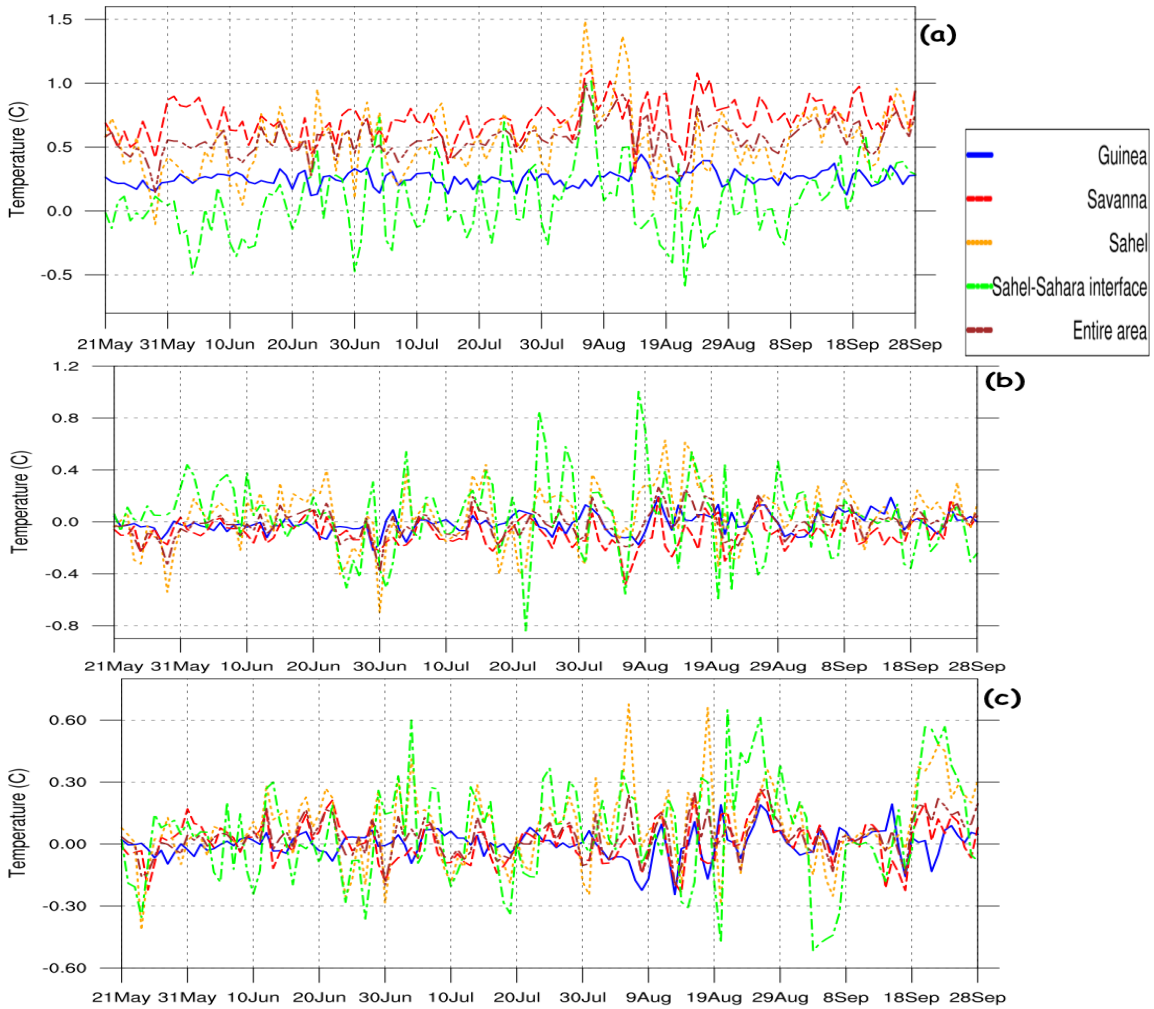

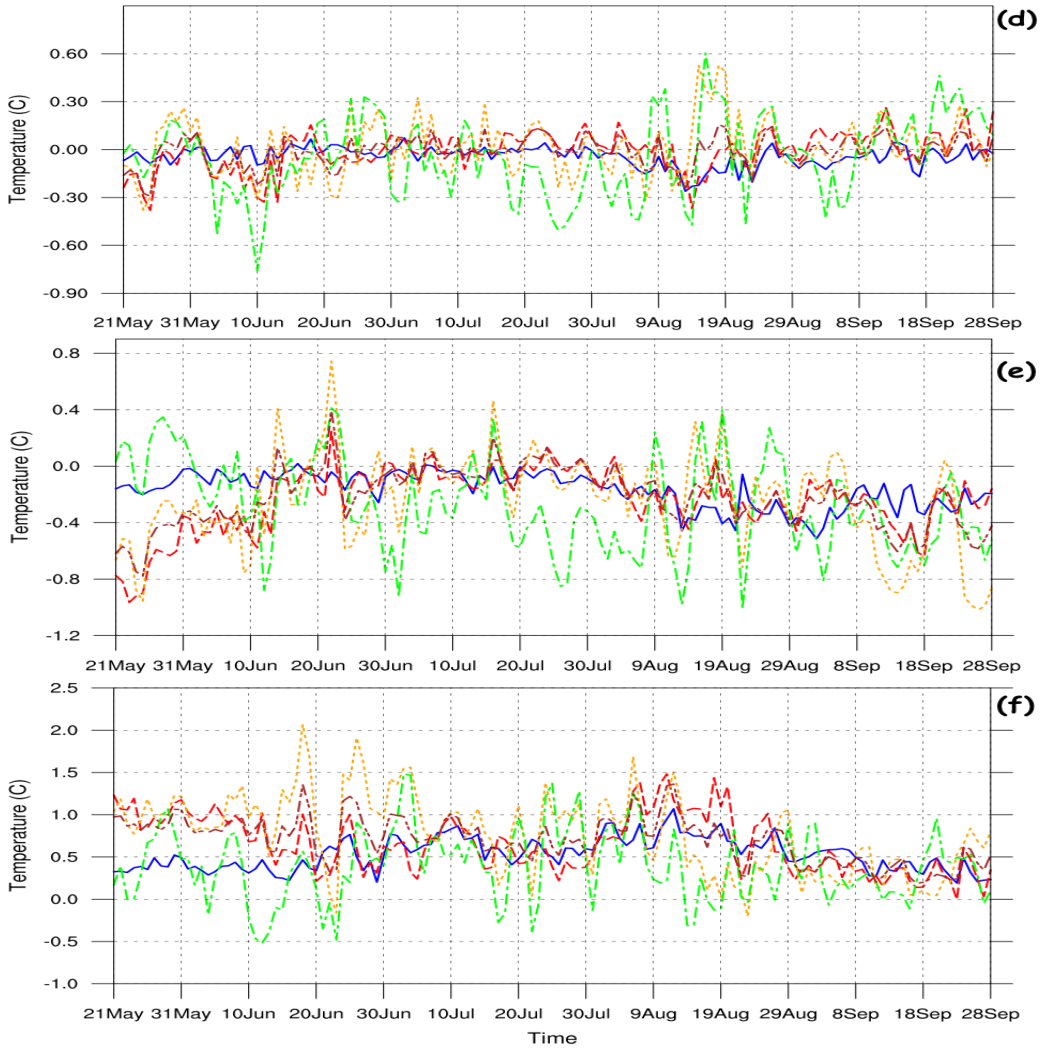

Figure 4.44: Time Series of Daily Temperature Difference for (a) Built Up, (b) Partial Deforest I, (c) Partial Deforest II, (d) Partial Afforest, (e) Total Afforest, (f) Total Deforest

Table 4.12: Percentage Change of Temperature (%) for Each LULC Scenario

Zone	Built-up	Partial Deforest II	Partial Deforest I	Partial Afforest	Total Afforest	Total Deforest
Guinea	1.00	-0.01	-0.05	-0.17	-0.67	2.06
Sudan	2.80	0.04	-0.34	-0.08	-1.20	2.79
Sahel	1.79	0.24	0.07	0.03	-0.97	2.76
Sahel-Sahara Interface	0.21	0.13	0.12	-0.11	-0.69	1.20
Entire area	2.10	0.10	-0.11	-0.07	-1.01	2.77

Figure 4.45 shows the spatial plot of daily average Sensible Heat (SH) flux for the LULC scenarios (Figure 4.45a-f), the control simulation (Figure 4.45g) and the spatial difference between the control simulation and the land use land cover experiments. From Figure 4.45a-g, sensible heat show north-south gradient with high values in the north and lower values in the south. High sensible heat flux was noted in the cropland and permanent wetland areas converted into built up lands in Figure 4.45a. The strengthening of sensible heat induced by the built up scenario could partly have led to an increase in temperature

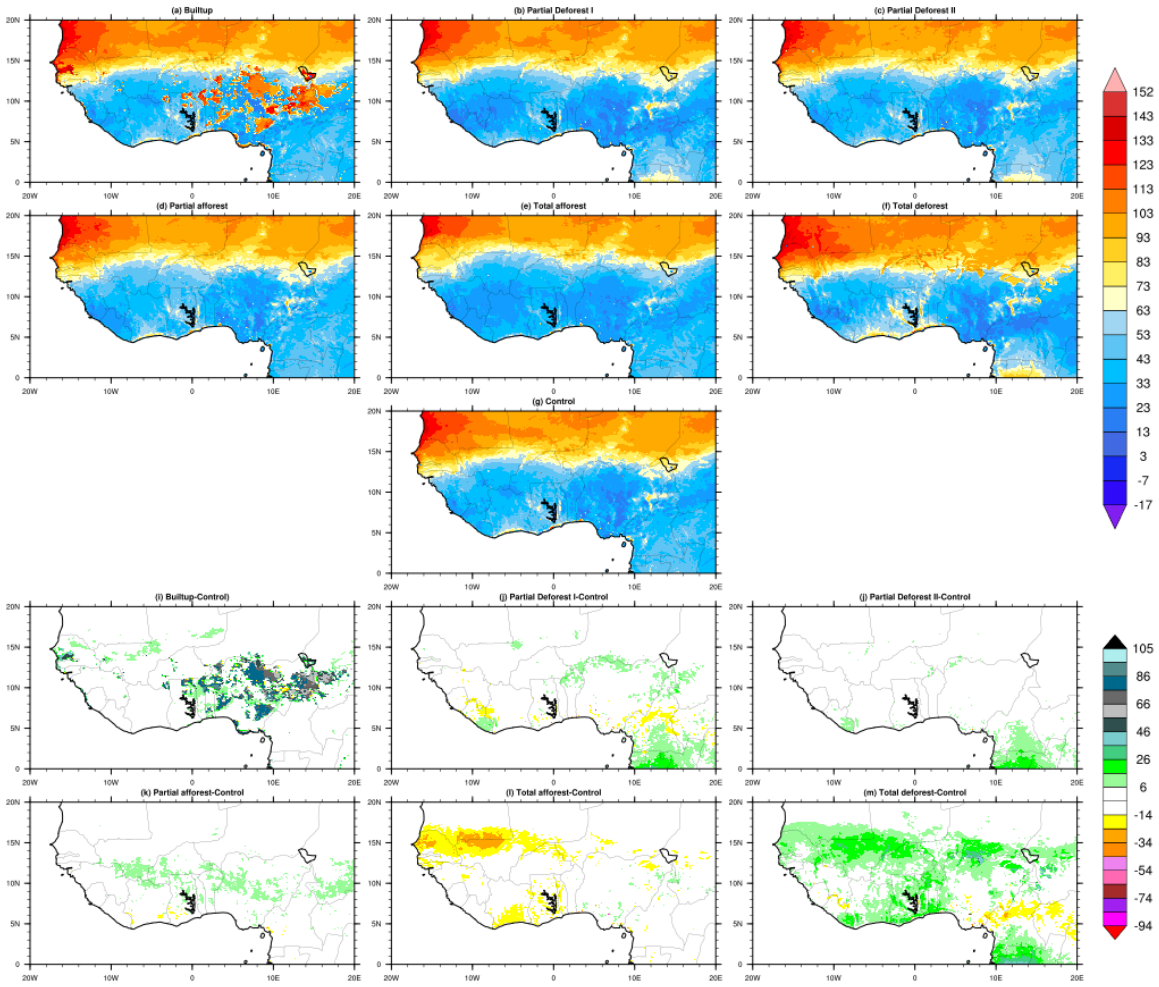

Figure 4.45: Spatial Average Sensible Heat Flux and Difference Between the Control Simulation and the Land Use Land Cover Experiments

(Diba *et al*. 2018; Wang and Cheung, 2017). It can also be observed that the boundary between value above 63 w/m^2 shifted upward in the total afforestation experiment (Figure 4.45e) and shifted southward in the total deforest experiment (Figure 4.45f). Also, there was a high increase in sensible heat flux over the areas converted into built up in the BU scenario. The simulation with the Partial deforest I LULC showed slight decrease in SH over some areas in the Guinea, and increase in some areas in the Sahel, while the simulation with the Partial deforest II LULC shows less effect on SH as most of the change falls between 6 and -14 W/m^2. The Partial afforest spatially shows appreciable sensible heat increase around the 8°N-11°N (Sudan) with some little decrease around the Guinea, while the total afforest scenario decreased sensible heat substantially around the Sahel and Sahel-Sahara interface. The total deforest scenario shows the highest impact as it increases sensible heat substantially in almost all the part of the study area, with an increase in few areas.

Furthermore, the conversion of the wetlands and croplands over the entire West Africa into built up lands (Figure 4.46) leads to an increase in Sensible heat flux over the entire area and each zone with Savanna having the highest increase and Sahel-Sahara interface having the least. Both the PDI caused a slight decrease on average over Guinea, Sudan, Sahel Sahara interface and the entire area, but a there was a slight increase in over the Sahel zone. Simulation with the PDI LULC decreased the sensible heat over Guinea, Sudan and the entire area with higher percentage decrease than that of the PDII (Table 4.13). The conversion of Woody Savanna into Evergreen Broadleaf Forests, and Savanna into Woody Savannas, and then converting Grasslands into Savanna (i.e., Partial Afforest PA) over West Africa decreases the sensible heat over Guinea and Sahel-Sahara

interface, but increased over Sudan, Sahel and the entire area. The total afforest decreased sensible heat over all the zones with Sudan zone having the highest percentage of decrease, and Sahel Sahara interface have the least. However, the total deforest scenario leads to an increase in sensible heat over all the zones with Sahel having the highest percentage of increase, and Sahel Sahara interface also having the least.

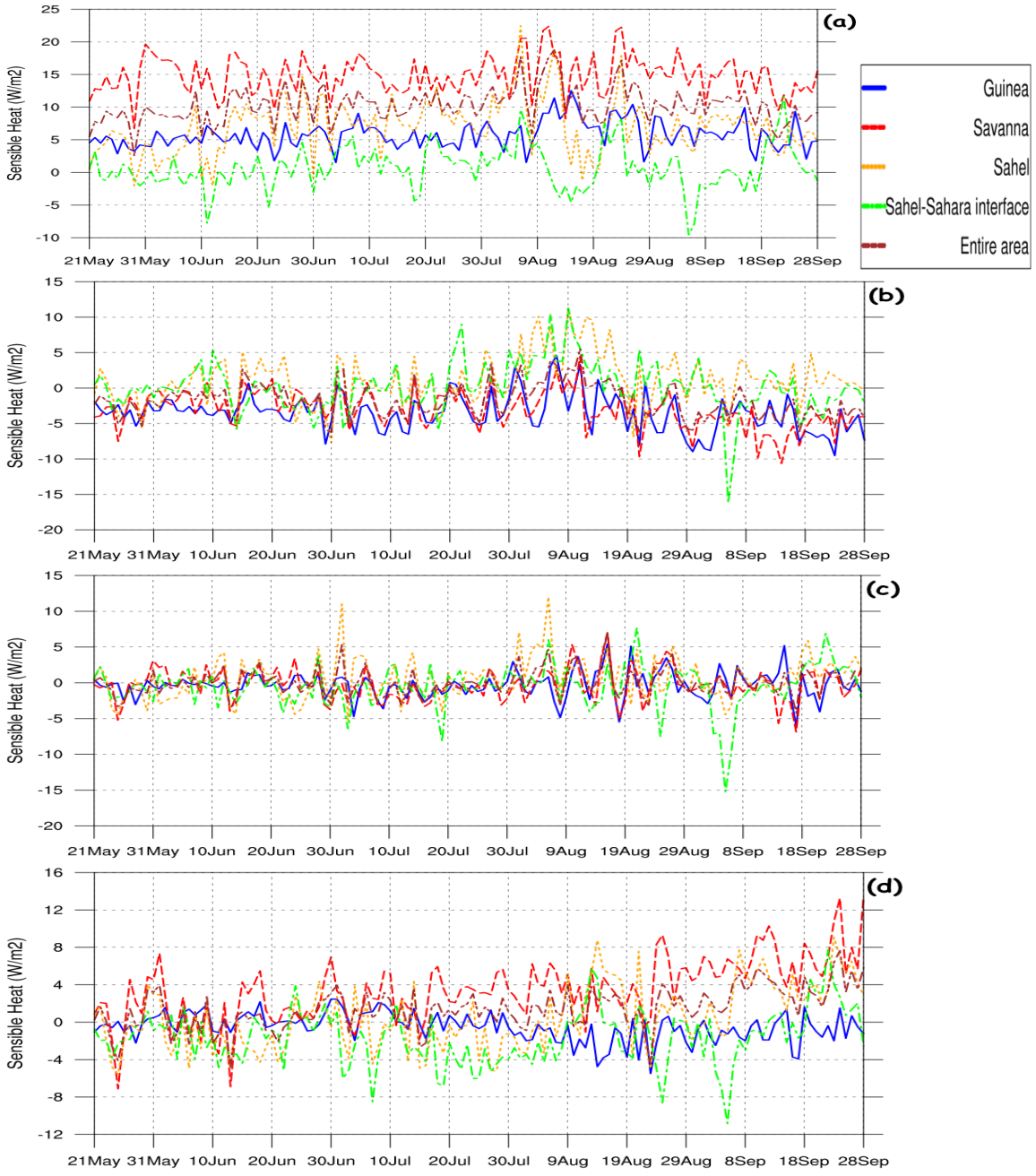

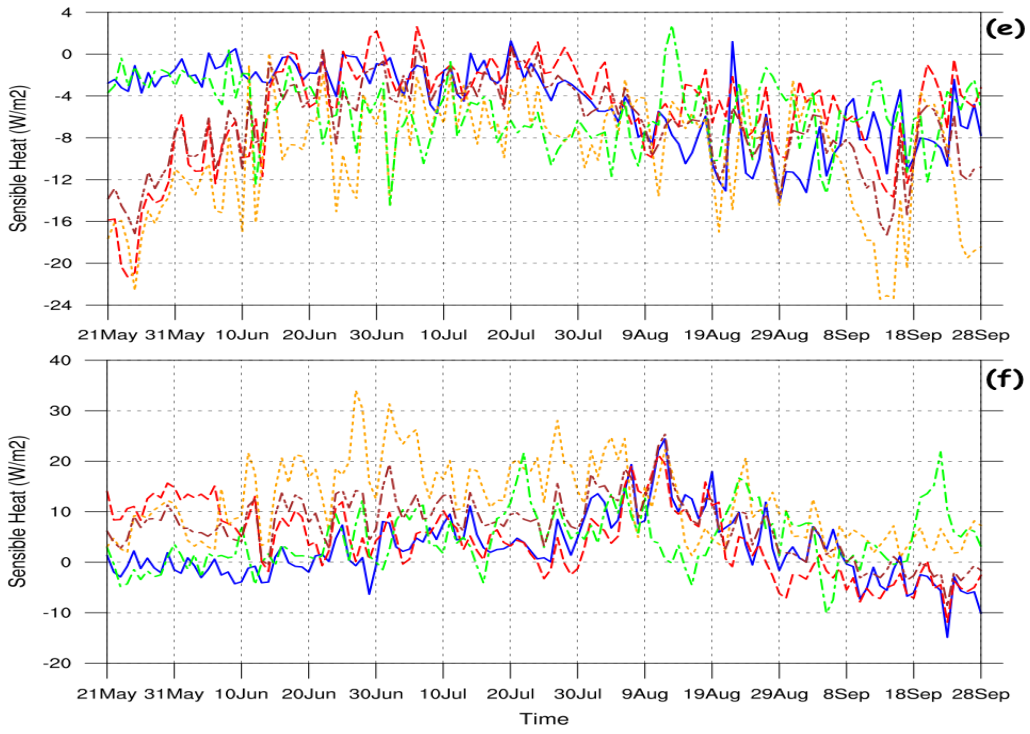

Figure 4.46: Time Series of Daily Sensible Heat Difference for (a) Built Up, (b) Partial Deforest I, (c) Partial Deforest II, (d) Partial Afforest, (e) Total Afforest, (f) Total Deforest

Table 4.13: Percentage Change of Sensible Heat Flux (%) for Each LULC Scenario

Zone	Built Up	Partial Deforest II	Partial Deforest I	Partial Afforest	Total Afforest	Total Deforest
Guinea	17.68	-1.18	-11.10	-1.61	-14.14	6.72
Sudan	37.90	-0.82	-8.04	8.19	-17.32	13.29
Sahel	9.83	0.57	1.16	0.56	-15.80	17.14
Sahel-Sahara Interface	0.57	-0.55	0.02	-1.57	-5.21	3.89
Entire area	21.18	-0.13	-4.21	2.79	-16.30	15.22

Impacts of LULC changes on precipitation are complex (Mahmood *et al*., 2010) as land conversions can lead to either increased or decreased precipitation (Li *et al*., 2018). Previous studies revealed that responses of precipitation to urbanization were not as evident as that of temperature (Tayanc and Toros, 1997; Laux *et al*., 2017; Li *et al*., 2018). Urbanization induces a series of complex changes in land surface roughness, soil moisture, and exchange of water and energy between land and the atmosphere (Lamptey *et al*., 2005). These changes can either offset or enhance each other and thus further complicate the spatial patterns of precipitation (Trusilova *et al*., 2008). From Figure 4.47a-f and Table 4.14, the conversion of all the permanent wetlands and croplands into

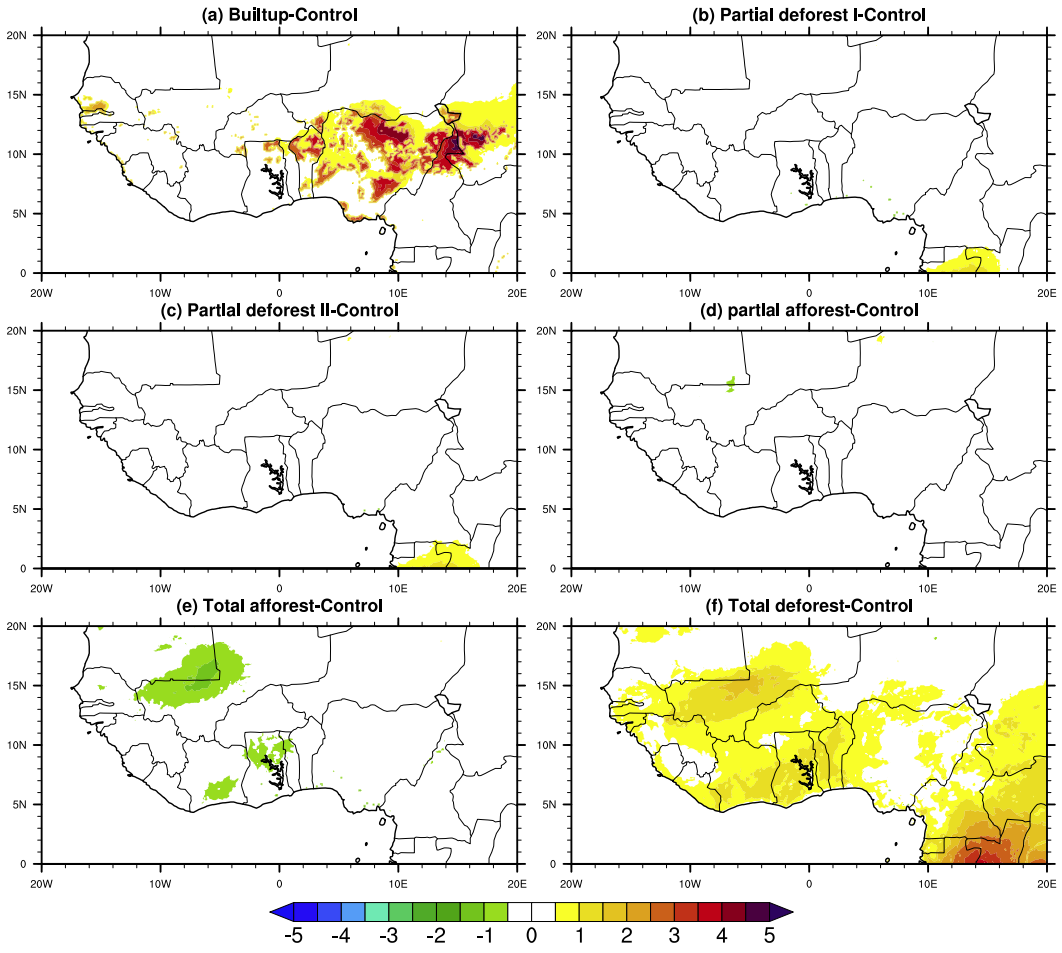

Figure 4.47: Average Precipitation Difference Between the Control Output and the Land Use Land Cover Experiments

built up lands increased precipitation over the Sahel and decreased precipitation over every other zone with the highest decrease in the Sahel-Sahara interface. The simulation with PDII scenario decreased precipitation over the Sahel, Sahara interface and the entire area, but increased precipitation over Guinea and Sudan zone. PDI scenario led to a decrease in precipitation over all the zones except the Guinea zone. Simulation with the partial afforest scenario increased precipitation over the entire area, the Sahel and Sudan zone, but decreased over Guinea and Sahel-Sahara interface.

For the simulation with total afforest scenario, precipitation was significantly enhanced over the Sahel-Saharan interface with a percentage increase of about 15.25%, while the total deforest scenario significantly decreased precipitation over same zone with about 21.1%. Total afforest scenario leads to an increased precipitation over all the entire zones except the Guinea zone with a low percentage decrease of about 0.19%. Total deforestation scenario also increased the precipitation in Sudan, Sahel and the entire zone. This is in line with the work of Xue *et al*. (1996) that there is an increase in rainfall as a result of deforestation. Sahel precipitation seems to be substantially influenced by the build up, partial afforest and partial deforest scenarios, as they seem to induce more precipitation over the Sahel. It can be said that deforestation in the Guinea zone could lead to a reduction of the precipitation in the Sahel and Sahel-Sahara interface as seen in the simulations with PDI and PDII LULC scenarios but also reduces precipitation over the entire area. This is in line with the work of Abiodun et al. (2007), which also stressed that deforestation increases the monsoon flow largely because of the reduced surface friction experienced by the flow over the Guinean region and also

reduces rainfall over the entire West African region. Also, this research also revealed that all deforestation option tends to decrease precipitation over the Sahel-Sahara interface.

According to Hagos *et al.* (2014), much of the change in precipitation is related to changes in circulation, particularly to the response of the intensity and latitudinal position of the African Easterly Jet, which varies with the changes in meridional surface temperature gradients. However, in-depth analysis on the general atmospheric circulation and large-scale system in play can throw more light on the question regarding the reason for this. This is a good avenue for future research. The desertification option (total deforest) leads to an increase in precipitation over the entire area (Abiodun *et al*. 2007). There was also an increase in Sudan and Sahel, but a decrease in the guinea as opposed to the findings of Abiodun *et al*. (2007).

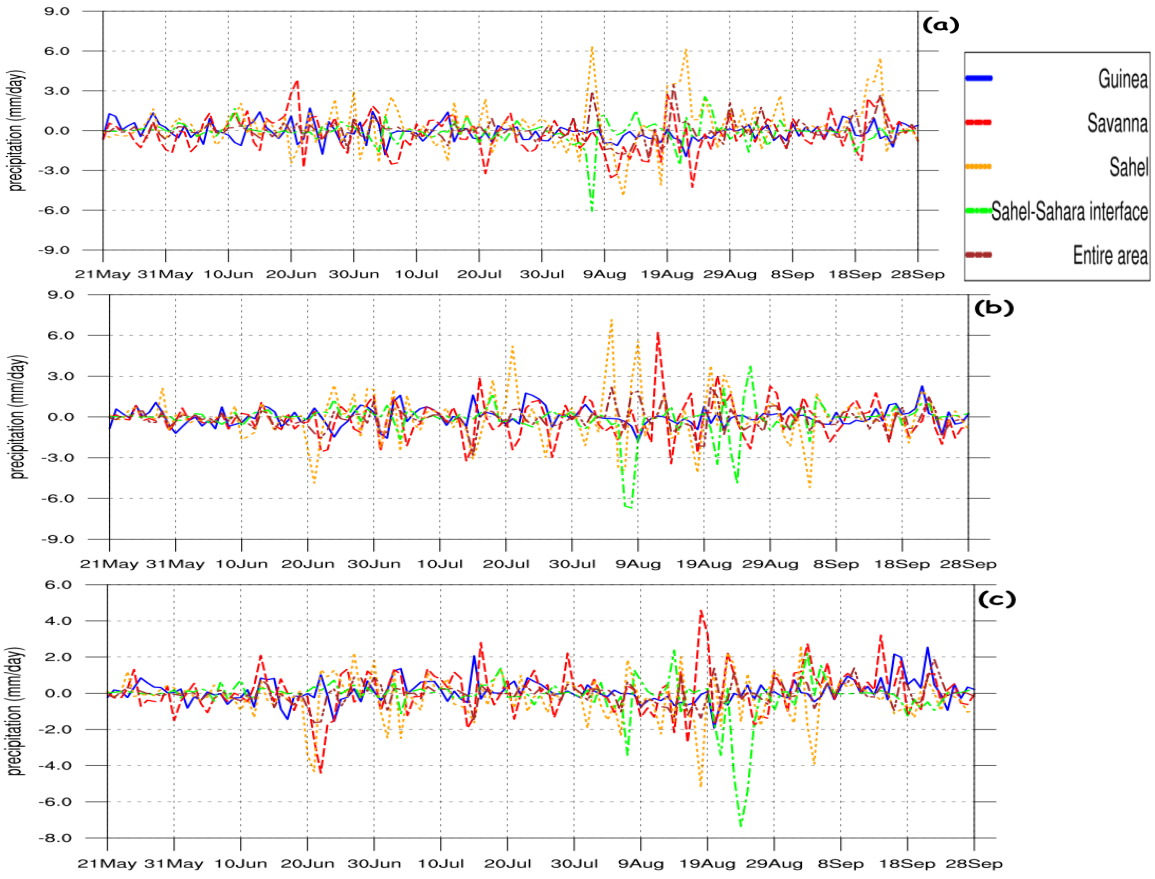

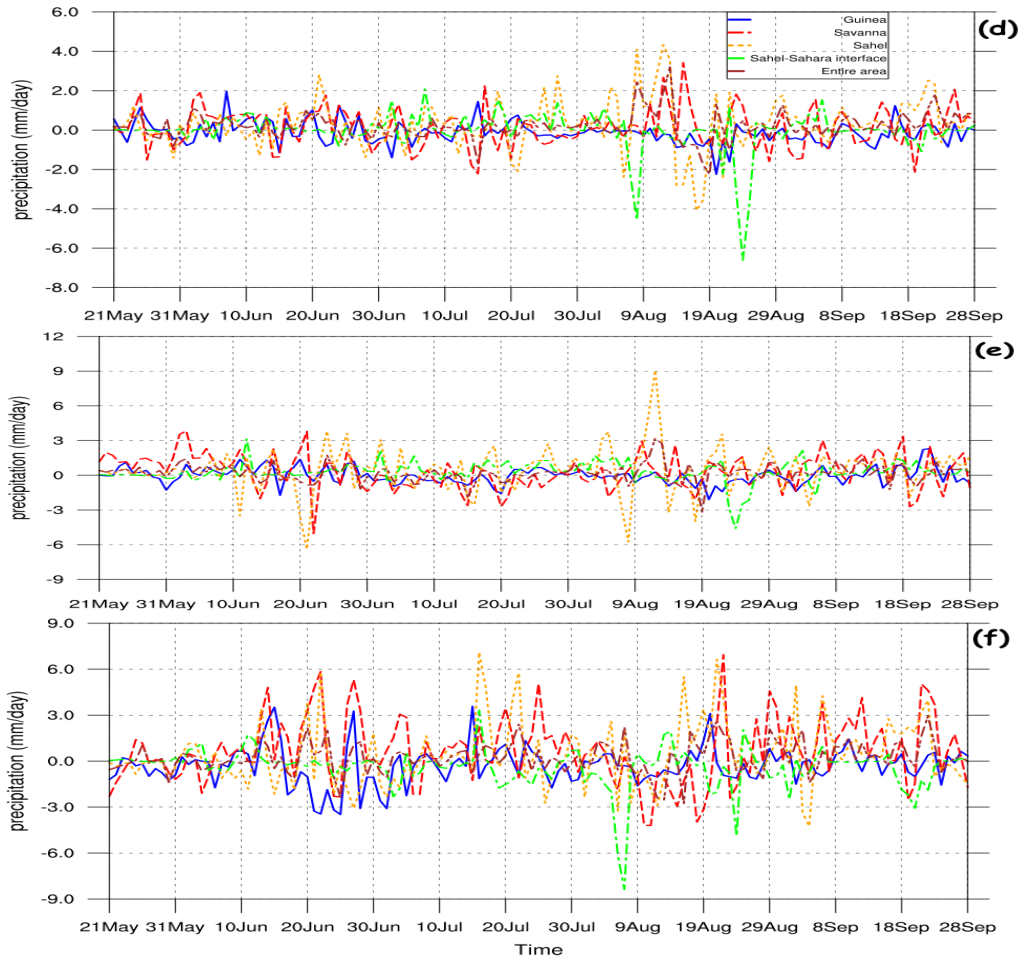

Figure 4.48: Time Series of Daily Precipitation Difference for (a) Built Up, (b) Partial Deforest I, (c) Partial Deforest II, (d) Partial Afforest, (e) Total Afforest, (f) Total Deforest

Table 4.14: Percentage Change of Precipitation for Each LULC Scenario

Zone	Built Up	Partial Deforest II	Partial Deforest I	Partial Afforest	Total Afforest	Total Deforest
Guinea	-0.52	1.55	0.30	-1.40	-0.19	-4.95
Sudan	-2.94	0.72	-2.01	1.29	5.46	6.59
Sahel	5.20	-3.49	-0.10	4.78	7.69	6.54
Sahel-Sahara Interface	-4.63	-7.33	-6.27	-1.95	15.25	-21.10
Entire area	-0.33	-0.16	-2.17	2.66	3.02	2.64

In other to throw more light on the impacts of the land surface conditions on rainfall, analysis of the impacts of LULCC on evapotranspiration was carried out. Figure 4.49 a-g shows the spatial representation of the daily average evapotranspiration over West Africa for the control simulation (Figure 4.49g) and for the LULCC experiments. From the control simulation, evapotranspiration increases to the south and decreases to the north of WA. The simulations with different LULC scenarios altered the outputs of the model as spatially shown in Figure 4.49h-m. The built up scenario significantly decreased Evapotranspiration (ET) over the converted areas. The PDI, PDII and TD scenarios tend

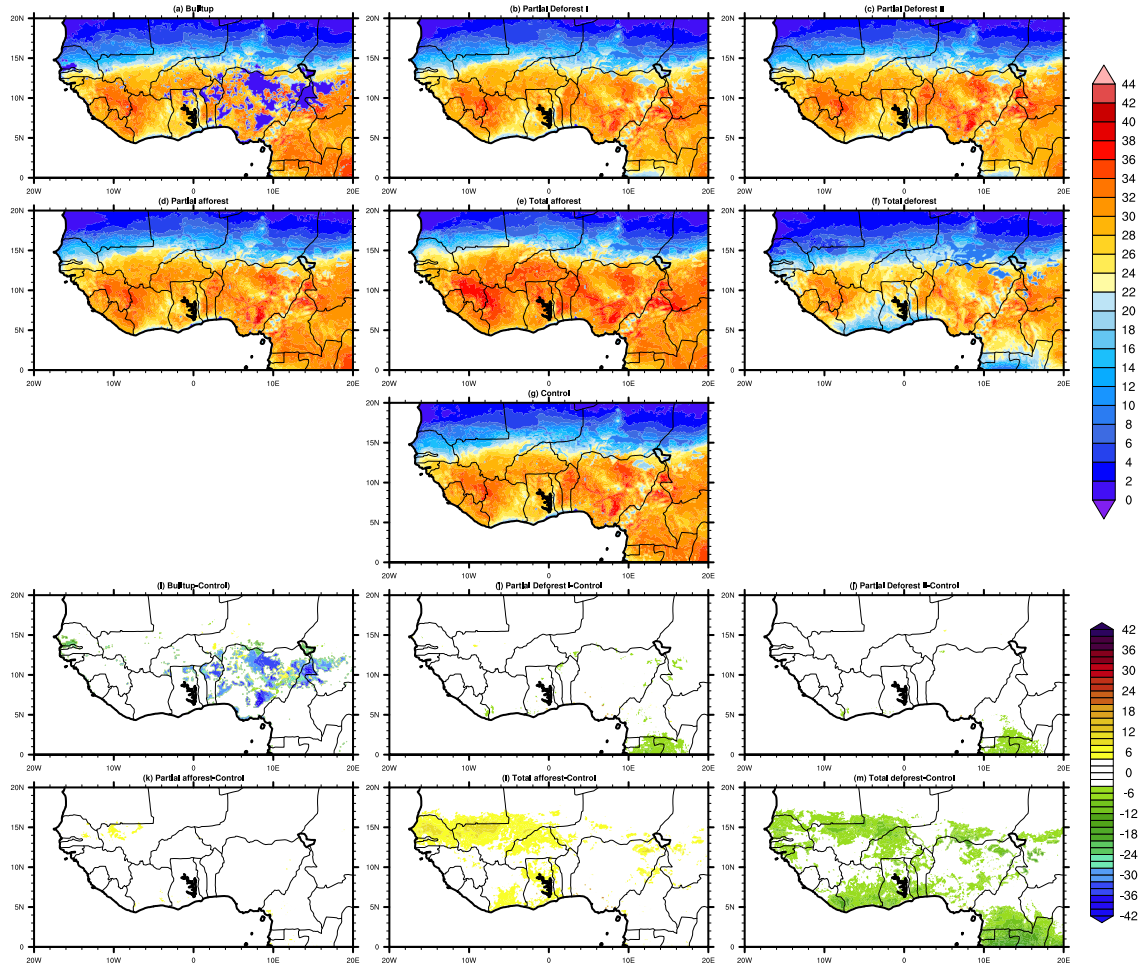

Figure 4.49: Spatial Average Evapotranspiration (a-g) and Difference Between the Control Output and the Land Use Land Cover Experiments (h-m).

to decrease ET over the area, but the PA and TA scenarios tend to increase ET. From Figure 4.50 and Table 4.15, the conversion of all permanent wetlands and croplands into built up in WA leads to a decrease in ET across the entire area and all the zones with the highest percentage decrease seen in Sudan zone, while the Sahel-Sahara interface has the least percentage decrease. ET was seen to increase with the PDII scenario over the Sudan and the Sahel-Sahara interface, but decreased in Guinea, Sahel and the entire area. Simulation with the PDI LULC scenario decreased ET in the entire area and all the zones except the Sahel-Sahara interface where there was an increase. The partial afforest scenario increased ET in the entire area and all the zones with Sahel-Sahara interface having the highest percentage increase and Sudan the least. The output from the run with total afforest scenario also show that ET increased over the entire area and all the zones with the Sahel-Sahara interface having the highest percentage increase and Guinea the least. Nevertheless, the run with the total deforest LULC scenario decreased the ET over the entire area and all the zones with the Sahel-Sahara interface having the highest percentage decrease in ET, and Sudan zone having the least.

It could be seen from the analysis that effect of LULCC on ET seems to be consistent with common belief about the relationship between vegetation cover and moisture availability as more deforestation tends to reduce ET. Analysis of the impact of LULCC on precipitation over WA shows that the afforestation tends to increase it. However, the increase of rainfall induced by the afforestation scenarios could be due to an increase of the evapotranspiration as shown in this work, and the strengthening of the atmospheric moisture as in Diba *et al*. (2018). The results have shown that all afforestation options (i.e. PA and TA) tend to decrease significantly the surface

temperature. A decrease in temperature caused by reforestation could be the result of the weakening of the sensible heat flux. The afforestation options tend to increase rainfall steadily over the entire area with the strengthening of the evapotranspiration and the atmospheric moisture content.

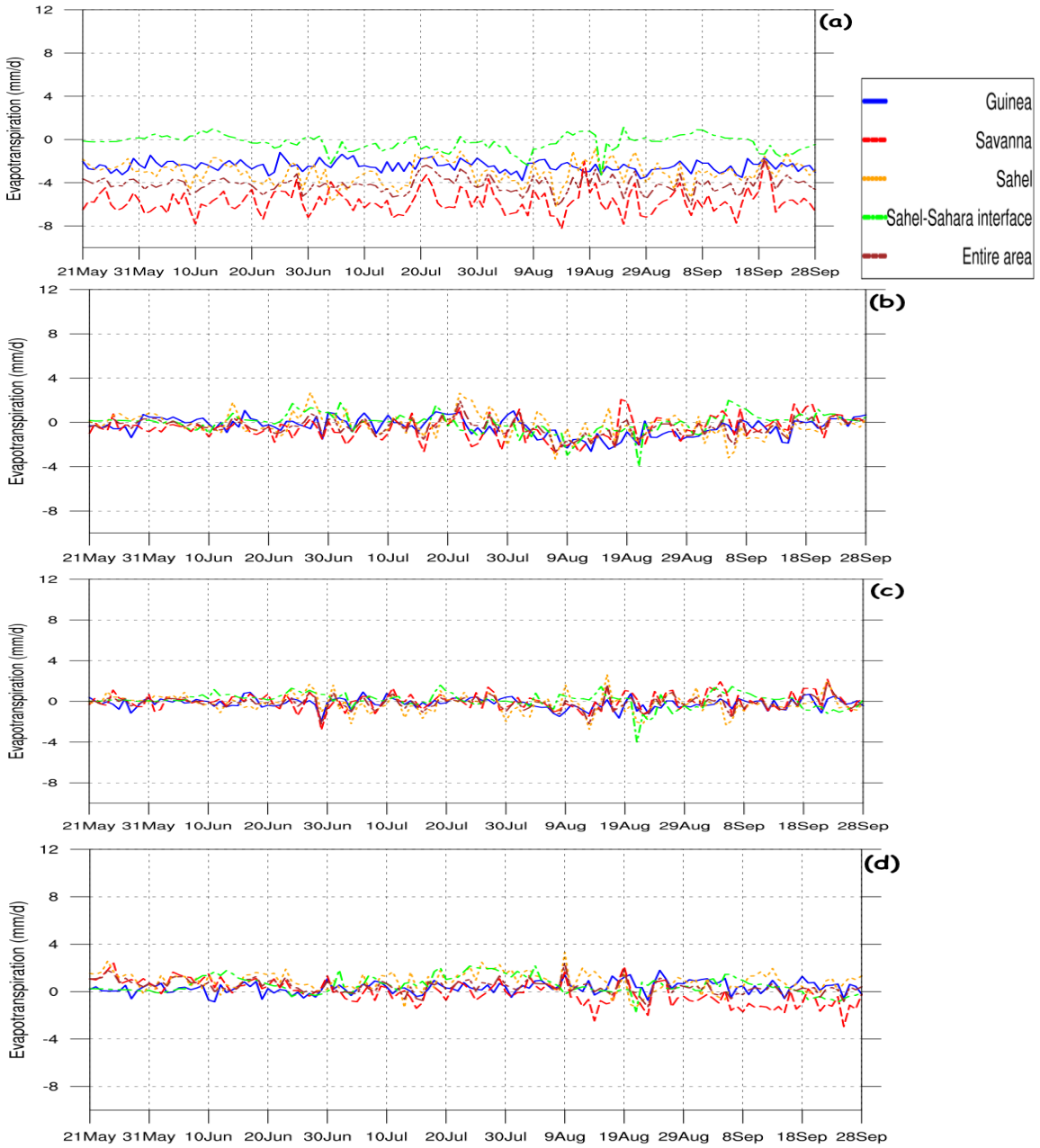

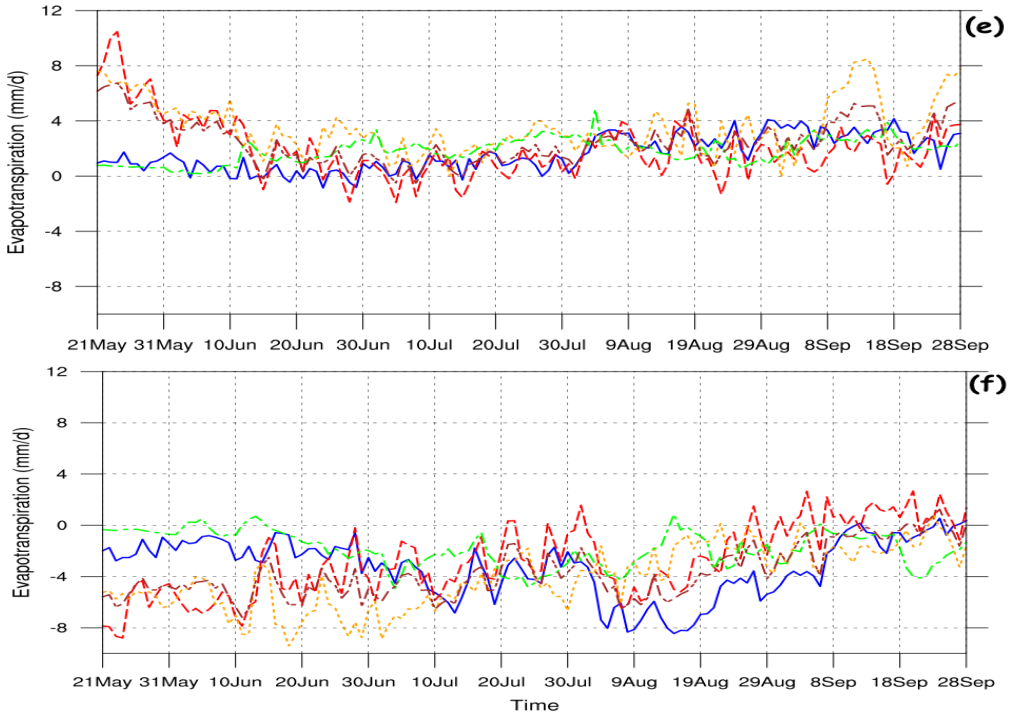

Figure 4.50: Time Series of Daily Evapotranspiration Difference for (a) Built Up, (b) Partial Deforest I, (c) Partial Deforest II, (d) Partial Afforest, (e) Total Afforest, (f) Total Deforest

Table 4.15: Percentage Change of Evapotranspiration for Each LULC Scenario

Zone	Built Up	Partial Deforest II	Partial Deforest I	Partial Afforest	Total Afforest	Total Deforest
Guinea	-12.34	-0.90	-1.86	1.60	7.71	-15.06
Sudan	-18.84	0.03	-1.63	0.31	8.73	-10.40
Sahel	-13.38	-0.68	-0.83	4.06	17.32	-19.05
Sahel-Sahara interface	-3.52	1.56	0.33	6.70	23.10	-22.19
Entire area	-15.51	-0.50	-1.42	1.86	10.99	-14.39

4.5 Impact of Land Use Land Cover Change (LULCC) on Streamflow Over Sokoto Rima River Basin

In other to study the impact of LULCC on streamflow, the WRF-hydro model was ran with five different LULC scenario and result of the differences between the outputs from each LULC scenario and the control run was analysed.

The performance of the streamflow calibration based on different REFKDT is summarized in Table 4.16. The simulations with REFKDT 1.0, 0.7, 0.6 and 0.5 all gave a good estimate compare to the observed flow as shown in Figure 4.51, but in other to have the best, all the statistics were considered for the best selection. However, the REFKDT 0.5 has a good correlation but with a high bias and low NSE value which made the other three (i.e. REFKDT 1.0, 0.7 and 0.6) to be more preferable. Among the best three calibration parameters, the REFKDT 0.7 was chosen for the WRF-hydro simulations because of its low bias as compared to others as all the best three has good correlation and good NSE value. From Figure 4.52, the calibrated model adequately captured the maximum peak streamflow with respect to the observed monthly streamflow at the Goronyo station.

Table 4.16: Model Performance at Different Calibration Parameters for Goronyo FP.

	REFKDT 3.0 (Def.)	REFKDT 1.5	REFKDT 1.0	REFKDT 0.7	REFKDT 0.6	REFKDT 0.5
Pearson Correlation (r)	0.924	0.691	0.950	**0.944**	0.958	0.958
Nash-Sutcliffe (NSE)	0.385	0.234	0.869	**0.887**	0.853	0.718
P-bias	-64.402	-60.482	-14.339	**-7.426**	31.982	53.385

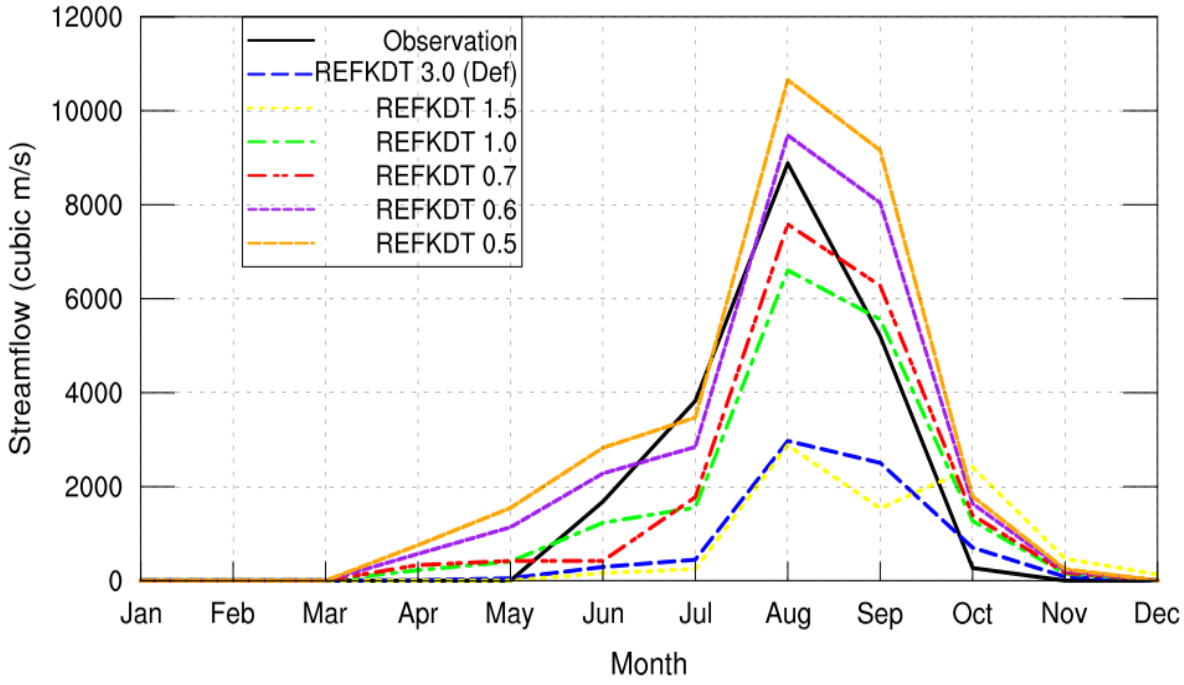

Figure 4.51: Streamflow Calibration Based on Different REFKDT Test for Goronyo FP

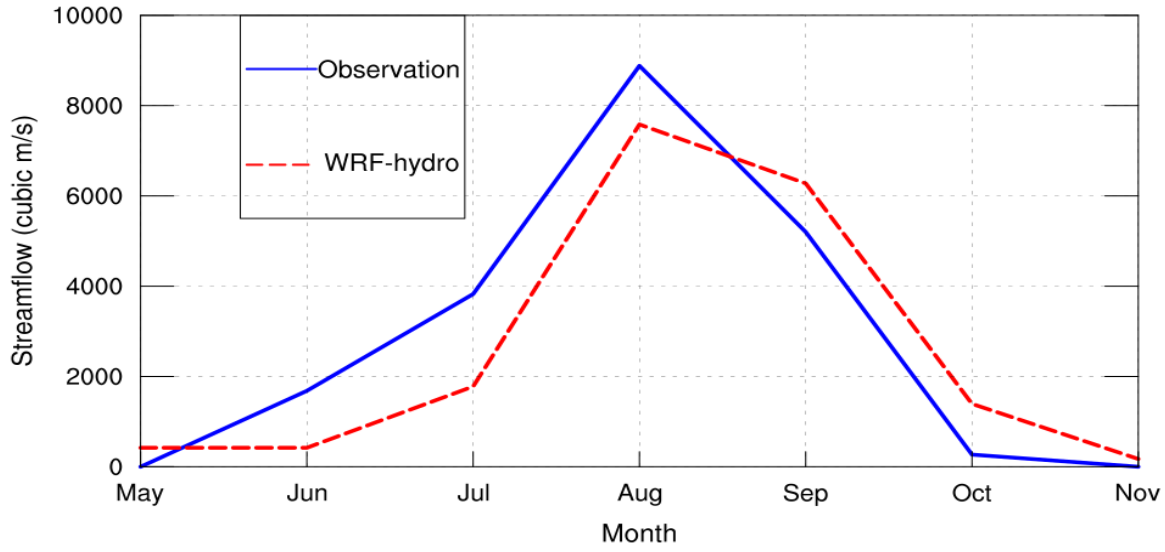

Figure 4.52: Calibrated Daily Stream Discharge With Observed Stream Discharge

Figure 4.53 shows the difference between the streamflow from the control simulation and each LULC scenario. The procedure used to generate the LULC scenarios are clearly presented in Table 3.6 in chapter three of this thesis. The conversion of all Permanent Wetlands (PW) and Croplands (Cr) in the basin into Built up lands increased the streamflow by about 41.79% in Sokoto, 82.11% in Goronyo and 98.48% in Bakolori (Table 4.17). This could not be far from the fact that urban built up lands has less infilteration capacity by creating impervious surface, removes vegetation and consequently removes transpiration. This is in line with the work of Zhou (2014) which emphasized that increasing peak flow has been generally taken as the major hydrologic implication of urbanization (Zhou, 2014). Also, almost all the upstream areas of Bakolori were converted into built up lands, and this could explain why we have much more higher percentage of increase in streamflow in this Forecast Point.

Simulation with the Partial Deforest PD scenario have been shown to increase streamflow by about 0.84% in Sokoto, 1.08% in Goronyo and 0.04% in Bakolori (Table 4.17). The conversion of open shrublands into Savannas; croplands and cropland/natural vegetation mosaics into grasslands, results into increased vegetation coverage. This finally led to intensifying soil water storage and increasing the infilteration of rainfall into the basin, and by this means, increases the streamflow as evapotranspiration is reduced. The conversion of grasslands into savannas (PA) however, decreased streamflow by -0.03% in Sokoto, increased it in Goronyo by 0.15% and then increases in Bakolori by 0.46%. The fact that the LCPs are not evenly distributed over the entire SRRB could be a good reason for the different response of the forecast points to conversion from grasslands into savanna. According to Teuling *et al*. (2019), changes that take place at the

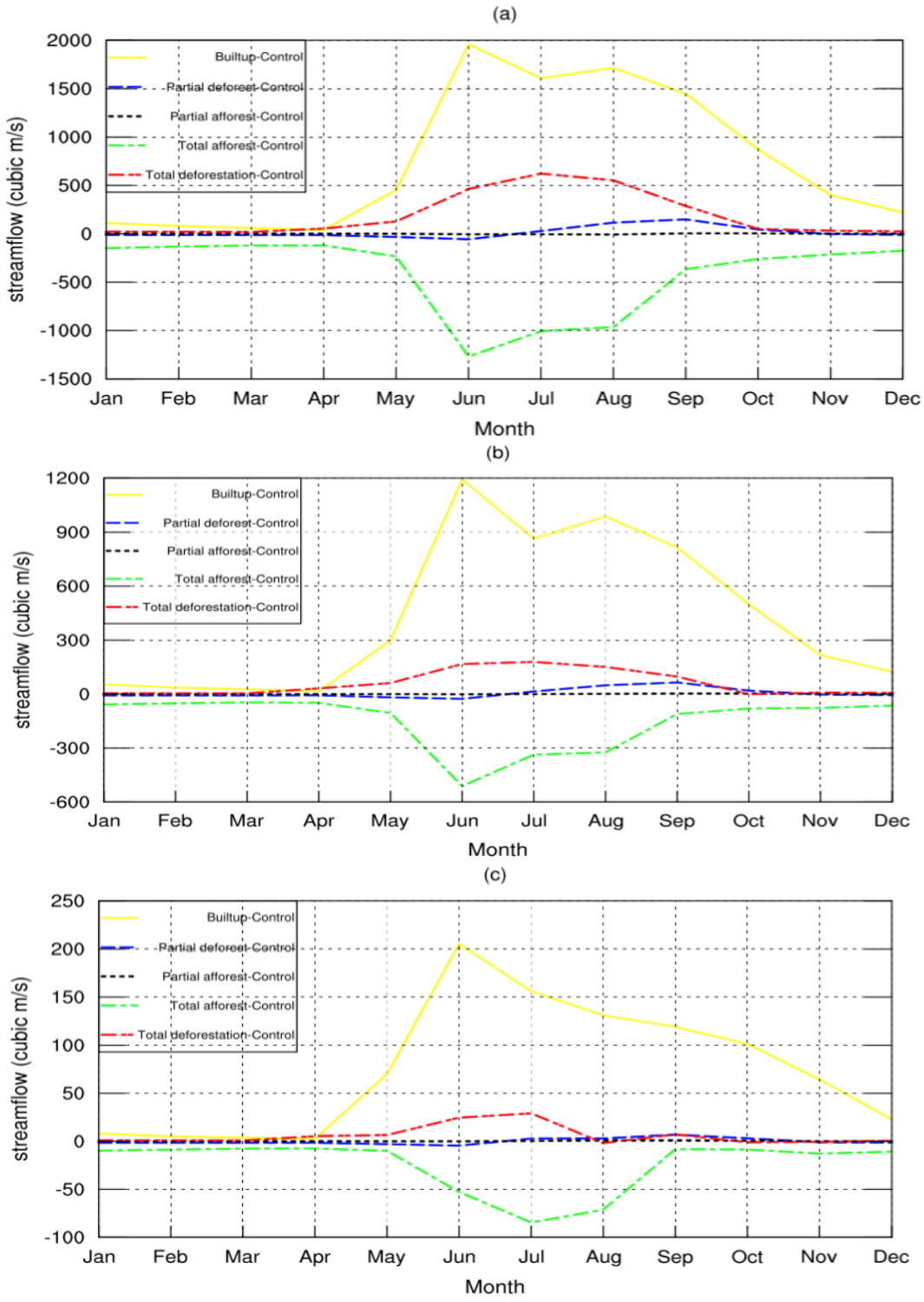

Figure 4.53: Difference between the Control Streamflow and Each LULC scenario for (a) Sokoto, (b) Goronyo and (c) Bakolori Forecast Points

Table 4.17: Percentage Change of Streamflow in Each Forecast Point in the SRRB

	LULC scenario	Annual change (%)
Sokoto	Built Up	41.97
	Partial Deforest	0.84
	Partial Afforest	-0.03
	Total Afforest	-23.51
	Total Deforest	10.63
Goronyo	Built Up	82.11
	Partial Deforest	1.08
	Partial Afforest	0.15
	Total Afforest	-28.93
	Total Deforest	11.46
Bakolori	Built Up	98.48
	Partial Deforest	0.04
	Partial Afforest	0.46
	Total Afforest	-32.30
	Total Deforest	8.07

sub-basin level are many a time obscured by opposing effects in other parts of the basin. The complete conversion of all the LCPs (except barren, built up lands and permanent wetlands) into Evergreen Broadleaf Forests (i.e. TA scenario) decreased the streamflow by -23.51% in Sokoto, -28.93% in Goronyo, and -32.30% in Bakolori. The effect of forest cover changes on mean streamflow is satisfactorily understood and data all over the world have revealed that increasing the forest cover of a catchment results into a decrease in the total volume of flow (Brown *et al*., 2013). Also, the rate of transpiration is generally different for various vegetation covers, as forested areas normally transpire at higher rates than shrubs and cultivated areas, hence could lead to a decreased streamflow. Lastly, the simulation with the Total Deforest scenario increased streamflow by 10.63% in Sokoto, 11.46% in Goronyo and 8.07% in Balkolori. When all vegetation is removed in the whole basin, there is obviously neither transpiration nor evaporation of precipitation, which is intercepted by the canopy. Consequently, evaporation is restricted

to only the one from the bare soil and therebe causing an increase in the streamflow. This is in line with the work of Li *et al*. (2007) who also concluded that deforestation increases streamflow.

The analysis have shown that afforestation decreases streamflow while deforestation leads to an increase, and this is in line with many researches like Aduah *et al*. (2017), Legesse *et al*. (2003), Ward *et al*. (2009), Li *et al*. (2007), Akpoti *et al*. (2016). Trimble *et al*. (1987) and Swank *et al*. (1988) also show a decrease in streamflow due to afforestation. According to Githui (2009), higher stream flow occurs as a result of increased agricultural lands and decreased forest areas. Thus, as the presence of forests can reduce flow, the smaller the forest area the more the flow.

CHAPTER FIVE

CONCLUSION AND RECOMMENDATION

5.1 Conclusion

The impacts of land use land cover change on hydrometeorological parameters such as air temperature, dew point temperature, precipitation, evapotranspiration, stremflow and their associated parameters over West Africa have been investigated in this research.

Land use land cover change analysis shows that between 2001 and 2016, there were ongoing land cover changes in West Africa. Analysis revealed that the percentage change in Land Cover Parameters (LCP) for Evergreen Needleleaf Forests, Evergreen Broadleaf Forests, Deciduous Broadleaf Forests, Mixed Forests, Closed Shrublands, Open Shrublands, Woody Savannas, Savannas, Grasslands, Permanent Wetlands, Croplands, Urban and Built-up Lands, Cropland/Natural Vegetation Mosaics, Barren and Water bodies between 2001 and 2016 is -5.71%, -1.20%, -22.54%, 52.38%, -81.03%, -11.78%, 12.14% -3.69%, 4.03%, 8.56%, -4.74%, 23.26%, 8.24%, -1.32%, -0.0042% respectively. Mutual exchange however exists between different types of LCP depending on the year understudy except for the UBL that has steady increase throughout the study period. The consequence of a steady increase in urban built up lands in an environment like West Africa is direct deforestation because of the need for buildings and construction purposes for settlements, food and basic infrastructural development. The decrease in water bodies can be connected to anthropogenic activities of land uses for housing, and road constructions.

In other to assess the performance of WRF land surface models over West Africa, simulations were carried out using four different land surface models, which include Noah, Noah-MP, CLM4 and the Noah-MP GW option with different physics combinations. The focus of the study is on daily precipitation, dew point temperature and air temperature at 2m for two periods representing wet and dry season (JAS and DJF). In order to provide a succinct statistical summary, the results were plotted in Taylor diagram. On average, the model outputs from all the LSMs have average values very close to the observed both for rainy and dry season except for precipitation with slightly wider ranges in some instances. It could be emphasized that the variable of interest is also a factor to be considered in the selection of LSMs. Each LSM could perform well for different variables in different seasons, which could be as a result of the difference in the models physics, soil/snow layers and columns, vegetation structure and level of model sophistication. However, Noah-MP performed best for simulation of precipitation for all season, both Noah-MP and the groundwater option performed best for temperature and dew point temperature for all seasons, and Noah-MP performed best overall for the three variables under study for all seasons. The models physics and level of sophistication/complexity affected the simulations either positively or negatively.

The study has shown that using an updated MODIS land use on the WRF model is feasible and that incorporation of remote sensing data into the WRF model improved the simulation. The study made the use of the biophysical parameters of the different LULC in order to ascertain the changes as a result of LULC change, specifically soil moisture, albedo, emissivity and Leaf area index were looked into. The changes in land use land cover data led to the alteration of the simulations like temperature, dew point

temperature, precipitation, some radiation variables and biophysical parameters. The alterations on the parameters could be attributed to the differences in the values of biophysical parameters between the two incorporated LULC data.

Studying the response of some hydrometeorological parameters to LULC change, six different land cover scenarios were generated for Built Up (BU), Partial Deforest I (PDI), Partial Deforest II (PDII), Partial Afforest (PA), Total Afforest (TA) and Total Deforest (TD). BU and TD scenarios decreased dew point temperature and evapotranspiration, and increased air temperature, sensible heat. TA generally increased dew point temperature, evapotranspiration, and decreased air temperature and Sensible heat. Analysis of the impact of LULCC on precipitation over WA showed that the afforestation tended to increase it. However, the increase of rainfall induced by the afforestation scenarios could be due to an increase of the evapotranspiration and the strengthening of the atmospheric moisture. The effect of LULCC on precipitation were complex and needs a deep analysis of the atmospheric circulation and other systems like the Tropical Easterly Jet (TEJ), African Easterly Waves (AEW), African Easterly Jet (AEJ), etc. thereby making the close to accurate simulation of precipitation to be more challenging.

In studying the response of streamflow to LULC change, WRF-hydro model was used to run simulations with five different land cover scenarios were generated for Built Up (BU), Partial Deforest (PD), Partial Afforest (PA), Total Afforest (TA) and Total Deforest (TD). The model was calibrated and validated by adjusting the infiltration parameter of the model. Result showed that afforestation generally decreased streamflow while deforestation led to an increase. The conversion of all Permanent Wetlands and

Croplands in the SRRB into built up lands increased the streamflow by about 41.79% in Sokoto, 82.11% in Goronyo and 98.48% in Bakolori which marks the highest percentage increase for all the LULC scenarios. This is because, urban and built-up lands has less infilteration capacity by creating impervious surface, removes vegetation and consequently removes transpiration.

In summary, the study have shown that land cover have changed over the years, and the adverse effect that will result if LULC changed to the extreme as it could increase temperature and discomfort and lead to flooding as stream flow increases. The combination of Remote Sensing, GIS and the WRF-hydro model provides a useful technique in assessing the impact of LULCC on catchment hydrology which is essential in selecting and developing feasible catchment management options that will promote sustainable utilization of land and water resources.

5.2 Recommendations

Based on the research findings, the followings are recommended;

i. The various governments in West Africa should employ the result of the LULC change analysis in their policy and decision making for effective solutions to the sustainability of the natural resources
ii. The government should be proactive in bringing up policies for proper land use management
iii. The use of Noah-MP should be intensified for land-atmosphere interaction studies over West Africa as it proves to be better than the others.
iv. Selection of LSM for research/forecast activities should be based on the parameter of interest as each parameter performs differently for each LSM.

v. Further work is recommended to capture all the area of the SRRB in other to have a better assessment of the impact of LULCC on the basin.

vi. Finally, incorporation of high-resolution satellite data like LANDSAT and SPOT is recommended for future work for so as to capture small-scale phenomena, which the after-match effect could be significant.

5.3 Contribution to Knowledge

1. The research work provided useful information on the trends of LULCC over the entire West Africa.
2. The research work studied the effects of LULCC on hydrometeorological parameters, which have not been carried out over WA.
3. The research has shown that Noah-MP LSM simulates 2m temperature, dew point temperature and precipitation better than Noah and CLM4.
4. The integration of different Remote Sensing (RS) and Geographic Information System (GIS) based data into WRF and WRF-Hydro model have not been carried out over WA.
5. This research will also help in making informed decisions in the selection and development of feasible catchment management choices to ensure sustainable use of land and water resources within the entire WA and the Sokoto Rima River Basin.

5.4 Limitations

The daily streamflow data were not available as at the period of the research, although, promises were made to make them available in the future. In consequence, only the monthly streamflow data were available for a few number of years in which 2012 was

judged the best. In addition, the tension in the area due to banditry and terrorism discouraged frequent visitation of the basin. The reason for selecting a smaller domain for the WRF-hydro simulation was due to the high computational cost of running WRF-hydro simulations over such a very large domain (i.e. the entire SRRB). Furthermore, building the routing grids using the WRF-Hydro GIS pre-processing tools was also difficult for a larger domain. A remotely sensed data with higher resolution (e.g. LANDSAT) would have been preferred over MCDI21Q1 MODIS data for the experiments and simulations, but owing to the time constraint and the ability to merge such numerous tiles (over 100 tiles) of LANDSAT data to cover the whole of West Africa, MODIS data were used. Finally, the reference data (i.e. ERA-interim, TRMM, NCEP FNL, GPCP) were used to validate the simulations over West Africa owing to lack of observed data over the region.

REFERENCES

Abdullahi S. A., Muhammad M. M., Adeogun B. K. and Mohammed, I. U. (2014). Assessment of Water Availability in the Sokoto Rima River Basin, Resources and Environment 4(5): 220-233 DOI: 10.5923/j.re.20140405.03

Abiodun, B. J., Pal, J., Afiesimama, E. A., Gutowski W. J. and Adedoyin, A. (2007). Simulation of West African monsoon using the Regcm3 Part II: Impact of Deforestation and Desertification. Theor. and Appli. Climatol. 93: 245-261

Adeel, M. (2010). Methodology for Identifying Urban Growth Potential Using Land Use and Population Data: A case study of Islamabad Zone IV. Procedia Environmental Sciences. 2: 32-41.

Aduah, M. S., Jewitt, G. P. W. and Toucher, M. L. W. (2017). Assessing Impacts of Land Use Changes on the Hydrology of a Lowland Rainforest Catchment in Ghana, West Africa. Water, 10(9): 1-15. doi:10.3390/w10010009

Akpoti, K., Antwi, E. O. Kabo-bah, A. T. (2016). Impacts of Rainfall Variability, Land Use and Land Cover Change on Stream Flow of the Black Volta Basin, West Africa. Hydrology 3, 26; 1-24. doi:10.3390/hydrology3030026

Alfred, B. Y., Gillian M. U., Mike O., Ofonedum O. L., Audu-Moses J. (2016). Urban Growth and Landuse Cover Change in Nigeria using GIS and Remote Sensing Applications. Case Study of Suleja L.G.A., Niger State. International Journal of Engineering Research & Technology, 5(8): 124-138

Alpert, P., Krichak, S. O., Shafir, H., Haim, D. and Osetinsky, I. (2008). Climatic trends to extremes employing regional modeling and statistical interpretation over the E. Mediterranean. Glob Plan Chang 63: 163-170.

Amani, A., Thomas, J., and Abou, M. N. (2007) Climate change adaptation and water resources management in West Africa. Synthesis report WRITESHOP. UNESCO. Retrived April 2014.

Amoo, O. T. and Dzwairo, B. (2017). Hydrological Characterization of a Watershed for Streamflow Prediction. World Academy of Science, Engineering and Technology International Journal of Environmental, Chemical, Ecological, Geological and Geophysical Engineering, 11(5): 382-396

Angelsen, A. and Kaimowitz, D. (1999). Rethinking the Causes of Deforestation: Lessons From Economic Models. The World Bank Research Observer 14: 73–98.

Antwi E.K., Boakye-Danquah J., Asabere S.B., Yiran G A.B., Ko L.S., Awere K.G., et al., (2014). LandUse and Landscape Structural Changes in the Ecoregions of Ghana. Journal of Disaster Research, 9: 452-464

Bai, J. H., Lu, Q. Q., Zhao, Q. Q., Wang, J. J. and Ouyang, H. (2013). Effects of Alpine Wetland Landscapes On Regional Climate. Adv. Meterol. 2013(5): 1-7.

Baidya, R. and Avissar, R. (2002). Impact of land use/land cover change on regional hydrometeorology in Amazonia. J Geophys Res 107(D20): 1−12

Ball, J. T., Woodrow, I. E. and Berry J. A. (1987). A model predicting stomatal conductance and its contribution to the control of photosynthesis under different environmental conditions, in Process in Photosynthesis Research, vol. 1, edited by J. Biggins, pp. 221–234, Martinus Nijhoff, Dordrecht, Netherlands.

Bartzen, B. A., Dufour, K. W., Clark, R. G. and Caswell, F. D. (2010). Trends in agricultural impact and recovery of wetlands in prairie Canada. Ecol. Appl. 20: 525-538.

Belward, A. S., Estes, J. E., and Kline, K. D. (1999). The igbp-dis global 1-km land-cover data set discover: A project overview. Photogrammetric Engineering and Remote Sensing, 65(9): 1013–1020.

Betts, A. K., Ball, J. H., Beljaars, A., Miller, M.J. and Viterbo, P. A. (1996) "The land surface−atmosphere interaction: a review based on observational and global modeling perspectives," J. Geophysical Research, 101 (3): 7209– 7225.

Bliefernicht, J., Berger, S., Salack, S., Guug, S., Hingerl, L., Heinzeller, D., Mauder, M., Steinbrecher, R., Steup, G., Bossa, A.Y., Waongo, M., Quansah, E., Balogun, A.A., Yira, Y., Arnault, J., Wagner, S., Klein, C., Gessner, U., Knauer, K., Straub, A., Schönrock, R., Kunkel, R., Okogbue, E. C., Rogmann, A., Neidl, F., Jahn, C., Diekkrüger, B., Aduna, A., Barry, B. and Kunstmann, H. (2018). The WASCAL Hydrometeorological Observatory in the Sudan Savanna of Burkina Faso and Ghana. Vadose Zone J. 17: 1-20 180065. doi:10.2136/vzj2018.03.0065

Bonan, G. B. (1996), A land surface model (LSM version 1.0) for ecological, hydrological, and atmospheric studies: Technical description and user's guide, NCAR Tech. Note NCAR/TN-417+STR, 150 pp., Natl. Cent. for Atmos. Res., Boulder, Colo.

Bonan, G. B. (2002). Landscapes as patches of plant functional types: An integrating concept for climate and ecosystem models. Global Biogeochemical Cycles, 16(2): 1021.

Boone A, Poccard-Leclerq I, Xue Y, Feng J, and de Rosnay P (2009a) Evaluation of the WAMME model surface fluxes using results from the AMMA land-surface model intercomparison project. Clim Dyn. doi:10.1007/s00382-009-0653-1

Boone, A., de Rosnay, P., bAlsAmo, G., beljAArs, A., choPin, F., Decharme, B., Delire, C., DuchArne, A., GAscoin, S., GriPPA, M., Guichard, F., Gusev, Y., Harris, P., Jarlan,

L., Kergoat, L., Mougin, E., Nasonova, O., Norgaard, A., Orgeval, T., ottlé, C., Poccard-Leclercq, I., Polcher, J., Sandholt, I., Saux-Picart, S., Taylor, C. andXue, Y. (2009b). The AMMA land surface model intercomparison project. Bul- letin of the American Meteorological Society 90: 1865–1880. DOI: 10.1175/2009BAMS2786.1.

Boone, A., Xue, Y., De Sales, F., Comer, R., Hagos, S., Mahanama, S., Schiro, K., Song, G., Wang, G., Li, S., & Mechoso, C. R. (2016). The Regional Impact Of Land-Use Land-Cover Change (LULCC) Over West Africa From An Ensemble Of Global Climate Models Under The Auspices of the WAMME2 project. Clim. Dyn., 47, 3547–3573.

Boori, M. S., Voze˘n´ılek V., Choudhary K., (2015). Land Use/Cover Disturbance Due To Tourism In Jesenı'ky Mountain, Czech Republic: A Remote Sensing And GIS Based Approach. Egypt. J. Remote Sensing Space Science, 18 (1): 17–26

Borge, R., V. Alexandrov, J. Jose´ del Vas, J. Lumbreras, and E. Rodrı´guez, (2008) A comprehensive sensitivity analysis of the WRF model for air quality applications over the Iberian Peninsula. Atmos. Environ., 42: 8560–8574.

Bossa, A. Y., Diekkrüger, B., and Agbossou, E. K. (2014). Scenario-Based Impacts of Land Use and Climate Change on Land and Water Degradation from the Meso to Regional Scale Aymar. Water, 6: 3152–3181; doi:10.3390/w6103152

Botai, C. M., Botai, J. O., Muchuru, S and Ngwana, I. (2015). Hydrometeorological Research in South Africa: A Review. Water, 7: 1580-1594; doi:10.3390/w7041580

Boucher, D. H., Elias, P., Lininger, K., May-Tobin, C., Roquemore, S., Saxon, E. (2011). The Root of the Problem: What's Driving Tropical Deforestation Today? (Cambridge, MA: Union of Concerned Scientists) (Online at :

https://theredddesk.org/sites/default/files/resources/pdf/ucs_rootoftheproblem_driversofdeforestation_fullreport.pdf)

Braimoh A. K. and Onishi, T. (2007). Spatial determinants of urban land use change in Lagos, Nigeria. Land Use Policy, 24, 502–515

Brink, A. B., Eva, H. D. (2009). Monitoring 25 years of land cover change dynamics in Africa: a sample based remote sensing approach. Appl. Geogr. 29: 501-512.

Bronstert, A., Niehoff, D. and Burger, G. (2002). Effects of Climate and Land-Use Change on Storm Runoff Generation: Present Knowledge And Modelling Capabilities. Hydrol. Process., 16: 509–529

Brown, A., Western, A., McMahon, T. and Zhang, Lu (2013). Impact of forest cover changes on annual streamflow and flow duration curves. Journal of Hydrology. 483:39-50.

Bruijnzeel, L.A. (1990). Hydrology of moist tropical forests and effects of conversion: a state of knowledge review. In: UNESCO International Hydrological Program, 224 pp.

Butt A., Shabbir R., Ahmad S.S., Aziz N. (2015a). Land use change map- ping and analysis using Remote Sensing and GIS: A case study of Simly watershed, Islamabad, Pakistan. The Egyptian Journal of Remote Sensing and Space Sciences, 18: 251–259

Butt A., Shabbir R., Ahmad S.S., Aziz N., Nawaz M., Shah, M. T. A. (2015b). Land Cover Classification and Change Detection Analysis of Rawal Watershed Using Remote Sensing Data. Journal of Biology and Environmental Science, 6 (1): 236–248

Cai, X. (2008). Water Stress, water transfer and social equity in Northern China-implications for policy reforms J. Environ. Manage. 87: 14-25

Cao, Q., Yu, D., Georgescu, M., Han, Z. and Wu, J. (2015): Impacts of land use and land cover change on regional climate: a case study in the agro-pastoral transitional zone of China, Environ. Res. Lett. 10, 124025, Environ. doi:10.1088/1748-9326/10/12/124025

Carrington, D. P., Gallimore, R. G. and Kutzbach, J. E. (2001). Climate Sensitivity to Wetlands And Wetland Vegetation in Mid-Holocene North Africa. Clim. Dyn. 17, 151e157.

Case, J. L., LaFontaine, F. J., Kumar, S. V. and Peters-Lidard, C. D. (2012) Using the NASA-Unified WRF to assess the impacts of real-time vegetation on simulations of severe weather. Preprints, 13th Annual WRF User's Workshop, Boulder, CO, p69.

Casse, C., Gosset, M., Vischel, T., Quantin, G. and Tanimoun, B. A. (2016). Model-based study of the role of rainfall and land use–land cover in the changes in the occurrence and intensity of Niger red floods in Niamey between 1953 and 2012. Hydrology and Earth System Sciences, 20:2841-2859. doi:10.5194/hess-20-2841-2016

Charney, J. G. (1975). Dynamics of Deserts And Drought in the Sahel. Q J R Meteorl. Soc. 101:193–202.

Charney, J. G., Quirk, W. J., Chow, S. H. and Kornfield, J. (1977). A comparative study of the effects of albedo change on drought in semi-arid regions. J Atmos Sci 34:1366–1385

Chase, T. N., Pielke, R., Kittel, T. G. F., Nemani, R. and Running, S. W. (1996). Sensitivity of a general circulation model to global changes in leaf area index J. Geophys. Res. 101(7): 393–408

Chen, F., Dudhia, J., (2001). Coupling an advanced land-surface/hydrology model with the Penn State/NCAR MM5 modeling system. Part I: model description and implementation. Mon. Weather Rev. 129: 569–585.

Chen, X. L., Zhao, H. M., Li, P. X. and Yin, Z. Y. (2006). Remote Sensing Image-Based Analysis of The Relationship Between Urban Heat Island and Land Use/Cover Changes. Remote Sens. Environ. 104: 133-146.

Chen, F., Manning, K. W., Lemone, M. A., Trier, S. B., Alfieri, J. G., Roberts, R., Tewari, M., Niyogi, D., Horst, T. W., Oncley, S. P., Basara, B. B. and Blanken, P. D. (2007). Description and Evaluation of the Characteristics of the NCAR High-Resolution Land Data Assimilation System. J. Appl. Meteorol. Climatol. 46:694–713

Chen, X., Yang, T., Wang, X., Xu, C.-Y. and Yu, Z. (2012) Uncertainty intercomparison of different hydrological models in simulating extreme flows. Water Resour. Manag. 27, 1393–1409. http://dx.doi.org/10.1007/s11269-012-0244-5

Chen, F., Liu, C. Dudhia, J. and Chen, M. (2014). A Sensitivity Study Of High-Resolution Regional Climate Simulations To Three Land Surface Models Over The Western United States. J. Geophys. Res., 119, 7271–7291, doi:10.1002/2014JD021827.

Clark, C. and Arrit, R. (1995). Numerical Simulations of the Effect of Soil Moisture and Vegetation Cover on the Development of Deep Convection. AMS. 34: 2039-2045.

Clark, D., Xue, Y., Harding, R. and Valdes, P. (2001). Modelling the impact of land surface degradation on the climate of tropical North Africa. J. of Climate. 14: 1809-1822.

Collatz, G. J., Ball, J. T., Grivet, C. and Berry, J. A. (1991). Physiological and environmental regulation of stomatal conductance, photosynthesis and transpiration: A model that includes a laminar boundary layer, Agric. For. Meteorol., 54(2–4): 107–136.

Collatz, G. J., Ribascarbo, M. and Berry, J. A. (1992). A coupled photosynthesis-stomatal conductance model for leaves of C4 plants, Aust. J. Plant Physiol., 19: 519–538.

Cook, H. K. (1999). Generation of the African Easterly Jet And Its Role In Determining West African Precipitation. J Climate 12: 1165–1184

Crétat, J., Pohl, B., Richard, Y. and Drobinski, P. (2012). Uncertainties in simulating regional climate of Southern Africa: sensitivity to physical parameterizations using WRF. Climate Dynamics, 38 (3-4): 613– 634.

Croke, B.F.W., Merritt, W.S., Jakeman, A.J., (2004). A dynamic model for predicting hydrologic response to land cover changes in gauged and ungauged catchments. J. Hydrol 291: 115–131.

Cunnington, W. M. and Rowntree, P. R. (1986). Simulations of the Saharan Atmosphere Dependence on Moisture And Albedo. Quart. J. Roy. Meteor. Soc., 112, 971–999.

Deb, S., T. Srivastava, and C. Kishtawal, (2008). The WRF model performance for the simulation of heavy precipitating events over Ahmedabad during August 2006. J. Earth Syst. Sci., 117: 589–602.

Decharme, B., Ottl, C., Boulain, N., Cappelaere, B., Ramier, D. and Zribi, M. (2009). A New Land Surface Hydrology within the Noah-WRF Land-Atmosphere Mesoscale Model Applied to Semiarid Environment: Evaluation over the Dantiandou Kori (Niger). Advances in Meteorology , 2009: 1-13.731874, doi:10.1155/2009/731874.

Dee, D. P., Uppala, S. M., Simmons, A, J., Berrisford, P., Poli, P., Kobayashi, S., Andrae, U, Balmaseda, M., Balsamo, G., Bauer, P., Bechtold. P. and Beljaars, C. M. (2011). The ERA-.Interim reanalysis: configuration and performance ,of the data assimilation system. Q J R Meteorol Soc 137(656): 553–597. doi:10.1002/qj.828

Dezfuli, A. and Nicholson, S. (2013). The Relationship of Rainfall Variability in Western Equatorial Africa to the Tropical Oceans and Atmospheric Circulation. Part II: The Boreal Autumn, Journal of Climate, 26: 66–84.

Diba, I., Camara, M., Sarr, A. B. and Diedhiou, A. (2018). Potential Impacts of Land Cover Change on the Interannual Variability of Rainfall and Surface Temperature over West Africa. Atmosphere, 9, 376: 1-32. doi:10.3390/atmos9100376

Dickinson, R. E., M. Shaikh, R. Bryant, and L. Graumlich (1998), Interac- tive canopies for a climate model, J. Clim., 11: 2823–2836, doi:10.1175/ 1520-0442(1998)011<2823:ICFACM>2.0.CO;2.

Dirmeyer, P. A. (2011). The Terrestrial Segment of Soil Moisture Climate Coupling. Geophys. Res. Lett., 38, L16702, doi:10.1029/ 2011GL048268

Domenico, P. A. and Schwartz, F. W. (1990). Physical and Chemical Hydrogeology; John Wiley and Sons, Inc. New York, NY, USA.

Donner, D. S. (Ed). (2004). Land Use, Land Cover, and Climate Change across the Mississippi Basin: Impacts on Selected Land and Water Resources. American Geophysical Union, 153: 249-261. DOI: 10.1029/153GM19.

Douville, H., Chauvin, F. and Broqua, H. (2001). Influence of Soil Moisture on the Asian and African monsoons. Part I: Mean Monsoon And Daily Precipitation. J. Climate, 14: 2381–2403.

Ekpoh, I. J. and EkpenyongNsa (FRGS) (2011). The Effects of Recent Climatic Variations on Water Yield in the Sokoto Region of Northern Nigeria; International Journal of Business and Social Science, 2(7): 251-256.

Eltahir, E. A. B. and Gong, C. (1996). Dynamics of Wet and Dry Years in West Africa. J. Climate, 9: 1030-1042.

Eltahir, E. and Bras, R. (1993). On the Response Of The Tropical Atmosphere to Large-Scale Deforestation. Q.J.R. Meteorol. Soc. 119: 779-793

Eva, H. D., Brink, A. and Simonetti, D. (2006). Monitoring Land Cover Dynamics in Sub-Saharan Africa. European Commission Directorate-General Joint Research Centre Institute for Environment and Sustainability, EUR 22498 EN, Office for Official Publications of the European Communities, Luxembourg.

Evans, J. P., Ekstro¨m M, Ji, F. (2012). Evaluating the performance of a WRF physics ensemble over South-East Australia. Clim. Dyn. doi:10.1007/s00382-011-1244-5

Fairhead, J. and Leach, M. (1998). Reframing Deforestation: Global Analysis and Local Realities: Studies in West Africa, Routledge, London, p. 238.

FAO, (2010). Global Forest Resources Assessment 2010. FAO Forestry Paper No. 163, UN Food and Agriculture Organisation, Rome.

FAO, (2015). Global Forest Resources Assessment 2015. FAO Forestry Paper, Un Food And Agriculture Organisation of the United Nations Rome.

FAO, (2016). State of the World's Forests 2016. Forest and Agriculture: Land Use Challenges and Opportunities. Rome.

FAO/UNEP, (1999). Terminology for Integrated Resources Planning and Management. Food and Agriculture Organisation/United Nations Environmental Program, Rome, Italy and Nairobi, Kenya.

Fearnside P. M. (1997). Transmigration in Indonesia: Lessons from its Environmental and Social Impacts. Environ. Manag. 21(4): 553–70.

Feddema. J. J., Oleson. K. W., Bonan. G. B., Mearns. L. O., Buja. L. E., Meehl. G. A. and Washington, W. M. (2005). The importance of land-cover change in simulating future climates. Science 310(5754): 1674–1678.

Foley, J. A., DeFries, R., Asner, G. P., Barford, C., Bonan, G., Carpenter, S. R., Chapin, F. S., Coe, M. T., Daily, G. C., Gibbs, H. K., Helkowski, J. H., Holloway, T., Howard, E. A., Kucharik, C. J., Monfreda, C., Patz, J. A., Prentice, I. C., Ramankutty, N., Snyder, P. K. (2005). Global Consequences of Land Use. Science, 309: 570-574.

Friedl, M. A., McIver, D. K., Hodges, J., Zhang, X. Y., Muchoney, D., Strahler, A. H., Woodcock, C. E., Gopal, S., Schneider, A., Cooper, A., Baccini, A., Gao, F., and Schaaf, C. (2002). Global land cover mapping from MODIS: algorithms and early results. Remote Sensing of Environment, 83(1): 287–302.

Friedl, M. A., Sulla-Menashe, D., Tan, B., Schneider, A., Ramankutty, N., Sibley, A., and Huang, X. (2010). MODIS Collection 5 global land cover: Algorithm refinements and characterization of new datasets. Remote Sensing of Environment, 114(1):168–182.

Friedl, M. and Sulla-Menashe, D. (2018). MCD12Q1 MODIS/Terra+Aqua Land Cover Type Yearly L3 Global 500m SIN Grid V006 [Data set]. NASA EOSDIS Land Processes DAAC. doi: 10.5067/MODIS/MCD12Q1.006

Fu, C., Yasunari, T. and Lütkemeier, S. (2004). The Asian monsoon climate. In P. Kabat et al. (Eds.), Vegetation, water, humans and the climate (pp. 115–127). Berlin: Springer-Verlag.

Fuller, D. O. and Ottke, C. (2002). Land Cover, Rainfall And Land-Surface Albedo In West Africa, Climatic Change, 54: 181–204.

Gallus, W., Jr., and Bresch, J. (2006). Comparison of impacts of WRF dynamic core, physics package, and initial conditions on warm season rainfall forecasts. Mon. Wea. Rev., 134: 2632–2641.

García-Díez, M., Fernández, J., Fita, L. and Yagüe, C. (2013) Seasonal Dependence of WRF Model Biases and Sensi- tivity to PBL Schemes over Europe. Quarterly Journal of the Royal Meteorological Society, 139: 501-514. http://dx.doi.org/10.1002/qj.1976

Gbobaniyi, E., Sarr, A., Sylla, M. B., and Diallo, I. (2013) Climatology, annual cycle and interannual variability of precipitation and temperature in CORDEX simulations over West Africa. Int J Climatol. doi:10.1002/joc.3834

Gbode, I. E., Dudhia, J., Ogunjobi, K.O and Ajayi, V. O. (2018). Sensitivity of different physics schemes in the WRF model during a West African monsoon regime, Theoretical and Applied Climatology. https://doi.org/10.1007/s00704-018-2538-x

Ge, Q., Zhang, X. and Zheng, J. (2014). Simulated effects of vegetation increase/decrease on temperature changes from 1982 to 2000 across the Eastern China Int. J. Climatol. 34: 187–96

Geist. H. J. and Lambin, E. F. (2001). What drives Deforestation? A Meta-Analysis of Proximate an underlying cause of deforestation Based on Sub National Case Study Envidence. LUCC Report Series 4, pp.116.

Georgescu, M. (2008). Evaluating The Effect Of Land-Use And Land-Cover Change On Climate In The Greater Phoenix, Az, Region. Phd Thesis Submitted To The Graduate School-New Brunswick Rutgers, The State University of New Jersey.

Georgescu, M., D. B. Lobell, and C. B. Field (2009). Potential Impact of U.S. Biofuels on Regional Climate, Geophys. Res. Lett., 36, L21806, doi:10.1029/2009GL040477

Ghaffari, G., Keesstra, S., Ghodousi, J. and Ahmadi, H. (2010). SWAT-Simulated Hydrological Impact Of Land-Use Change in the Zanjanrood Basin, Northwest Iran. Hydrol. Process. 24: 892–903

Githui, F., Mutua, F. and Willy, B. (2009). Estimating the Impacts Of Land-Cover Change On Runoff Using the Soil And Water Assessment Tool (SWAT): Case Study Of Nzoia Catchment, Kenya. Hydrol Sci J 54: 899−908

Gochis, D. J. and Chen, F. (2003). Hydrological enhancements to the community Noah land surface model. NCAR Technical Note, NCAR/TN-454+STR, 68.

Gochis, D.J., M. Barlage, A. Dugger, K. FitzGerald, L. Karsten, M. McAllister, J. McCreight, J. Mills, A. RafieeiNasab, L. Read, K. Sampson, D. Yates and W. Yu, (2018). The WRF-Hydro modeling system technical description, (Version 5.0). NCAR Technical Note. 107 pages. Available online at: https://ral.ucar.edu/sites/default/files/public/WRFHydroV5TechnicalDescription.pdf.

Gong, C. and Eltahir, E. (1996). Sources of Moisture for Rainfall in West Africa, Water Resources Research, 32: 3115–3121, doi:10.1029/96WR01940.

Gornitz, V. (1985). A Survey of Anthropogenic Vegetation Changes in West Africa During The Last Century—Climatic Implications. Clim Change 7:285–325

Green, J.K.,. Konings, A.G., Alemohammad, S.H., Berry, J., Entekhabi, D., Kolassa, J., Lee, J-E. and Gentine P. (2017). Regionally strong feedbacks between the atmosphere and terrestrial biosphere. Nat. Geosci. 10:410–414. doi:10.1038/ngeo2957

Grimmond, S. (2007). Urbanization and Global Environmental Change: Local Effects Of Urban Warming. Geogr. J. 173: 83-88.

Gupta, H. V., Kling, H., Yilmaz, K. K., Martinez, and G. F. (2009). Decomposition of the mean squared error and NSE performance criteria: implications for improving hydrological modeling. J. Hydrol. 377: 80–91.

Gupta, H. V., Sorooshian, S. and Yapo, P. O. (1999). Status of Automatic Calibration for Hydrologic Models: Comparison with Multilevel Expert Calibration. Journal of Hydrologic Engineering. 4(2): 135-143

Hagos, S., Leung, L. R, Xue, Y. K., Boone, A., de Sales, F., Neupane, N., Huang, M. and Yoon, J-H. (2014). Assessment of uncertainties in the response of the African monsoon precipitation to land use change simulated by a regional model. Clim Dyn 43:2765–2775. doi:10.1007/s00382-014-2092-x

Han, S. H., Meng, L., Park, G. S., Kim, S. B., Cho, M. S., Park, B. B. (2017). Characteristics of Soil Carbon and Nutrient Stocks Across Land Use Types in a Forest Region of Central Korea, Forest Science and Technology, 13(3): 93-99.

Hansen, M. C., Defries, R. S., Townshend, J. R., and Sohlberg, R. (2000). Global land cover classification at 1 km spatial resolution using a classification tree approach. International Journal of Remote Sensing, 21(6-7):1331–1364.

He, C., Wang, S., Xu, J. and Zhou, C. (2002) Using remote sensing to estimate the change of carbon storage: A case study in the estuary of Yellow River delta, International Journal of Remote Sensing, 23(8): 1565-1580. DOI: 10.1080/014311602753590887

Hegazy , I. R. and Kaloop , M. R. (2015). Monitoring urban growth and land use change detection with GIS and remote sensing techniques in Daqahlia governorate Egypt. International Journal of Sustainable Built Environment. 4, 117-124.

Hong, S. Y. and Lim, J. O. J. (2006) The WRF Single-Moment 6-Class Microphysics Scheme (WSM6), J. Korean Meteor. Soc., 42, 129– 151.

Hong, S. Y., Lim, K. S. S., Kim, J. H., Lim, J. O. J. and Dudhia, J. (2009). Sensitivity study of cloud-resolving convective simulations with WRF using two bulk microphysical parameterizations: Ice-phase microphysics versus sedimentation effects. J. Appl. Meteor. Climatol., 48: 61–76.

Hough, J. (1986). Management Alternatives for Increasing Dry Season Base Flow in The Miombo Woodlands of Southern Africa. Ambio 15(6): 341-346.

Houghton, J., Ding, Y., Griggs, D.J., Noguer, M., van der Linden, P.J., Xiaosu, D. (2001). Climate Change 2001: The Scientific Basis. Contribution of Working Group I to the 3rd Assessment Report of the Intergovernmental Panel on Climate Change. Cambridge University Press, Cambridge.

Houghton, R. A. and J. L. Hackler (2006). Emissions of carbon from land use change in sub-Saharan Africa, J. Geophys. Res., 111, G02003, doi:10.1029/2005JG000076.

Huffman, G. J., Bolvin, D. T., Nelkin, E. J., Wolff, D. B., Adler, R. F., Gu, G., Hong, Y., Bowman, K. P., Stocker, E. F. (2007) The TRMM multisatellite precip- itation analysis (TMPA): quasi-global, multiyear, combined-sensor precipitation estimates at fine scales. J Hydrometeorol 8(1): 38–55

Huffman, G. J., Adler, R. F., Bolvin, D. T. and Gu, G. (2009) Improving the global precipitation record: GPCP version 2.1. Geophys Res Lett 36(17).

Huffman G. J., Bolvin, D. T., Adler, R. F. (2016). GPCP Version 1.2 One- Degree Daily Precipitation Data Set. Research Data Archive at the National Center for Atmospheric Research, Computational and Information Systems Laboratory.

Iacono, M. J., Delamere, J. S., Mlawer, E. J., Shephard, M. W., Clough, S. A. and Collins, W. D. (2008) Radiative forcing by long- lived greenhouse gases: Calculations with the AER radiative transfer models. J. Geophys. Res., 113, D13103, doi:10.1029/2008JD009944.

Ichoku C., Ellison, L. T., Willmot, K. E., Matsui, T., Dezfuli, A. K., Gatebe, C. K., Wang, J., Wilcox, E. M., Lee, J., Adegoke, J., Okonkwo, C., Bolten, J., Policelli, F. S. and Habib, S. (2016). Biomass Burning, Land-Cover Change, and the Hydrological Cycle in Northern Sub-Saharan Africa Environ. Res. Lett. 11. doi:10.1088/1748-9326/11/9/095005.

Ifatimehin O. O., Essoka, P. A. and Ahmed, A. (2012). Analysis Of Land Use Changes And Its Hydrological Implication On River Niger, Lokoja, Nigeria. Con. J. Envtal Std, 7:112-119

IGBP-IHDP. (1999). Land-use and land-cover change, implementation strategy. IGBP Report 46/IHDP Report 10. Prepared by Scientific Steering Committee and International Project Office of LUCC. Stockholm and Bonn.

Indian Natl. Sci. Acad., Chin. Acad. Sci., US Natl. Acad. Sci. (2001). Growing Populations, Changing Landscapes: Studies from India, China, and the United States. Washington, DC: Natl. Acad. 324 pp.

IPCC (2001). Climate Change 2001: The Scientific Basis. Contribution of Working Group I to the Third Assessment Report of the Intergovernmental Panel on Climate Change, Houghton, J.T., Ding, Y., Griggs, D.J., Noguer, M., van der Linden, P.J., Dai, X., Maskell, K. and Johnson, C.A. (Eds.), Cambridge University Press, Cambridge, UK and New York, NY, USA, p.881.

IPCC (2013). Climate change 2013: The Physical Science Basis, the Contribution of Working Group I to the Fifth Assessment Report of the Intergovernmental Panel on Climate Change Cambridge, Cambridge University Press.

Jankov, I., Gallus Jr. W., Segal, M. Shaw, B. and Koch, S. (2005) The impact of different WRF model physical parameterizations and their interactions on warm season MCS rainfall. Wea. Forecasting, 20: 1048–1060

Jimoh, H. I., Iroye, K. A. (2010). Managing High Runoff Discharge in the Urbanized Basins of Asa River Catchment Area of Ilorin, Nigeria. Canadian Social Science, 6(4): 210-223

Jin. J, Miller. N. L., Schlegel, N. (2010). Sensitivity study of four land surface schemes in the WRF model. Adv. Meteorol. 167436, DOI: 10.1155/2010/167436.

Jonckheere, I., Fleck, S., Nackerts, K., Muys, B., Coppin, P. and Baref, M. (2004). Review of methods for in situ leaf area index determination: theories, sensors and hemispherical photography. Agricultural and Forest Meteorology 121(1-2): 19-35.

Jones, A. D., Calvin, K. V., Collins, W .D., Edmonds, J. (2015). Accounting for radiative forcing from albedo change in future global land-use scenarios. Clim. Change 131, 691–703. doi:http://dx.doi.org/10.1007/s10584-015-1411-5.

Kain, J. S., Weiss, S. J., Levit, J. J., Baldwin, M. E. and Bright, D. R. (2006). Examination of convection-allowing configurations of the WRF model for the prediction of severe convective weather: The SPC/NSSL spring program 2004. Wea. Fore., 21: 167–181.

Kalnay, E. and Cai, M (2003) Impact of Urbanization And Land-Use Change On Climate, Nature, 423: 528–531.

Karanja, A. K., China, S. S., and Kundu, P. M. (1986). The influence of land use on Njoro River Catchment between 1975 and 1985. Department of Agricultural Engineering, Egerton University College, Njoro.

Keenan, R. J., Reams, G. A., Achard, F., de Freitas, J. V., Grainger, A. and Lindquist, E. (2015). Dynamics of Global Forest Area: Results from the FAO Global Forest Resources Assessment 2015. Forest Ecology and Management 352: 9-20

Kilianova´ H., Pechanec V., Brus J., Kirchner K. and Machar I. (2017). Analysis of the development of land use in the Morava River ood- plain, with special emphasis on the landscape matrix. Moravian Geographical Reports, 25(1): 46–59.

Kinter, J .L. and Shuka, J. (1999). The global hydrologic and energy cycles: Suggestions for studies in the pre-global energy and water cycle experiment (GEWEX) period. Bull. Am. Meteorol. Soc., 71: 181–189.

Kissinger, G., Herold, M., De Sy, V. (2012). Drivers of Deforestation and Forest Degredation: A Synthesis Report for REDD+ Policymakers. Lexeme Consulting, Vancourver Canada, August 2012.

Kitoh, A., Yamzaki, K. and Takiota, T. (1988). Influence of Soil Moisture and Surface Albedo Changes Over African Tropical Rainforest on Summer Climate Investigated with MRI-GCM-I. J. Meteor. Soc. Japan, 66: 65–85.

Klein, C., Heinzeller, D., Bliefernicht, J. and Kunstmann, H. (2015). Variability of West African monsoon patterns generated by a WRF multi-physics ensemble. Climate Dyn., 45: 2733–2755, doi:10.1007/s00382-015-2505-5.

Klein, C., Bliefernicht, J., Heinzeller, D., Gessner, U., Klein, I., and Kunstmann, H. (2016). Feedback of observed interannual vegetation change: A regional climate model analysis for the West African monsoon. Clim. Dyn. 48: 2837–2858.

Knauer, K., Gessner, U., Fensholt, R., Forkuor, G. and Kuenzer, C. (2017). Monitoring agricultural expansion in Burkina Faso over 14 years with 30 m resolu- tion time series: The role of population growth and implications for the environment. Remote Sens. 9:132. doi:10.3390/rs9020132

Koster, R. D., Dirmeyer, P. A., Guo, Z., Bonan, G., Chan, E., Cox, P., Gordon, C. T., Kanae, S., Kowalczyk, E., Lawrence, D., Liu, P., Lu, C-H., Malyshev, S., McAvaney, B., Mitchell, K., Mocko, D., Oki, T., Oleson, K., Pitman, A., Sud, Y. C., Taylor, C. M., Verseghy, D., Vasic, R., Xue, Y., and Yamada, T. (2004). Regions of strong coupling between soil moisture and precipitation. Science, 305: 1138–1140.

Koster, R. D., Dirmeyer, P. A., Hahmann, A. N., Ijpelaar, R., Tyahla, L., Cox, P. and Suarez, M. J. (2002). Comparing the degree of land–atmosphere interaction in four atmospheric general circulation models. J. Hydrometeorol. 3: 363–375.

Koster, R. D., Guo, Z., Dirmeyer, P. A., Bonan, G. B., Chan, E., Cox, P., Gordon, C. T., Kanae, S., Kowalczyk, E., Lawrence, D.M., Liu, P., Lu, C.H., Malyshev, S., McAvaney, B., Mitchell, K., Mocko, D., Oki, T., Oleson, K., Pitman, A., Sud, Y.C., Taylor, C.M., Verseghy, D., Vasic, R., Xue, Y., Yamada, T. (2006) GLACE: The Global Land-Atmosphere Coupling Experiment. Part I: Overview. Journal of Hydrometeorology, 7: 590-610

Kumar, A., Chen, F., Barlage, M., Ek, M. B. and Niyogi, D. (2014). Assessing impacts of integrating MODIS vegetation data in the weather research and forecasting (WRF)

model coupled to two different canopy-resistance approaches J. Appl. Meteorol. Climatol. 53: 1362–80

Kunstmann, H. and Jung, G. (2006). Influence of Soil-Moisture and Land Use Change on Precipitation in the Volta Basin of West Africa. Intl. J. Riv. Basin Mana. 5(2): 1–8

Kutzbach, J., Bonan, G., Foley, J. and Harrison, S. P. (1996). Vegetation and soil feedbacks on the response of the African monsoon to orbital forcing in the early to middle Holocene Nature 384: 623–626

Kwun, J. H., Kim, Y. K. Seo, J. W. Jeong, J. H and You, S. H. (2009). Sensitivity of MM5 and WRF mesoscale model predictions of surface winds in a typhoon to planetary boundary layer parameterizations. Nat. Hazards, 51: 63–77.

Lakshmi, V., Hong, S., Small, E. E. and Chen, F. (2011). The influence of the land surface on hydrometeorology and ecology: new advances from modeling and satellite remote sensing. Hydrology Research. 42: 95-112

Lal, R. (1997). Deforestation and Land-Use Effects on Soil Degradation and Rehabilitation in Western Nigeria. IV. Hydrology and Water Quality. Land Degradation. Dev. 8: 95–126.

Lambin, E. F., Geist. H. J. and Lepers. E. (2003). Dynamics of land use and land cover change in tropical regions. Annu. Rev. Environ. Resour. 28: 205- 41

Lamptey, B.L., Barron, E.J., Pollard, D., 2005. Impacts of agriculture and urbanization on the climate of the Northeastern United States. Glob. Planet. Chang. 49, 203-221.

Laurence, W. F. (2007). A New Initiative to Use Carbon Trading For Tropical Forest Conservation. Biotropica, 39: 20-24.

Laurence, W. F. and Bierregaard R. o. jr. (eds). (1997). Tropical Forest Remnants: Ecology,Management and Conservation of Fragmented Communities. The University of Chicago, Illinois 616, pp. ISBN 0-226-46898-4.

Laux, P., Nguyen, N. B. P., Cullmann, J. and Kunstmann, H. (2017). Impacts of Land-Use/Land-Cover Change and Climate Change on the Regional Climate in the Central Vietnam. DOI: 10.1007/978-981-10-2624-9_9

Laval, K. and Picon, L. (1986). Effect of a Change of the Surface Albedo of the Sahel on Climate, Journal of the Atmospheric Sciences, 43 (21): 2418–2429

Lavender, S. L., Taylor, C. M. and Matthews, A. J. (2010). "Coupled Land-Atmosphere Intraseasonal Variability Of The West African Monsoon in a GCM," Journal of Climate, 23(21). 5557–5571, 2010.

Lawrence, D. M., Oleson, K. W., Flanner, M. G., Thornton, P. E., Swenson, S. C., Lawrence, P. J., Zeng, X., Yang, Z-L., Levis, S., Sakaguchi, K., Bonan, G. B., Slater, A. G. (2011). Parameterization Improvements And Functional And Structural Advances in Version 4 of the Community Land Model. J Adv Model Earth Syst 3:1942–2466.

Lee, C. B., Kim, J-C., Belorid, M. and Zhao, P. (2016). Performance Evaluation of Four Different Land surface Models in WRF Asian Journal of Atmospheric Environment, 10(1), 42-50.

Legesse, D., Vallet-Coulomb, D. and Gasse F. (2003). Hydrological Response of a Catchment to Climate and Land use Changes in Tropical Africa: Case Study South Central Ethiopia, J. Hydrol., 275: 67–85.

Li, K.Y., Coe, M.T., Ramankutty, N. and De Jong, R. (2007). Modeling the hydrological impact of land-use change in West Africa. Journal of Hydrology. 337: 258– 268

Li, Q. P. and Ding, Y. H. (2004). Research process in the effect of vegetation change on regional climate. Journal of Nanjing Institute of Meteorology (in Chi- nese), 27(1): 131-140.

Li, S. C., He, F. N. and Zhang, X. Z (2015). A Spatially Explicit Reconstruction Of Cropland Cover In China from 1661 to 1996. Regional Environment Change. doi: 10.1007/s10113-014-0751-4.

Li, W.-P., Xue, Y. and Poccard, I. (2007). Numerical investigation of the impact of vegetation indices on the variability of West African summer monsoon. Journal of Meteorological Society of Japan, 85A: 363–383.

Li, W., Guo, W., Xue Y., Fu, C. and Qui B. (2015). Sensitivity of a regional climate model to land surface parameterization schemes for East Asian summer monsoon simulation Climate Dynamics, 47(7-8), DOI 10.1007/s00382-015-2964-8

Li, X. and Pu, Z. (2009). Sensitivity of numerical simulations of the early rapid intensification of Hurricane Emily to cumulus parameterization schemes in different model horizontal resolutions. J. Meteor. Soc. Japan, 87: 403–421.

Li, X., Mitra, Marzen, C., Dong, L. and Yang, Q. (2018). Understanding Land Use Change Impacts On Microclimate Using Weather Research and Forecasting (WRF) Model. Physics and Chemistry of the Earth, 103: 115-126.

Liang, X., Xie, Z. and Huang, M. (2003). A new parameterization for surface and groundwater interactions and its impact on water budgets with the variable infiltration capacity (VIC) land surface model, J. Geophys. Res., 108(D16), 8613. doi:10.1029/2002JD003090.

Liu, X., Ren, L., Yuan, F., Singh, V P., Fang, X., Yu, Z. and Zhang, W. (2009). Quantifying the effect of land use and land cover changes on green water and blue water in northern part of China. Hydrol. Earth Syst. Sci., 13: 735–747.

Loveland, T. R. and Belward, A. S. (1997). The international geosphere biosphere programme data and information system global land cover data set (DISCover). Acta Astronautica, 41(4): 681–689.

Lu, Y. and Kueppers, L. M. (2012). Surface Energy Partitioning Over Four Dominant Vegetation Types Across the United States in A Coupled Regional Climate Model (Weather Research and Forecasting Model 3-Community Land Model 3.5). J. Geophys Res, 117:D06111. doi:10.1029/2011jd016991

MacKellar, N., Tadross, M. and Hewitson, B. (2010). Synoptic-Based Evaluation of Climate Response to Vegetation Change Over Southern Africa. Int. J. of Climo. 30: 774-789.

Mahapatra, K. and Kant, S. (2003). Tropical deforestation: A Multinominal Logistic Model and some Country Specific Policy Prescriptions, Journal of Forest and Economics, 7:1-8

Mahe, G., Paturel, J., Servat, E., Conway, D. and Dezetter, A. (2005). The impact of land use change on soil water holding capacity and river flow modelling in the Nakambe River, Burkina-Faso. J. Hydrol., 300: 33–43.

Mahe, G. (2006). The impacts of land-use/land-cover change and climate variability on the hydrology of the Sahel. Climate Variability and Change—Hydrological Impacts (Proceedings of the Fifth FRIEND World Conference held at Havana, Cuba, November 2006), IAHS Publ. 308, 2006.

Mahmood, R., Pielke R.A. Sr., Hubbard, K.G., Niyogi, D., Bonan, G., Lawrence, P., Baker,

B., McNider, R., McAlpine, C., Etter, A., Gameda, S., Qian, B., Carleton, A., Beltran-Przekurat, A., Chase, T., Quintanar, A.I., Adegoke, J.O., Vezhapparambu, S., Conner, G., Asefi, S., Sertel, E., Legates, D.R., Wu, Y., Hale, R., Frauenfeld, O.W., Watts, A., Shepherd, M., Mitra, C., Anantharaj, V.G., Fall, S., Lund, R., Nordfelt, A., Blanken, P., Du, J., Chang, H.-I., Leeper, R., Nair, U.S., Dobler, S., Deo, R., and Syktus, J. (2009). Impacts Of Land Use Land Cover Change On Climate And Future Research Priorities, *Bulletin of the American Meteorological Society*, 91(1): 37-46

Mahmood, R., Quintanar, A. I., Conner, G., Leeper, R., Dobler, S., Pielke, R. A. and Syktus, J. (2010). Impacts of Land Use/Land Cover Change On Climate And Future Research Priorities. Bull. Amer. Meteor. Soc. 91: 37-46.

Malick, D. and Inoussa, B. (2009). Deforestation in Sub-Saharan Africa. Presentation at the Southern Agricultural Economics Association Annual Meeting, Atlanta, Georgia, January 31-February 3, 2009.

Matsangouras, I. T., Nastos P. T, Pytharoulis I. (2011) Synoptic-mesoscale analysis and numerical modeling of a tornado event on 12 February 2010 in northern Greece. Adv Sci Res 6: 187–194

Matthews, E. (2001). Understanding the FRA 2000. Forest Briefing 1, World Resource. Institute Washington, DC

McGuffie, K., Henderson-Sellers, A., Zhang, H., Durbridge, T. B. and Pitman, A. J. (1995). Global climate sensitivity to tropical deforestation. Global and Planetary Change. 10: 97-128.

McNally A., Arsenault, K., Kumar, S., Shukla, S., Peterson, P., Wang, S., Funk, C., Peters-Lidard C. and Verdin, J. (2017). A land data assimilation system for sub-Saharan

Africa food and water security applications. Sci. Data 4:170012 doi: 10.1038/sdata.2017.12

Mengistu, D. A. (2008). Remote Sensing and GIS-based Land Use and Land Cover Change detection in the Upper Dijo River Catchment, Silte zone, Southern Ethiopia. Working papers on Population and Land Use Change in Central Ethiopia, nr. 17 Acta Geographica-Trondheim Serie A, Nr. 23 Series A, No 23.

Merritt, W. S., Letcher R.A. and Jakeman A. J. (2003). A review of erosion and sediment transport models. Environmental Modelling & Software 18: 761–799.

Meyer, W.B. and Turner, B. L. (1994). Changes in Land Use And Land Cover: A Global Perspective. Cambridge: Cambridge University Press. New York.

Miao, J.-F., Chen, D., Borne, K. (2007) Evaluation and Comparison of Noah and Pleim-Xiu Land Surface Models in MM5 Using GOTE2001 Data : Spatial and Temparal Variations in Near-Surface Air Temperature. Journal of Applied Meteorology and Climatology 46: 1587-1605.

Miller, J., Barlage, M., Zeng, X., Wei, H., Mitchell, K., Tarpley, D. (2006) Sensitivity of the NCEP/Noah land surface model to the MODIS green vegetation fraction data set. Geophys. Res. Lett. 33: doi:10.1029/2006GL026636

Mkaya, D. M. (2013). Evaluation of the Impact of Land Use Change On Catchment Hydrology: The Case of Wundanyi River Catchment in Taita Hills, Kenya. A Master's Thesis Submitted to the Graduate School in Partial Fulfilment for the Requirements of the Master of Science Degree, department of Agricultural Engineering, Egerton University

Mora, D. E., Campozano, L., Cisneros, F., Wyseure, G. and Willems, P. (2004). Climate changes of hydrometeorological and hydrological extremes in the Paute basin, Ecuadorean Andes. Hydrol. Earth Syst. Sci., 18: 631–648.

Morales-Hidalgo, D., Oswalt, S. N. and Somanathan, E. (2015). Status And Trends in Global Primary Forest, Protected Areas, and Areas Designated for Conservation of Biodiversity From the Global Forestresources Assessment 2015. Forest Ecology and Management 352: 68–77

Mustafa, Y. M., Amin, M. S. M., Lee, T. S., and Shariff, A. R. M. (2005). Evaluation of Land Development Impact on a Tropical Watershed Hydrology Using Remote Sensing and GIS. Journal of Spatial Hydrology, 5(2): 16 - 30.

Myneni, R. B., Hoffman, S., Knyazikhin, Y., Privette, J. L., Glassy, J., Tian, Y., Wang, Y., Song, X., Zhang, Y., Smith, G. R., Lotsch, A., Friedl, M., Morisette, J. T., Votava, P., Nemani, R. R., and Running, S. V. (2002). Global products of vegetation leaf area and fraction absorbed PAR from year one of MODIS data. Remote Sensing of Environment, 83(1): 214–231.

Naabil, E., Lamptey, B. L., Arnault, J., Olufayo, A., Kunstmann, H. (2017). Water resources management using the WRF-Hydro modelling system : Case-study of the Tono dam in West Africa. Journal of Hydrology : Regional Studies, 12: 196-209.

Nakanishi, M., and Niino, H. (2006). An Improved Mellor–Yamada level-3 model: Its numerical stability and application to a regional prediction of advection fog. Bound.-Layer Meteor., 119: 397–407, doi:10.1007/s10546-005-9030-8.

Nash, J. E. and Sutcliffe, J. V., 1970. River flow forecasting through conceptual models, 1. A discussion of principles. J. Hydrol. 10: 282–290.

National Centers for Environmental Prediction/National Weather Service/ NOAA/U.S. Department of Commerce (2000). Updated Daily NCEP FNL Operational Model Global Tropospheric Analyses, continuing from July 1999. Research Data Archive at the National Center for Atmospheric Research, Computational and Information Systems Laboratory. doi:https://doi.org/10.5065/D6M043C6.

Ndehedehe, C. (2019). The water resources of tropical West Africa: problems, progress, and prospects. Acta Geophys. 67(2): 621-649.

Newson, M. (1995). Hydrology and the River Environment (Reprinted). Oxford University Press.

Ngana, J. O. (2002). Integrated Water Resources Management: The Case of the Pangani River Basin. In Ngana, J. O. (ed.). Water Resources Management in the Pangani River Basin: Challenges and Opportunities. Dar es Salaam: Dar es Salaam University Press: 1 – 8

Nicholson, S. E. (2013). The West African Sahel: A Review of Recent Studies on the Rainfall Regime and its Interannual Variability, ISRN Meteorology, 1–32, doi:10.1155/2013/453521.

Niu, G.-Y., Z.-L. Yang, K. E. Mitchell, F. Chen, M. B. Ek, M. Barlage, L. Longuevergne, A. Kumar, K. Manning, D. Niyogi, E. Rosero, M. Tewari, and Y. Xia (2011). The community Noah land surface model with multiparameterization options (Noah-MP): 1. Model description and evaluation with local-scale measurements, J. Geophys. Res., doi:10.1029/2010JD015139

Niu, G.-Y., and Yang, Z.-L. (2004), The effects of canopy processes on snow surface energy and mass balances, J. Geophys. Res., 109: D23111, doi:10.1029/2004JD004884.

Niu, G.-Y., and Yang, Z.-L. (2006), Effects of frozen soil on snowmelt run- off and soil water storage at a continental scale, J. Hydrometeorol., 7: 937–952, doi:10.1175/JHM538.1.

Nobre, C. A., Silva Dias, M. A., Culf, A. D., Polcher J., Gash, J. H. C., Marengo, J. A. and Avissar R. (2004). The Amazon climate. In P. Kabat et al. (Eds.), Vegetation, water, humans and the climate 79–92. Berlin: Springer-Verlag.

Nolan, D. S., Zhang, J. A. and Stern, D. P. (2009) Evaluation of planetary boundary layer parameterizations in tropical cyclones by comparison of in situ observations and high-resolution simulations of Hurricane Isabel (2003). Part I: Initialization, maximum winds, and the outer-core boundary layer. Mon. Wea. Rev., 137: 3651–3674.

Nwaogu, C., Okeke, J. O., Fadipe, O. O., Bashiru, K. A. and Pechanec, V. (2017). Is Nigeria Losing Its Natural Vegetation And Landscape? Assessing The Landuse-Landcover Change Trajectories And Effects in Onitsha Using Remote Sensing and GIS, Open Geosci. 9: 707–718

Obiri, B. D. and Damnyag, L. (2011). Socio-Economic Contribution of Illegal Chaninsaw Milling to the Ghanian Rural Economy. Ghana Journal of Forestry, 27: 50-57.

Ojekunle, O. Z. (2014). The Effects of Linkages of Deforestation and Temperature on Climate Change in Nigeria. Global Journal of Science Frontier Research: H Environmental and Earth Science, 14(6): 9-18.

Okalebo, J. A., Oglesby, R. J., Feng, S., Hubbard, K., Kilic, A., Hayes, M., Hays, C. (2016). An Evaluation of the Community Land Model (Version 3.5) and Noah Land Surface Models for Temperature and Precipitation Over Nebraska (Central Great Plains): Implications for Agriculture in Simulations of Future Climate Change and Adaptation, Leal Filho, W., Musa, H., Cavan, G., O'Hare, P., Seixas, J. (Eds.), Climate Change

Adaptation, Resilience and Hazards, Climate Change Management, DOI 10.1007/978-3-319-39880-8_2.

Okpara, J., Tarhule, A. A., and Perumal, M. (2013). Study of climate change in niger river basin, west africa: reality not a myth. INTECH Open science. doi:10.5772/55186.

Oleson, K. W., Lawrence, D. M., Bonan, G. B., Flanner, M. G., Kluzek, E., Lawrence, P. J., Levis, S., Swenson, S. C., Thornton, P. E., Dai, A., Decker, M., Dickinson R., Feddema, J., Heald, C. L., Hoffman, F., Lamarque, J., Mahowald, N., Niu, J., Qian, Taotao., Randerson, J., Running, S.,Sakaguchi, K., Slater, A., Stöckli.,R., Wang, A., Yang L., Zeng, X. and Zeng, X. (2010). Technical description of version 4.0 of the Community Land Model (CLM). Technical Note NCAR/TN-478+STR, National Center for Atmospheric Research, Boulder, Colorado, 257 pp

Olorunfemi, I. E., Fasinmirin, J. T. and Akinola, F. F. (2018). Soil physic-Chemical Properties and Fertility Status of Long-Term Land Use and Cover Changes: A Case Study in Forest Zone of Nigeria. Eurasian J. Soil Sci., 7(2): 133-150.

Omotosho, J. B., Abiodun, B. J., (2007) A numerical study of moisture build-up and rainfall over West Africa. Meteorol. Appl. 14 (3): 209–225.

Ott, B. and Uhlenbrook S. (2004). Quantifying the Impact of Land-Use Changes at the Event and Seasonal Time Scale Using a Process-Oriented Catchment Model, Hydrol. Earth Syst. Sci., 8(1): 62–78.

Ouedraogo, I., Savadogo, P., Tigabu, M., Cole, R., Odén, P.C., and Ouadba. J.M. (2009). Is rural migration a threat to environmental sustainability in southern Burkina Faso? Land Degrad. Dev. 20: 217–230. doi:10.1002/ldr.910

Pal, J. S. and Eltahir, E. A. B. (2001). Pathways relating soil moisture conditions to future summer rainfall within a land-atmosphere system, J. Clim.,12: 1227–1242.

Patricola, C. M. and Cook, K. H. (2009). Northern African climate at the end of the twenty-first century: an integrated application of regional and global climate models. Clim Dyn 35:193–212 DOI 10.1007/s00382-009-0623-7

Pellikka, P. K. E., Lötjönen, M., Siljander, M. and Lens, L. (2009). Airborne remote sensing of spatiotemporal change (1955–2004) in indigenous and exotic forest cover in the Taita Hills, Kenya. International Journal of Applied Earth Observation and Geoinformation. 11(4): 221-232

Pereira, H. C. (1989). Policy and Practice of Water Management in Tropical Areas. Boulder, Co: Westview Press.

Pereira, H. C. (1992). Keynote paper. In: 10th World Forestry Congress, Proc. 3, Paris, 1991, 139–150.

Petchprayoon, P., Blanken, P. D., Ekkawatpanit, C. and Hussein, K. (2010). Hydrological impacts of land use/land cover change in a large river basin in central–northern Thailand. Int. J. Climatol. 30: 1917–1930

Pielke, R. (2001). Influence of the Spatial Distribution of Rainfall and Soil on the Prediction of Cumulus Convective Rainfall. Reviews of Geophysics. 39: 151-177.

Pitman, A. J. (2003): The Evolution of, and Revolution in, Land Surface Schemes Designed For Climate Models Int. J. Climatol. 23: 479–510 DOI: 10.1002/joc.893

Pitman, A. J., de Noblet-Ducoudre, N., Avila, F. B., Alexander, L. V., Boisier, J.-P., Brovkin, V., Delire, C., Cruz, F., Donat, M. G., Gayler, V., van den Hurk, B., Reick, C. and

Voldoire, A. (2012). Effects of land cover change on temperature and rainfall extremes in multi-model ensemble simulations. Earth Syst. Dynam., 3: 213–231.

Polcher, J. (1995). Sensitivity of Tropical Convection to Land Surface Processes. Amer. Meteorol. Soc. 52: 3143-3161.

Qi, X. and Chopping, M. (2007). Expansion of Urban Area in the Yellow River Zone, Inner Mongolia Autonomous Region, China, from DMSP OLS Nighttime Lights Data, Proc. IEEE International Geoscience and Remote Sensing Symposium 2007, Barcelona, Spain, July 23-27, 2007 doi:10.1109/IGARSS.2007.4423222

Qu, R., Cui, X., Yan, H., Ma, E. and Zhan, J. (2013). Impacts of Land Cover Change on the Near-Surface Temperature in the North China Plain. Advances in Meteorology . http://dx.doi.org/10.1155/2013/409302

Rademaekers K., Eichler L., Berg, J., Obersteiner M. and Havlik, P. (2010). Study on the Evolution of Some Deforestation Drivers and their Potential Impacts on the Costs of an Avoiding Deforestation Scheme. Prepared for the European Commission by ECORRYS and IIASA. Rotterdam, Netherlands.

Ramankutty, N. and Foley, J. A. (1999) Estimating historical changes in global land cover: croplands from to 1700 to 1992. Global Biogeochemical Cycles, 13: 997–1027.

Rawat, J. S. and Kumar, M. (2015). Monitoring land use/cover change using remote sensing and GIS techniques: A case study of Hawalbagh block, district Almora, Uttarakhand, India. The Egyptian Journal of Remote Sensing and Space Sciences 18: 77–84

Ray, D. K., Welch, R. M., Lawton, R. O. Nair, U. S. (2006). Dry Season Clouds And Rainfall In Northern Central America: Implications For The Mesoamerican Biological Corridor. *Global and Planetary Change* 54: 150 – 162.

Redelsperger, J. L., Thorncroft, C. D., Diedhiou, A., Lebel, T., Parker, D. J., and Polcher, J.(2006). African monsoon multidisciplinary analysis, Bulletin of the American Meteorological Society, 87(12): 1739–1746, doi:10.1175/BAMS-87-12-1739.

Ren, G., Zhou, Y., Chu, Z., Zhou, J., Zhang, A., Guo, J., Liu, X., 2008. Urbanization ef- fects on observed surface air temperature trends in north China. J. Clim. 21, 1333e1348. http://dx.doi.org/10.1175/2007JCLI1348.1.

Rodriguez-Iturbe, I., Entekhabi, D. and Bras, R. L. (1991). Nonlinear dynamics of soil moisture at climate scales: 1. Stochastic analysis. Water Resour. Res., 27: 1899–1906.

Rogers, D. and Tsirkunov, V. (2011). Implementing Hazard Early Warning Systems; Global Facility for Disaster Reduction and Recovery: Washington, DC, USA.

Rowell, D. P. and Blondin, C. (1990). The Influence of Soil Wetness Distribution on Short Range Rainfall Forecasting in the West African Sahel. Quart. J. Roy. Meteor. Soc., 116: 1471–1485.

Roy, S., and Avissar, R. (2002). Impact of land use/land cover change on regional hydrometeorology in Amazonia. Journal of Geophysical Research, 107(D20), DOI 10.1029/2000JD000266

Ruiz-Arias, J. A, Pozo-Vazquez D, Sanchez–Sanchez N, Montavez JP, Hayas-Barru A, Tovar- Pescador J (2008) Evaluation of two MM5-PBL parameterizations for solar radiation and temperature estimation in the south-eastern area of the Iberian peninsula. Il Nuovo Cimento 31(5–6): 825–842

Running, S. W., Nemani, R. R., Heinsch, F. A., Zhao, M., Reeves, M. C., and Hashimoto, H. (2004). A Continuous Satellite-Derived Measure of Global Terrestrial Primary Production. BioScience, 54(6): 547-560.

Ruti, P. M., Williams, J. E., Hourdin, F., Guichard, F., Boone, A., Van Velthoven, P., Favot, F., Musat, I., Rummukainen, M., Domınguez, M., Gaertner, M. A., Lafore, J. P., Losada, T., Rodriguez de Fonseca, M. B., Polcher, J., Giorgi, F., Xue, Y., Bouarar, I., Law, K, Josse, B., Barret, B., Yang, X., Mari, C. and Traore, A. K. (2011). The West African climate system: a review of the AMMA model inter-comparison initiatives. Atmos. Sci. Let. 12: 116–122. DOI: 10.1002/asl.305

Santos-Munoz D, Wolff J, Santos C, García-Moya JA, Nance L (2009) Implementation and validation of WRF model as ensemble member of a probabilistic prediction system over Europe. 10th Annual WRF Users' Workshop, Boulder, USA, 23–26 June 2009

Sato, T. and Xue, Y. (2013) Validating a Regional Climate Model's Downscaling Ability for East Asian Summer Monsoonal Interannual Variability. Clim Dyn 41:2411–2426.

Savenije, H.H.G. (1995). New definitions for moisture recycling and the relation with land use changes in the Sahel. H. Hydrol. 167: 57–78.

Schaaf, C. B., Gao, F., Strahler, A. H., Lucht, W., Li, X., Tsang, T., Strugnell, N. C., Zhang, X., Jin, Y., and Muller, J.-P. (2002). First operational BRDF, albedo nadir reflectance products from MODIS. Remote Sensing of Environment, 83(1):135–148.

Schaake, J. C., Duan, Q., Koren, V., Mitchell, K. E., Houser, P. R., Wood, E. F., Robook, A., Lettenmaier, D. P., Lohmann, D., Cosgrove, B., Sheffield, J., Luo, L., Higgins, R. W., Pinker, R. T. and Tarpley, J. D. (2004). An Intercomparison Of Soil Moisture Fields in the North American Land Data Assimilation System (NLDAS), J. Geo- phys. Res., 109, D01S90, doi:10.1029/2002JD003309.

Schär, C., Lüthi, D., Beyerle, U. and Heise, E. (1999). "The Soil-Precipitation Feedback: A Process Study with a Regional Climate Model," Journal of Climate, 12: 722–741

Schlosser, C. A., Slater, A. G., Robock, A., Pitman, A. J., Vinnikov, K. Y., Henderson-Sellers, A., Speranskaya, N. A., Mitchell, K. and the PIPLS 2(d) contributors (2000). Simulations of a Boreal Grassland Hydrology at Valdai, Russia: PILPS Phase 2 (d), Mon. Weather Rev., 128: 301–321

Sellers, P. J., Randall, D. A., Collatz, G. J., Berry, J. A., Field, C. B., Dazlich, D. A., Zhang, C., Collelo, G. D. and Bounoua, L. (1996), A revised land surface parameterization (SiB2) for atmospheric GCMs: Part I. Model formulation, J. Clim., 9, 676–705.

Semazzi, F. and Song, Y. (2001). A GCM Study Of Climate Change Induced By Deforestation in Africa. Climate Research 17:169-182.

Semwal R.L., Nautiya S., Sen K.K., Rana U., Maikhuri R.K., Rao K.S., et al., (2004). Patterns and ecological implications of agricultural land-use changes: a case study from central Himalaya, India. Agriculture, Ecosystem, & Environment, 102: 81–92.

Sertel, E., Robock, A., Ormeci, C. (2010). Impacts of land cover data quality on regional climate simulations. Int. J. Climatol. 30(13): 1942–1953.

Sertel, E., Ormeci, C. and Robock, A. (2011) 'Modelling land cover change impact on the summer climate of the Marmara Region, Turkey', Int. J. Global Warming, 3(1/2): 194–202.

Shepherd, J. M., Pierce, H. and Negri, A. J. (2002). Rainfall modification by major urban areas: observations from spaceborne rain radar on the TRMM satellite. J. Appl. Meteor 41: 689-701.

Shuster, W., Bonta, J. and Thurston, H. (2005). Warnemuende, E.; Smith, D. Impacts of impervious surface on watershed hydrology: A review. Urban Water J., 2 (4): 263–275

Singh, A. P., Mohanty, U. C., Sinha, P., Mandal, M. (2007) Influence of different land-surface processes on Indian summer monsoon circulation. Natural Hazards 42, 423-438. Olerud, D., Sims, A. cited. (2003) MM5 sensitivity modeling in support of VISTAS (Visibility Improvement- State and Tribal Association): Task 2e deliverable.

Skamarock, W., Klemp, J., Dudhia, J., Gill, D., Barker, D., Duda, M., yu Huang, X., and Wang, W. (2008). A Description of the Advanced Research WRF Version 3, Tech. rep., Mesoscale and Microscale Meteorology Division, National Center for Atmospheric Research, doi:10.5065/D68S4MVH, available at: http://nldr.library.ucar.edu/repository/collections/ TECH-NOTE-000-000-000-855 (last access: 13 Decem- ber 2013).

Sörensson, A., Menéndez, C., Samuelsson, P., Willén, U. and Hansson U (2010) Soil-Precipitation Feedbacks During The South American Monsoon as Simulated by a Regional Climate Model. Clim Change 98: 429–447. doi:10.1007/s10584-009-9740-x

Steiner, A., Pal, J., Rauscher, S., Bell, J., Diffenbaugh, N., Boone, A., Sloan, L. C. and Giorgi, F. (2009). Land surface coupling in regional climate simulations of the West African monsoon. Climate Dynamics, 33: 869–892.

Stohlgren, T. J., Chase, T. N., Pielke, R. A., Kittel, T. G. F. and Baron, J. S. (1998). Evidence that local land use practices influence regional climate, vegetation, and stream flow patterns in adjacent. Glob. Chang. Biol. 4: 495-504.

Sud, Y. C. and Fennessy, M. J. (1982). A study of the influence of surface albedo on July circulation in semiarid regions using the GLAS GCM. J. of Climatol., 2, 105–125.

Sud, Y. C. and Molod, A. (1988). A GCM Simulation Study of The Influence of Saharan Evapotranspiration And Surface Albedo Anomalies On July Circulation And Rainfall. *Mon. Wea. Rev.,* **116,** 2388–2400.

Sud, Y. C., and Fennessy, M. J. (1984). Influence of Evaporation in Semi-Arid Regions on the July Circulation: A Numerical Study. J. Climatol., 4, 383–398.

Sulla-Menashe, D. and Friedl, M. A. (2018) User Guide to Collection 6 MODIS Land Cover (MCD12Q1 and MCD12C1) Products.

Sulla-Menashe, D., Gray, J. M., Abercrombie, S. P. and Friedl, M. A. (2019) Hierarchical mapping of annual global land cover 2001 to present: The MODIS Collection 6 Land Cover product, Remote sensing and environment, 222: 183-194

Sultan B, Janicot S (2000) Abrupt shift of the ITCZ over West Africa and intraseasonal variability. Geophys Res Lett 27: 3353–3356

Sultan B, Janicot S (2003) The West African monsoon dynamics. Part II: the ‘‘Pre-onset’’ and ‘‘onset’’ of the summer monsoon. J Clim 16: 3407–3427

Swank, W. T., Swift, L. W. and Douglass, J. E. (1988). Stream flow changes associated with forest cutting, species conversions, and natural disturbances. In: Swankand, W. T. and Crossley, D. A. (eds.). Forest hydrology and ecology at Coweeta. Ecological Studies 66. New York City, NY, USA

Swann, A. L. S., Fung, I. Y. and Chaing, J. C. H. (2012). Mid-latitude Afforestation Shifts General Circulation And Tropical Precipitation. PNAS. 109(3): 712-716.

Tan, K.C., San Lim, H., MatJafri, M.Z., Abdullah, K. (2010). Landsat data to evaluate urban expansion and determine land use/land cover changes in Penang Island, Malaysia. Environ. Earth Sci. 60: 1509-1521.

Tang, Z., Engel, B. A., Pijanowski, B. C. and Lim, K. J. (2005). Forecasting Land-Use Change and its Environmental Impact at a Watershed Scale, J. Enviro. Managt. 76: 35–45.

Tayanc, M. and Toros, H. (1997). Urbanization Effects On Regional Climate Change In The Case Of Four Large Cities Of Turkey. Clim. Chang. 35: 501-524.

Taylor, R.W. (1993). Urban Development in Nigeria—Planning, Housing and Land Policy. Avebury, Aldershot.

Taylor, K. E. (2001) Summarizing Multiple Aspects of Model Performance in a Single Diagram. J. Geophys. Res., 106: 7183– 7192, doi:10.1029/2000JD900719.

Taylor, C. M., Lambin, E. F., Stephenne, N., Harding, R. J, Essery, R. L. H. (2002). The influence of land use change on climate in the Sahel. J Clim 15:3615–3629

Taylor, C. M. (2008). Intraseasonal Land-Atmosphere Coupling in the West African Monsoon. Journal of Climate, 21, 6636–6648.

Teuling, A. J., de Badts, E. A. G., Jansen, F. A., Fuchs, R., Buitink, J., van Dijke, A. J. H. and Sterling, S. M (2019). Climate Change, Reforestation/Afforestation, and Urbanization Impacts on Evapotranspiration and Streamflow in Europe. Hydrol. Earth Syst. Sci., 23, 3631–3652. https://doi.org/10.5194/hess-23-3631-2019

Tiwari, P. R., Kar, S. C., Dey, S., Sinha, P., Raju, P. V. S., Shekhar, M. S. (2015). The Role Of Land Surface Schemes In The Regional Climate Model (Regcm) For Seasonal Scale Simulations Over Western Himalaya, Atmósfera 28(2): 129-142.

Trail. M., Tsimpidi. A. P., Liu. P., Tsigaridis. K., Hu, Y., Nenes, A., Stone, B., Russell, A. G. (2013). Potential impact of land use change on future regional climate in the

Southeastern U.S.: Reforestation and crop land conversion. J. Geophys. Res. Atmos. 118(20): 11577–11588, doi: 10.1002/2013JD020356.

Trier, S. B., Davis, C. A. and Ahijevyc, D. (2010a). "Environmental Controls On The Simulated Diurnal Cycle Of Warm-Season Precipitation in the Continental United States." Journal of Atmospheric Science 67: 1066-1099, doi:10.1175/2009JAS3247.1.

Trier, S. B., Sharman, R. D., Fovell, R. G. and Frehlich, R. G. (2010b), Numerical Simulation Of Radial Cloud Bands Within The Upper-Level Outflow Of An Observed Mesoscale Convective System, J. Atmos. Sci., 67(9): 2990– 2999, doi:10.1175/2010jas3531.1

Trimble, S. W., Weirich, F. H. and Hoag, B.L. (1987). Reforestation and the reduction ofwater yield on the Southern Piedmont since circa 1940. Water Resources Research 23(3): 425–437.

Trusilova, K., Jung, M., Churkina, G., Karsten, U., Heimann, M. and Claussen, M. (2008). Urbanization impacts on the climate in Europe: numerical experiments by the PSU-NCAR mesoscale model (MM5). J. Appl. Meteor. Climatol. 47: 1442-1455.

United Nations Environmental Programme (UNEP), (2006). Africa Environmental Outlook 2: Our Environment, Or Wealth, retrieved on 13th October, 2018.

Vågen, T. G., Lai, R. and Singh, B. R., (2005). Soil carbon sequestration in sub-Saharan Africa: A review. Land Degradation and Development 16(1): 53–71.

Van Asselen, S. and Verburg, P. H. (2013). Land cover change or land-use intensification: simulating land system change with a global-scale land change model. Glob. Chang. Biol. 19: 3648-3667. http://dx.doi.org/10.1111/gcb.12331.

Veldkamp, A., and Verburg, P. H.(2004). Modelling land use change and environmental impact. Journal of Environmental Management 72(1–2): 1–3.

Viterbo, P. (2002) The role of the land surface in the climate system, Meteorological Training Course Lecture Serie ECMWF 2002.

Vitousek, P. M., Mooney, H. A., Lubchenco, J., Melillo, J. M. (1997). Human domination of Earth's ecosystems. Science 277: 494–499

Walker, J. and Rowntree, P. R. (1977). The effect of soil moisture on circulation and rainfall in a tropical model. Quarterly Journal of the Royal Meteorological Society, 103: 29–46.

Wang, A. and Zeng, X. (2009). Improving the treatment of vertical snow burial fraction over short vegetation in the NCAR CLM3. Adv. Atmos. Sci. 26: 877-886.

Wang, G. L. and Eltahir, E. A. B. (2000a) Ecosystem dynamics and the Sahel drought. Geophys Res Lett 27(6): 795–798

Wang, G. L. and Eltahir, E. A. B. (2000b) The role of ecosystem dynamics in enhancing the low-frequency variability of the Sahel rainfall. Water Resour Res 36(4): 1013–1021

Wang, L. and Cheung, K.W. (2017). Potential impact of reforestation programmes and uncertainties in land cover effects over the loess plateau: A regional climate modeling study. Clim. Chang. 2017.

Wang, W., Barker, D., Bruyere, C., Duda, M., Dudhia, J., Gill, D., Michalakes, J. and Rizvi, S. (2008a). WRF Version 3 Modeling System User's Guide. http://www.mmm.ucar.edu/wrf/users/docs/user guide V3/.

Wang, X., Zheng, D. and Shen, Y. (2008b). Land use change and its driving forces on the Tibetan Plateau during 1990-2000 Catena, 72: 56-66

Ward, P. J., van Balen, R.T., Verstraeten, G. and Renssen, H. (2009). Vandenberghe, J. The impact of land use and climate change on late Holocene and future suspended sediment yield of the Meuse catchment. Geomorphology. 103: 389–400.

Wei, J., Dirmeyer, P. A., Guo, Z., Zhang, L. and Misra, V. (2009) How Much do Different Land Models Matter For Climate Simulation? Part 1: climatology and variability. J Climate 23: 3120–3134

Weng, Q. (2001). A remote sensing? GIS evaluation of urban expansion and its impact on surface temperature in the Zhujiang Delta, China. International Journal of Remote Sensing, 22(10): 1999-2014.

Weng, Q., Lu, D., Schubring, J. (2004). Estimation of Land Surface Temperature-Vegetation Abundance Relationship for Urban Heat Island Studies. Remote Sens. Environ. 89: 467-483.

WFSE Working group, (2009). Making Sub-Saharan African Forest Work for People and Nature; Policy approaches in a changing global environment. ISBN 978-92-9059-2563

Wharton, S., Simpson, M., Osuna, J, Newman, J. and Biraud, S (2013) Assessment of Land Surface Model Performance in WRF for Simulating Wind at Heights Relevant to the Wind Energy Community S. LLNL-TR-643914 DOI: 10.2172/1097768

Wood, E. F., Lettenmaier, D. P., Kian, X., Lohmann, D., Boone, A., Chang, S., Chen, F., Dai, Y., Dickinson, R. E., Duan, Q., Ek, M., Gusev, Y. M., Habets, F., Irannejad, P., Koster, R., Mitchell, K. E., Nasonova, O. N., Noilhan, J., Schaake, J., Schlosser, A., Shao, Y., Shmakin, A. B., Verseghy, D., Warrach, K., Wetzel, P., Xue, Y., Yang, Z.-L. and Zeng, Q.-C. (1998). The Project For Intercomparison Of Land-Surface Parameterization Schemes (PILPS) Phase 2(C) Red-Arkansas River Basin

Experiment: 1. Experiment Description And Summary Intercomparisons, Global Planet. Change, 19: 115-135.

Wood, E. F., Lettenmaier, D. P. and Zartarian, V. G. (1992) "A land- surface hydrology parameterization with subgrid variability for general circulation models," Journal of Geophysical Research, 97(3): 2717–2728.

World Bank, (2017). Forests, Trees and Woodlands in Africa: An Action Plan for World Bank Engagement. World Bank Africa Region Report. 73026

Xue, Y., Liou, K.-N. and Kasahara, A. (1990) "Investigation of the Biophysical Feedback on the African Climate Using a Two-Dimensional Model," Journal of Climate, 3: 337–352.

Xue, Y. K. and Shukla, J. (1993) The Influence of Land Surface Properties on Sahel Climate. Part I: desertification. J Clim 6: 2232–2245

Xue, Y. and Shukla, J. (1996). The Influence of Land Surface Properties On Sahel Climate. Part II: Afforestation. Journal of Climate, 9: 3260–3275.

Xue, Y., Bastable, H. G., Dirmeyer, P. A. and Sellers, P. J. (1996). Sensitivity of Simulated Surface Fluxes to Changes In Land Surface Parameterizations – A Study using ABRACOS Data. J. of. App. Meteorol. 35: 386-400.

Xue, Y. (1997). Biosphere Feedback On Regional Climate in Tropical North Africa. Q J R Meteorol. Soc. 123:1483–1515

Xue, Y., Hutjes, R. W. A., Harding, R. J., Claussen, M., Prince, S., Lambin, E. F., Allen, S. J., Dirmeyer, P. and Oki, T. (2004a). The Sahelian Climate (Chapter A5). In P. Kabat et al. (Eds.), Vegetation, Water, Humans and the Climate (59–77). Berlin: Springer-Verlag.

Xue, Y., Juang, H. M., Li, W., Prince, S., DeFries, R., Jiao, Y. and Vasic, R. (2004b). Role of Land Surface Processes In Monsoon Development: East Asia and West Africa. J Geophys Res 109(D03105). doi:10.102 9/2003JD003556

Xue, Y., De Sales, F., Vasic, R., Mechoso, C. R., Arakawa, A. and Prince, S. (2010a). Global and Seasonal Assessment Of Interactions Between Climate and Vegetation Biophysical Processes: a GCM Study with Different Land–Vegetation Representations. J Clim 23: 1411–1433. doi:1 0.1175/2009jcli3054.1

Xue Y, De Sales F, Vasic R, Mechoso CR, Prince SD, Arakawa A (2010b). Global and temporal characteristics of seasonal climate/ vegetation biophysical processes (VBP) interactions. J Clim 23:1411–1433

Xue, Y., Boone, A. and Taylor, C. M. (2012). Review and Prospective of Recent Development in West African Atmosphere/Land Interaction Studies. Int J Geophys. 2012: 1-12. doi:10.1155/2012/748921

Yang, R., and M. A. Friedl (2003), Modeling the effects of three-dimensional vegetation structure on surface radiation and energy balance in boreal forests, J. Geophys. Res., 108(D16), 8615. doi:10.1029/ 2002JD003109.

Yang, Y., Chou, S., Li, A. and Li Z. (1992). A Study On The Water Conservation Function of the Natural Forest of Ge's Evergreen Chinquapin J. Nat. Resour. 3: 217–23

Yang, Z.-L., and Niu G.-Y. (2003), The versatile integrator of surface and atmosphere processes (VISA) part I: Model description, Global Planet. Change, 38: 175–189.

Yeh, T.-C., Wetherald, R. T. and Manabe, S. (1984). The Effect Of Soil Moisture on the Short-Term Climate and Hydrology Change—A Numerical Experiment. Mon. Wea. Rev., 112: 474–490.

Yu, Y. and Xie, Z.-H. (2013). A Simulation Study On Climatic Effects of Land Cover Change in China. Adv. Clim. Change Res., 4(2): 117-126. doi: 10.3724/SP.J.1248.2013.117.

Yucel, I., Onen, A., Yilmaz, K. K. and Gochis, D. J. (2015). Calibration and Evaluation Of A Flood Forecasting System; Utility Of Numerical Weather Prediction Model, Data Assimilation And Satellite-Based Rainfall. J. Hydrol., 523: 49–66.

Zeng, N. and Neelin, J. D. (1999) A Land-Atmosphere Interaction Theory for the Tropical Deforestation Problem. J. Climate, 12: 857-872.

Zeng, N., Neelin, J. D., Lau, K. W. and Tucker, C. J. (1999) Enhancement of inter-decadal climate variability in the Sahel by vegetation interaction. Science 286: 1537–1540

Zeng, X. and Decker, M. (2009). Improving the Numerical Solution Of Soil Moisture-Based Richards Equation For Land Models With a Deep or Shallow Water Table. J. Hydrometeor. 10: 308-319.

Zhang, C., Wang, Y. and Hamilton, K. (2011). Improved representation of boundary layer clouds over the Southeast Pacific in ARW-WRF using a modified tiedtke cumulus parameterization scheme. Mon Weather Rev 139: 3489–3513

Zhang, H., Henderson-Sellers, A. and McGuffie, K. (1996). Impacts of Tropical Deforestation. Part I: Process analysis of local climate change. Amer. Meteorol. Soc. 9: 1497-1514.

Zhang, N., Gao, Z., Wang, X., Chen, Y. (2010). Modeling the Impact Of Urbanization On The Local And Regional Climate in Yangtze River Delta, China. Theor. Appl. Climatol. 102 (3-4), 331-342.

Zhao, L., Jin, J., Wang, S.-Y., and Ek, M. B. (2012), Integration of remote-sensing data with WRF to improve lake-effect precipitation simulations over the Great Lakes region, J. Geophys. Res., 117, D09102, doi:10.1029/2011JD016979.

Zhao, L., Wang, S.-Y., Jin, J. and Clark, A. J. (2014). Weather Research and Forecasting model simulations of a rare springtime bow echo near the Great Salt Lake, USA. Meteorol. Appl. DOI: 10.1002/met.1455.

Zhao, W. and Li, A (2015) A Review on Land Surface Processes Modelling over Complex Terrain Advances in Meteorology Volume 2015, Article ID 607181, 17 pages http://dx.doi.org/10.1155/2015/607181 Review

Zheng, H. W., Shen, G. Q., Wang, H. and Hong, J. (2015). Simulating land use change in urban renewal areas: A case study in Hong Kong, Habitat International, 46, 23-34.

Zheng, H., Chen, F., Ouyang, Z., Tu, N., Xu, Weihua, Wang, X., Miao, H., Li, X., Tian, Y. (2008). Impacts of Reforestation Approaches on Run-Off Control in The Hilly Red Soil Region of Southern China. Journal of Hydrology 356: 174-184.

Zheng, X. Y. and Eltahir, E. A. B. (1997) The Response To Deforestation And Desertification in a Model Of West African Monsoons. Geophys. Res. Lett. 24:155–158

Zheng, X.Y., and Eltahir, E.A.B. (1998). The role of vegetation in the dynamics of West African monsoons. Journal of Climate, 12: 1368-1381.

Zhou Y. (2014). Watershed Hydrology and Land-Use and Land-Cover Change (LULCC) Encyclopedia of Natural Resources 892 - 895. DOI: 10.1081/E-ENRW-120048174

Zhou, L., Chen, H. and Dai, Y. (2015). Stronger warming amplification over drier ecoregions observed since 1979 Environ. Res. Lett. 10 064012

Zhou, L., Dickinson, R. E., Tian, Y., Jin, M., Ogawa, K., Yu, H. and Schmugge, T. (2003). A sensitivity study of climate and energy balance simulations with use of satellite-derived emissivity data over Northern Africa and the Arabian Peninsula J. Geophys. Res. 108(D24): 4795-4803.

Zhou, Y. and Wang, Y. Q. (2008). Extraction of impervious surface areas from high spatial resolution imagery by multiple agent segmentation and classification. Photogramm. Eng. Rem. S., 74 (7), 857–868.

Zittis, G., Hadjinicolaou, P. and Lelieveld, J. (2014). Comparison of WRF Model Physics Parameterizations over the MENA-CORDEX Domain. American Journal of Climate Change, 3: 490-511. http://dx.doi.org/10.4236/ajcc.2014.35042

theredesk.org

www.mongabay.com